Doctoral Thesis

Synthetic Natural Gas from Woody Biomass

carried out for the purpose of obtaining the degree of

Doctor technicae (Dr. techn.)

submitted at TU Wien, Faculty of Mechanical and Industrial Engineering
by

Alexander Bartik
Matr.Nr.: 01327352

under the supervision of
Univ.-Prof. Dipl.-Ing. Dr.techn. Hermann Hofbauer

and the co-supervision of
Ing. Dipl.-Ing. Dr.techn. Stefan Müller
Dipl.-Ing. Dr.techn. Florian Benedikt

at the
Institute of Chemical, Environmental and Bioscience Engineering

reviewed by

Univ.-Prof. Dr.-Ing.
Jürgen Karl

Friedrich-Alexander-Universität
Erlangen-Nürnberg
Schloßplatz 4
91054 Erlangen, Germany

Univ.-Prof. Dr.-Ing.
Markus Lehner

Montanuniversität Leoben

Franz-Josef-Straße 18
8700 Leoben, Austria

Imprint

alexander.bartik@tuwien.ac.at
Institute of Chemical, Environmental and Bioscience Engineering
TU Wien
Getreidemarkt 9/166
1060 Vienna, Austria

Synthetic natural gas from woody biomass
ISBN: 978-3-9503671-5-7

Printed and distributed by:

TU Wien
Institute of Chemical, Environmental and Bioscience Engineering
Getreidemarkt 9/166
1060 Vienna, Austria

reproduction requires color print

+43 1 58801 16600
`www.tuwien.at/tch/icebe/e166-07`

Examination committee

Supervisor:	Univ. Prof. Dipl.-Ing. Dr.techn. Hermann Hofbauer
Co-supervisors:	Ing. Dipl.-Ing. Dr.techn. Stefan Müller Dipl.-Ing. Dr.techn. Florian Benedikt
Reviewer 1:	Univ.-Prof. Dr.-Ing. Markus Lehner
Reviewer 2:	Univ.-Prof. Dr.-Ing. Jürgen Karl
Chairwoman:	Dipl.-Ing. Dr.techn. Bettina Mihalyi-Schneider

I confirm, that the printing of this thesis requires the approval of the examination board.

Acknowledgment

This work was supported by the Austrian Klima- und Energiefonds within the framework of the projects ReGas4Industry (871732) and AdoreSNG (881135). Furthermore, this work was carried out within the doctoral college CO_2Refinery at TU Wien.

CO_2Refinery supervisors

PI:	Ing. Dipl.-Ing. Dr.techn. Stefan Müller
Co-PI:	Ao.Univ.-Prof. Dipl.-Ing. Dr.techn. Michael Harasek
Labcoach:	Dipl.-Ing. Dr.techn. Florian Benedikt

Affidavit

I declare in lieu of oath, that I wrote this thesis and performed the associated research myself, using only literature cited in this volume. If text passages from sources are used literally, they are marked as such. I confirm that this work is original and has not been submitted elsewhere for any examination, nor is it currently under consideration for a thesis elsewhere.

Vienna, 5th February 2024

Alexander Bartik

Danksagung

Ich bedanke mich bei allen, die mich auf diesem spannenden Weg begleitet und unterstützt haben. Ohne euch wäre es nicht möglich gewesen. Bei Hermann Hofbauer bedanke ich mich für die Möglichkeit, meine Dissertation in diesem Themenfeld zu verfassen. Danke für die wissenschaftliche Leitung, die anregenden Diskussionen und die Offenheit und Menschlichkeit, die du uns entgegenbringst. Bei Stefan Müller bedanke ich mich für das angenehme Arbeitsumfeld und das entgegengebrachte Vertrauen. Ein großer Dank gebührt Florian Benedikt. Die unzähligen fachlichen und persönlichen Gespräche haben wesentlich zum Gelingen dieses Vorhabens beigetragen. Vielen Dank für deine Zeit, Hingabe und Freundschaft!

Ebenfalls möchte ich mich bei allen Mitgliedern des Forschungsbereichs bedanken. Danke für den einzigartigen Teamgeist, die anregenden Diskussionen und die harmonische gemeinsame Zeit. Ich könnte mir keine besseren KollegInnen wünschen!

Bei meiner Familie bedanke ich mich für die immerwährende Unterstützung und die Möglichkeit, meinen Weg frei zu wählen. Allein dadurch war es mir erst möglich an diesem Punkt im Leben anzukommen.

Nicht zuletzt bedanke ich mich bei dir, Veronica. Du sitzt sprichwörtlich im gleichen Boot und kannst die Herausforderungen, die am Weg entstehen, sehr gut nachvollziehen. Danke für deine Zuneigung und deine bedingungslose Unterstützung in allen Lebenslagen. Ohne dich wäre dieser Weg nur halb so schön!

Abstract

Evolution has allowed humankind to prosper and flourish, culminating in unparalleled growth and abundance where a sustainable existence seems unfeasible. The exorbitant resource consumption and greenhouse gas emissions must be reduced dramatically to reach climate neutrality and lay down a sustainable pathway for future generations. Sustainable energy carriers are one technical solution to contribute to these goals. A promising approach to partially replace natural gas is dual fluidized bed (DFB) gasification of biomass and catalytic fluidized bed methanation to synthetic natural gas. Dual fluidized bed gasification is an established technology that produces a nearly nitrogen-free product gas that has been utilized for heat and electricity generation and demonstrations of synthetic natural gas production. The demonstrations showed that technical and economic issues must be addressed to prepare for successful commercialization. Methanation in adiabatic fixed-bed reactors is already well-known from coal-based production plants and is applied to syngas methanation from biomass alike. However, fluidized bed reactors offer the advantage of an increased heat transfer and less risk of carbon deposition on the catalyst, allowing for a simpler process layout.

Hence, this work aims to elaborate on innovative concepts that increase the efficiency, the carbon utilization of the biomass, and the gas quality while simultaneously reducing the complexity of the process and creating economic advantages. The investigations include i) thermodynamic analyses of methanation, ii) design, construction, and investigation of a 10 kW fluidized bed methanation reactor and gas cleaning units, iii) investigation of a full process chain including a 100 kW_{th} advanced dual fluidized bed pilot plant, and, iv) conceptualization, simulation, techno-economic analysis, and CO_2 footprint calculations of industrial scale synthetic natural gas production from woody biomass.

The results lead to the conclusion that unpressurized fluidized bed methanation with an optimized catalyst in combination with a fixed-bed polishing reactor and advanced dual fluidized bed gasification represents an attractive concept that leads to compliance with the specified thresholds of the natural gas grid (e.g. CO $<$ 0.1 mol.-%) and reduces the electricity consumption by 17%–38%. From an economic point of view, the process can almost compete with industrial natural gas prices at around 90 €/MW h in 2022, presuming revenues from secondary products

like district heat and CO_2. If revenues from CO_2 are unlikely, sorption enhanced reforming, an advanced operation mode of dual fluidized bed gasification with in-situ CO_2 removal, leads to a significant cost reduction requiring fewer and smaller equipment. Ecologically favorable hybrid concepts with external H_2 addition allow a doubling of the carbon utilization of the biomass but penalize the economic feasibility by increasing production costs by roughly 60%.

Overall, synthetic natural gas from woody biomass could lead to a CO_2 reduction potential of 12%–39% when applied in the Austrian energy or industrial sectors, thus significantly contributing to the national climate targets.

Kurzfassung

Die Evolution hat es der Menschheit ermöglicht, sich ungestört zu entwickeln und entfalten, was zu einem beispiellosen Wachstum und Überfluss geführt hat, bei dem eine nachhaltige Existenz nicht mehr möglich scheint. Der exorbitante Ressourcenverbrauch und die Treibhausgasemissionen müssen drastisch gesenkt werden, um Klimaneutralität zu erreichen und einen nachhaltigen Weg für künftige Generationen zu ebnen. Nachhaltige Energieträger stellen eine technische Lösung dar, um diesem Ziel näherzukommen. Ein vielversprechender Ansatz, um Erdgas teilweise zu ersetzen, könnte die Zweibettwirbelschicht-Gaserzeugung (DFB) aus Biomasse und die katalytische Wirbelschichtmethanierung zu synthetischem Erdgas sein. Die Zweibettwirbelschichttechnologie hat sich zur Erzeugung von Strom und Wärme bereits etabliert. Durch das erzeugte, nahezu stickstofffreie Produktgas wurde die Technologie auch zur Produktion von synthetischem Erdgas bereits demonstriert. Im Hinblick auf technische und ökonomische Aspekte bedarf es jedoch einer Weiterentwicklung der bisher betriebenen Demonstrationsanlagen. An sich ist die Methanierung in adiabatischen Festbettreaktoren bereits aus kohlebasierten Anlagen bekannt und wird auch bei der Methanierung von Synthesegas aus Biomasse angewandt. Wirbelschichtreaktoren bieten jedoch den Vorteil eines verbesserten Wärmetransports und eines geringeren Risikos von Kohlenstoffablagerungen auf dem Katalysator, wodurch eine einfachere Prozessgestaltung ermöglicht wird.

Ziel dieser Arbeit ist es daher, innovative Konzepte zu erarbeiten, die die Effizienz, den Biomasse-Kohlenstoffnutzungsgrad und die Gasqualität erhöhen, und gleichzeitig eine Reduktion der Prozesskomplexität und eine Senkung der Produktionskosten erreichen. Die Untersuchungen umfassen i) thermodynamische Analysen der Methanierung, ii) Entwurf, Bau und Untersuchung eines 10 kW Wirbelschicht-Methanierungsreaktors sowie von Gasreinigungsapparaten, iii) Untersuchung einer vollständigen Prozesskette, einschließlich einer 100 kW_{th} Zweibettwirbelschicht-Pilotanlage, und, iv) Konzeption, Simulation, techno-ökonomische Analyse und Berechnung des CO_2-Fußabdrucks von industriellen Konzepten zur Erzeugung von synthetischem Erdgas aus Biomasse.

Aus den Ergebnissen lässt sich schlussfolgern, dass eine drucklose Wirbelschichtmethanierung mit optimiertem Katalysator in Kombination mit einem Festbett-Polishing-Reaktor und der

Zweibettwirbelschicht-Gaserzeugung ein attraktives Konzept darstellt, welches zu einem hochwertigen Gas entsprechend den Anforderungen des Gasnetzes (z.B. CO $< 0,1$ mol-%), bei einer gleichzeitigen Senkung des Stromverbrauchs von 17–38 %, führt. Mit Produktionskosten von circa 90 €/MW h im Jahr 2022 kann das so erzeugte synthetische Erdgas annähernd mit großtechnisch gehandelten Erdgaspreisen konkurrieren, wobei Einnahmen aus Beiprodukten wie Fernwärme und CO_2 vorausgesetzt werden. Sind Einnahmen aus CO_2 nicht zu erwarten, führt die sorptionsgestützte Gaserzeugung (SER), eine spezielle Betriebsart der Zweibettwirbelschichttechnologie mit in-situ CO_2-Abscheidung, zu einer erheblichen Kostenreduktion mit weniger und kleineren Anlagenkomponenten. Ökologisch relevante Hybridkonzepte, mit externer H_2-Zudosierung, ermöglichen eine Verdopplung des Biomasse-Kohlenstoffnutzungsgrads, beeinträchtigen aber die wirtschaftliche Machbarkeit durch eine Erhöhung der Produktionskosten um etwa 60 %.

Allgemein erlaubt die Produktion von synthetischem Erdgas aus holzartiger Biomasse ein CO_2-Reduktionspotential von 12–39 % bei Anwendung im österreichischen Energie- oder Industriesektor und kann somit einen wertvollen Beitrag zum Erreichen der nationalen Klimaziele leisten.

Contents

List of Appended Publications

Paper I

Thermodynamic investigation of SNG production based on dual fluidized bed gasification of biogenic residues
Alexander Bartik, Florian Benedikt, Andreas Lunzer, Constantin Walcher, Stefan Müller, Hermann Hofbauer
Biomass Conversion and Biorefinery, **2020**, Vol. 11, pp. 95–110
https://doi.org/10.1007/s13399-020-00910-y

Paper II

Development of an internally circulating fluidized bed for catalytic methanation of syngas
Alexander Bartik, Josef Fuchs, Stefan Müller, Hermann Hofbauer
in Proceedings of the 16th Minisymposium Verfahrenstechnik, September 21st–22nd, **2020**, TU Wien, Vienna
https://doi.org/10.34726/566

Paper III

Experimental investigation on the methanation of hydrogen-rich syngas in a bubbling fluidized bed reactor utilizing an optimized catalyst
Alexander Bartik, Josef Fuchs, Gernot Pacholik, Karin Föttinger, Hermann Hofbauer, Stefan Müller, Florian Benedikt
Fuel Processing Technology, **2022**, Vol. 237, 107402
https://doi.org/10.1016/j.fuproc.2022.107402

Paper IV

Experimental investigation of hydrogen-intensified synthetic natural gas production via biomass gasification: a technical comparison of different production pathways
Alexander Bartik, Florian Benedikt, Josef Fuchs, Hermann Hofbauer, Stefan Müller
Biomass Conversion and Biorefinery, **2023**, article in press
https://doi.org/10.1007/s13399-023-04341-3

Paper V

Economic and ecological impacts on the integration of biomass-based SNG and FT diesel in the Austrian energy system
Martin Hammerschmid, Alexander Bartik, Florian Benedikt, Marton Veress, Simon Pratschner, Stefan Müller, Hermann Hofbauer
Energies, **2023**, Vol. 16(16), 6097
https://doi.org/10.3390/en16166097

Author's Contributions

Paper I Alexander Bartik was responsible for conceptualization, methodology, investigation, visualization, and writing the original draft.

Paper II Alexander Bartik was responsible for methodology, analysis, visualization, writing the original draft, most of the investigations, and partially responsible for conceptualization and validation.

Paper III Alexander Bartik was responsible for conceptualization, methodology, analysis, investigation, visualization, and writing the original draft.

Paper IV Alexander Bartik was responsible for analysis, writing the original draft, visualization, and partially responsible for conceptualization, methodology, investigation, and validation.

Paper V Alexander Bartik was partially responsible for conceptualization, investigation, and writing and reviewing the draft.

List of Additional Publications

Additional Paper I

Experimental demonstration of 80kW$_{th}$ chemical looping combustion of biogenic feedstock coupled with direct CO_2 utilization by exhaust gas methanation
Benjamin Fleiß, Alexander Bartik, Juraj Priscak, Florian Benedikt, Josef Fuchs, Stefan Müller, Hermann Hofbauer
Biomass Conversion and Biorefinery, **2023**, article in press
https://doi.org/10.1007/s13399-023-04311-9

Additional Paper II

Nitrogen recovery from low-value biogenic feedstocks via steam gasification to methylotrophic yeast biomass
Roghayeh Shirvani, Alexander Bartik, Gustavo A.S. Alves, Daniel Garcia de Otazo Hernandez, Stefan Müller, Karin Föttinger, Matthias Steiger
Frontiers in Bioengineering and Biotechnology, **2023**, Vol. 11
https://doi.org/10.3389/fbioe.2023.1179269

Additional Paper III

Methodology for the Development of Virtual Representations within the Process Development Framework of Energy Plants: From Digital Model to Digital Predictive Twin - A Review
Martin Hammerschmid, Daniel C. Rosenfeld, Alexander Bartik, Florian Benedikt, Josef Fuchs, Stefan Müller
Energies, **2023**, Vol. 16(6), 2641
https://doi.org/10.3390/en16062641

Additional Paper IV

Dynamic modeling of dual fluidized bed steam gasification for control design
Lukas Stanger, Alexander Schirrer, Florian Benedikt, Alexander Bartik, Stefan Jankovic, Stefan Müller, Martin Kozek
Energy, **2023**, Vol. 265, 126378
https://doi.org/10.1016/j.energy.2022.126378

Additional Paper V

Conversion of CO_2 during the DFB biomass gasification process
Anna M. Mauerhofer, Stefan Müller, Alexander Bartik, Florian Benedikt, Josef Fuchs, Martin Hammerschmid, Hermann Hofbauer
Biomass Conversion and Biorefinery, **2021**, Vol. 11(1), pp. 15–27
https://doi.org/10.1007/s13399-020-00822-x

Additional Paper VI

CO_2 gasification of biogenic fuels in a dual fluidized bed reactor system
Anna M. Mauerhofer, Stefan Müller, Florian Benedikt, Josef Fuchs, Alexander Bartik, Hermann Hofbauer
Biomass Conversion and Biorefinery, **2021**, Vol. 11(1), pp. 1101–1116
https://doi.org/10.1007/s13399-019-00493-3

Additional Paper VII

Thermodynamic investigation of SNG production based on dual fluidized bed gasification of biogenic residues
Alexander Bartik, Florian Benedikt, Andreas Lunzer, Constantin Walcher, Stefan Müller, Hermann Hofbauer
in Proceedings of the ICPS19 – International Conference on Polygeneration Strategies, November 18th–20th, **2019**, Vienna, pp. 223–233
http://dx.doi.org/10.34726/105

Additional Paper VIII

SNG production via gasification and catalytic methanation: Latest developments at TU Wien
Alexander Bartik, Florian Benedikt, Josef Fuchs, Hermann Hofbauer, Stefan Müller
in Proceedings of the 7th International Conference on Renewable Energy Gas Technology (REGATEC 2020), September 20th–21st, **2021**, Weimar, Germany, pp. 61–64
ISBN 978-91-981149-6-6

Additional Paper IX

Development and Techno-Economical Evaluation of an Optimized Concept for Industrial Bio-SNG Production from Sewage Sludge
Marton Veress, Alexander Bartik, Florian Benedikt, Martin Hammerschmid, Josef Fuchs, Stefan Müller, Hermann Hofbauer
in Proceedings of the 28th European Biomass Conference and Exhibition (e-EUBCE), July 6th–9th, **2020**, virtual, pp. 901–911
ISSN 2282-5819

Additional Paper X

Steam gasification of sewage sludge for synthesis processes
Johannes C. Schmid, Alexander Bartik, Florian Benedikt, Anna M. Mauerhofer, Josef Fuchs, Ellen Schanz, . . . , Hermann Hofbauer
in Proceedings of the ICPS19 – International Conference on Polygeneration Strategies, November 18th–20th, **2019**, Vienna, pp. 45–53
http://doi.org/10.34726/45

Additional Paper XI

Experimental development of chemical looping combustion with biogenic solid fuels at TU Wien

Benjamin Fleiß, Josef Fuchs, Alexander Bartik, Florian Benedikt, Stefan Müller, Hermann Hofbauer

in Proceedings of the 6th International Conference on Chemical Looping, September 19th–22nd, **2022**, Zaragoza, Spain

https://doi.org/10.34726/3726

Chapter 1

Introduction

1.1 Motivation

Climate change is seen as one of the most pressing issues of our time [1]. Many institutions warn of the impacts on the planet and on future generations, resulting in global resolutions to combat the downwards spiral. The Paris Agreement states a limit on global warming of 1.5 °C [2]. Furthermore, a transition away from fossil fuels was declared at the UN Climate Change Conference in Dubai in 2023, simultaneously acknowledging that progress was far too slow in the past [3]. Meanwhile, the exploitation of our planet continues at an ever growing pace and the set climate goals seem almost unreachable. The IPCC's report on climate change paints a grim picture of the future following the current trajectory [4]. Thus, a tremendous global effort that tackles climate change from every aspect of life seems necessary. Technological advances are only one tool that can be instrumentalized toward this goal. The utilization of biomass resources, for example, enables us to replace energy carriers and products currently based on fossil fuels. Natural gas is an important energy carrier worldwide, with an annual consumption of 4250 bn m^3 in 2021 [5]. Gaseous fuels, in general, are predicted to remain crucial energy carriers in the foreseeable future [6]. Thus, a sustainable replacement is advisable. Synthetic natural gas (*SNG*) from woody biomass via dual fluidized bed (*DFB*) gasification is one possibility to produce such a natural gas substitute. This technology produces syngas from woody (waste) biomass through gasification with steam and consecutively converts it to a methane-rich gas in a catalytic methanation process.

In general, the following benefits result if an SNG production approach is followed. [7, 8]

- The already existing gas infrastructure (e.g. pipelines) and end-use equipment (e.g. natural gas burners) can be utilized.

- The energy supply security is increased, and domestic, biogenic resources can be used further.
- A (nearly) pure stream of biogenic carbon dioxide (CO_2) can be obtained for further utilization or sequestration with the possibility of creating negative emissions.
- Baseload and peak-load power can be provided with the possibility to equalize fluctuations in the electricity grid caused by stochastic renewable energy sources (RESs) like photovoltaics and wind power. This is enabled by supplying SNG to e.g. gas-fired power plants or converting excess electricity to methane (CH_4).
- SNG is easily stored and transported over long spatial and temporal (even seasonal) distances creating flexibility in the energy system.

However, other aspects need to be considered as well.

- CH_4 is a greenhouse gas 28-times more potent than CO_2 [9]. Direct emissions to the air occur through leaking equipment or poorly maintained gas pipelines.
- Biomass resources are limited and the demand for natural gas is far higher than the supply through biogenic resources if sustainably managed.
- CH_4 is usually quite short-lived considering its application as a combustion fuel, re-emitting CO_2 (even though biogenic) to the atmosphere once combusted.

Nevertheless, on the mid-term, there is a need for gaseous, sustainable energy carriers like SNG [5]. Thus, legislation is prepared in Austria ("Erneuerbare-Gase-Gesetz") for a mandatory quota of 7.5 TW h p.a. of "green gases" in 2030 [10].

In the past, several investigations concerning SNG production via biomass gasification and catalytic methanation have been carried out (e.g. [11–13]). However, there is room for process improvements, as some aspects have not been addressed, require more attention, and can be optimized further. Hence, this work aims to push innovative concepts forward, improve the methanation process itself, and optimize SNG production from an economic perspective, eventually showing the potential greenhouse gas emissions reduction within the Austrian energy system.

1.2 Aim and Scope

This thesis aims to optimize SNG production from woody biomass from multiple angles. Even though lab-scale and demonstration-scale plants already exist, new aspects of this technology are treated in this thesis.

- Unpressurized fluidized bed methanation with a tailored catalyst to reduce the compression energy and increase the catalyst's performance and lifetime.
- Innovative process concepts combining advanced DFB gasification, sorption enhanced reforming (*SER*), fluidized bed methanation and optional external hydrogen (H_2) addition to increase the carbon utilization of the biomass, increase the efficiency and comply with the gas grid specifications (e.g. CO limit).
- Reduce the capital and operational expenditures through the innovations above.

To this end, thermodynamic, experimental, and simulation-based investigations are carried out. A new fluidized bed methanation reactor, including an optimized catalyst for fluidized bed applications, is designed and investigated. Full process chain investigations from woody biomass to raw synthetic natural gas (*raw-SNG*) are performed, comparing and assessing the alternative and novel process configurations. Finally, the proposed process configurations are transferred to commercial-scale concepts via process simulation. A technical, techno-economic, and CO_2 footprint assessment provides the basis for the integration of SNG production from woody biomass into the Austrian energy system.

1.3 Methodology of this Thesis

This thesis is based on five publications, as depicted in Fig. 1.1. The structure of the thesis follows the genesis of the publications, which aligns with the general structure of any scientific work. Chapter 2 is based on extended literature sources of all publications. Additionally, a new subchapter is presented in this thesis, which has not been published before (section 6.2).

In **Paper I**, the thermodynamic modeling is performed to investigate the impact of advanced DFB gasification and SER on methanation at varying parameters like methanation temperature, pressure, and steam content. The investigations in this paper also provide valuable information about the methanation reactor design. **Paper II** deals with the design, construction, and fluid dynamic investigation of the chosen fluidized bed methanation reactor. A catalyst tailored for fluidized beds is manufactured and tested together with the reactor under methanation conditions. Systematic experimental investigations with synthetically premixed syngas allow a deeper insight

into fluidized bed methanation (**Paper III**). The investigations reveal the catalyst stability and activity, the performance of the reactor, and the applicability of DFB and SER product gases for fluidized bed methanation, ultimately allowing statements on optimized SNG production possibilities. In **Paper IV**, a full process chain is set up and investigated to show the technical feasibility of raw-SNG production from woody biomass. The fluidized bed methanation reactor is connected to upstream gas cleaning units, comprising a biodiesel scrubber and activated carbon (AC) beds, and to a 100 kW_{th} advanced DFB pilot plant. The full process chain operation allows the tracking of impurities and the comparison of different process configurations. The comparison involves the direct methanation of syngas from advanced DFB gasification, external H_2 addition to this syngas for increased carbon utilization, and the direct methanation of syngas from SER. The results allow statements on the advantages and disadvantages of the alternative process configurations. Eventually, it is important to translate the gained knowledge to commercial-scale concepts and assess and compare them on a techno-economic and ecological basis. Thus, **Paper V** shows a simulation study on the integration of SNG and Fischer-Tropsch (FT) diesel into the Austrian energy system. In the previously unpublished subchapter (section 6.2), the alternative process configurations are translated to commercial-scale concepts and compared from a technical and techno-economic perspective. Based on the knowledge gained from the theoretical, experimental, and simulation-based investigations, conclusions toward optimized SNG production pathways are drawn.

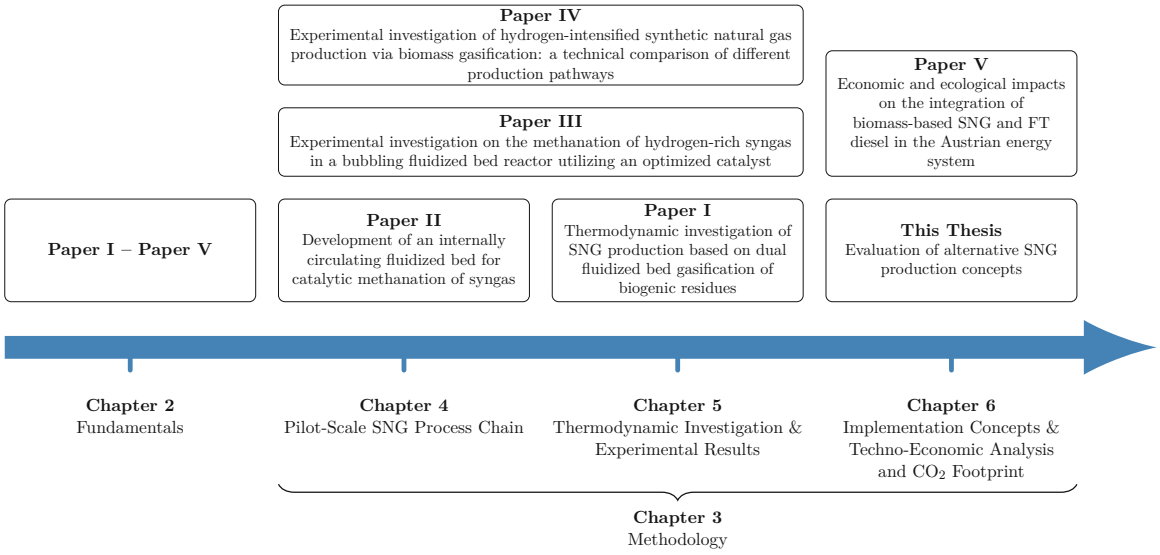

Fig. 1.1: Schematic methodology of this thesis

Chapter 2

Fundamentals

This chapter discusses the fundamentals of methanation (section 2.1) and the gasification and gas cleaning technologies to provide syngas for methanation (section 2.2). Furthermore, section 2.3 introduces process concepts converting woody biomass to synthetic natural gas (*SNG*).

2.1 Methanation

Methanation is understood as a technology of producing CH_4 from carbon oxides and H_2 [14]. The technology became industrially relevant at a time when natural gas had already replaced town gas and was established as an essential pillar of the energy system [15]. Especially the abundance of coal, the expected shortage of natural gas, and the oil crisis in the 1970s ramped up the efforts to produce a natural gas substitute, usually referred to as SNG [7]. The technology per se had been known before: Sabatier and Senders discovered the methanation reaction already in 1902 [16] and for a long time it was applied as a gas cleaning step to convert carbon monoxide (CO) in ammonia synthesis plants [14].

Over the last two decades, the focus has shifted toward the production of renewable CH_4. Biomass-to-Gas (*BtG*) and Power-to-Gas (*PtG*) concepts have been developed to combat global warming and reduce anthropogenic greenhouse gas emissions [17, 18]. In this context, biological processes also gained importance [19]. Fig. 2.1 gives an overview of methods applied to CH_4 production. Generally, all combinations of the displayed gas production and methanation technologies are possible and have been looked at during the last decades. In the following paragraphs, these major technologies are described shortly.

Thermochemical processes in the context of SNG production focus on the conversion of biomass or coal to product gas via gasification, utilizing gasification agents such as steam, air, oxygen (O_2), CO_2, H_2, or a mixture of those [20]. The resulting product gas is then cleaned and catalytically converted to raw synthetic natural gas (*raw-SNG*), which can be injected into the

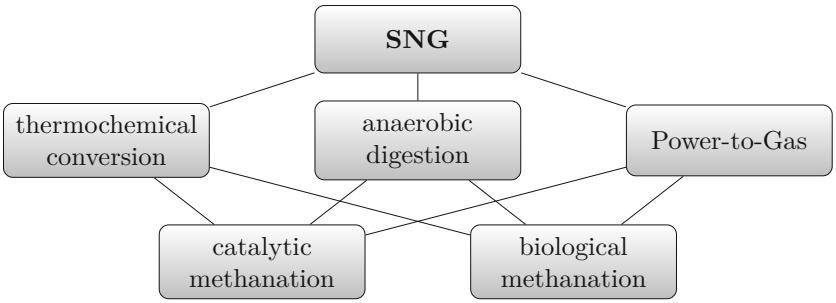

Fig. 2.1: Overview of methods for SNG production

natural gas grid after upgrading [7]. Since the present thesis focuses on this process, a more detailed description follows in this chapter. Investigations also focus on the biological conversion of product gas to CH_4. Schwede et al. [21] successfully produced CH_4 with methanogenic archaea immobilized on biochar to improve the mass transfer. Because of the inhibitory effect of CO, further investigations in this direction are necessary. A further subcategory of thermochemical conversion processes is hydrothermal gasification (*HTG*). The aim is to exploit the changing chemical and physical properties of water near or above the critical point, which increases the reactivity compared to steam significantly. A gas rich in CH_4 and CO_2 is obtained under typical reaction conditions between 350 and 450 °C and 200 and 300 bar. For a sufficient CH_4 yield, a heterogeneous catalyst (e.g. Ru on activated carbon (*AC*)) is required [22]. Two similar pilot-scale units have been designed and operated by the Paul Scherrer Institute and the Pacific Northwest National Laboratory, converting 1–10 kg/h of various biomass feedstocks (including algae) to a methane-rich gas [23, 24]. Overall the HTG process should be considered for wet biomass feedstocks, where conventional gasification processes show disadvantages because of the energy penalty related to drying [22].

Anaerobic digestion is the process of converting organic substrates like manure, energy crops, municipal waste, or industrial byproducts to biogas, mainly consisting of CH_4 and CO_2. The conversion itself is a biological process involving fermentative bacteria, acid-forming bacteria and methanogens in a four-step process: hydrolysis, acidogenesis, acetogenesis, and methanogenesis [25]. Typically, biogas is utilized in cogeneration plants to produce heat and electricity [26]. However, increasing attention is paid to upgrading biogas to SNG (mainly referred to as biomethane synonymously). Upgrading steps involve the removal of impurities and the bulk removal of CO_2. The removed CO_2 is either just vented to the atmosphere or utilized as a source of biogenic carbon for PtG processes. The same applies to removed CO_2 from thermochemical conversion processes. Such a PtG process typically produces H_2 via electrolysis, which is further used for the hydrogenation of CO_2—in this particular case for the catalytic or biological methanation to SNG. The latter uses hydrogenotrophic methanogenic archaea in trickle

bed reactors, for example. High CH_4 concentrations above 95 vol.-% have been obtained—the poor solubility of H_2 being the limiting factor [27]. While this is referred to as ex-situ biological methanation, in-situ concepts and combinations of both have been investigated as well. During in-situ biological methanation, H_2 is directly injected into the biogas fermenter. This concept comes with some additional limitations regarding the interference of H_2 with the metabolic pathway of microorganisms used in biogas fermenters [28, 29].

Much research is also put into the catalytic hydrogenation of CO_2. In the context of PtG, the publicly familiar term "e-fuels" is often used as an umbrella term for these processes. Advantages thereof are (i) the possibility to store electricity from fluctuating renewable energy sources (RESs) in the long-term, (ii) the coupling of the power and the gas grid which increases the flexibility and stability of the former, and (iii) the production of sustainable fuels - in this case, CH_4 [7]. However, there are a few hurdles along the way [30]: (i) Due to the fluctuating nature of RESs, a dynamic operation of the plant and H_2 storage capacities are required, (ii) low efficiency can be expected due to the losses connected to electrolysis and the exothermic methanation reaction, and (iii) high costs can be expected due to the current price of electricity (also see section 6.2). To date, the largest and most prominent example is the Audi e-gas plant in Germany with an installed capacity of 6 MW_{el}, utilizing a molten-salt cooled tube bundle reactor [7]. For these processes, the origins of H_2 and CO_2 are crucial for an ecologically sound concept. The most widely discussed and matured source of renewable H_2 is water electrolysis [31]. Nevertheless, alternatives are also investigated, including electrical or thermochemical water splitting [32, 33], biomass gasification [34], and dark or photo-fermentation of biogenic materials [35]. Biogas plants, on the other hand, can serve as a source of renewable CO_2, like in the above-mentioned Audi e-gas plant. Furthermore, off-gases from steelworks—though not renewable—are also investigated in methanation processes as a way of carbon recycling [36, 37].

Also for catalytic methanation processes, the combination of PtG and BtG has been realized. Adding H_2 to product gas or biogas increases the utilization of biomass carbon within a single process setup. There is no requirement for a CO_2 separation step [38, 39] and O_2 from electrolysis could be utilized as a secondary product, for example, directly as a gasification agent [40]. Nevertheless, the same limitations and benefits apply as for straight PtG concepts. This approach is investigated and will be described further throughout this thesis.

2.1.1 Thermodynamics

The main chemical species involved in the methanation of syngas are CH_4, H_2, CO, CO_2, and H_2O. The thermodynamic equilibrium can be formulated via the CO methanation reaction (Eq. 2.1),

$$CO + 3\,H_2 \rightleftharpoons CH_4 + H_2O \qquad \Delta H_R^0 = -206\,\mathrm{kJ/mol} \tag{2.1}$$

the water-gas shift (*WGS*) reaction (Eq. 2.2),

$$CO + H_2O \rightleftharpoons CO_2 + H_2 \qquad \Delta H_R^0 = -41\,\mathrm{kJ/mol} \tag{2.2}$$

or the CO_2 methanation reaction (Eq. 2.3).

$$CO_2 + 4\,H_2 \rightleftharpoons CH_4 + 2\,H_2O \qquad \Delta H_R^0 = -165\,\mathrm{kJ/mol} \tag{2.3}$$

The equations are linearly dependent, requiring only two of the three equations for a unique solution of the equilibrium state. Since these reactions are all exothermic and the methanation reactions lead to a volume reduction according to Le Chatelier's principle, low temperatures and high pressures generally favor the conversion to CH_4. As can be seen from the reaction equations, an H_2/CO ratio of 3 and an H_2/CO_2 of 4 is required for stoichiometric methanation.

Because of the low temperatures required, the methanation reactions are heterogeneously catalyzed for industrial applications. Therefore, carbon deposition and coke formation on the catalyst surface are issues that can lead to fouling and catalyst deactivation and need to be considered (see section 2.1.2) [41]. From a thermodynamic point of view, the Boudouard reaction (Eq. 2.4),

$$2\,CO \rightleftharpoons CO_2 + C(s) \qquad \Delta H_R^0 = -174\,\mathrm{kJ/mol} \tag{2.4}$$

the hydrogenation of the solid carbon to CH_4 (Eq. 2.5),

$$C(s) + 2\,H_2 \rightleftharpoons CH_4 \qquad \Delta H_R^0 = -82\,\mathrm{kJ/mol} \tag{2.5}$$

and the gasification with steam (Eq. 2.6)

$$C(s) + H_2O \rightleftharpoons CO + H_2 \qquad \Delta H_R^0 = 134\,\mathrm{kJ/mol} \tag{2.6}$$

can be considered. Increased amounts of H_2O, H_2, and CO_2 could therefore prevent carbon depositions [42].

Syngas from gasification—especially from dual fluidized bed (*DFB*) gasification—also contains small amounts of hydrocarbons like ethylene (C_2H_4) [43]. Especially in fluidized bed methanation reactors, a conversion of C_2H_4 to ethane (C_2H_6) or CH_4 has been observed by Kopyscinski et al. [44]. Therefore, the hydrogenation of C_2H_4 is included here. It can proceed to C_2H_6 or CH_4 (Eqs. 2.7 and 2.8), for example.

$$C_2H_4 + H_2 \rightleftharpoons C_2H_6 \qquad \Delta H_R^0 = -137\,\mathrm{kJ/mol} \tag{2.7}$$

$$C_2H_4 + 2\,H_2 \rightleftharpoons 2\,CH_4 \qquad \Delta H_R^0 = -202\,\mathrm{kJ/mol} \tag{2.8}$$

Thermodynamic models are often used to describe the main methanation reactions since a good estimation of the real gas composition can be given. For example, Gao et al. [45] systematically investigated CO and CO_2 methanation under varying temperatures, pressures, and H_2/CO ratios. Other researchers propose novel process configurations and find optimal process conditions based on thermodynamic analysis (see section 2.3.2). Of course, temperature limits have to be obeyed, below which kinetic limitations govern the reactions. Such temperature limits are around 320 °C for fluidized bed applications [11, 46, 47]. Additionally, heat and mass transfer limitations can lead to deviations [7, 11]. Conversely, carbon depositions are often governed by kinetics and an exact description is an intricate matter. Nevertheless, thermodynamic models using graphitic carbon as a model substance have been used by Frick et al. [48] and Bai et al. [49] to give a rough estimation, since kinetic models are often only valid for specific reaction conditions and catalysts [48].

2.1.2 Catalysts

As stated in section 2.1.1, a high conversion to CH_4 occurs at relatively low temperatures, requiring the application of catalysts for industrially relevant reaction rates. Generally, group VIII–X elements of the periodic table have been found to catalyze methanation reactions [17]. Vannice [50] ranked these metals by their activity and selectivity, Mills and Steffgen [51] shortened the list to relevant methanation catalysts, and Kuznecova and Gusca [52] added a cost ranking, resulting in the following order:

- Activity: Ru > Fe > Ni > Co > Mo
- Selectivity: Ni > Co > Fe > Ru

- Cost: Ru > Mo > Co > Ni > Fe

According to this ranking, ruthenium is the most active (120 times more active than nickel [53]), nickel is the most selective, and iron is the cheapest. If these properties are combined, nickel turns out to be the preferred solution and is, in fact, widely applied. Nevertheless, a significant amount of research is put into developing methanation catalysts, as some reviews show [53, 54]. Since PtG applications gain importance, tailored catalysts for CO_2 methanation are developed in parallel. Also for this application, nickel-based catalysts are the front-runners [55]. Another critical factor is the stability of the catalyst, where nickel shows some issues, as will be discussed further down.

The support on which the active metal is immobilized also plays a vital role in shaping the catalyst's performance. The most commonly applied support for nickel catalysts is Al_2O_3 in its γ-configuration because of its high surface area, developed pore structure, and known surface properties. Alternative metals, such as SiO_2, TiO_2, ZrO_2, CeO_2, SiC, and perovskites, are also studied, each showing specific advantages and drawbacks [54]. Furthermore, promoters are used, which alter the properties of the catalyst. In combination with Ni/Al_2O_3, MgO and boron have been found to increase the resistance against carbon depositions and minimize Ni particle sintering [56, 57]. Finally, the preparation method and conditions also affect the dispersion of the active metal and the metal-support interaction. Well-known preparation methods include impregnation [58], precipitation [59], and sol-gel methods [60]. Also, the calcination temperature of the support [61] and the active metal loading on the support [62] influence the activity and stability of the catalyst. Overall, there are even more parameters that have an impact on the properties of the catalyst. This shows that there are many angles from which catalyst optimizations can be carried out, possibly explaining the wealth of literature available in this field. Gao et al. [54] summarized this literature and provided a good overview of applied catalysts, supports, promoters, and preparation methods.

Catalyst Deactivation

A major issue encountered in catalytic methanation processes is the deactivation of the catalyst over time. Bartholomew [41] defined chemical, mechanical, and thermal deactivation mechanisms, which he further broke down into the following categories.

Poisoning A strong chemisorption of species (e.g. impurities) occurs on the active catalyst sites. In other words, the bond of the poison is stronger than the bond of the desired reacting species. Sulfur compounds are one of the most problematic substances in this context. H_2S,

COS, and organic sulfur species, like thiophene, are typical substances found in product gas from biomass gasification [63], which may react with nickel directly (Eq. 2.9) or after hydrogenation (Eq. 2.10) [17].

$$H_2S + NiO(s) \rightleftharpoons NiS(s) + H_2O(g) \tag{2.9}$$

$$2\,H_2(g) + C_4H_4S(g) \rightleftharpoons H_2S(g) + C_4H_6(g) \tag{2.10}$$

Especially nickel catalysts are reported to be very sensitive to sulfur poisoning, resulting in stringent requirements for sulfur contents down to *ppb* levels [7, 64, 65].

Fouling Fouling occurs through the physical deposition or chemisorption of gaseous species on the catalyst. When talking about methanation, fouling mainly refers to carbon or coke depositions. While adsorbed carbon is a necessary reaction intermediate during methanation, the formation of stable deposits can lead to catalyst deactivation [49]. This happens when the carbon deposition rate is higher than the reaction of the adsorbed carbon with reactants, such as H_2 or H_2O. The tendency to form carbon deposits greatly depends on the temperature, the H_2 and CO partial pressure, and the catalyst properties. The term coking is usually used when talking about carbon depositions resulting from C_2 species and aromatics, such as C_2H_4 and benzene, which are typically in product gas from biomass gasification [63]. Various types of carbon species can be formed thereof. If the adsorbed carbon (C_α) does not desorb, it can diffuse into the bulk nickel, forming nickel carbide (C_γ). Adsorbed carbon can also polymerize to an amorphous carbon film (C_β), which can turn into graphitic carbon (C_C) over time. Both species can deactivate the catalyst by covering active sites with a film or encapsulating nickel crystallites. Additionally, carbon whiskers (C_v) can form via an intermediate nickel carbide, blocking the pores and physically destroying the particles. Especially C_β and C_v occur at relatively low temperatures ($< 500\,°C$), making it relevant for low-temperature methanation as well. Fluidized beds show some advantages in this regard, as will be discussed in section 2.1.4. [7, 57, 66]

Vapor-solid reactions Below temperatures of 230 °C, nickel can be carried over to the gas phase via the reaction with CO to nickel tetracarbonyl ($Ni(CO)_4(g)$). It is highly toxic but only plays a role during start-up and shutdown since it is formed at temperatures where methanation catalysts only show low activity. [17]

Thermal degradation Especially in adiabatic fixed-bed reactors, temperature hot spots can lead to the sintering of the nickel particles and a loss of surface area and catalyst activity. This problem occurs due to the high heat flux and the poor heat conductivity, which can be overcome by the application of alternative reactor concepts (see section 2.1.4). [17, 41]

Attrition and crushing In fluidized bed applications, high mechanical forces act on the bed material, i.e. the catalyst particles. Therefore, attrition is an issue that can cause a loss of catalyst material (i.e. lead to operational expenditures) and potentially requires a downstream particle separation. Attention must be paid to the development of attrition-resistant catalysts, if fluidized beds are applied. Crushing, on the other hand, refers to the destruction of catalyst particles by mechanical stress (e.g. pressure fluctuations) or thermal stress (e.g. fast temperature changes). This phenomenon is mainly problematic for fixed-bed applications during start-up and shutdown. [41]

2.1.3 Kinetics

The methanation reactions can be described in approximation by the thermodynamic equilibrium down to a certain temperature level. Below, kinetic effects govern the conversion. Even at higher temperatures, mass transfer and kinetic limitations must be considered for an exact description of the gas composition. Different pathways have been proposed concerning kinetic mechanisms. One mechanism suggests the adsorption and dissociation of CO to an adsorbed C_α and the following stepwise hydrogenation to CH_4. Another mechanism proposes an oxygenated COH-complex without the dissociation step. The hydrogenation of CO_2 is believed to proceed via CO_2 adsorption, dissociation to CO, and subsequent hydrogenation of the adsorbed CO. The presence of CO can cause a reduced CO_2 reaction rate because CO is preferentially adsorbed on the catalyst surface [67]. Overviews of available literature in this context can be found in Rönsch et al. [17] and Schildhauer et al. [7].

The Langmuir-Hinshelwood mechanism is widely used as a mathematical description of the reaction rate. When formulating the rate equation, the question of the rate-determining step arises. In recent literature, such rate equations for fluidized bed methanation were formulated by Kopyscinski et al. [68], Witte et al. [39], and Rönsch et al. [69]. The models combine fluid dynamic aspects of fluidized beds, mass transfer between bubble and dense phase (two-phase theory), thermodynamic equilibrium, and kinetics. Grossgasteiger utilized these models and performed a parameter fitting to adjust the kinetic parameters to the catalyst prepared in this work. Furthermore, he designed an algorithm that calculates the optimal reaction temperature based on the syngas composition and a controller, which controls the reaction temperature based

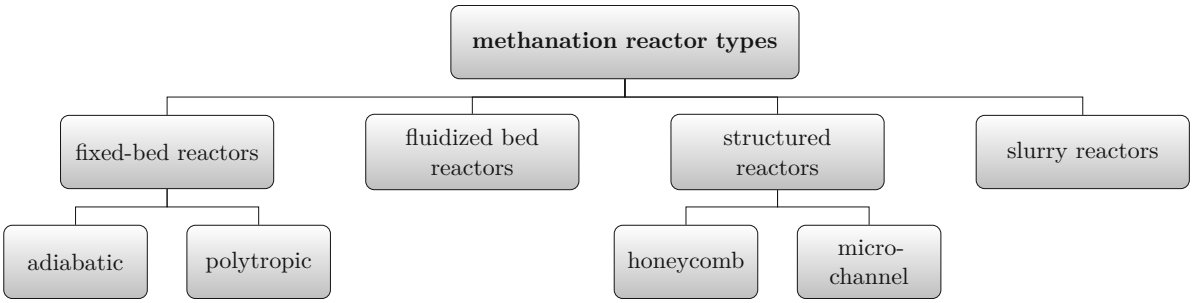

Fig. 2.2: Types of reactors used for catalytic methanation, adapted with permission from [17]

on the algorithm's results. This topic is, however, not within the scope of this work, and a reference to the supervised master thesis is made here [70].

2.1.4 Methanation Reactor Types

A wide range of reactor types have been developed for catalytic methanation processes—some more advanced than others regarding their technology readiness level (*TRL*). Fig. 2.2 gives an overview of applied reactor types. The only commercially available reactor types thereof are adiabatic fixed-bed reactors [7]. Operating conditions ranging from 250 to 700 °C and pressures from 1 to 87 bar_a have been applied due to the wealth of reactor types and specific conditions they are used in [42]. In the following, the reactor types are briefly discussed.

Fixed-bed reactors

Adiabatic fixed-bed reactors are commercially utilized in coal-to-SNG plants. These concepts consist of a reactor cascade with 2–7 fixed-bed reactors, including intermediate gas cooling and partial gas recycling. These measures are necessary to control the temperature peaks caused by the highly exothermic methanation reactions since no heat is directly extracted from the reactors and the heat transfer in fixed-bed reactors is limited anyway. Additionally, fixed-bed reactors are prone to catalyst sintering due to the high temperatures and catalyst deactivation by carbon depositions. Because of the multiple reactors necessary, the overall concept is relatively complex. Nevertheless, the Lurgi, the HICOM, and the TREMP processes have been developed, giving a few examples. In 1984, 14 of the Lurgi reactors were installed in the Great Plains Synfuels Plant in North Dakota, producing up to 4.8 mil. m^3 of SNG per day [71]. For a long time, this was the only operational SNG production plant worldwide. Only more recently, the HICOM and TREMP processes were installed in coal-to-SNG plants in China. An adapted version of the TREMP process from Haldor Topsøe is also installed in the GoBiGas biomass-to-SNG plant in Gothenburg, Sweden (see section 2.3.1). Fig. 2.3 depicts a schematic diagram of the TREMP process. It consists of 3 (sometimes 4) adiabatic fixed-bed reactors and a partial recycle of

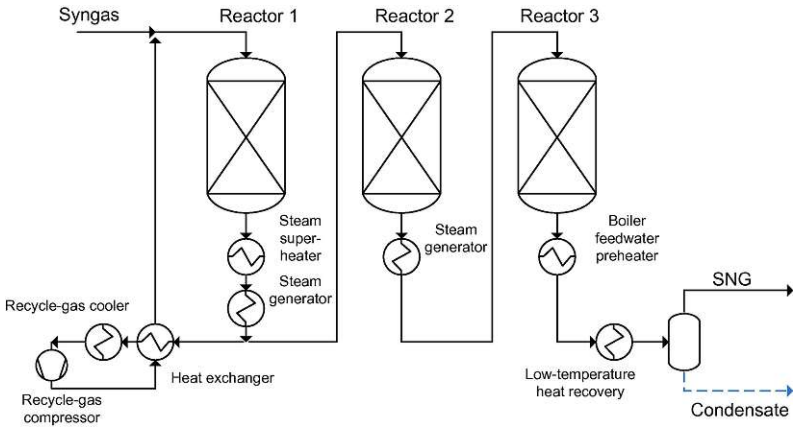

Fig. 2.3: Scheme of the TREMP process, reproduced with permission from [17]

raw-SNG in the first reactor stage. As it is a high-temperature methanation process (< 700 °C), high-temperature steam can be recovered at the intermediate gas cooling steps. [8, 15, 17, 72]

Linde has developed, but not commercially applied, a cooled fixed-bed reactor using contorted cooling tube bundles in the reactor. More recently, a molten-salt cooled tube bundle reactor was installed in the 6 MW PtG plant in Werlte, Germany [72]. According to Rönsch et al. [17], these reactor types can be categorized as polytropic reactors since a temperature increase is still expected due to the heat transfer limitations.

Structured reactors

Research is put into dispersing the catalyst particles onto thermally highly conducting structures to improve the heat transfer and reduce pressure drops in comparison to traditional fixed beds, thus reducing temperature hotspots. Typically, metal monoliths are coated with catalyst particles, often referred to as honeycomb structures. The Engler-Bunte-Institute applied this concept to the load-flexible methanation of gasifier product gas with additional H_2 from electrolysis [72] and Biegger et al. [73] to a PtG concept. Similarly, micro-channel reactors have been investigated, which allow a conversion at very high space velocities [74, 75]. However, these concepts are still on a research level (TRL 4–5) and envisaged for smaller-scale operations. Such reactors can be categorized as polytropic. They advantageously combine high reaction rates due to the temperature increase at the inlet with high conversions due to the lower temperature at the exit. A drawback is the difficult and expensive catalyst preparation and renewal, once spent.

Fluidized bed reactors

Fluidized beds are known for their high heat and mass transfer capabilities due to the movement of the particles [76]. Hence, fluidized beds have been under investigation for catalytic methanation processes just as long as fixed beds. One of the most prominent examples is the COMFLUX

project, which successfully demonstrated the production of 20 MW_{SNG} from coal in the 1980s. The construction and operation of the large-scale plant was accompanied by a pilot unit (0.4 m diameter, 200 kg catalyst) and a bench-scale unit at the University of Karlsruhe. In this unit, they investigated deactivation mechanisms, kinetics, attrition resistance, and influence of sulfur compound concentrations [8]. Fig. 2.4 shows a scheme of the bench-scale unit (left) and a picture of the pilot plant (right).

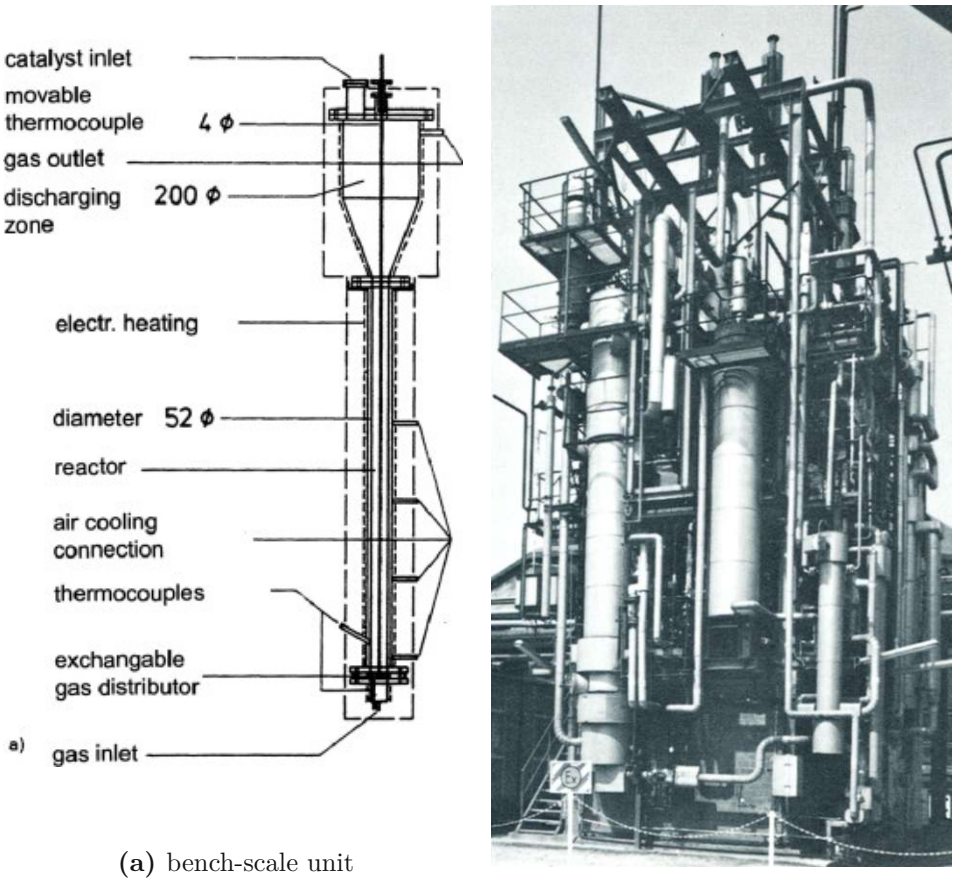

(a) bench-scale unit

(b) pilot plant

Fig. 2.4: Bench-scale fluidized bed methanation unit at the University of Karlsruhe (a), and COMFLUX pilot plant (b), reproduced with permission from [8]

The Paul Scherrer Institute recently picked up on these developments and investigated the fluidized methanation process more closely. They performed spatially resolved concentration and temperature measurements along the height of the catalytic bed. The results show that the particle movement leads to an in-situ regeneration of the catalyst particles and, therefore, reduces the risk for carbon depositions even in the presence of C_2H_4 [44, 47]. The main advantages of fluidized beds are the intrinsic catalyst regeneration and the nearly isothermal operating conditions, eliminating temperature hotspots. The limiting factor of fluidized beds, on the other hand, is the mass transfer between the bubble phase and the dense phase in the upper part of the bed, reducing conversion [11]. Furthermore, catalyst particles have to cope with high mechanical

Tab. 2.1: Advantages and disadvantages of fluidized beds in comparison to fixed-bed methanation reactors [7, 8, 17, 57, 72]

fixed-bed reactor	fluidized bed reactor
advantages – commercially available concept – commercially available catalyst – heat recovery at higher temperatures – higher degrees of freedom through WGS unit	**advantages** – conversion in one step possible – no WGS or pre-methanation unit necessary – catalyst fouling better manageable – olefine hydrogenation possible in reactor – formed C_2H_6 in SNG increases LHV – lower amounts of catalyst needed – better heat and mass transfer
disadvantages – difficult heat management and temperature control – more complex process through reactor cascade – gas recycling often needed – higher risk of catalyst fouling especially at higher temperatures – higher efforts on gas cleaning and gas conditioning	**disadvantages** – no manufacturer established – fluidized bed methanation catalysts not established – potential catalyst attrition and elutriation – reactor design more complex

stress, necessitating the development of attrition-resistant catalysts. This, and the more complex control of the reactor itself compared to fixed beds, might have prevented the commercialization since only research and demonstration projects are available so far (see section 2.3). Nevertheless, the Swiss company AlphaSYNT currently works on commercializing the technology [77]. Rönsch et al. [17] assign a TRL of 7 to fluidized bed methanation. Table 2.1 aims to summarize the advantages and disadvantages of fluidized beds in comparison to fixed-bed methanation reactors.

Slurry reactors

A few investigations also looked at slurry (or three-phase) reactors for catalytic methanation processes. Slurry reactors show the advantage of isothermal operating conditions even under load fluctuations due to the additional heat capacity of the liquid phase. Drawbacks are the additional mass transfer barrier to and from the liquid phase and possible decomposition and evaporation of the liquid phase [78, 79]. This technology also started out in the 1970s for converting syngas from coal. A quite large-scale pilot plant was erected and operated at that time [8]. Nevertheless, a TRL of 4–5 can be assumed for these types of reactors [17].

2.1.5 Natural Gas Grid Specifications

Natural gas is typically transported in pipelines. The same is envisaged for SNG and biogas if it is not utilized in the direct vicinity of the production site. Specific criteria have to be fulfilled for

Tab. 2.2: Excerpt from the Austrian gas grid specifications according to ÖVGW G B210 at 25 °C/0 °C

parameter	unit	value	parameter	unit	value
Wobbe-Index	MJ/m^3	$47.7 - 56.92$	CO	mol-%	0.1
HHV[a]	MJ/m^3	$33.73 - 47.63$	NH_3	mg/m^3	≤ 10
rel. density	-	$0.5 - 0.7$	total sulfur	mg/m^3	≤ 21
H_2	mol-%	≤ 10	H_2S+COS	mg/m^3	≤ 5
CO_2	mol-%	≤ 2.5	O_2	mol-%	0.001
N_2	mol-%	≤ 5	H_2O dew point[b]	°C	−8

[a] higher heating value (HHV)
[b] at 70 bar_a, or the maximum allowed pressure of the grid

pipeline transportation, ensuring high-quality gas and meeting safety standards. Unfortunately, there is no unified standard in the EU, and each country defines its own specifications [80]. In Austria, the specifications are regulated by "Österreichische Vereinigung für das Gas- und Wasserfach (ÖVGW)" directive G B210. Table 2.2 shows an excerpt of the specifications. While the maximum allowed H_2 content has been increased in the last years, the demanded CO content of 0.1 mol-% poses a challenge for catalytic methanation processes. The limitations regarding impurities show that not only the deactivation of the catalyst gives reason for rigorous gas cleaning but also the grid specifications.

2.2 Product Gas Generation and Gas Cleaning

Conventional syngas for methanation is produced through the gasification of solid feedstock (biomass, coal) and consecutive gas cleaning. Coal gasification has been carried out for decades to produce SNG—for example, in the Great Plains synfuel plant, as already introduced in section 2.1. Over the last two decades, biomass gasification gained importance due to the rising awareness of climate change. For biomass, alternative gasification technologies have been developed in comparison to coal because of the different physical and chemical properties and the different feedstock potentials and utilization strategies.

A stoichiometric syngas for methanation would have an H_2/CO ratio of 3 and an H_2/CO_2 ratio of 4. Unfortunately, woody biomass has an average elemental composition of $CH_{1.44}O_{0.66}$ [20], requiring an active conversion to reach more suitable gas compositions. The parameters that can be used to adjust the gas composition and quality are the operating mode, the gasification agent, and the reactor type, as Fig. 2.5 shows. Only the most widely applied combinations are shown. Other combinations of gasification agents and reactor types are generally applied as well. Furthermore, the type of woody biomass itself plays a crucial role. For methanation, low nitrogen and high H_2 contents are obligatory, reducing the possibilities to O_2, mixed O_2/H_2O, and pure H_2O gasification in entrained flow or fluidized bed gasifiers. The downside of utilizing O_2 as a

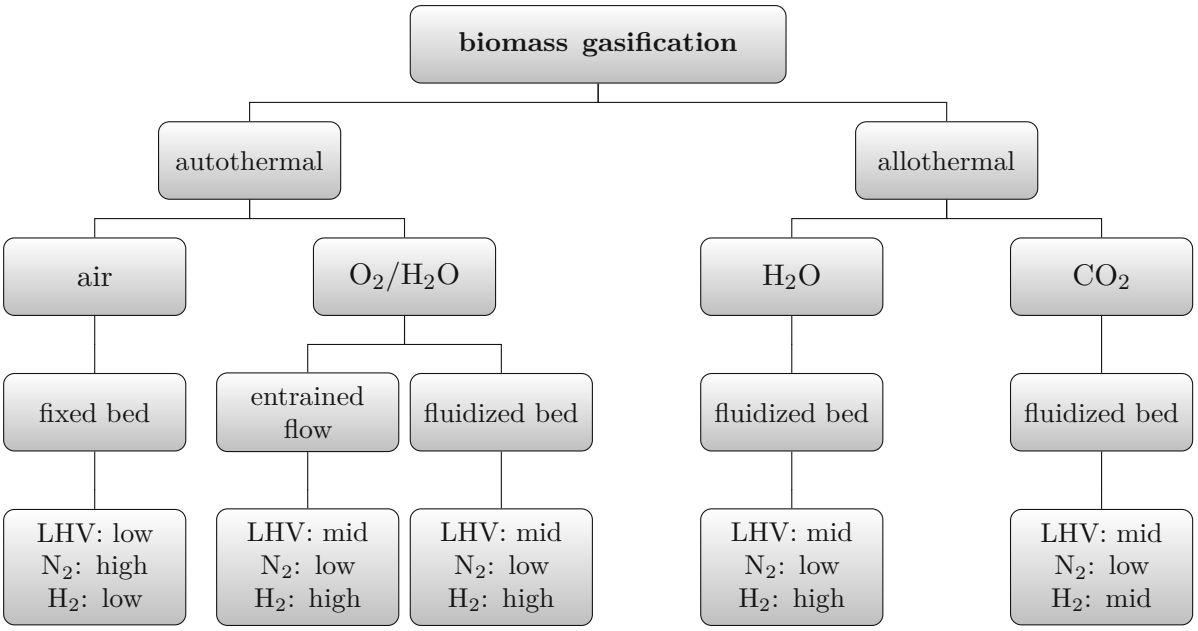

Fig. 2.5: Classification of gasification technologies, adapted from [20]

gasification agent is the requirement of an air separation unit (or an electrolyzer). Additionally, entrained flow gasifiers are quite complex. Both issues make these concepts feasible at large scales (e.g. for coal gasification). Thus, allothermal gasification with H_2O as a gasification agent has proven to be advantageous for syngas production. The following section will introduce the DFB gasification technology as an example of allothermal, fluidized bed gasification. [20]

2.2.1 Dual Fluidized Bed Gasification

DFB steam gasification has been successfully demonstrated in several industrial-scale plants in Austria, Germany, Sweden, Thailand, and Japan. Over the last two decades heat and electricity as well as SNG have been produced from woody biomass via this technology [81]. The basic principle of DFB gasification is depicted in Fig. 2.6 and follows the description in **Paper IV** [38].

In the gasification reactor (*GR*), biogenic feedstock is converted to a product gas containing mainly H_2, CO, CO_2, and CH_4 with steam as a gasification agent. Due to the allothermal operation of the GR, a nearly nitrogen-free product gas is obtained. However, impurities, like tars and nitrogen- and sulfur-containing species, might need to be removed in a downstream gas cleaning section, depending on the quality of the feedstock. The GR is coupled with a combustion reactor (*CR*) through a solids circulation loop. In the CR, ungasified char and additional fuel (e.g. recycled product gas) is combusted with air to heat up the bed material. Since the CR is operated as a fast fluidized bed, the hot bed material is transported back to the GR, where it sustains the endothermic gasification process. Numerous investigations have been conducted looking at different aspects of the process. Wilk et al. [82], Benedikt et al. [83, 84], Mauerhofer et al. [85],

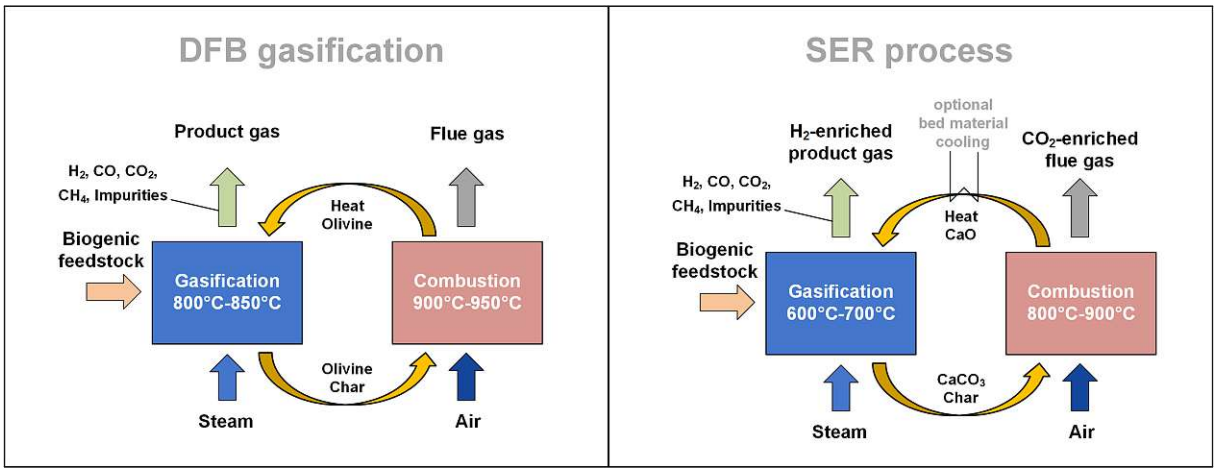

Fig. 2.6: Basic principle of DFB gasification (left) and DFB gasification with in situ CO_2 removal (SER process) (right), reproduced from [38]

Schweitzer [86], and Schmid et al. [87, 88] looked at different feedstocks, ranging from high-quality softwood pellets to sewage sludge, showing the broad applicability of DFB gasification, even for low-value waste material and residues. Others looked at the application of alternative gasification agents, such as CO_2 [89, 90]. Furthermore, the type of bed material plays a crucial role, defining its catalytic activity and, therefore, influencing the product gas composition and quality [91–93]. The influence on the tar content is especially well documented [43, 94, 95], as it influences the operational stability of the plant. Over the last couple of years, the advanced DFB gasification technology has been developed and investigated at TU Wien. It increases the fuel flexibility, allows the production of a higher-quality gas, and the application of soft bed materials like limestone [63, 96]. A closer description of this reactor concept follows in Chapter 4, as it is the technology used for the investigations in this thesis.

If limestone is used as bed material, the in-situ removal of CO_2 from the GR can be facilitated. This advanced operation mode is also referred to as sorption enhanced reforming (*SER*) (Fig. 2.6 (right)). At comparable low temperatures of 600 to 750 °C in the GR, $CaCO_3$ is formed out of CaO and gaseous CO_2. Removing gaseous CO_2 from the product gas stimulates the WGS reaction and increases the H_2 content (up to 70 vol.-$\%_{db}$). The captured CO_2 is transported to the CR as $CaCO_3$ together with the bed material and char. At elevated temperatures in the CR, the $CaCO_3$ is calcined. Thus, gaseous CO_2 is released again in the CR and CaO is formed out of $CaCO_3$. The gasification temperature [97, 98] and the bed material cycle rate [99] are the two main parameters that allow the targeted adjustment of the product gas composition. Therefore, the product gas from the SER process might be more suitable for methanation than the conventional product gas. Fig. 2.7 depicts the evolution of the product gas composition over the gasification temperature of the SER process, according to Fuchs et al. [97]. The data was

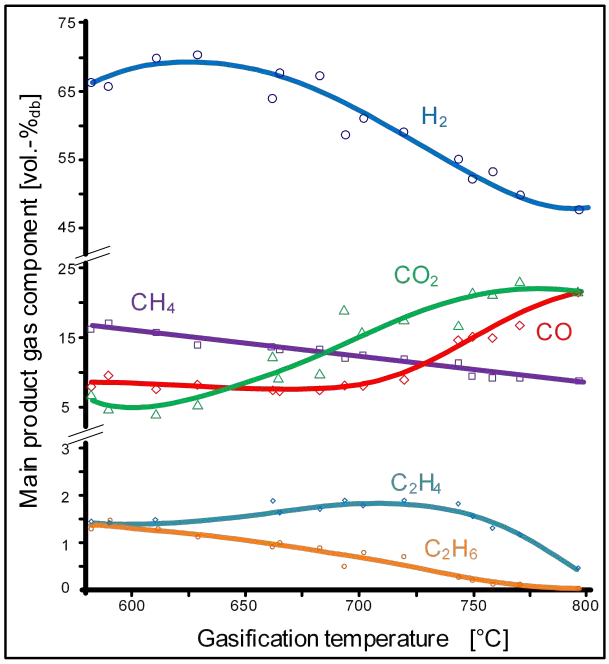

Fig. 2.7: Product gas composition over gasification temperature for the SER process according to Fuchs et al., reproduced from [97]

recorded at the 100 kW_{th} advanced DFB pilot plant at TU Wien and will be used throughout this work to assess fluidized bed methanation in combination with the SER process.

2.2.2 Gas Cleaning

Product gas cleaning is probably the most critical area when it comes to high plant availability and a long catalyst lifetime. At the same time, it is the most difficult segment to assess fundamentally because of the many potentially involved substances [100, 101]. In this context, gas cleaning aims to remove impurities from the gas stream which are harmful to downstream syntheses, cause technical and operational problems in gas utilization appliances, and would result in environmental and health issues if emitted to the atmosphere. The amount and nature of substances that need to be removed depends on the biomass feedstock and the primary measures already carried out during gasification. Nevertheless, the main concerning species remain the same.

- Particulate matter,
- alkali metals,
- tar,
- sulfur-containing substances (H_2S, COS, C_4H_4S, ...),
- nitrogen-containing substances (NH_3, HCN, ...), and

- halogen-containing substances (HCl, ...).

Another main distinction is made whether gas cleaning is performed hot or cold. The latter is commonly applied, reliable, and allows high separation efficiencies. Hot gas cleaning, on the other hand, has the benefit of being more energy efficient and results in less effluent streams that need to be taken care of. However, the TRL is lower and typically applied catalysts tend to deactivate rapidly [100]. In this work, primarily cold gas cleaning approaches are utilized and further discussed.

From a catalyst perspective, sulfur-containing species are the most critical, leading to a fast deactivation, especially when nickel is used. Conventionally, absorption-based processes, like Selexol, Rectisol, or amine-based solutions, are utilized. These processes allow a simultaneous removal of H_2S and CO_2 [102]. Another possibility is adsorption on AC, the preferred solution in smaller-scale plants. Additionally, metal oxides, like ZnO and CuO, are applied to chemically bond H_2S for a deep sulfur removal down to *ppb* levels [103]. Since product gas also contains organic sulfur species, which are not necessarily removed by the mentioned technologies, a catalytic conversion to H_2S can be targeted in a hydro-desulfurization unit [104].

Tars consist of a complex mixture of organic molecules resulting from incomplete gasification. They lead to fouling on equipment and catalyst deactivation and must be removed beforehand. Wet scrubbing is commonly applied, where tars condense or absorb in the washing liquid. Initially, water has been used for this task, which lacks the ability to dissolve non-polar tar components. Thus, oil-based scrubbers have been developed, which simultaneously condense and adsorb tars [7, 100]. In this work, rapeseed methyl ester (*RME*) is used as a solvent, which has previously been used for tar removal in DFB plants [105]. However, lighter (poly)aromatic compounds, such as benzene, toluene, xylene, or naphthalene, do not fully separate in the scrubber. Thus, consecutive adsorption on AC can be carried out. In the GoBiGas plant (see section 2.3.1), AC was used in a temperature swing adsorption (*TSA*) unit for this purpose [13].

NH_3 and HCN are highly water-soluble [100]. Therefore, water scrubbing is an efficient removal technology. Since the product gas of a DFB gasifier contains large amounts of water, the solvent is already inherently available. Thus, a significant NH_3 removal capacity has been reported in oil scrubbers since tars and water condense there [106]. Acidic scrubbers can be applied if the required purity level is not reached [107].

Much more could be said on the complex topic of gas cleaning, including other impurity families such as particulate matter, halogenated compounds, or alkali metals. For the purpose of this work, only the excerpt mentioned above is provided, and further details are documented in literature [100, 108].

2.3 Process Concepts

Methanation concepts to produce SNG from woody biomass have been proposed in literature and even demonstration projects have been realized. In this section, existing demonstration concepts (section 2.3.1), recent developments on a research level (section 2.3.2), and the concepts conceived in this thesis (section 2.3.3) are presented.

2.3.1 Demonstration Plants

The most prominent examples of SNG production from woody biomass are the 1 MW_{SNG} process development unit (*PDU*) connected to the DFB gasification plant in Güssing (Austria) and the 20 MW_{SNG} GoBiGas plant in Gothenburg (Sweden). Fig. 2.8 shows pictures of the two demonstration plants.

The two realized projects differ in terms of the applied concepts, as Fig. 2.9 and Fig. 2.10 show. While both product gas generation sections are based on the DFB technology, a fluidized bed methanation reactor is installed in the PDU in Güssing, and a down-scaled TREMP process from Haldor Topsøe is installed at the GoBiGas plant. The latter uses 4 adiabatic fixed-bed reactors, a WGS unit, a gas conditioning reactor, and a pre-methanation unit, while only a single fluidized bed is used in the PDU in Güssing. This obvious advantage is opposed by the fact that the TREMP process is industrially proven and commercially available. As a result, the gas cleaning and upgrading sections also differ substantially. The GoBiGas plant uses an

(a) GoBiGas plant Gothenburg **(b)** PDU Güssing

Fig. 2.8: Pictures of the demonstration plants, reproduced from [109] and [110]

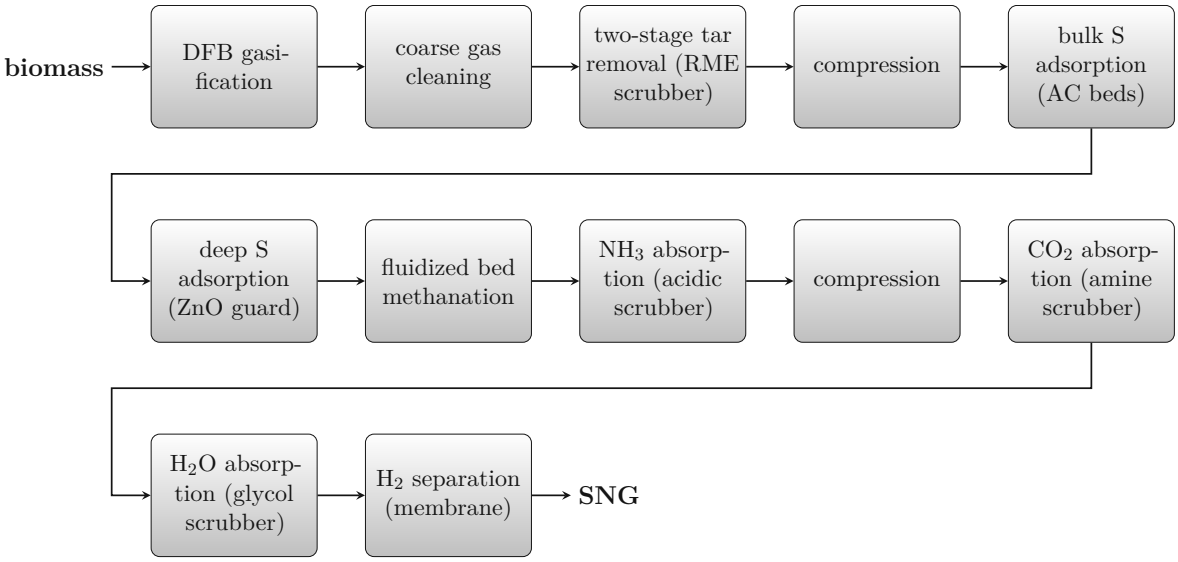

Fig. 2.9: Basic flow chart of the 1 MW_{SNG} PDU in Güssing (Austria) [110]

olefine hydrogenator and a COS hydrolyzer to convert C_2-species and sulfur compounds upstream to an H_2S scrubber. In Güssing, C_2-species are converted in the methanation reactor and AC beds remove H_2S. In both cases, light (poly)aromatic compounds such as benzene, toluene, and naphthalene are removed by AC. The effects of the different methanation concepts show up when it comes to gas upgrading and conditioning. In the GoBiGas plant, only drying is required downstream of the methanation section. CO_2 separation is performed upstream the methanation section and downstream the WGS unit. This is enabled by the WGS unit shifting the gas before methanation and therefore producing CO_2. In a single fluidized bed methanation concept, CO_2 separation needs to be placed downstream since the gas shifting is typically carried out in the methanation reactor [42]. Due to the lower operating pressure and the higher final methanation temperature in the fluidized bed methanation reactor, an additional H_2 separation is required in the PDU. Despite the different concepts, both plants demonstrated the production of grid-feedable SNG, the GoBiGas plant being already a scaling step more advanced. However, the plans for a 100–200 MW_{SNG} industrial-scale plant based on GoBiGas were discontinued. Good documentation on the GoBiGas plant is available in literature [13, 109, 111]. Unfortunately, the Güssing PDU lacks open information, apart from the thesis of Rehling [110].

More recently, another fluidized bed methanation project at a scale of 400 kW_{SNG} was realized. In France, the GAYA platform went into operation and produced SNG via DFB gasification of woody biomass and solid recovered fuels [112]. Even PtG, hydrolyzing CO_2 with H_2, was experimentally investigated [113]. Announcements were made by ENGIE, which indicated that this process will be scaled-up. Starting in 2026, approximately 20 MW_{SNG} should be produced from non-recyclable waste within the SALAMANDRE project [114, 115].

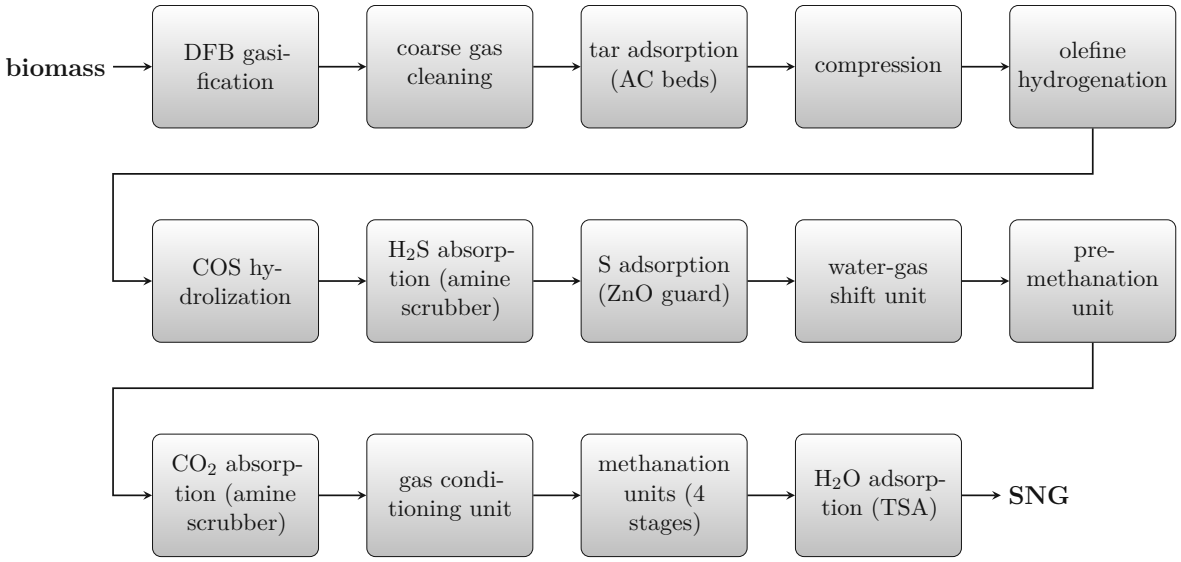

Fig. 2.10: Basic flow chart of the 20 MW_{SNG} GoBiGas plant in Gothenburg (Sweden) [13, 109]

2.3.2 Research Concepts

Some more advanced and novel research concepts for catalytic methanation processes of syngas have been published in literature. This section aims to present some of the ideas which have been investigated. For example, Gassner and Maréchal [40] proposed on a theoretical basis the addition of renewable H_2 to the syngas to improve the carbon utilization of the biomass. Some other works followed up on this idea of a hybrid concept, as summarized in **Paper IV** [38]: Alamia et al. [116] simulated the integration of H_2 in an optimized GoBiGas plant and calculated cold gas efficiencies between 70% and 73% for SNG production. Some experimental investigations were carried out by Salbrechter and Schubert [117]. They performed methanation experiments in fixed-bed reactors with varying H_2 contents in the premixed syngas. Multiple alternative concepts for the integration of H_2 in the SNG production process have been proposed. Giglio et al. [118] conceptualized a catalytic methanation process in isothermal reactors in combination with solid oxide electrolysis and O_2/steam-blown gasification and calculated cold gas efficiencies as high as 71.7%. From an experimental point of view, Leimert et al. [119] combined the heatpipe reformer gasification technology with a polytropic fixed-bed methanation reactor and demonstrated the production of raw-SNG with additional H_2. Another demonstration of a hybrid process concept was shown by Witte et al. [120]. They directly upgraded biogas in a fluidized bed methanation reactor with external H_2 over more than 1000 h with an average CH_4 yield of 96%.

Another novel concept is the combination of the SER process with methanation. Brellochs [121] modeled such a combination and defined a small gasification temperature window between 697.5 °C and 702.5 °C, where the product gas composition in the gasifier can be adjusted close enough to the stoichiometric requirements of methanation so that no CO_2 separation unit is

required. Martínez et al. [122] modeled a cold gas efficiency of 62% for a combination of the SER process with the TREMP methanation process. However, neither the hybrid concept, combining DFB gasification, H_2 addition, and catalytic methanation, nor the SER process in combination with catalytic methanation, have been experimentally investigated and presented in literature. Therefore, this work deals with these aspects, as section 2.3.3 describes more closely.

2.3.3 Applied Process Concepts

Fig. 2.11 depicts basic flowcharts of investigated process chains in this work. The investigations focus on three novel configurations, as introduced in section 2.3.2:

- advanced DFB gasification and direct methanation of the DFB product gas (DFB-Std)
- advanced DFB gasification with external H_2 addition to the product gas and methanation of the hydrogen-enriched product gas (DFB+H_2)
- SER process with direct methanation of the hydrogen-enriched product gas without external H_2 addition (SER)

All three concepts are investigated with the same advanced DFB pilot-plant and the gas cleaning and methanation units set-up in this work (see Chapter 4). Gas upgrading is looked at from a simulation perspective in Chapter 6 but is not investigated experimentally.

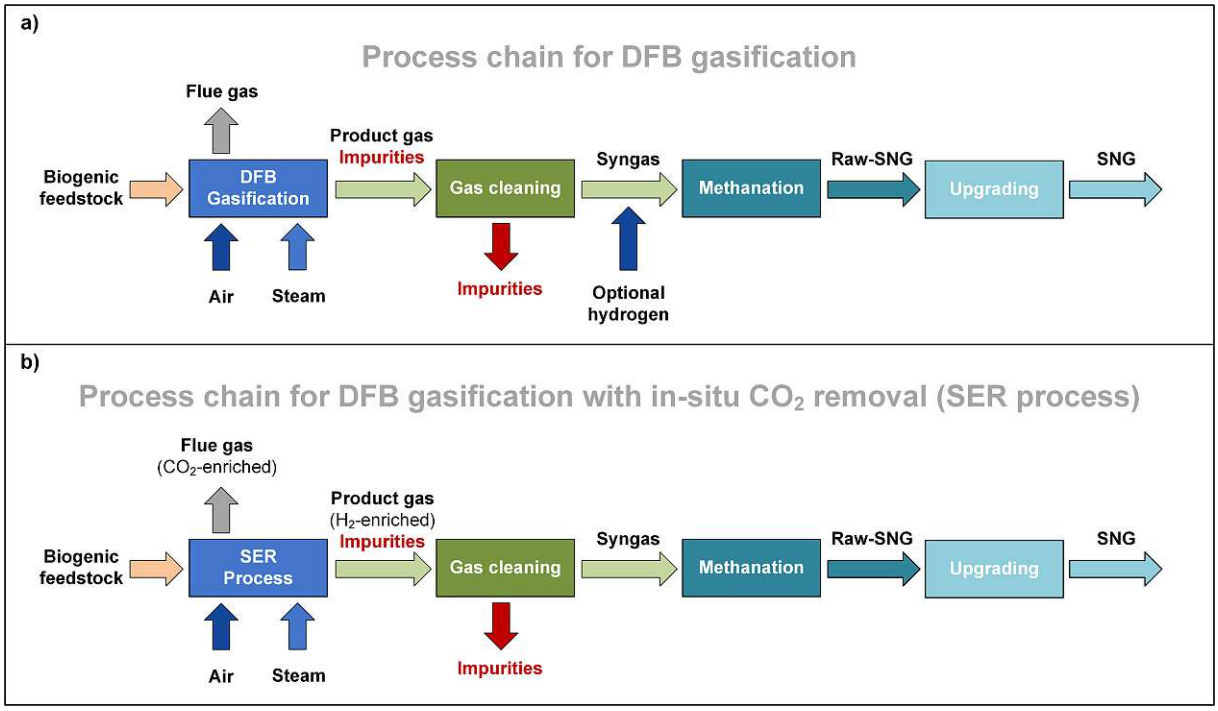

Fig. 2.11: Basic process chains investigated in this work, (a) DFB gasification with optional H_2 addition to the syngas, (b) DFB gasification with in-situ CO_2 removal (SER process), reproduced from [38]

Chapter 3

Methodology

This thesis covers catalytic methanation from a thermodynamic, experimental, and simulative point of view. Therefore, the applied methods are manifold, combining modeling, experiments, analytical methods, and measurement data.

Thermodynamic modeling of the methanation reactions is performed in HSC Chemistry 6 and MATLAB to investigate the influence of syngas composition, temperature, and pressure on the process (see **Paper I**). The developed MATLAB code numerically solves the equilibrium constant expressions for each reaction equation, eventually computing the equilibrium concentrations. Basic fluid dynamic and heat transfer calculations are carried out to design the fluidized bed methanation reactor. Additionally, a model in the process simulation software IPSEpro 8.0 is developed to support the design (see **Paper II**). The developed fluidized bed methanation catalyst is analyzed using temperature-programmed reduction, temperature-programmed oxidation (*TPO*), pulse chemisorption, N_2 physisorption, and laser diffraction methods. Methanation experiments with the designed reactor and catalyst provide numerous temperature, pressure, and gas composition measurement data, which are evaluated and validated with the previously developed model in IPSEpro (see **Paper III**). A similar approach is chosen to evaluate and validate full process chain experiments (see **Paper IV**). Eventually, industrial-scale concepts are set up and simulated in IPSEpro. This data provides the technical basis for the economic and ecological evaluation (see **Paper V**). In the following, the technical parameters and key performance indicators (KPIs) (section 3.1) and the techno-economic KPIs and the CO_2 footprint (section 3.2) are introduced. Further information on the measurement setup can be found in **Paper III** and **Paper IV**. A more detailed description of the methodology used for the techno-economic analysis has been published in related works [81, 123].

3.1 Technical Parameters

The CH_4 yield (Y_{CH_4}) is calculated according to Eq. 3.1, where $\dot{n}$ is the molar flow of species j and N is the number of carbon atoms in the respective gas component in the feed gas ($feed$) and the raw synthetic natural gas ($raw\text{-}SNG$) (out). Eqs. 3.2, 3.3, 3.4 define the CO conversion (X_{CO}), the CO_2 conversion (X_{CO_2}), and the H_2 conversion (X_{H_2}), respectively. [124]

$$Y_{CH_4} = \frac{\dot{n}_{CH_4,out}}{\sum_j N_j \, \dot{n}_{j,feed}} * 100 \tag{3.1}$$

$$X_{CO} = \frac{\dot{n}_{CO,feed} - \dot{n}_{CO,out}}{\dot{n}_{CO,feed}} * 100 \tag{3.2}$$

$$X_{CO_2} = \frac{\dot{n}_{CO_2,feed} - \dot{n}_{CO_2,out}}{\dot{n}_{CO_2,feed}} * 100 \tag{3.3}$$

$$X_{H_2} = \frac{\dot{n}_{H_2,feed} - \dot{n}_{H_2,out}}{\dot{n}_{H_2,feed}} * 100 \tag{3.4}$$

In this work, ethylene (C_2H_4), as the main hydrocarbon species in the dual fluidized bed (DFB) product gas besides CH_4, is investigated in the methanation reactor. Thus, it is helpful to define a selectivity of C_2H_4 towards C_2H_6 ($S_{C_2H_6}$) (Eq. 3.5) as the results will show. Furthermore, CO can react to CO_2 via the water-gas shift (WGS) reaction, especially if a substoichiometric product gas is methanated. Thus, a selectivity of CO towards CO_2 (S_{CO2}) is defined (Eq. 3.6).

$$S_{C_2H_6} = \frac{\dot{n}_{C_2H_6,out} - \dot{n}_{C_2H_6,feed}}{\dot{n}_{C_2H_4,feed} - \dot{n}_{C_2H_4,out}} * 100 \tag{3.5}$$

$$S_{CO_2} = \frac{\dot{n}_{CO_2,out} - \dot{n}_{CO_2,feed}}{\dot{n}_{CO,feed} - \dot{n}_{CO,out}} * 100 \tag{3.6}$$

The stoichiometric number (SN) (Eq. 3.7) assesses the stoichiometry of the feed gas for methanation according to the reaction equations (Eqs. 2.1, 2.2, 2.3) [124].

$$SN = \frac{y_{H_2}}{3\,y_{CO} + 4\,y_{CO_2} + 2\,y_{C_2H_4}} \tag{3.7}$$

For the evaluation of the performance of the whole process chain, the carbon utilization (η_C) is defined, which relates the amount of carbon in the raw-SNG or synthetic natural gas (SNG) to the amount of carbon in the feedstock (Eq. 3.8). Two different definitions of the cold gas efficiency are used, depending on the investigated case. For pilot-scale investigations, the chemical energy of the raw-SNG (P_{rawSNG}) is compared to the chemical energy of the fuel input to the

gasification reactor (GR) ($P_{GR,fuel}$) and the combustion reactor (CR) ($P_{CR,fuel}$) minus heat losses ($\dot{Q}_{loss}$) plus the chemical energy introduced through external H_2 addition (P_{H_2})(Eq. 3.9) [38]. In industrial-scale plants, the additional fuel input to the CR is replaced by an internal product gas recycling, resulting in the definition of Eq. 3.10.

$$\eta_C = \frac{\dot{m}_{C,CH_4,SNG}}{\dot{m}_{C,GR,fuel}} \tag{3.8}$$

$$\eta^*_{CGE,o} = \frac{P_{rawSNG}}{P_{GR,fuel} + P_{CR,fuel} - \dot{Q}_{loss} + P_{H_2}} \tag{3.9}$$

$$\eta_{CGE,o} = \frac{P_{SNG}}{P_{GR,fuel} + P_{H_2}} \tag{3.10}$$

3.2 Techno-Economic Assessment & CO_2 Footprint

The main KPIs used for the techno-economic assessment in Chapter 6 are the levelized costs of products ($LCOP$), calculated according to Eq. 3.11. The calculation follows the net present value (NPV) method and is based on the IPSEpro simulation results for a plant scale of 100 MW fuel input. The LCOP depend on the capital investment costs (I_0), the annual expenditures (E), the annual revenues of secondary products ($R_{sec.prod.}$), and the annual quantity of the produced SNG ($M_{t,SNG}$). The cumulative discount factor (CDF) is used to discount the expenditures and revenues of the secondary products to the present, depending on the interest rate (i) and the plant lifetime (n) (Eq. 3.12). [125, 126]

$$LCOP = \frac{I_0 + (E - R_{sec.prod.})\, CDF}{M_{t,SNG}\, CDF} \tag{3.11}$$

$$CDF = \frac{(1+i)^n - 1}{i\,(1+i)^n} \tag{3.12}$$

The capital investment costs are determined in two ways. The costs of the DFB plant section are estimated from the existing industrial-scale DFB plants in Güssing, Oberwart, and Senden. For the downstream fine gas cleaning and SNG synthesis part, single equipment costs are researched and multiplied with a Lang factor of 4.87 for a solid-fluid processing plant [127]. The researched equipment costs $C_{eq,base}$ are scaled to the required size according to the cost-scaling method and are inflation-adjusted to the years 2019 and 2022 via the chemical engineering plant cost index ($CEPCI$)(Eq. 3.13). $C_{eq,design}$ refers to the equipment cost at the design scale and S_{design} and

S_{base} to the scale itself, with r being the scaling factor. The overall installation factor Z accounts for equipment transportation. [125, 127]

$$C_{eq,design} = C_{eq,base} \left(\frac{S_{design}}{S_{base}}\right)^{r} Z \frac{CEPCI_{ref}}{CEPCI_{base}} \tag{3.13}$$

From an ecological perspective, the water consumption of the processes and the CO_2 footprint are evaluated in Chapter 6. The water consumption simply results from the mass and energy balances in IPSEpro. The CO_2 footprint, on the other hand, aims to calculate the greenhouse gas emissions in CO_2 equivalent (CO_2e). Therein, the direct and indirect emissions of the main utilities are calculated via ecological factors for e.g., the biomass, the operating utilities, or the construction material. For an ecologically viable concept, green electricity is assumed. Most of the data is sourced from the Federal Environmental Agency of Austria [128] and Germany [129], as well as the software tool GEMIS 5.1 [130]. Since two products are produced—SNG and district heat—the emissions are evenly distributed to the two products by their respective energy content. Furthermore, the implementation of SNG in different sectors of the Austrian energy system is evaluated in Chapter 6. Therefore, a CO_2 reduction potential per sector i is defined (CO_2e_{red,sec_i}). It compares the substituted gas consumption of sector i (E_{gas,sec_i}) multiplied by the difference in CO_2 footprint of natural gas (FP_{NG}) and SNG (FP_{SNG}) to the overall annual CO_2e emissions of sector i (CO_2e_{tot,sec_i}) (Eq. 3.14). Thus, a quantitative statement on CO_2 reduction potentials of different sectors can be made.

$$CO_2e_{red,sec_i} = \frac{E_{gas,sec_i}\ (FP_{NG} - FP_{SNG})}{CO_2e_{tot,sec_i}} \tag{3.14}$$

Chapter 4

Pilot-Scale SNG Process Chain

In this work, a full process chain converting woody biomass to raw synthetic natural gas (*raw-SNG*) was designed, set up, and experimentally investigated. The following description of the process chain is partly taken from **Paper IV** [38]. The main units are,

- an existing 100 kW_{th} advanced dual fluidized bed (*DFB*) gasification pilot plant,
- a biodiesel (rapeseed methyl ester (*RME*)) scrubber,
- activated carbon (*AC*) and zinc oxide (ZnO) adsorber beds,
- and a 10 kW_{SNG} fluidized bed methanation reactor.

Fig. 4.1 shows a basic flow sheet of the process chain at TU Wien. The left part of the diagram depicts the fuel-feeding system. Three fuel hoppers are available to feed the feedstock via screws into the lower gasification reactor (*GR*) where the gasification with steam occurs. The generated product gas further reacts in the upper GR and leaves the DFB system after particle separation in a gravity separator and a cyclone. The advanced DFB design, incorporating a counter-current column with constrictions in the upper GR and gravity separators, allows a better conversion due to the increased residence time and turbulence in the counter-current column. This results in a higher quality product gas and the possibility to use softer and catalytically more active bed materials like limestone [84, 131]. Therefore, this pilot plant is used to investigate product gas from the DFB process and the sorption enhanced reforming (*SER*) process. Fig. 4.2 shows a picture and a schematic drawing of the 100 kW_{th} advanced DFB pilot plant at TU Wien. No further details are provided here since the design of the pilot plant and the experimental results are well documented in literature [63, 83, 84, 96, 97, 99, 132].

Downstream the DFB system, a partial flow of the product gas is directed towards the synthetic natural gas (*SNG*) process chain. This partial stream is cleaned in a filter stuffed with glass

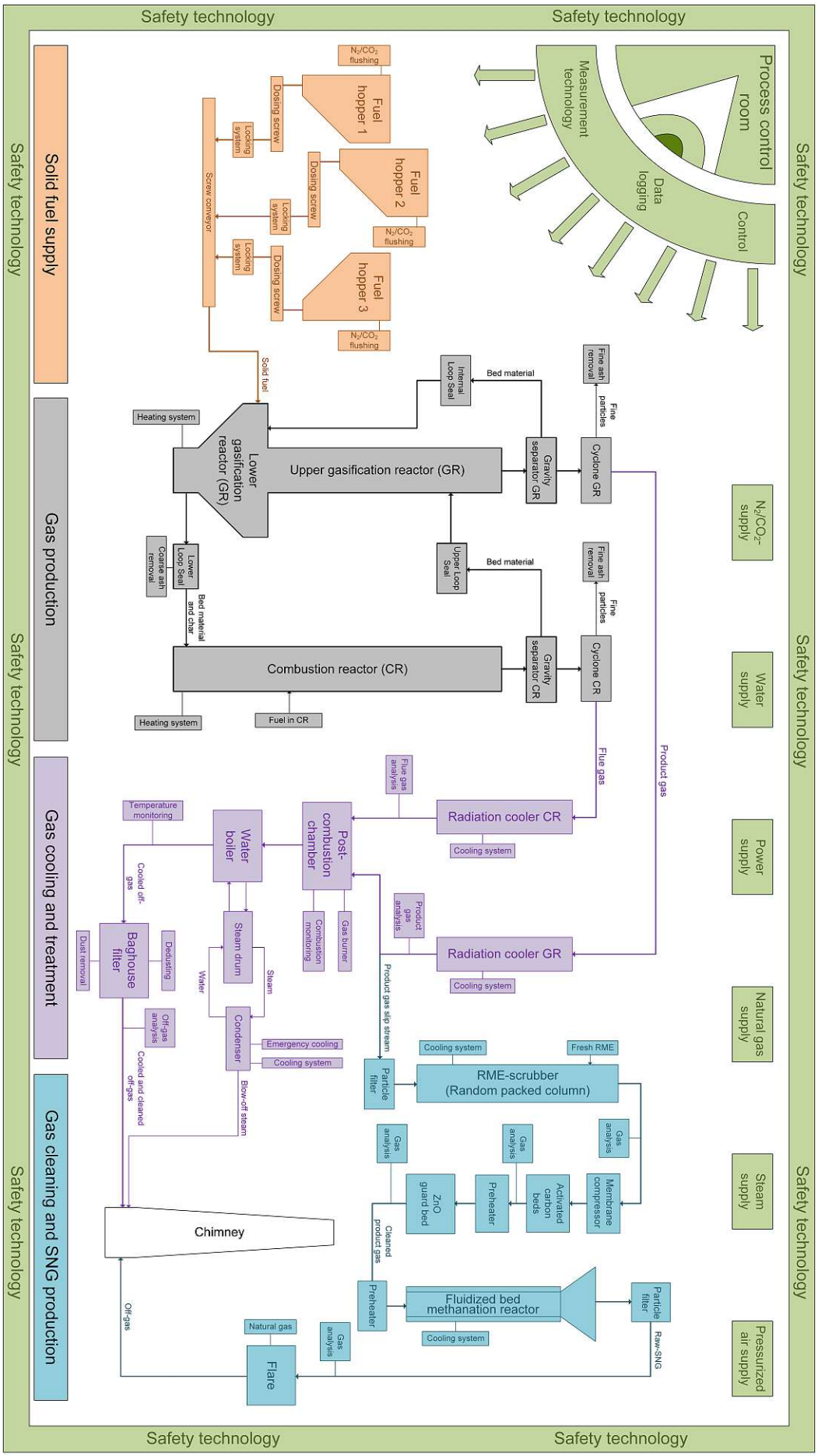

Fig. 4.1: Basic flow sheet of the SNG process chain at TU Wien, reproduced from [38]

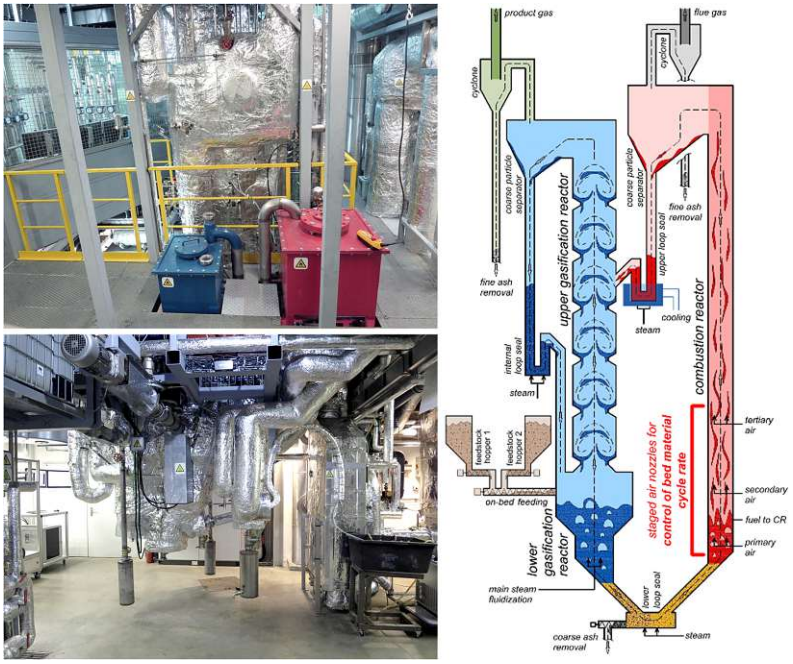

Fig. 4.2: Picture (left) and schematic drawing (right) of the 100 kW advanced DFB pilot plant at TU Wien, reproduced from [38]

wool[1] and enters the RME scrubber. In the RME scrubber (Fig. 4.3 left), tar compounds and water-soluble substances, like NH_3, partially separate from the gas stream. An emulsion phase and a water-rich phase are obtained in the connected phase separator, while the RME phase recirculates to the scrubber column. Further information on this topic is documented in [105]. The following membrane compressor is used as a blower to set the required volume flow for the methanation reactor. Since the process chain is operated at almost atmospheric pressure,

Fig. 4.3: Pictures of the gas cleaning units: RME-scrubber (left) and AC beds (right), reproduced from [38]

[1]At the time of writing the glass wool filter had already been upgraded to a hot gas filter with ceramic filter candles.

no significant pressure increase is desired at this point. To further remove impurities from the product gas stream, the gas passes through two AC beds and a ZnO bed at approximately 300 °C (Fig. 4.3 right). These beds remove (poly)aromatic compounds such as benzene, toluene, naphthalene, and sulfur compounds (e.g. H_2S) from the gas stream. The preheated gas then enters the fluidized bed methanation reactor, where the syngas is converted to raw-SNG. A glass wool filter holds back potentially carried-out catalyst particles and a natural gas operated flare is used to burn the raw-SNG downstream of the gas analysis measurements. Auxiliary systems, like process media supply, measurement technology, a process control system and safety measures accompany the main process chain.

4.1 Design and Construction of the Fluidized Bed Methanation Reactor

The methanation reactor is designed as an internally circulating fluidized bed (*ICFB*), following the work of Hofbauer [134]. Fig. 4.4 shows a schematic drawing of the reactor concept. It consists of two individually fluidized reaction zones—the inner draft tube and the outer annular region. By adjusting the volume flows $\dot{Q}_a$ and $\dot{Q}_d$, and therefore the superficial gas velocities u_a and u_d, a bed material (or catalyst) circulation between the two bubbling fluidized bed regions via the upper gap and the lower gap can be established (gray arrows). This should allow additional circulation, increasing the heat exchange of the bed material with the cooling surfaces.

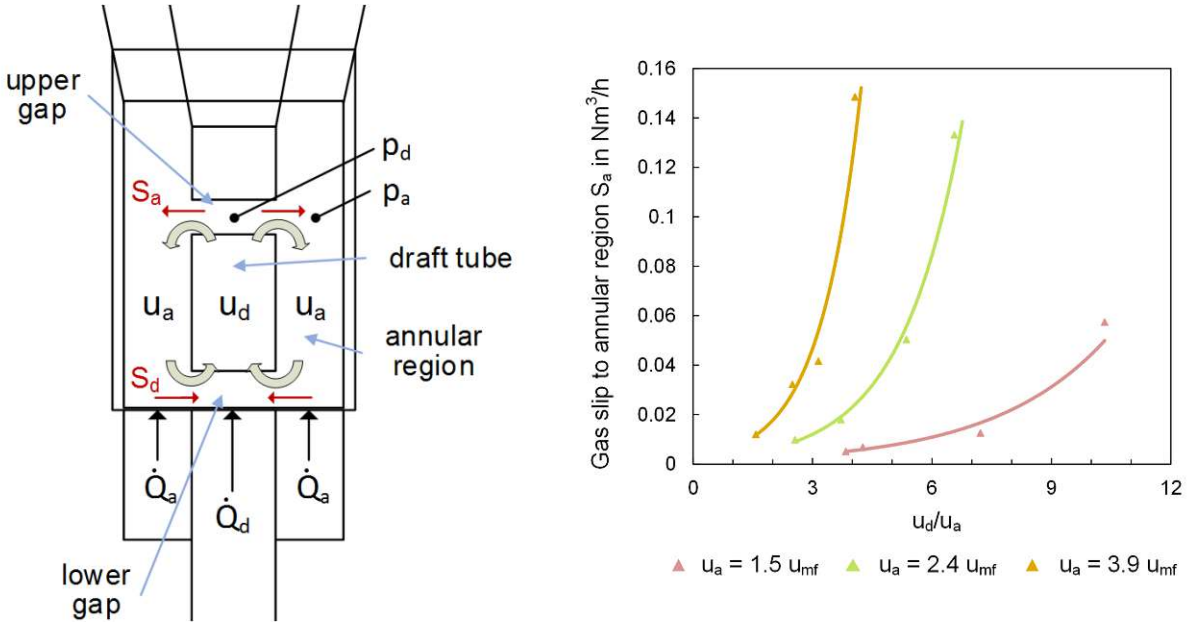

Fig. 4.4: Schematic drawing of the internally circulating fluidized bed reactor concept (left) and results of the gas slip investigations showing the gas slip from the draft tube to the annular region S_a over the fluidization ratio u_d/u_a (right), adapted from [133]

Furthermore, increased load flexibility could be achieved by the individual fluidization of the two regions. For example, only one of the two regions could be active under partial load while the other is in standby mode. Eventually, even a two-stage concept in one reactor is thinkable. For example, after a first conversion in the annular region, the gas could be withdrawn, water could be externally condensed, and redirected to the draft tube for a final conversion (or polishing) step. However, not only the bed material circulates between the two zones, but also a gas slip occurs (denoted by red arrows and S_a and S_d). The fluid dynamic investigations carried out in **Paper II** [133] confirm the gas slip and show a correlation of the gas slip with the fluidization ratio u_d/u_a (cf. Fig. 4.4). Furthermore, the fluidization ratio was found to be directly proportional to the pressure difference in the upper gap $p_d - p_a$. Further details are provided in the respective publication.

Fig. 4.5 shows a 3D CAD drawing of the fluidized bed reactor setup. Two wind boxes allow the individual fluidization of the two reaction zones. A distributor plate with integrated nozzles provides the necessary pressure drop. Pneumatic silencers [2] are used as nozzles in the small-scale reactor to ensure a uniform gas distribution. Both reaction zones are cooled individually to manage the heat released by the exothermic reaction. An air-perfused coil cools the inner reaction zone, while an outer cooling jacket is used to cool the annular reaction zone. Thus, an isothermal operation of the methanation reactor is ensured. At the same time, the fluidization in the two reaction zones is not disturbed by internals. The catalyst, however, can move freely between the zones through the upper gap and the lower gap. [124]

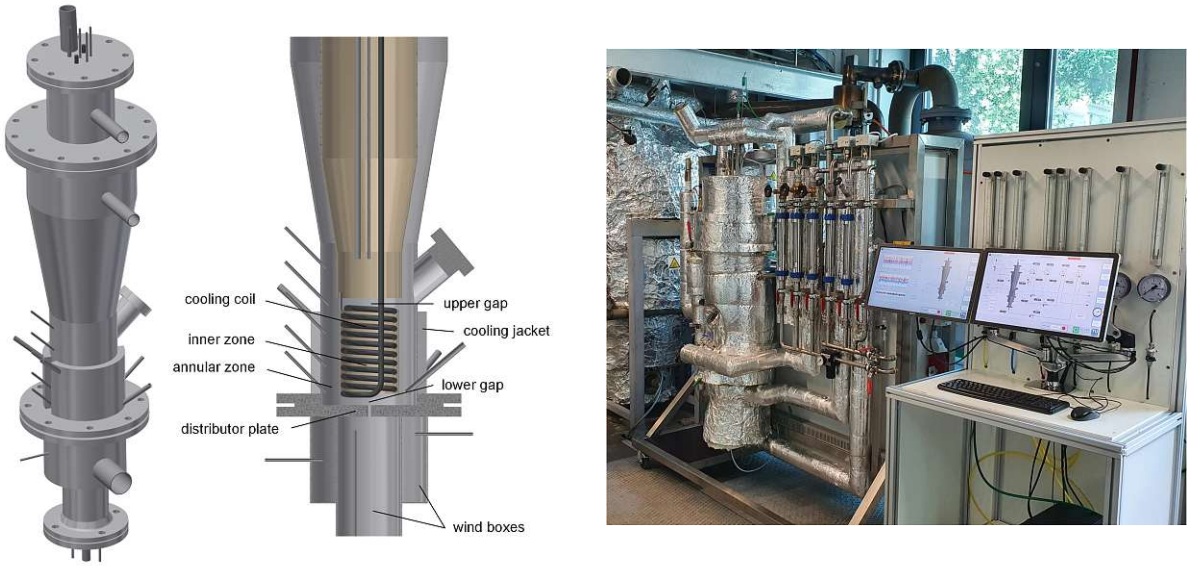

Fig. 4.5: 3D CAD drawing (left) and picture (right) of the fluidized bed reactor, reproduced from [38]

[2] PKS GmbH Type SDD 18
https://pks.fittingline.com/artikel/de/schalldaempfer-g-18-drahtgewebe-messing/SDD18

The design of the methanation reactor considered the following steps, targeting a chemical raw-SNG power of 10 kW.

- Thermodynamic calculation of the raw-SNG gas composition, volume reduction and the heat of reaction, considering a stoichiometric H_2/CO and H_2/CO_2 inlet composition as well as a typical advanced DFB and SER product gas at 300–350 °C and 1 bar_a.
- Fluid dynamic calculation of the minimum fluidization velocity u_{mf} in IPSEpro according to Grace [135], utilizing the property data of the gas in the thermodynamic equilibrium.
- Calculation of a suitable pressure drop in the gas distributor plate, determining the number of required nozzles.
- Estimation of the heat exchanger surface area and cooling air volume flow according to VDI Wärmeatlas [136] to remove the reaction heat from the reactor and ensure an isothermal operation.

The drawings of the fluidized bed methanation reactor, the whole assembly, and the gas cleaning units are attached to Appendix B. Table 4.1 additionally summarizes the main properties and dimensions of the fluidized bed methanation reactor. Further information on the design is documented in **Paper II** [133].

Tab. 4.1: Main design values of the fluidized bed methanation reactor

parameter	unit	value
inner diameter draft tube	cm	8.0
inner diameter annular region	cm	16.4
unfluidized bed height	cm	20
number of nozzles draft tube	-	8
number of nozzles annular region	-	14
nominal chemical energy SNG	kW	10
operating temperature reaction zone	°C	280–400
gas preheating temperature	°C	250
operating pressure	bar	atmospheric

Fig. 4.6 depicts a simplified piping and instrumentation (*P&I*) diagram of the fluidized bed methanation reactor setup. The test rig can either be used with synthetically premixed gases or connected to the process chain for the live gas methanation of DFB syngas. For the former, the gases ($H_2/CO/CO_2/CH_4/C_2H_4$) are withdrawn from gas cylinders and premixed according to the volume flow set by valves and rotameters. After splitting and preheating, the gas stream enters the wind boxes. Here, water vapor can be added if the syngas composition requires so. The reaction zones are equipped with thermocouples type K to measure the axial temperature distribution along the reactor height. The gas outlet is equipped with a particle filter and

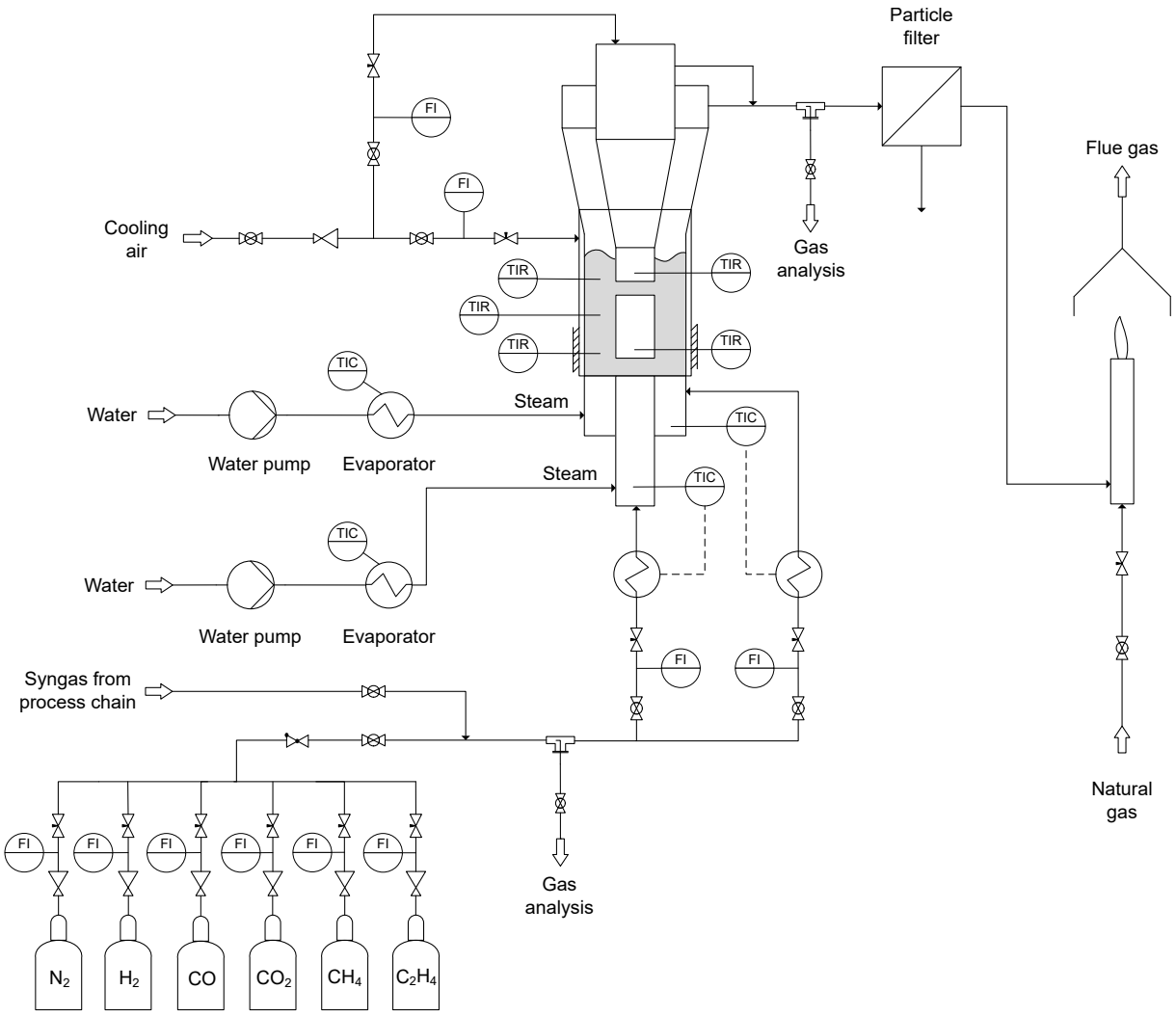

Fig. 4.6: Simplified P&I diagram of the fluidized bed reactor setup, reproduced from [124]

downstream the raw-SNG is burnt in a flare. The syngas and raw-SNG compositions are analyzed online with Emerson NGA-2000 modules.

4.2 Catalyst Preparation and Properties

Disclaimer: A declaration error occurred in ***Paper III*** *[124]. The catalyst support material was wrongly declared as* α*-*Al_2O_3*. Instead, the Puralox SCCa-150/200* Al_2O_3 *support material from SASOL shows a* γ/δ *crystal phase structure. A corrigendum was published (see* ***Paper IV*** *[137]).*

A considerable amount of research on methanation catalysts is available in literature, following the wealth of available preparation methods and influencing parameters, as explained in section 2.1.2. Only limited information is available on the preparation of methanation catalysts for fluidized bed applications. Cui et al. [138] added binders to a spray-granulated Ni-Mg/Al_2O_3 catalyst

Fig. 4.7: Picture of the prepared catalyst

Tab. 4.2: Measured properties of the Al_2O_3 support and the prepared NiO/Al_2O_3 catalyst [124]

parameter	unit	Al_2O_3	NiO/Al_2O_3
Geldart group	-	B	B
Sauter diameter d_{SV}	µm	140	150
bulk density ρ_b	kg/m^3	787	902
BET surface area	m^2/g	183	142
Ni surface area	m^2/g	-	2.8
Ni mean particle size	nm	-	37

and found the highest attrition resistance for acidic silica sol. Others generally showed the superiority of fluidized beds over fixed beds in small lab-scale test rigs. However, no holistic approach combining the investigation of the fluidization behavior with the catalytic activity seems to be available. Thus, a catalyst designed for fluidized bed applications was prepared in this work. Composition-wise, a typical 20 wt.-% NiO and 2 wt.-% MgO catalyst was prepared by impregnation on an Al_2O_3 catalyst support, following Hu et al. [56]. The catalyst support was a Puralox SCCa-150/200 γ-Al_2O_3 from SASOL, particularly designed for fluidized beds and exhibiting a high attrition resistance, a narrow particle size distribution, and high sphericity [139].

Table 4.2 shows the main properties of the prepared catalyst and the unimpregnated Al_2O_3. Both are classified as group B particles close to the transition area to group A, according to Geldart [140]. An increase in the mean Sauter diameter d_{SV} and the bulk density ρ_b is observed through the impregnation, while the surface area is reduced by approx. 22%. Most likely, some pores were blocked by NiO particles. Nevertheless, the surface area is in the range of commonly used NiO/Al_2O_3 catalysts [11, 56]. For the operation of the fluidized bed methanation reactor, 1.6 kg of the prepared catalyst and 1.5 kg of unimpregnated Al_2O_3 is used, which amounts to an unfluidized bed height of 20 cm. A picture of the catalyst in the fluidized bed methanation reactor during operation is shown in Fig. 4.7. It captures a bursting bubble at the bed's surface, dispersing the catalyst horizontally in the reactor. Further results concerning the catalyst's stability and activity are documented in section 5.2. More information on the catalyst preparation and the experimental conditions are documented in the respective publication [124].

Chapter 5

Thermodynamic Investigation & Experimental Results

This chapter summarizes the main findings of this work considering the thermodynamic analyses of methanation (see section 5.1), the experimental investigation with the designed catalyst and the methanation reactor (see section 5.2), and the experimental investigation of the full synthetic natural gas (*SNG*) process chain (see section 5.3)—all in the context of advanced dual fluidized bed (*DFB*) gasification.

5.1 Thermodynamic Analyses

In **Paper I**, thermodynamic analyses of the methanation reactions considering different operation modes and product gas compositions of the advanced DFB gasification technology are carried out. The aim is to reveal and assess the potential of this combination in terms of the achievable SNG gas composition and the carbon utilization η_C by varying operating conditions of the methanation reactor. The parameters are the reaction temperature, pressure, product gas composition, and necessary steam addition to prevent carbon deposition from a thermodynamic point of view. Since a fluidized bed is the focus of the investigations, the water-gas shift (*WGS*) reaction is assumed to occur entirely in the fluidized bed methanation reactor without a prior WGS reactor.

Table 5.1 shows the product gas compositions used for the thermodynamic modeling of the methanation reactions. The product gas compositions result from different feedstocks like bark (BA), lignin (LI), sewage sludge (SS), rapeseed cake (RSC), and softwood (SW). For product gas no. 5, the admixture of CO_2 to steam as a gasification agent is investigated additionally. Furthermore, the bed material selection between olivine and limestone influences the product gas composition. At low temperatures, the utilization of limestone leads to an in-situ CO_2 removal from the product gas (sorption enhanced reforming (*SER*)), represented by product gas nos. 1 and 6. In **Paper I** [42], product gas no. 6 is selected from the possible operating range of the

Tab. 5.1: Investigated product gas compositions and related gasification parameters (BA = bark, LI = lignin, SS = sewage sludge, RSC = rapeseed cake, SW = softwood, L = limestone, O = olivine), adapted from [42]

DFB parameters	unit	product gas number					
		1	2	3	4	5	6
source	–	[141]	[83]	[63]	[87]	[85]	[97]
gasification agent	–	H_2O	H_2O	H_2O	H_2O	CO_2/H_2O[a]	H_2O
feedstock	–	BA	BA	LI	SS	RSC	SW
bed material	–	L	L	O	O/L[b]	O	L
gasification temperature	°C	625	761	789	800	840	683
combustion temperature	°C	820	998	945	945	938	n.a.[c]
product gas composition to methanation (water-free feed)							
H_2	vol.-%	68.3	51.1	42.6	35.6	25.8	67.8
CO	vol.-%	6.5	17.9	21.2	13.7	32.1	7.3
CO_2	vol.-%	8.9	22.4	21.8	36.5	33.7	9.8
CH_4	vol.-%	14.5	8.0	12.0	11.7	7.3	13.3
C_2H_4	vol.-%	1.9	0.6	2.4	2.5	1.1	1.7

[a] CO_2/H_2O=68/32 vol.-%
[b] O/L=80/20 wt.-%
[c] not available

SER process (cf. Fig. 2.7) so that the CH_4 content is maximized in the raw synthetic natural gas (*raw-SNG*) (not shown here).

The results of the raw-SNG composition in equilibrium at 1 bar_a and 300 °C are depicted in Fig. 5.1—the related key performance indicators (KPIs) are shown in Table 5.2. When product gas from conventional DFB gasification is used (no. 2–4), the main raw-SNG components are CH_4 and CO_2. CO_2 can even be the main raw-SNG component if the product gas already contains a large portion of CO_2—as is the case with sewage sludge gasification (product gas no. 4). Because of the WGS reaction, CO_2 is produced instead of consumed (negative CO_2 conversion X_{CO_2}). Utilizing CO_2 as a gasification agent further increases the surplus of CO_2 and only a very limited CH_4 yield Y_{CH_4} is possible because of the low stoichiometry. Nevertheless, residual hydrogen remains in the raw-SNG, owed to the thermodynamic limitations at atmospheric pressure. On the other hand, a high CO conversion X_{CO} and thus low residual CO contents between 600–700 $ppm_{v,db}$ remain, despite the low SN. Though this seems low, the gas grid regulations demand 0.1 mol-% (1000 ppm) CO after CO_2 separation. Considering that the selected methanation temperature is already quite low at 300 °C, this limitation could become problematic if kinetic or mass transfer limitations are considered. To prevent carbon depositions caused by the low H_2/CO ratio, up to 52 vol.-% of steam needs to be added to the methanation reactor from a thermodynamic point of view. However, at low temperatures, like in the fluidized bed methanation reactor, a considerable discrepancy between a thermodynamic description of carbon deposition and reality must be expected [7], possibly allowing a much lower steam content.

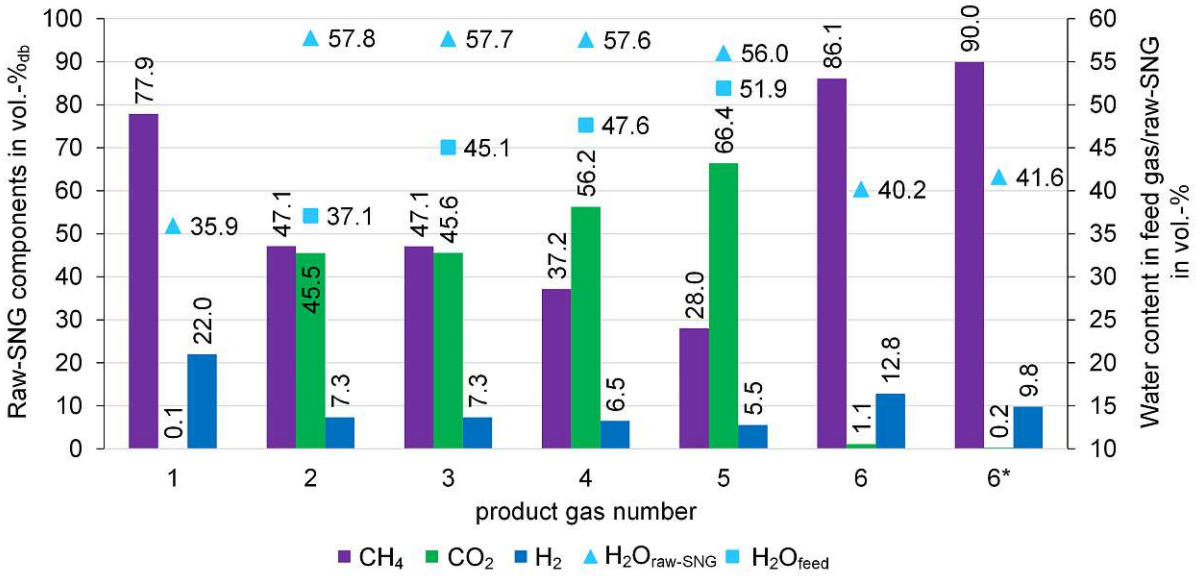

Fig. 5.1: Raw-SNG composition at equilibrium for feed gas nos. 1-6 at 1 bar_a and 300 °C including the amount of steam needed to prevent carbon deposition, 6*: feed gas no. 6 at a methanation pressure of 4 bar_a, adapted from [42]

Looking at product gas from the SER process (nos. 1, 6, and 6*), a much more favorable composition for methanation with an SN around 1 is possible. Theoretically, almost all the CO_2 can be converted in this case, resulting in a Y_{CH_4} above 98.8% (see Table 5.2). Furthermore, only trace amounts of CO remain (7–51 $ppm_{v,db}$) and no steam addition is necessary to prevent carbon deposition. However, SN must be kept rather close to 1 to prevent excessive amounts of H_2 in the raw-SNG. Another measure is a pressurized operation. Increasing the methanation pressure of product gas no. 6 to 4 bar_a (no. 6*) leads to increased Y_{CH_4}, X_{CO_2}, and X_{CO} and a residual H_2 content just below the allowed threshold level of 10 mol-%. Composition-wise, a grid-feedable gas is obtained in this setting. Another indicator to describe the efficiency of the whole process, including gasification, is the carbon conversion η_C. Even though almost all the carbon can be converted in the methanation reactor if an SER product gas is utilized, the overall η_C remains in a comparable range to conventional DFB gasification between 35% and 38%. The nature of the SER process explains this behavior: The in-situ removal of CO_2 in the gasification reactor

Tab. 5.2: KPIs of the equilibrium calculations, adapted from [42]

parameter	unit	product gas number						
		1	2	3	4	5	6	6*
SN	-	1.16	0.35	0.27	0.19	0.11	1.05	1.05
Y_{CH_4}	%	99.9	50.8	50.8	39.8	29.6	98.8	99.7
X_{CO}	%	100	99.8	99.8	99.7	99.8	99.97	99.99
X_{CO_2}	%	99.7	−8.5	−34.9	−10.3	−57.1	95.8	99.1
η_c	%	36.5	37.0	47.0	34.6	23.1	37.9	38.3

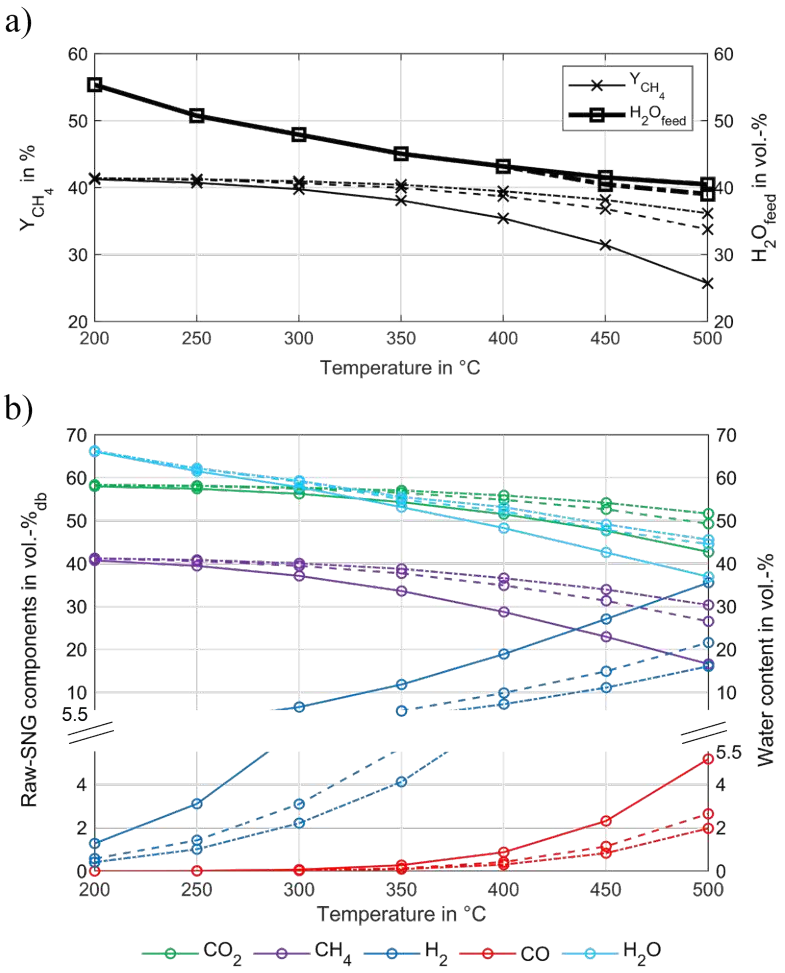

Fig. 5.2: Temperature and pressure variation for the sewage sludge product gas (no. 4) in the thermodynamic equilibrium: 1 bar_a (full line), 5 bar_a (dashed line), 10 bar_a (dash-dotted line), a) CH_4 yield and feed water content, b) raw-SNG gas composition, reproduced from [42]

lowers the carbon utilization in the gasification reactor to low levels. Whereas, for conventional gasification the low η_C results from the low carbon utilization in the methanation reactor. In both cases, carbon is "lost" either through the flue gas of the SER process or the unreacted CO_2 which needs to be separated from the raw-SNG during gas upgrading. Two outliers are lignin gasification with olivine (no. 3) and the mixed CO_2/H_2O (no. 5) operating points. As expected, the latter shows a poor η_C. On the other hand, the former shows an exceptionally high η_C resulting from the high carbon conversion in the DFB system. This is, however, only a single test run and other factors, like the amount of auxiliary fuel introduced to the combustion reactor of the DFB system, would have to be considered as well.

The investigations above were conducted at a fixed methanation temperature. The increased pressure for operating point no. 6 already showed the influence on the gas composition. Hence, a temperature and pressure variation is carried out to see the influence on the raw-SNG composition, Y_{CH_4}, and the necessary feed water content to prevent carbon deposition (H_2O_{feed}). The sewage

sludge product gas (no. 4) is chosen as an example (Fig. 5.2). As expected, Y_{CH_4} and the CH_4 content decrease strongly with increasing temperatures while the residual H_2 and CO contents increase. The most pronounced influence of pressure is visible at high temperatures, diminishing at lower temperatures. Especially the pressure increase from 1 to 5 bar_a significantly improves the composition, while a further increase shows only limited improvements. In the range of 300–350 °C, where fluidized bed methanation is operated, a pressure increase still has a significant impact. It can lead to the desired reduction in residual H_2 and CO contents while improving the carbon utilization. At 350 °C and 10 bar_a or 320 °C and 5 bar_a, the allowed H_2 threshold of 10 mol-% in the final SNG is complied with after CO_2 separation. Even lower temperatures or higher pressures would be needed to fulfill the CO threshold of 0.1 mol-%.

Generally, the other product gases follow the same trends. However, it has to be noted that these statements premise a full conversion within thermodynamic limitations. In reality, other constraints, like kinetics, catalyst deactivation, and mass transfer phenomena occur, further impeding the conversion and the reachable raw-SNG composition. Hence, experimental investigations need to be carried out in an actual fluidized bed methanation reactor.

5.2 Fluidized Bed Methanation

The experimental investigations of the fluidized bed methanation reactor and the prepared catalyst in **Paper III** [124] focus on the performance and characterization of the catalyst and the reactor, as well as the application of DFB and SER product gas methanation. For this purpose, variations in temperature, weight hourly space velocity ($WHSV$), and gas composition are carried out utilizing synthetically premixed gases at a constant near-ambient operating pressure. The findings in the section should also provide further knowledge for the following full process chain investigations.

The goal of the catalyst preparation (see section 4.2) was to develop a methanation catalyst suitable for fluidized beds. It should fulfill the requirements of mechanical and chemical stability, activity, and a suitable fluidization behavior. Fig. 5.3 (left) depicts the particle size distribution of the freshly prepared catalyst in comparison to the spent catalyst after about 200 h of operation. The uniform, narrow particle size distribution could be maintained, showing only a slight, negligible deviation of the mean Sauter diameter d_{SV}, which the catalyst reduction could have influenced[1]. Furthermore, 100 h of operation under methanation conditions[2] showed the chemical stability of the catalyst. The temperature-programmed oxidation (TPO) curve (Fig. 5.3 right)

[1] The measurement of the fresh catalyst was performed before reduction.

[2] Varying syngas compositions including synthetically premixed gases partially containing C_2H_4 as well as real product gas from the 100 kW_{th} DFB pilot plant.

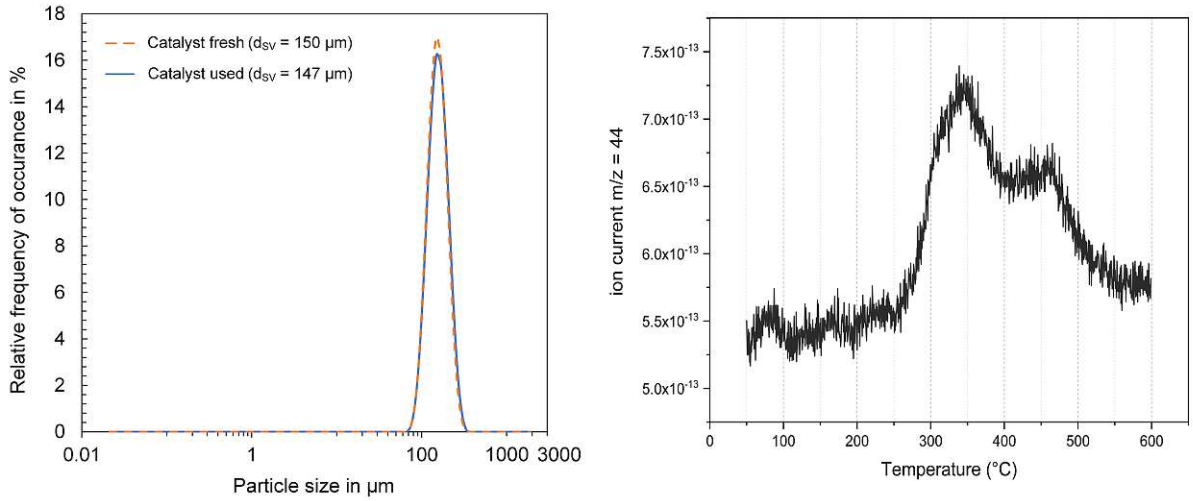

Fig. 5.3: Comparison of the particle size distribution of the fresh and the used catalyst (left) and TPO of the used catalyst (right); the x-axis is displayed from 0.01 µm–3000 µm to show that only a single peak is visible over the entire measurement range; reproduced from [124]

suggests only minimal amounts of rather weakly bound amorphous carbon on the catalyst surface, even though methanation experiments with syngas containing C_2H_4 were carried out. Unfortunately, a quantitative statement from the TPO measurements is not possible. Nevertheless, no apparent catalyst deactivation could be observed from a macroscopic point of view. Repeatedly carried out methanation experiments during the 100 h operation time with a stoichiometric H_2/CO ratio of 3 at 360 °C showed no significant deviation in the raw-SNG gas composition, i.e. the catalyst's activity.

The same stoichiometric H_2/CO ratio of 3 was used to carry out a temperature and $WHSV$ variation. Fig. 5.4 plots the results thereof. The main findings can be summarized as follows:

- Highest CH_4 content and lowest H_2 and CO contents reached between 320–360 °C depending on the applied $WHSV$ as a result of the kinetic temperature dependency.
- Close to equilibrium conversion at higher temperatures with a slight remaining deviation possibly caused by mass transfer limitations and the back-mixing behavior of fluidized beds.
- Slight selectivity of CO towards C_2H_6 at low temperatures (< 300 °C).
- Nearly isothermal operation during methanation with a maximum temperature gradient of 10 °C at 280 °C and 1 $NL/g_{cat}h$ and a maximum deviation of only 2 °C for temperatures above 320 °C (not depicted here).

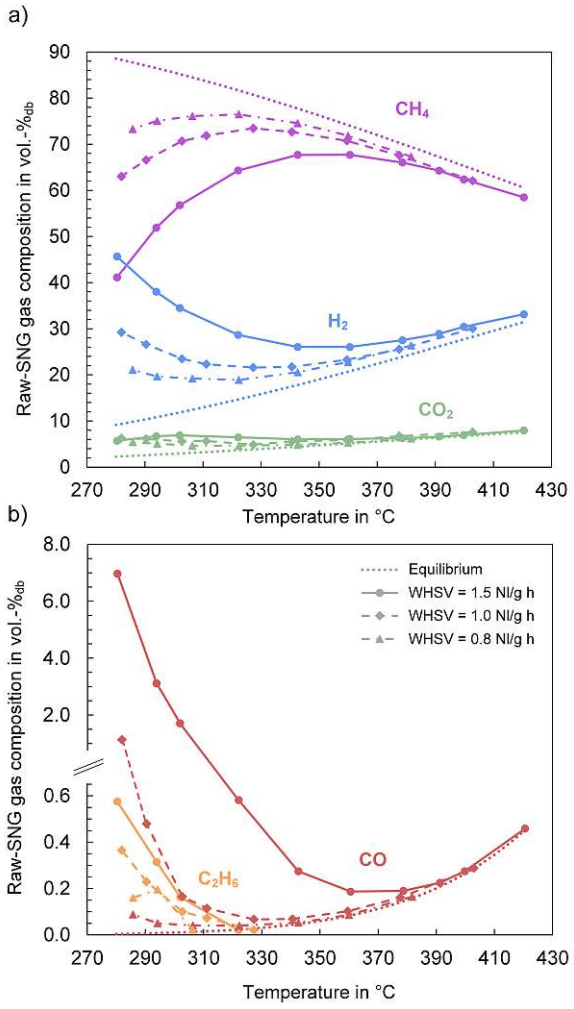

Fig. 5.4: Experimentally determined raw-SNG composition for stoichiometric H_2/CO methanation (75/25 vol.-%) as a function of reaction temperature and $WHSV$ and raw-SNG composition in the thermodynamic equilibrium (dotted lines), a) CH_4, H_2 and CO_2 concentrations, b) CO and C_2H_6 concentrations, reproduced from [124]

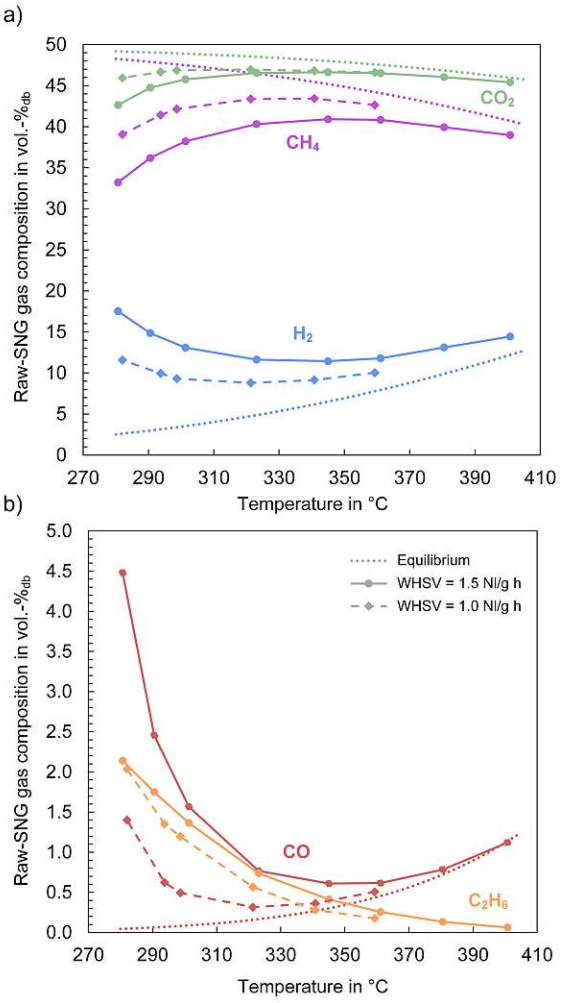

Fig. 5.5: Experimentally determined raw-SNG composition for a typical DFB product gas as a function of reaction temperature and $WHSV$ and raw-SNG composition in the thermodynamic equilibrium (dotted lines), a) CH_4, H_2 and CO_2 concentrations, b) CO and C_2H_6 concentrations, reproduced from [124]

Similar curves can be recorded when premixing a typical advanced DFB product gas composition[3] (Fig. 5.5). Because of the substoichiometric composition, large amounts of CO_2 remain in the raw-SNG. Again, at 320–360 °C the highest conversion can be observed. However, the influence of the reaction temperature is less pronounced. The CO content reaches a minimum of 0.32 vol.-%$_{db}$ at 320 °C and 1 NL/g_{cat}h. Even the thermodynamic limit at this temperature would not be below the demanded limit of 0.1 mol-%, especially considering that a downstream CO_2 separation approximately doubles the residual CO content. Thus, further measures must be taken to fulfill the gas grid regulations (see Chapter 6). Furthermore, C_2H_6 can be found to some degree in the raw-SNG. In this case, it is a result of the selectivity of C_2H_4 towards

[3] 42.3 vol.-% H_2, 23.1 vol.-% CO, 21.9 vol.-% CO_2, 10.4 vol.-% CH_4, 2.4 vol.-% C_2H_4

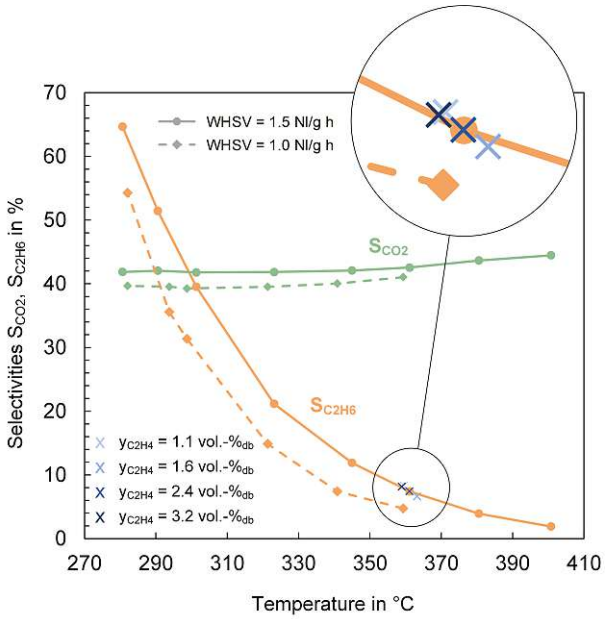

Fig. 5.6: $S_{C_2H_6}$ as a function of reaction temperature, $WHSV$, and syngas ethylene concentration, and S_{CO_2} as a function of reaction temperature and $WHSV$ for a typical DFB syngas, reproduced from [124]

C_2H_6 ($S_{C_2H_6}$) and not the selectivity of CO towards C_2H_6 (see **Paper III**). Fig. 5.6 plots the increasing $S_{C_2H_6}$ at declining temperatures, showing a gradually increasing kinetic limitation concerning the C_2H_6 conversion. The variation in $WHSV$ follows this trajectory, whereas the C_2H_4 concentration shows no impact on $S_{C_2H_6}$. The C_2H_4 conversion, on the other hand, shows no limitation. Interestingly, the selectivity of CO towards CO_2 (S_{CO_2}) is almost independent of the temperature. At lower $WHSV$ it is decreased, showing that the methanation reactions gain more importance and lead to an increased CO conversion to CH_4. The higher CO_2 concentrations in the raw-SNG are therefore attributed to dilution effects.

One option to diminish the CO_2 content in the raw-SNG is the utilization of a hydrogen-enriched product gas produced via the SER process. Through the variation of, e.g. the gasification temperature, the product gas composition can be adjusted in a wide range, as was introduced in section 2.2.1 (cf. Fig. 2.7). If these available SER operating points are reconstructed with bottled gases and methanated at a constant reaction temperature of 360 °C and 1.5 $NL/g_{cat}h$, the raw-SNG compositions over the stoichiometric number SN, depicted in Fig. 5.7, result. If SN is greater than 1.2, a large portion of the CO_2 ($> 90\%$) can be converted and no downstream CO_2 separation would be required to fulfill the threshold level of 2.5 mol-% of CO_2 for grid injection. However, excessive amounts of H_2 remain, which would need to be separated and recirculated. An SN of around 1 results in the highest CH_4 content but requires a CO_2 and H_2 separation under the investigated operating conditions. Nevertheless, the CO limit could be complied with for all SN down to around 1.

Fig. 5.8 compares the operating points of the DFB and SER product gas methanation, displaying the maximum achieved conversion in both cases. The maximum achieved conversion corresponds to a methanation temperature of 360 °C, a $WHSV$ of 1 NL/g_{cat}h, and an SN of 1.05 in the case of SER[4]. The CH_4 content increases by more than 30 percentage points and the CH_4 yield Y_{CH_4} doubles by utilizing the SER syngas. Conversely, the CO and CO_2 concentrations decrease to low levels. A large portion of CO_2 can be converted, whereas CO_2 is produced via the WGS reaction in the case of the DFB product gas. However, the low CO_2 content in the SER raw-SNG doubles the residual H_2 content, despite the higher hydrogen conversion X_{H_2}. This is because of the dilution of the DFB raw-SNG with CO_2. After CO_2 separation, the residual H_2 concentrations are in a similar range. Nevertheless, both raw-SNG gases require an H_2 and CO_2 separation unit before grid feeding under the considered reaction conditions. On the contrary, the residual CO concentration of the SER raw-SNG is within the limit of 0.1 mol-%, whereas a further reduction for the DFB raw-SNG is required. In general, the SER raw-SNG is much closer to the specifications of the gas grid. [124]

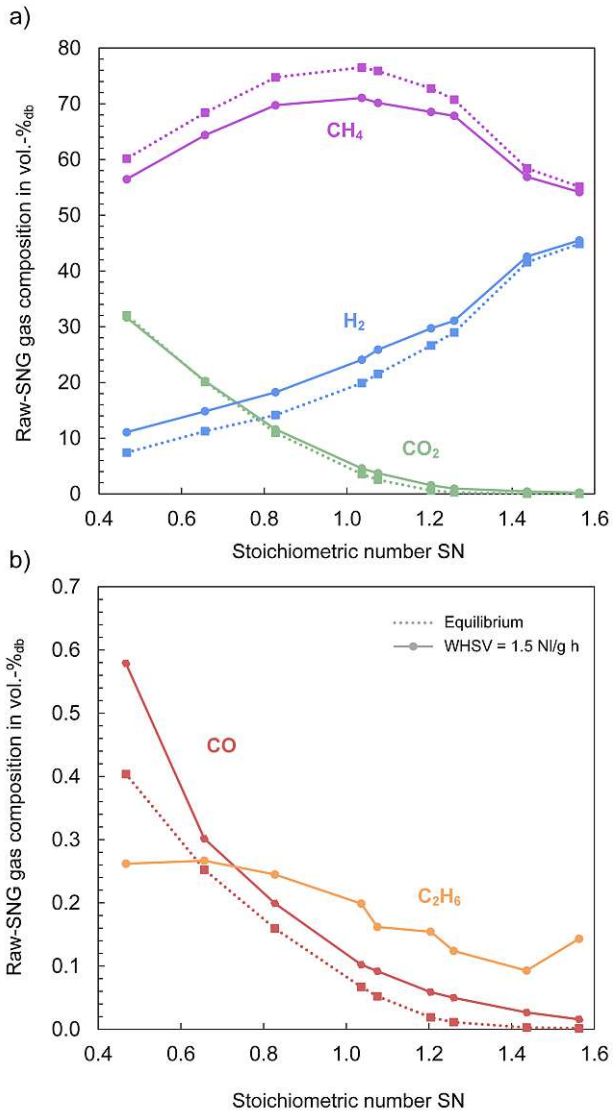

Fig. 5.7: Experimentally determined raw-SNG composition and raw-SNG composition in the thermodynamic equilibrium (dotted lines) for different SER syngas compositions as a function of the stoichiometric number SN at 360 °C and a $WHSV$ of 1.5 NL/g_{cat}h, a) CH_4, H_2 and CO_2 concentrations, b) CO and C_2H_6 concentrations, reproduced from [124]

In any way, the full process chain must be studied to understand the potential benefits of the SER process in combination with methanation. A high CO_2 conversion or CH_4 yield in the methanation reactor alone does not necessarily improve the whole process's efficiency or economy. Additionally, it is necessary to look at process configurations that potentially allow the

[4] An SN closer to 1 might result in even more conversion, but no operating point is available there.

production of grid-feedable SNG without the need for CO_2 and H_2 separation (see section 6.2). A pressurized operation could also help to achieve the necessary gas quality, as was discussed in section 5.1.

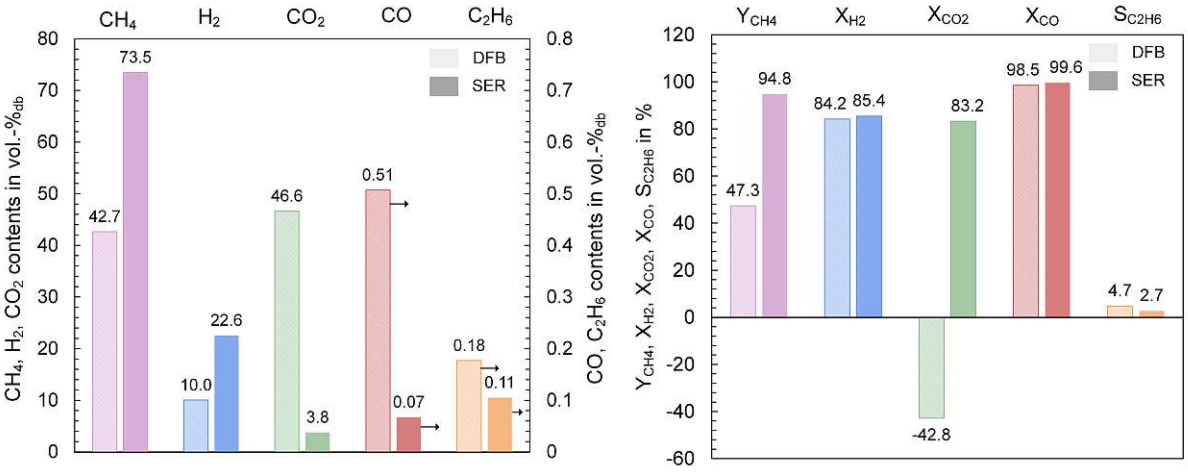

Fig. 5.8: Comparison of the raw-SNG composition (left) and the key figures (right) of the DFB (hatched) and the SER (filled) syngas methanation experiments at 360 °C and a $WHSV$ of 1 $NL/g_{cat}h$, reproduced from [124]

5.3 Process Chain Investigations

A holistic evaluation of the investigated SNG production processes requires the operation of a full process chain. Within this work, a fluidized bed methanation reactor and gas cleaning units were designed, set up, and connected to the 100 kW_{th} advanced DFB pilot plant at TU Wien (see Chapter 4). This section shows an excerpt of the results gained from the process chain operation. As stated before, the three investigated configurations are:

- DFB gasification and direct methanation of the DFB product gas (DFB-Std).
- DFB gasification with external hydrogen addition to the product gas and methanation of the hydrogen-enriched product gas (DFB+H_2).
- The SER process with direct methanation of the hydrogen-enriched product gas without external hydrogen addition (SER).

Softwood pellets are used as a comparable reference feedstock for all investigations in this context. More details on the results, the methodology used, and the operating parameters are documented in **Paper IV** [38].

Fig. 5.9 shows the raw product gas analysis values of the DFB product gas (top) and the raw-SNG (bottom) on a dry and nitrogen-free basis over time for the DFB-Std configuration. Nitrogen

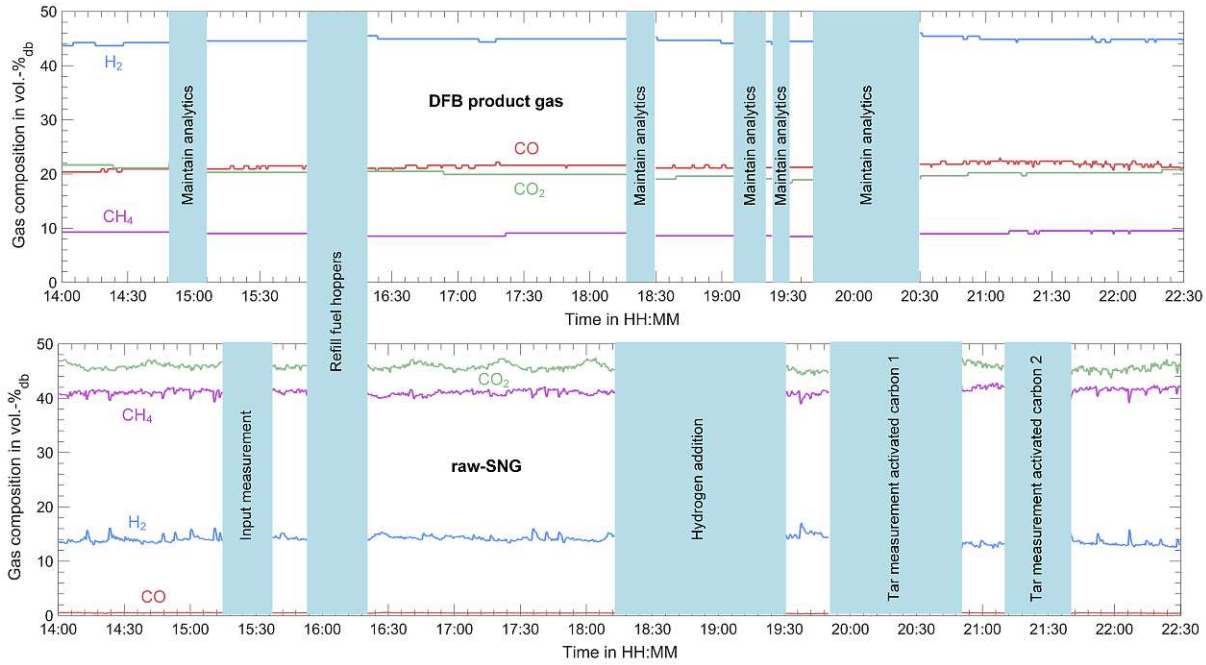

Fig. 5.9: Raw measurement values of the DFB product gas composition (top) and the raw-SNG composition (bottom) for the DFB-Std configuration on a dry and nitrogen-free basis over time, reproduced from [38]

is excluded because it results from flushing the fuel hoppers and the pressure measurement points. Hardly any nitrogen is expected from the fuel in the case of softwood pellets. Internal investigations not depicted in the current study showed that CO_2 can be used as a flushing agent, which reduced the nitrogen content in the product gas to about 0.13 vol.-$\%_{db}$. The product gas and the raw-SNG compositions show a stable trend over the displayed 8.5 h. The excluded parts of the diagram are mainly caused by the maintenance of the gas measurement equipment, while the process itself remains in a steady state. Exceptions are the refilling of fuel hoppers and tar measurements after the activated carbon (*AC*) adsorber beds. Furthermore, hydrogen addition (DFB+H_2) was investigated between 18:15 and 19:30. [38]

Fig. 5.10a) depicts via mass and energy balances validated data of the DFB-Std operation for all units throughout the process chain (denoted by stream numbers 1–12). Each stream number can be allocated to a certain point in the process chain according to the process flow diagram in Fig. 5.10b). The data shows the evolution of temperature and pressure (top) and the evolution of the gas components (bottom). The illustration of the gas composition is divided into two sections: from stream nos. 1–8, the evolution of impurities such as BTEX[5], GCMS[6] tar, NH_3, and H_2S are depicted, while for stream nos. 9–12, the evolution of the main gas components (H_2, CO_2, CO, CH_4) and the water content is displayed. The illustration of impurities and main

[5]benzene, toluene, ethyl-benzene, xylene (BTEX)
[6]gas chromatography/mass spectroscopy (*GCMS*)

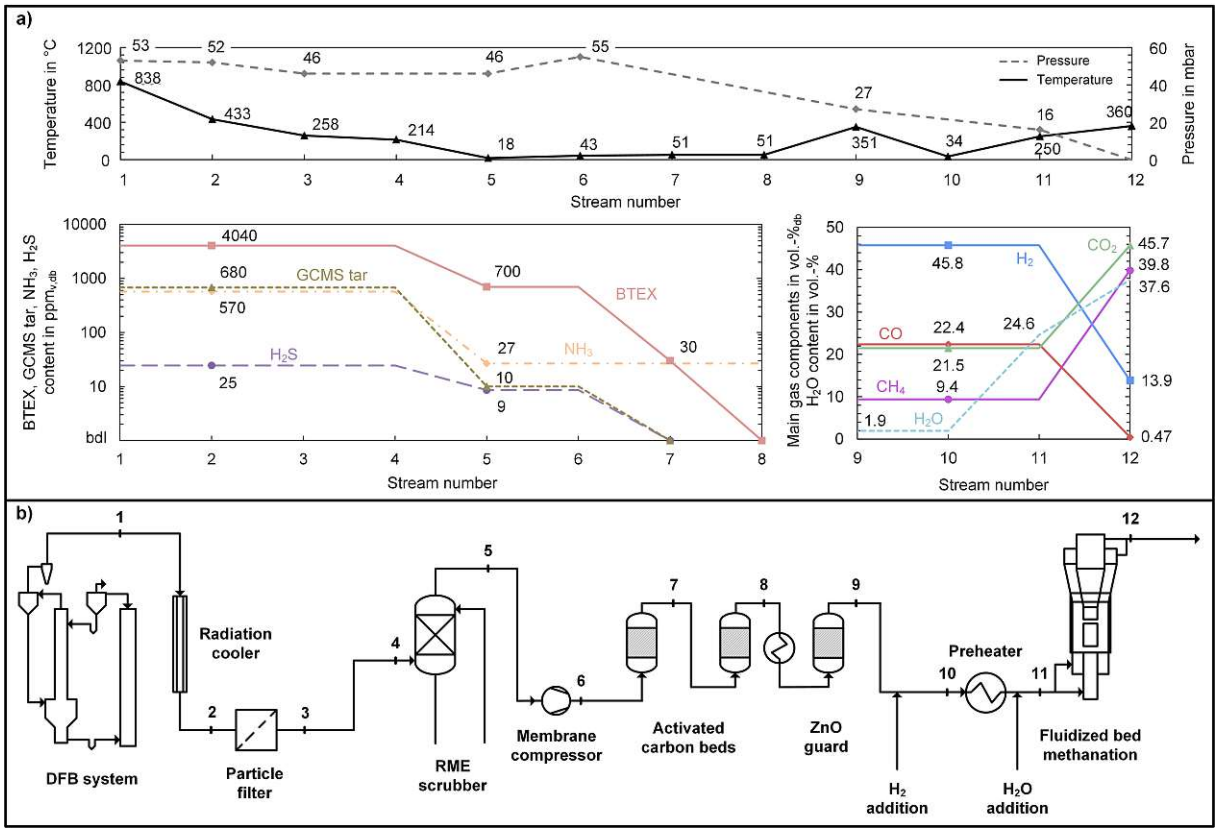

Fig. 5.10: Process conditions over the whole process chain during the direct methanation of the DFB product gas (DFB-Std): a) evolution of temperature, pressure (top), and concentration of impurities and main gas components (bottom), b) process flow diagram with stream numbers, reproduced from [38]

gas components for the other stream numbers is omitted because the gas composition does not change there. [38]

The main observations taken from this figure can be summarized as follows.

- Low H_2S concentrations in the raw product gas because of the high quality of the feedstock.
- Low GCMS tar concentrations because of high gasification temperature and limestone-share in the bed material.
- BTEX amount to the highest share of impurities, but only benzene and toluene were detected.
- Impurities are efficiently removed in the RME scrubber. Separation efficiencies are 98.5%, 95%, and 83% for GCMS tar, NH_3, and BTEX, respectively. Naphthalene, which makes up two-thirds of the GCMS tar concentration, is removed below the detection limit and mainly benzene remains from the BTEX sum downstream of the scrubber because of the low boiling point. Interestingly, some high molecular weight tars (particularly anthracene, fluoranthene, and pyrene) remain, which should have been removed due to their high boiling point. The high NH_3 separation efficiency results from the dissolution in the condensed

steam (see Additional Paper II [142] for more information about NH_3 in the scrubber). Literature reports substantial variations of separation efficiencies in the scrubber, depending on the operating conditions and the scale [95, 105, 143].

- H_2S is removed below the detection limit in the first adsorber bed and benzene in the second adsorber bed.
- In the raw-SNG after the fluidized bed methanation reactor, approx. 40 vol.-$\%_{db}$ of CH_4 was reached at 360 °C and near ambient pressure conditions. The high CO_2 content is a result of the WGS reaction. Residual H_2 remains because of thermodynamic and kinetic limitations at these operating conditions. CO is almost completely converted, but still 0.47 vol.-$\%_{db}$ remains which is too high for grid injection. Similar results were achieved by Seemann et al. [12], factoring in the deviating operating conditions and a different catalyst.

Similarly, the DFB+H_2 and the SER process configurations were investigated. Details can be found in the respective publication [38]. Here, a comparison of the results of the three process configurations is discussed. Fig. 5.11 depicts the raw-SNG composition and the KPIs of the methanation reactor for a DFB-Std, two DFB+H_2, and one SER operating point. The horizontal lines indicate the theoretically achievable gas composition at equilibrium. Compared to the DFB-Std configuration, the CH_4 content increases up to 70 vol.-$\%_{db}$ for SER, similar to the results with synthetically premixed gases. Furthermore, CO_2 is converted and not produced, lowering the residual CO_2 concentration. The amount of residual CO_2 and H_2 depends on the SN of the syngas, which is controlled by the amount of external H_2 added and the operating conditions of the gasifier. In the case of SER, a substoichiometric product gas ($SN = 0.71$) with an H_2 content of approx. 60 vol.-$\%_{db}$ was produced, resulting in a higher CH_4 content, but also a higher residual CO_2 content compared to DFB+H_2. Although this increases Y_{CH_4} to 80%, it is significantly lower than the results with synthetically premixed gases, where a near stoichiometric SER product gas composition ($SN = 1.05$) resulted in a Y_{CH_4} of 95%. If hydrogen is added externally to produce a slightly substoichiometric ($SN = 0.91$) and a slightly overstoichiometric ($SN = 1.04$) syngas, much more CO_2 can be converted (see X_{CO_2}). Naturally, the more H_2 is added, the more CO_2 is converted—however, at the cost of a lower X_{H_2} and a substantial amount of residual H_2 in the raw-SNG. Nevertheless, X_{H_2} is still higher compared to the DFB-Std operation, where the steam addition to the methanation reactor leads to a production of H_2 via the WGS reaction. To reach an SN of 0.91 and 1.04, 91% and 111% of H_2 in relation to the syngas volume flow upstream of the H_2 addition must be added, respectively. Thus, the distance to the equilibrium is increased because of the resulting higher $WHSV$ and

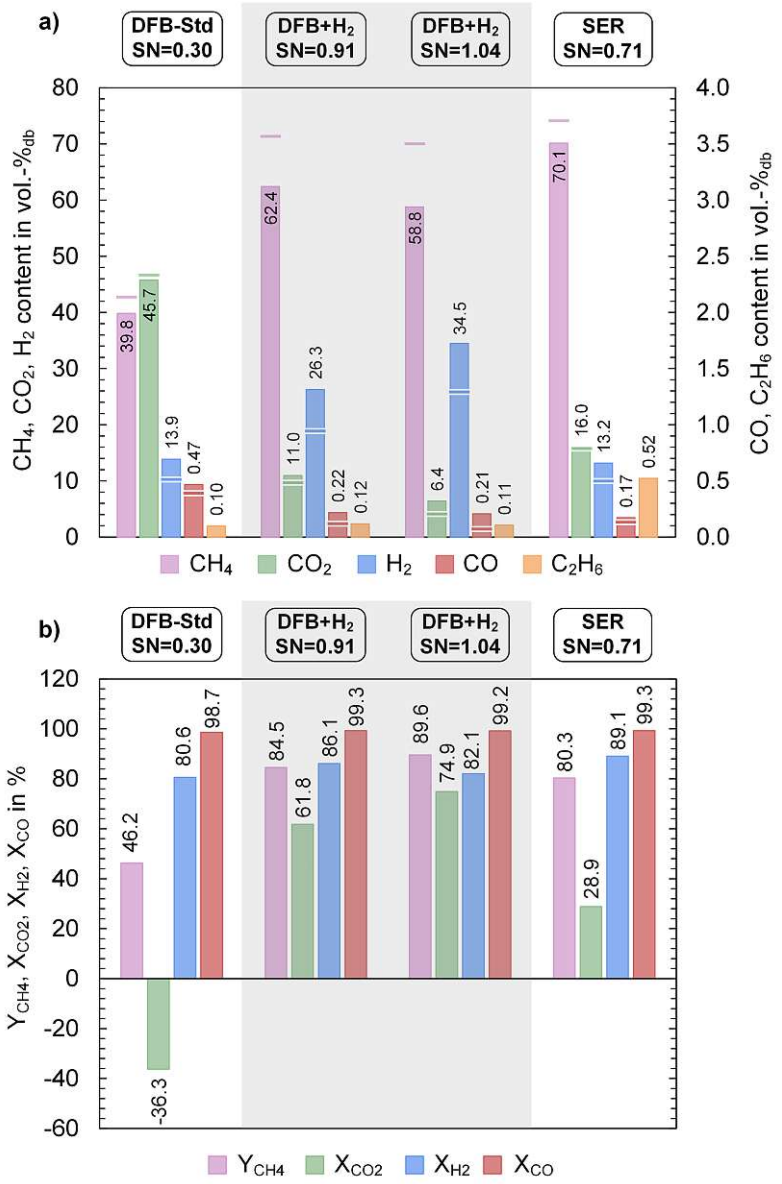

Fig. 5.11: Comparison of the four operating points, a) raw-SNG composition, b) KPIs of the methanation reactor; the horizontal lines indicate the thermodynamic equilibrium; reproduced from [38]

the kinetic limitations. The residual CO content, on the other hand, is reduced and X_{CO} is increased. Nevertheless, the required CO limit of 0.1 mol-%$_{\mathrm{db}}$ could not be reached. Once more, this confirms that further measures are necessary (see Chapter 6).

For the performance of the methanation reactor alone, it is unimportant how the adjustment of the syngas towards high H_2 contents is achieved. The main influencing parameter is SN at the inlet of the methanation reactor and, to some extent, the changing $WHSV$ due to H_2 addition. However, the performance of the whole process chain depends very much on the origin of the syngas. Therefore, to compare the KPIs of the whole process chain, Fig. 5.12 depicts the overall cold gas efficiency ($\eta^*_{CGE,o}$) and the carbon utilization (η_C) [38]. Interestingly, the DFB-Std and the DFB+H_2 configurations show a very similar $\eta^*_{CGE,o}$. On the contrary, the SER configuration

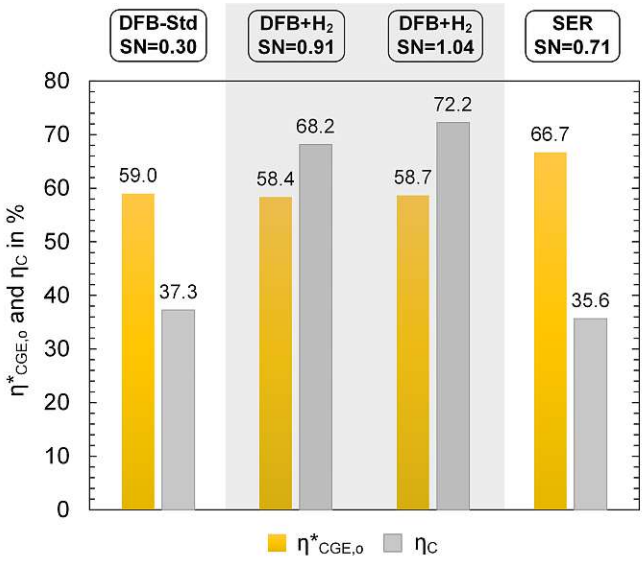

Fig. 5.12: Comparison of the KPIs of the overall process chain for the four operating points, reproduced from [38]

leads to an increased $\eta^*_{CGE,o}$. The lower temperatures in the DFB reactor, more available char for combustion, less heating oil consumption, and a higher product gas CH_4 content, allow a more efficient process. Brellochs [121] calculates a similar efficiency at 67.5% for a simulated 10 MW_{th} SNG plant. For the DFB+H_2 route, a much higher $\eta^*_{CGE,o}$, between 67% and 73%, has been calculated on a theoretical basis in literature [40, 116]. η_C, on the other hand, can be increased to roughly 70% via H_2 addition. From a technical and ecological perspective, it is highly desirable to utilize limited biomass resources as efficiently as possible. Of course, economic perspectives also have to be considered (see Chapter 6). Through the SER process, no increase in η_C can be achieved, since this process only shifts some carbon from the product gas to the flue gas, not changing the overall hydrogen availability. Hence, values around 36%–37% are reached for both the DFB-Std and the SER process, which is in the range of reported values for the GoBiGas plant (30%). Of course, a comparison to large-scale plants is always tricky since the fully integrated process is not available at pilot-scale, and e.g., the amount of heating oil used at pilot-scale has to be provided by product gas recirculation in large-scale plants, reducing η_C of the latter.

Chapter 6

Implementation Concepts, Techno-Economic Analysis and CO_2 Footprint

Based on the previously established knowledge and results in this work, the question arises how an industrial concept for the production of synthetic natural gas (*SNG*) could look like and how such a process could be implemented and assessed. In this chapter, the bigger picture is captured by the "Reallabor" case study, which puts the technology in the context of the Austrian energy system (see section 6.1 and section 6.3). In section 6.2, alternative SNG production concepts beyond the state-of-the-art are proposed, assessments are made, and suggestions are derived. The focus of the quantitative analysis lies in the evaluation of technical, economic, and ecological parameters relevant to this technology. The investigations provide a basis for the realization of the "Reallabor" and the rollout of the technology. Furthermore, the introduced concepts in this chapter provide possible research topics to be investigated and demonstrated in such an industrial-scale laboratory setting.

6.1 Case Study "Reallabor"

In 2020, the "Reallabor" study was conducted by Hofbauer et al. [81], showing the technical, economic, ecological, and legislative aspects of integrating dual fluidized bed (*DFB*) gasification based processes for the production of SNG and Fischer-Tropsch (*FT*) diesel to defossilize the agricultural sector (excluding fertilizers) in Austria. A more general approach in terms of the utilization of the products within the Austrian energy sector was investigated by Hammerschmid et al. [125] (**Paper V**). This section and section 6.3 summarize the paper's main findings concerning SNG. The FT part of the paper can be found in the respective publication.

6.1.1 Process Flow Diagram of the Proposed Concept

Fig. 6.1 depicts the process flow diagram (*PFD*) of the proposed SNG process chain for 100 MW thermal fuel input. Only the main process units, but no heat displacement or regeneration steps, are depicted for better legibility. 100 MW thermal fuel input was chosen as a trade-off between a realistic, manageable size and the impact of economy of scale [81]. The calculation of mass- and energy balances was carried out in IPSEpro 8.0 (cf. Chapter 3). The following description of the PFD is largely taken from **Paper V**. The modeling assumptions can be found in the appendix of **Paper V** [125].

The resource supply section consists of the on-site fuel handling and storage as well as a dryer to reduce the water content of the fuel to an optimal and constant level for gasification, which is about 20%. In this study, the considered fuel is woody biomass. The heat required for drying is supplied internally through heat displacement. The gasification section is based on the advanced DFB steam gasification technology utilizing a mixture of olivine and limestone as bed material, similar to the experiments in section 5.3. Product gas leaves the gasification reactor (*GR*) and is cooled to 180 °C in heat exchangers (PG cooler). In the coarse gas cleaning section, dust and some tar compounds are removed in a baghouse filter (PG filter). The main amount of tar compounds are separated in a biodiesel scrubber at 40 °C based on the solvent rapeseed methyl ester (*RME*). Additionally, steam condenses in the biodiesel scrubber and enables the separation of water-soluble substances from the product gas, like ammonia (NH_3). The tar-rich RME and the condensed water are directed into a phase separator (solvent regen.). Here, the liquid separates into a clear RME phase, an emulsion phase, and a water phase. The clear RME phase is recirculated to the scrubber while the water phase is evaporated, superheated, and reused as a gasification agent in the gasification reactor. Through that, the freshwater consumption of the DFB system is minimized. The emulsion phase consists of a mixture of RME, absorbed tar compounds, and water and is utilized as additional fuel in the combustion reactor. Downstream of the biodiesel scrubber, a part of the product gas is recirculated to the combustion reactor to provide the necessary heat for gasification (PG recycle to CR). This way, there is no need for an external fuel supply to the combustion reactor of the process. In the fine gas cleaning section, all remaining impurities are removed that harm the catalysts during the synthesis processes and are unwanted in the final product. Activated carbon (*AC*) adsorbers remove light aromatic compounds such as benzene, toluene, or naphthalene and sulfur compounds such as hydrogen sulfide (H_2S). The AC filters are operated as temperature swing adsorption (*TSA*), and the regeneration is carried out with steam at 250 °C.

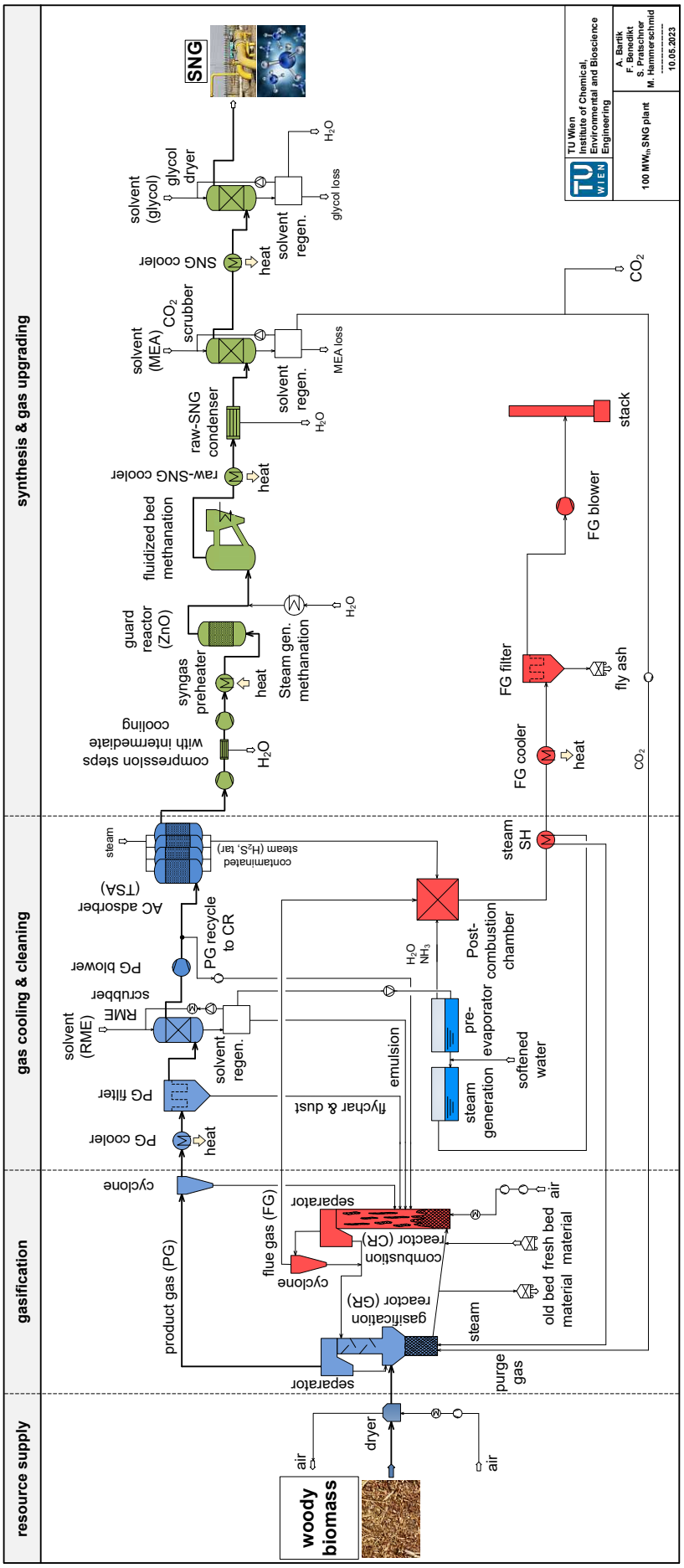

Fig. 6.1: PFD of an SNG production process chain for 100 MW fuel input, adapted from [125] (**Paper V**)

For SNG synthesis, the product gas is compressed to 10 bar_a in a two-stage intercooled compressor. 10 bar_a is chosen to reach the required CO conversion in the methanation reactor, thus limiting the CO content in the SNG to 0.1 mol.-% according to natural gas grid regulations. Simultaneously, it is the assumed pressure at the transfer point to the gas grid operator. Downstream the compressor, the product gas is preheated to 250 °C and enters a ZnO guard reactor, which acts as a protection layer against sulfur break-through. The conversion of syngas to raw synthetic natural gas (*raw-SNG*) takes place in a cooled fluidized bed methanation reactor at 320 °C in the presence of a nickel catalyst. After heat recovery, a condenser separates water from the raw-SNG, and the gas enters an amine scrubber for CO_2 removal. The condensed water is fully reused within the process, e.g. for steam regeneration of the AC or steam addition upstream of the methanation reactor. In the last step, the gas is dried in a glycol scrubber and transferred to the natural gas grid following the specifications of the Austrian gas grid (ÖVGW G B210 [144]). Furthermore, CO_2 and district heat are generated as secondary products from these processes, creating additional revenues.

The flue gas line starts at the combustion reactor (*CR*) of the DFB system. In the CR, the biomass char and recycled product gas is burnt with air. After particle separation in a cyclone, the remaining CO content in the flue gas is converted in a post-combustion chamber. Here, contaminants, like NH_3, H_2S, and BTX, coming from the pre-evaporator and the AC TSA unit, are combusted. After heat recovery and particle filtration, the flue gas leaves the stack via the FG blower. No additional gas cleaning is necessary due to the application of woody biomass. If residues and waste materials would be used, additional flue gas cleaning efforts would have to be considered.

6.1.2 Results of the Techno-Economic Analysis and CO_2 Footprint Calculations

The techno-economic analysis (*TEA*) is based on the calculation of the mass- and energy balances in IPSEpro 8.0. More details on the methodology of the TEA can be found in section 3.2 and in **Paper V**. The most important input and output streams are summarized in Table 6.1 "reference case" (section 6.2.1) and can be found in more detail in **Paper V**.

Fig. 6.2a shows the production costs (including taxes) of the proposed process chain compared to the market price of fossil natural gas for 2019 and 2022. The decision to distinguish between 2019 and 2022 results from the significantly changed prices caused by global disruptions. In 2019, the production costs of SNG were almost equal to the household price of natural gas at approximately 70 €/MW h. In 2022, the production costs of SNG are almost identical to the industrial price of natural gas at around 90 €/MW h. This shows that SNG production can be

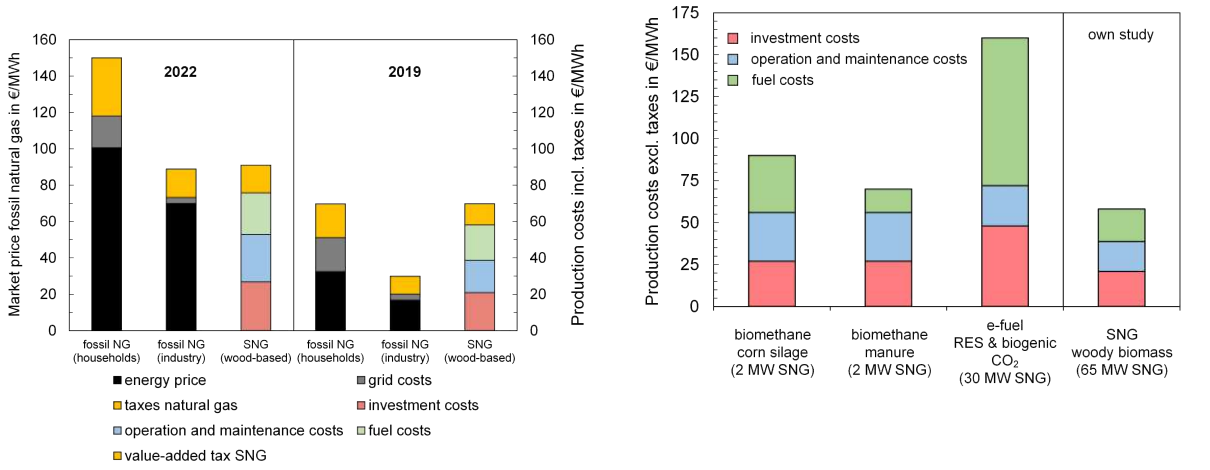

(a) comparison to fossil natural gas in 2019 and 2022

(b) comparison to biomethane [145] and e-fuels [30] in 2019

Fig. 6.2: Comparison of the production costs of SNG for 100 MW fuel input to fossil natural gas and renewable alternatives, adapted from [125]

competitive with fossil natural gas, assuming that revenues from CO_2 (69.60 €/t_{CO2} (2022), 24.90 €/t_{CO2} (2019)) and district heat (37.4 €/MW h (2022), 31.3 €/MW h (2019)) are created. Furthermore, the production costs are split into investment, operation and maintenance, and fuel costs. The most pronounced increase of 57% between 2019 and 2022 is found for the operation and maintenance costs due to the doubling of the electricity price during that time.

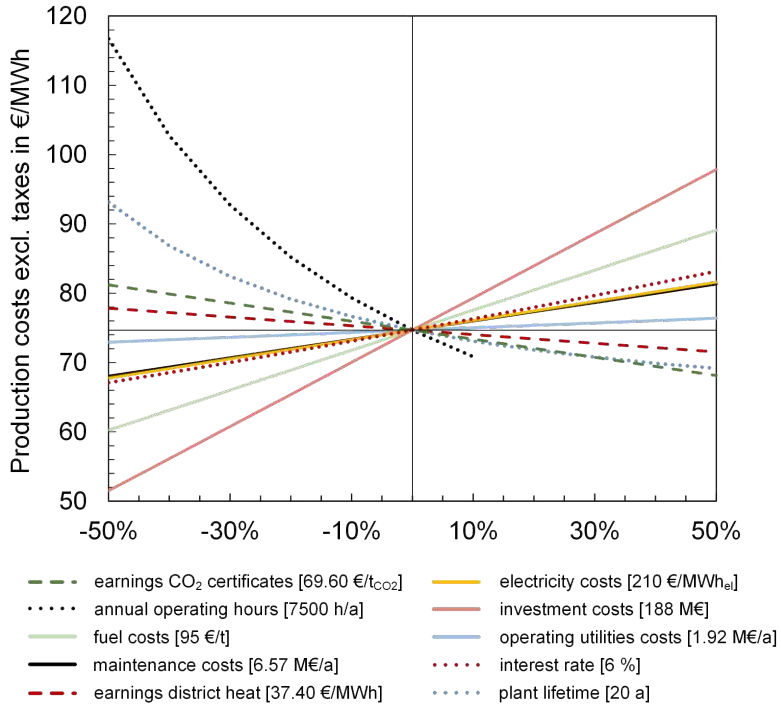

Fig. 6.3: Sensitivity in production costs of SNG for 100 MW fuel input in 2022, numbers in brackets indicate the baseline costs, adapted from [125]

Fig. 6.2b compares the production costs (excluding taxes) of the proposed process chain to the production costs of other renewable alternatives. Fermentative biomethane production routes show 20% to 55% higher production costs, depending on the used feedstock [145]. As of 2019, much higher production costs can be expected from e-fuels produced from biogenic CO_2 and renewable energy sources (RESs) (plus 175%), mainly driven by the high electricity costs. Of course, a fair comparison is hardly possible due to the different plant sizes (2 MW_{SNG} compared to 65 MW_{SNG}). Fermenters are not subject to economies of scale as thermochemical routes are. Instead, they are built on a smaller scale but in higher numbers, which is preferable for decentralized applications. On the other hand, thermochemical routes only reveal their economic advantages at relatively large scales, making them suitable for centralized production facilities. This shows that the plant location, the feedstock supply, and the operator's goals are crucial factors when evaluating different technology options.

Additionally, a sensitivity analysis is carried out to investigate the sensitivity of the production costs to the most prominent commodities and cost drivers (Fig. 6.3). The most influential parameters are the annual operating hours, plant lifetime, investment costs, and fuel costs. To a lesser extent, earnings from CO_2 certificates and district heat, interest rate, electricity costs, and maintenance costs impact production costs. Thus, high plant availability and lifetime, low investment costs, e.g. through less equipment, or less fuel costs, e.g. by utilizing residual and waste materials [123], are measures to keep the production costs low.

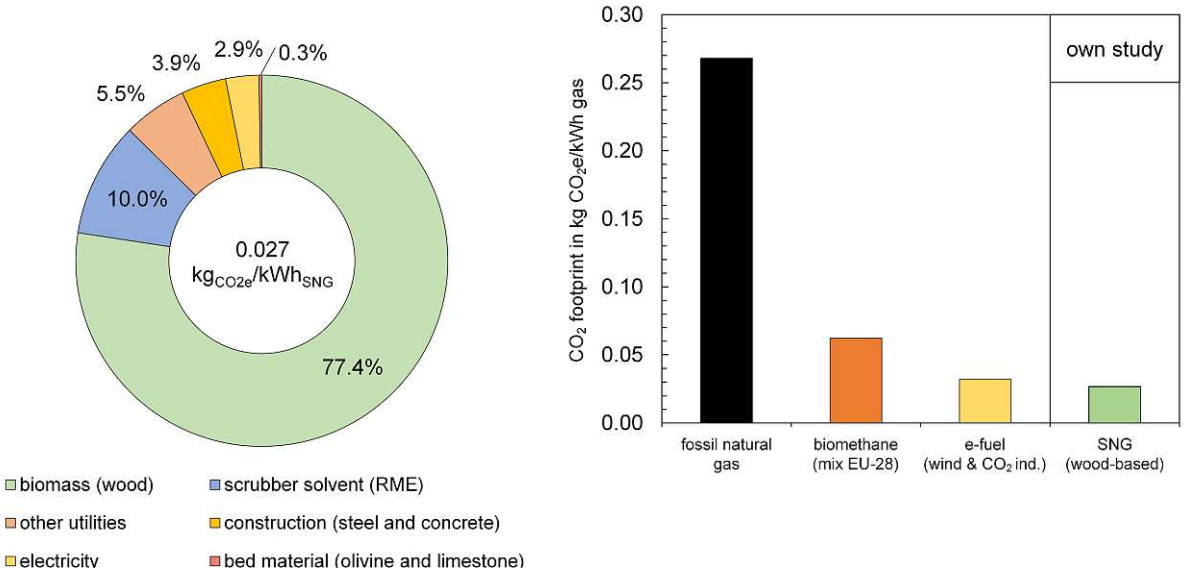

(a) Breakdown of CO_2 footprint

(b) CO_2 footprint in comparison to fossil natural gas [128], biomethane, and e-fuels [146, 147]

Fig. 6.4: Breakdown of the CO_2 footprint of SNG and comparison to fossil natural gas and renewable alternatives, adapted from [125]

From an ecological perspective, the CO_2 footprint of SNG based on woody biomass is evaluated (Fig. 6.4). Compared to fossil natural gas, an emission reduction of 90% results. Even in comparison to biomethane via anaerobic digestion, a lower CO_2 footprint is observed—only e-fuels show comparatively low emissions. The remaining emissions very much depend on the applied parameters, like the substrate mix used to evaluate the biomethane route or the electricity and CO_2 source for e-fuels. For the investigated SNG route, renewable electricity is assumed. Thus, the highest share of the remaining emissions originates from the direct and indirect emissions of the biomass itself (77%). The rest is split between utilities like RME and bed material, electricity, and the plant's construction. Of course, the CO_2 footprint gives only a hint at the ecological impacts of these processes. A full life cycle assessment could provide further insights into this issue.

6.2 Evaluation of Alternative Concepts

In this work, alternative process concepts have been introduced, which are now translated to industrial-scale concepts utilizing the same methodology as in section 6.1. This includes an optimized layout to the "reference case" in section 6.1, as well as advanced concepts utilizing external H_2 and the sorption enhanced reforming (*SER*) process. The three process concepts are

- an optimized layout for advanced DFB gasification with direct methanation of the syngas (DFB-Std),
- a hybrid route including external H_2 addition and methanation of the hydrogen-enriched syngas (DFB+H_2),
- DFB gasification with in-situ CO_2 removal and direct methanation of the hydrogen-enriched syngas (SER).

A sensitivity analysis again shows the main influencing parameters. Furthermore, the input and output streams and key performance indicators (KPIs), such as cold gas efficiency for industrial-scale concepts ($\eta_{CGE,o}$) and carbon utilization (η_C), are evaluated and compared. The following analysis omits displaying the DFB section of the process since the layout and the assumptions are identical to section 6.1.

6.2.1 Optimized Conventional Concepts (DFB-Std)

The concept introduced in section 6.1 (reference case) can theoretically produce injectable SNG if the thermodynamic equilibrium is almost perfectly reached at 10 bar_a and 320 °C. Especially the

demanded CO content of <0.1 mol-% is challenging to reach, considering practical kinetic limitations and theoretical thermodynamic limitations even under elevated pressures (cf. Chapter 5) [38, 42, 124]. Therefore, some adaptions should be made to ensure a high-quality gas and increase the operational flexibility. A second-stage adiabatic fixed-bed polishing reactor is suggested after condensing water from the raw-SNG downstream the methanation reactor. The water condensation drives the CO methanation reaction (Eq. 2.1) in the polishing reactor—according to Le Chatelier's principle—towards CH_4 and away from CO. However, the same principle would also imply a production of CO via the reversed water-gas shift (*WGS*) reaction (Eq. 2.2), which can be counteracted by removing CO_2 beforehand. Therefore, the polishing reactor must be placed downstream of the CO_2 removal step. The polishing reactor also opens up the possibility of placing the compression unit downstream the fluidized bed methanation reactor, thus reducing the energy consumption for compression. From a design point of view, a rather simple adiabatic fixed bed is chosen. This is sufficient because only minor amounts of CO are reacting, resulting in a low reaction heat, and carbon deposition is unproblematic due to the high H_2/CO ratio (approx. 20) at this point.

Fig. 6.5 shows PFDs of two variants of such a concept. Variant 1 (Fig. 6.5 a)) places the compression unit in-between the fluidized bed methanation unit and the CO_2 scrubber (framed in red), while in variant 2 (Fig. 6.5 b)), it is placed downstream the CO_2 scrubber. The main difference lies in the monoethanolamine (*MEA*) regeneration heat required in the desorber of the

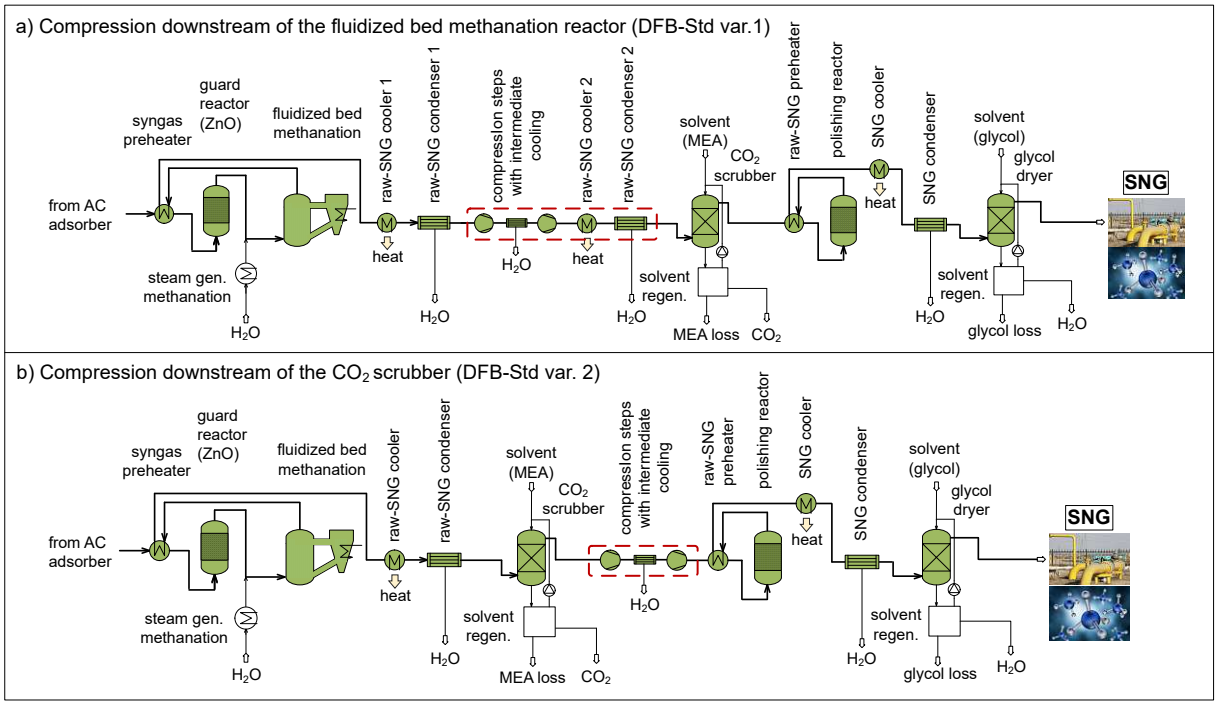

Fig. 6.5: PFD of two alternative DFB-Std variants, compression is carried out a) downstream of the fluidized bed methanation reactor (var. 1), b) downstream of the CO_2 scrubber (var. 2)

CO_2 scrubber and the electricity requirement of the compression unit. Amine scrubbing is known, for example, from post-combustion CO_2 capture, to be a large consumer of thermal energy [148]. Li et al. [149] calculate with a reboiler energy duty of 3.6 MJ/kg_{CO2}, which is used in variant 2 due to the near-ambient pressure conditions similar to flue gas CO_2 capture.[1] If compression takes place upstream the CO_2 scrubber (variant 1), a significant reduction in reboiler energy duty to 0.83 MJ/kg_{CO2} is achieved, according to data from the GoBiGas plant[2] [150]. Thus, variant 1 aims to minimize the thermal energy requirement and maximize the output of district heat. Additionally, higher CO_2 separation efficiencies are reached under pressurized conditions. In contrast, variant 2 minimizes the electricity consumption due to the lower volume flow, i.e., the lower compression energy (about 50 % of the total raw-SNG volume flow is CO_2).

Table 6.1 summarizes the input and output streams, the KPIs, and the levelized costs of products (*LCOP*) of the two discussed variants in comparison to the reference case in section 6.1. The modeling assumptions deviating from the reference case are found in Appendix A. At this point, it should only be mentioned that the reaction temperatures of the fluidized bed methanation unit and the polishing reactor are set to 340 °C and 360 °C, respectively. At this temperature, the highest conversion rates could be observed (cf. Chapter 5) in the pilot-scale fluidized bed methanation unit. Furthermore, a sufficiently high inlet temperature to the polishing

Tab. 6.1: Production costs, input and output streams, and KPIs of DFB-Std variants 1 and 2 in comparison to the DFB-Std reference case for 100 MW fuel input

parameter	unit	variant 1	variant 2	reference case
input				
electricity	kW_{el}	3371	2716	4340
fresh water	kg/h	148	161	-
output				
SNG	Nm^3/h	6780	6810	6840
district heat	kW	12550	2770	14170
captured CO_2	Nm^3/h	6140	6140	6150
waste water	kg/h	-	-	320
KPIs				
$\eta_{CGE,o}$	%	64.95	64.96	64.96
η_C	%	34.47	34.42	34.36
SNG CH_4 content	vol.-%	95.76	95.18	94.62
SNG CO content	vol.-%	0.042	0.035	0.093
SNG CO_2 content	vol.-%	2.21	2.32	2.34
SNG H_2 content	vol.-%	1.87	2.33	2.82
production costs				
LCOP excl. taxes	€/MW h	74.88	76.51	75.84

[1] The influence of the lower CO_2 partial pressure of flue gas (~12 vol.-%) compared to raw-SNG (50 vol.-%) is neglected.

[2] In the GoBiGas plant, actually a mixture of methyldiethanolamine and piperazine is used instead of MEA as a solvent. The different costs and absorption enthalpies are neglected.

reactor can be maintained due to heat recuperation if the exothermic reactions are allowed to heat up the gas stream in the adiabatic polishing reactor to 360 °C. The pressure is kept constant at 10 bar_a.

The results show almost identical numbers in terms of KPIs, SNG output, and captured CO_2. Most importantly, the two variants are able to reduce the CO content well below the threshold level despite the higher, but more realistic, methanation reaction temperatures. Simultaneously, the CH_4 content is increased and the H_2 and CO_2 contents are below 10 mol.-% and 2.5 mol.%, respectively. As discussed previously, the placement of the compression unit largely influences its electricity consumption and, inversely, the amount of usable district heat. A district heat penalty of 80% must be accepted for a 37% reduction in electricity consumption when comparing variant 2 with the reference case. This instance also influences the production costs, resulting in the lowest costs for variant 1 despite the larger number of equipment. However, the margin is small when thinking about a ±30% prediction accuracy of the applied TEA methodology [151, 152].

Nevertheless, it is worth considering the production cost sensitivity of the two variants to the electricity price and the district heat revenues. Fig. 6.6 displays these dependencies, assuming 5800 district heat operating hours per year. If the earnings from district heat were reduced by more than 38%, variant 2 would have a slight economic advantage due to the low amount of district heat and, thus, the low sensitivity. Regarding the electricity costs, variant 1 is superior throughout the displayed range, despite the higher electricity consumption, i.e. the higher sensitivity. In the end, the most favorable variant will be determined by the location of the plant and the availability of surrounding district heat consumers.

Summing up, DFB-Std variant 1 is chosen as the overall best trade-off considering the investigated parameters. The main advantages compared to the reference case are

- an SNG CO content securely below the threshold level of 0.1 mol-%,
- an increased CH_4 content despite the slightly lower SNG amount,
- a significantly reduced electricity consumption due to the volume reduction in the fluidized bed methanation unit and water condensation (40% less volume flow),
- fluidized bed methanation at near-ambient pressure (no pressure vessel) and potentially more space for heat exchanger surfaces in the reactor to handle the highly exothermic reactions,
- similar production costs.

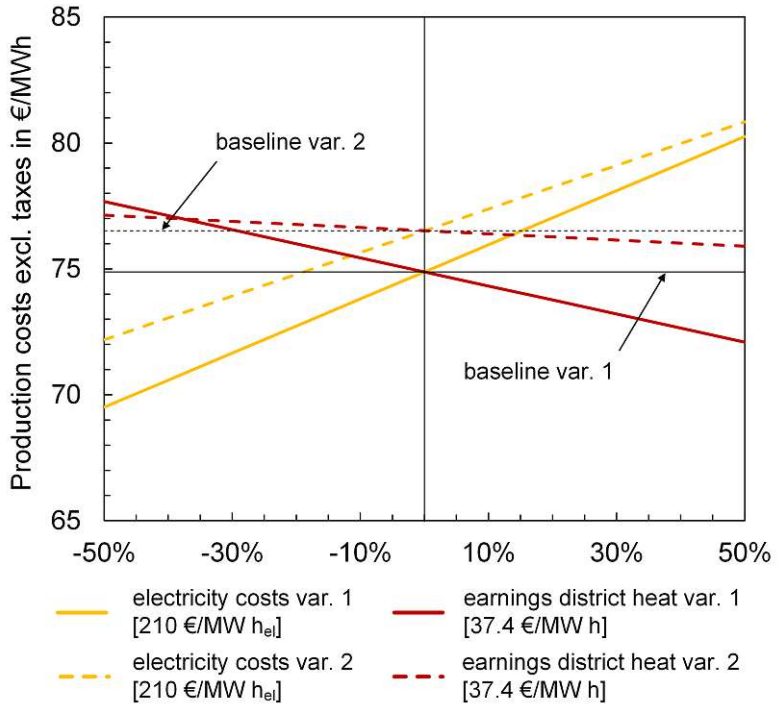

Fig. 6.6: Sensitivity in production costs to electricity costs and district heat revenues for DFB-Std variant 1 and 2

Therefore, variant 1 will be used in section 6.2.4 as the prevailing DFB-Std route for a comparison to alternative concepts.

6.2.2 Hybrid Route with External Hydrogen Addition (DFB+H_2)

The inclusion of additional H_2 to Biomass-to-Gas (*BtG*) processes can significantly increase the carbon utilization of the biomass. Fig. 6.7 depicts a PFD of such a concept. The layout is identical to the DFB-Std variant 1, except for the omittable CO_2 scrubber and the H_2 addition upstream of the fluidized bed methanation reactor. The process layout is chosen for the same reasons as previously: reducing compression energy, less pressure vessels, and enhanced, more flexible conversion to CH_4. The origin of the external H_2 is considered outside of the investigation's boundary. Nevertheless, it must be acknowledged that a renewable, continuous supply of H_2 is a crucial factor for the success of this process from a technical, economic, and ecological point of view [40, 153]. In this study, only the H_2 price (4.5 €/kg_{H_2} [125]) is considered. For a fair comparison, the simulation parameters are identical to previous concepts.

H_2 addition has multiple other effects besides increased carbon conversion and high CO_2 utilization: (i) The amount of SNG produced is increased, thus increasing the equipment size; (ii) both CO and CO_2 can be converted in the methanation unit, i.e., the heat flux density increases

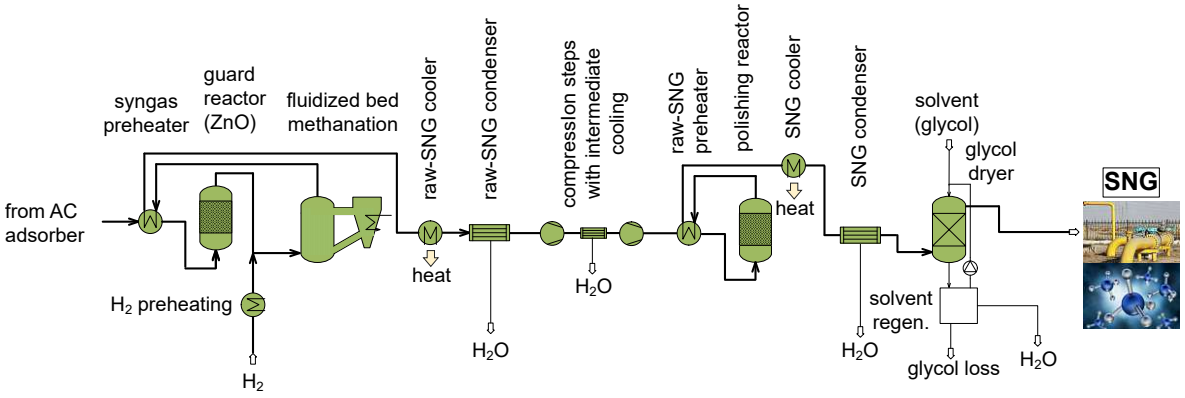

Fig. 6.7: PFD of the hybrid concept including external H_2 (DFB+H_2)

and more attention must be paid to the design of the heat exchange system; (iii) H_2 costs play a major role in determining the production costs of SNG due to the large amount of H_2 required; (iv) the stoichiometric number (SN) must be kept in a rather narrow range to ensure low enough H_2 and CO_2 contents in the SNG. The latter is shown in Fig. 6.8, where variations in SN are plotted to determine the influence of the amount of H_2 added on production costs, KPIs, and input and output streams.

To keep within the requirements of the gas grid, a narrow range fulfilling $0.975 < SN < 1.04$ must be adhered to, assuming fixed simulation parameters otherwise. Within this range, higher production costs can be expected if more H_2 is added since the costs for the additional H_2 outweigh the additional revenues from the increased amount of SNG. For the same reason, the absolute production costs are high at 121–123 €/MW h. Looking at the CH_4 content and the SNG amount at higher SN, it can be interpreted as a dilution with H_2, i.e., an increasing amount of H_2 passes through unreacted until the threshold of 10 vol.-% is reached. Of course, the amount of consumed H_2 increases accordingly. 2200–2450 kg/h H_2 are required, corresponding to 73–82 MW of chemical energy. $\eta_{CGE,o}$ and η_C are only slightly affected from the SN variation, showing a minor increase at higher numbers. Additionally, about 9500–10100 kg/h of waste water are produced, mainly in the raw-SNG condenser. The waste water from the raw-SNG condenser should be largely free of impurities and could be used to lower the fresh water consumption of electrolysis used for H_2 production. An estimation results in a remaining fresh water consumption of about 10 t/h if all of the waste water is recycled. However, the electrolyzer is not within the scope of this study and disposal costs are assumed for the waste water.

For further analyses, an SN of 0.98 is chosen to keep the H_2 consumption low. For this setting, a sensitivity analysis is performed (Fig. 6.9), showing the sensitivity of the production costs to the H_2 price, investment costs, fuel costs, and annual operating hours. The other parameters shown in section 6.1 are not displayed because of their comparatively insignificant influence. As

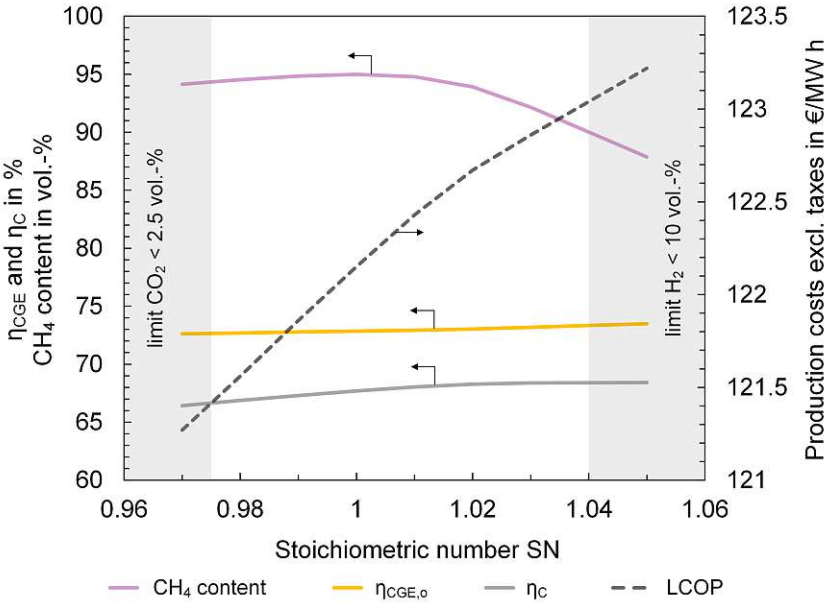

(a) Influence on the CH_4 content, cold gas efficiency ($\eta_{CGE,o}$), carbon utilization (η_C), and the production costs (LCOP)

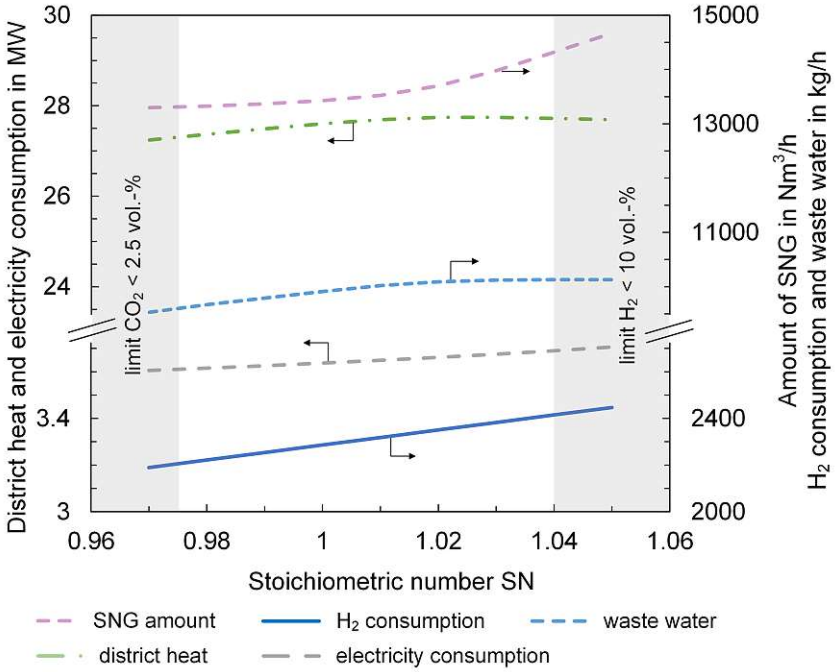

(b) Influence on the SNG amount, H_2 consumption, district heat, electricity consumption, and waste water amount

Fig. 6.8: Variation in SN showing the influence on different parameters for the 100 MW fuel input DFB+H_2 concept

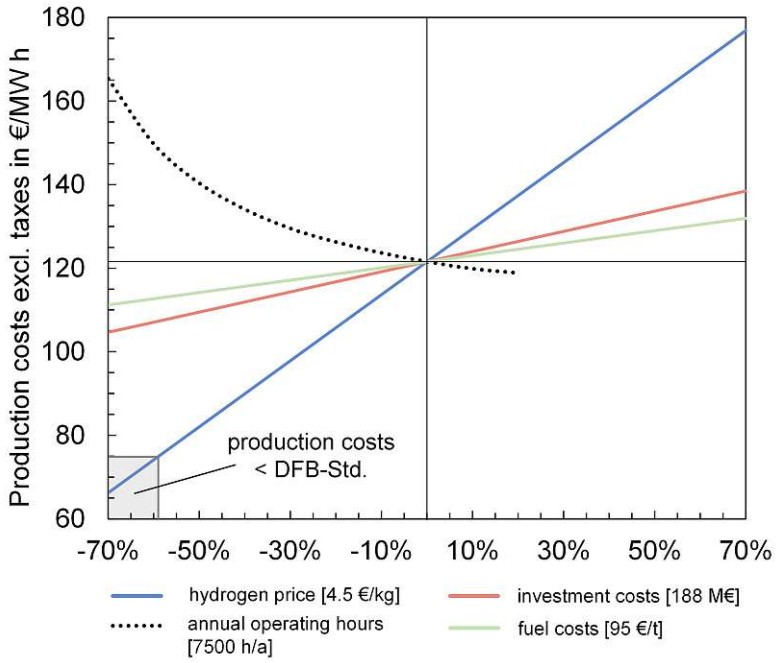

Fig. 6.9: Sensitivity in production costs to the H_2 price, investment costs, fuel costs, and annual operating hours for the DFB+H_2 concept at $SN = 0.98$

expected, the H_2 costs are the main cost driver for this concept. Only if the H_2 price is 59% lower, corresponding to 1.85 €/kg_{H_2}, equal production costs as the DFB-Std variant 1 concept would be reached. This H_2 price reduction cannot be expected even when forecasts for 2040 are considered [154, 155]. Barbuzza et al. [156] argue that integrating H_2 in SNG production can nevertheless become economically feasible if off-peak hour electricity becomes largely available due to variable renewable energy sources. However, even if this came into effect in the future, a fluctuating supply of H_2 would impose high demands on the dynamic operation of the plant or require, for example, buffer tanks to equalize these fluctuations [157, 158]. An unconsidered influence on the process is the O_2 produced by electrolysis. It could be considered as a secondary product creating revenues or utilized as a gasification or combustion agent in adapted concepts.

6.2.3 Sorption Enhanced Reforming (SER)

DFB gasification with in-situ CO_2 removal (SER) can be applied to produce syngas with a stoichiometric composition without the need for external H_2, as was discussed in section 2.2.1 and Chapter 5. Fig. 6.10 shows a PFD of the methanation section for a SER syngas. The flowsheet is almost identical to the DFB+H_2 flowsheet, except for the not needed H_2 addition.[3] Compared to the other concepts, the equipment is smaller because the removal of CO_2 already takes place in the gasifier, resulting in a lower syngas volume flow. Again, an SN variation can be carried out.

[3]The raw-SNG cooler is not displayed because no extractable heat is available between the syngas preheater and the raw-SNG condenser under the investigated process conditions.

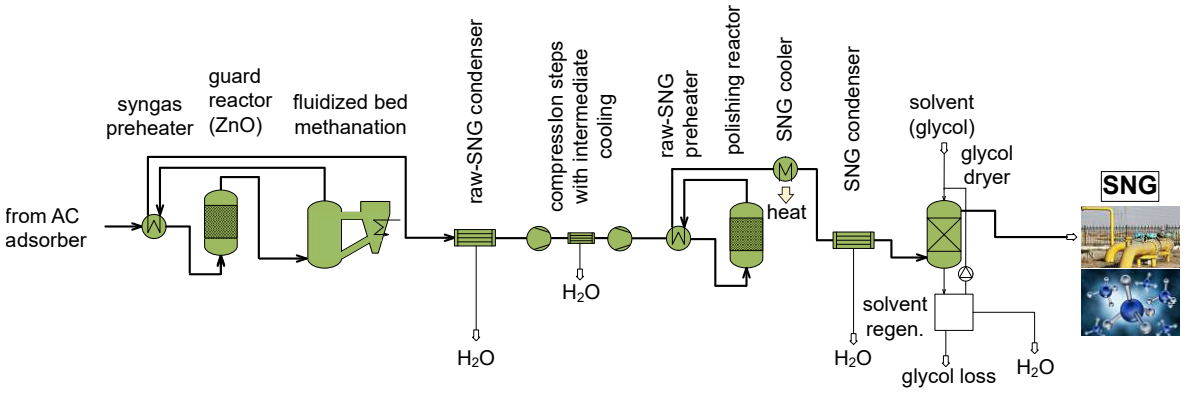

Fig. 6.10: PFD of the SER concept

In this case, the SN variation is achieved by varying the gasification parameters. The modeling follows data on the SER process provided by Brellochs [121] and Fuchs et al. [141]. The input parameters are summarized in Appendix A. Else, the same assumptions apply as for the two other concepts.

Fig. 6.11 displays the influence of the SN variation on the same parameters as in Fig. 6.8. Additionally, the gasification temperature is depicted, which is the main gasification parameter used to model the different syngas compositions. SN must be kept between 0.97 and 1.07 to adhere to the gas grid specification. The production costs show a decreasing trend towards higher SN, while $\eta_{CGE,o}$ slightly increases. The CH_4 content and η_C show maxima at $SN = 1.0$, while the electricity consumption is minimal at around $SN = 1.07$. Also, some amount of waste water needs to be disposed of. The decreasing production costs are mainly attributed to the rising energy content of the SNG with increasing SN. This brings down the energy-specific (per MW h) production costs even though the SNG amount is not monotonously increasing and the district heat amount is decreasing.

Modeling suggests a quite narrow gasification temperature window between 696 °C and 702 °C to limit SN to the needed range, similar to the results of Brellochs [121]. Of course, this is a very idealistic approach. In reality, syngas fluctuations resulting from, e.g., inhomogeneous biomass feedstock, must be considered. Additionally, other gasification parameters, like the bed material circulation rate have been found to impact the syngas composition [99]. Therefore, it is crucial to control the syngas composition and amount efficiently, factoring in all disturbances inherent to the complex gasification system. Ongoing research is performed in this context at TU Wien, setting up and testing a model predictive controller (MPC) for the DFB gasification system (Additional Paper IV) [159]. Promising results have been obtained, demonstrating a close setpoint tracking of the gasification temperature and the product gas mass flow. The methanation

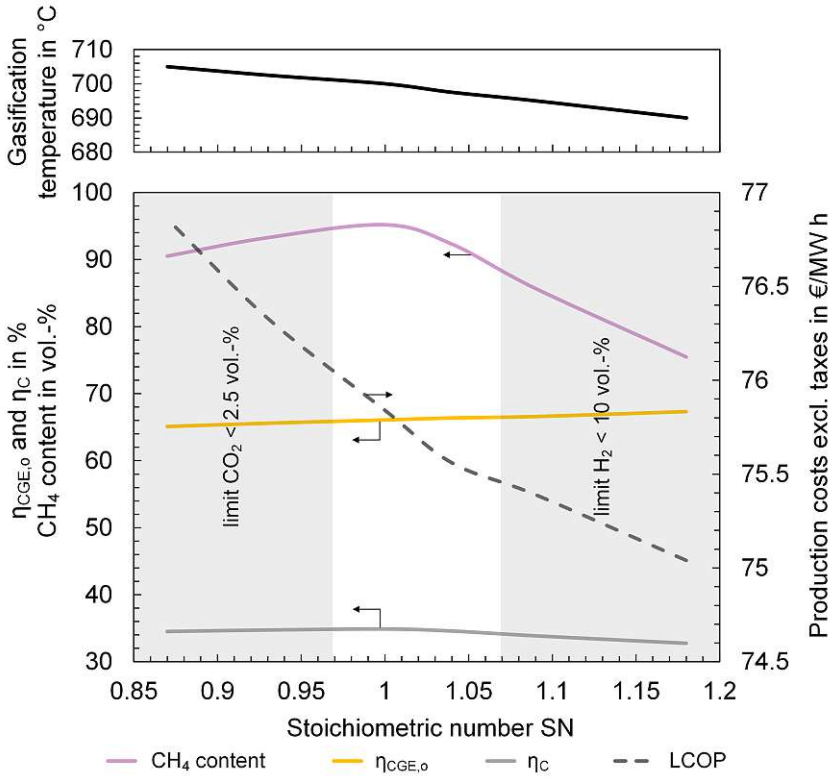

(a) Influence on the CH_4 content, cold gas efficiency ($\eta_{CGE,o}$), carbon utilization (η_C), and the production costs (LCOP)

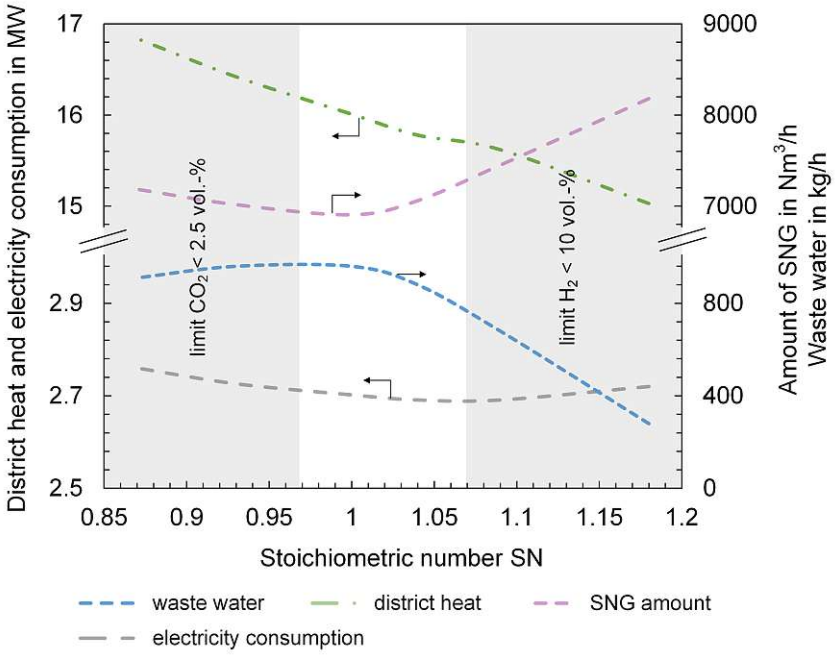

(b) Influence on the SNG amount, electricity consumption, district heat and waste water

Fig. 6.11: Variation in SN showing the influence on different parameters for the 100 MW fuel input SER concept

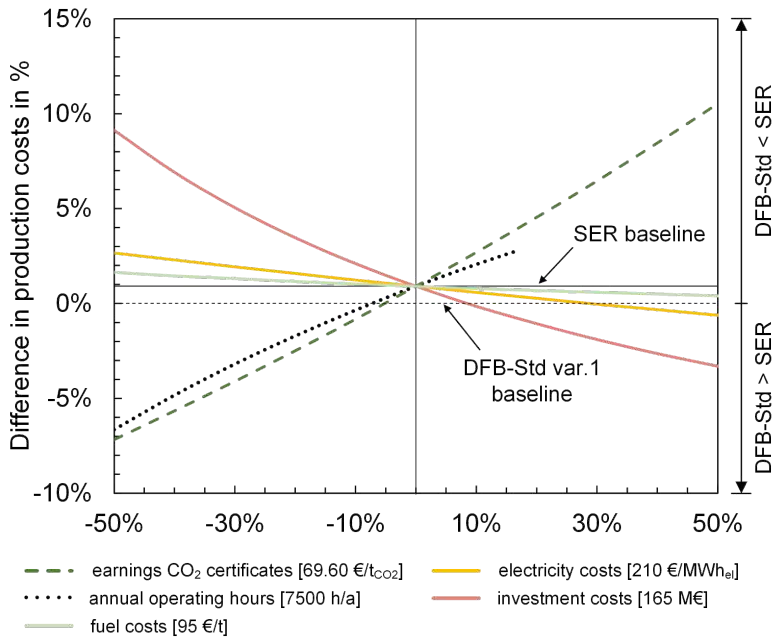

Fig. 6.12: Sensitivity in production costs to the electricity price, investment costs, fuel costs, annual operating hours, and earnings from CO_2 certificates for the SER concept at $SN = 1.06$

temperatures in the fluidized bed methanation and the polishing reactor give additional degrees of freedom in ensuring the SNG quality.

For further analysis, an overstoichiometric SN of 1.06 is chosen to exploit the advantages of this setting (e.g. lower production costs). Again, a sensitivity analysis of the production costs for the most prominent parameters is carried out. Fig. 6.12 depicts the relative sensitivity to the investment costs, electricity costs, annual operating hours, fuel costs, and the earnings from CO_2 certificates of the SER process in comparison to the DFB-Std variant 1. The earnings from CO_2 certificates are especially interesting since no concentrated CO_2 stream is acquired from the SER concept. Instead, a diluted CO_2 stream is vented to the atmosphere via the combustion reactor, while the DFB-Std concept produces around $12\,t_{CO_2}/h$ at a spot market price of $69.60\,€/t_{CO_2}$ in 2022. The base case shows 0.9% higher production costs for the SER variant. However, the SER concept would be more cost-efficient if the earnings from CO_2 certificates or the annual operating hours were 5% or 7% lower, respectively. The same is valid if the investment or electricity costs are 8% and 28% higher, respectively. Of course, vice versa, the DFB-Std concept would be more favorable.

6.2.4 Comparison of the Process Concepts

Table 6.2 summarizes and compares the main inputs and outputs, the KPIs, and the production costs of the three proposed process chains. The DFB-Std variant 1 is the cheapest overall despite producing the least amount of SNG and district heat. Thus, the efficiencies are the lowest in

Tab. 6.2: Comparison of the three proposed industrial scale process concepts for 100 MW_{th} fuel input

parameter	unit	DFB-Std variant 1	DFB+H_2	SER
input				
electricity	kW	3371	3620[a]	2690
fresh water	kg/h	148	-	-
H_2	MW	-	74.1	-
output				
SNG	Nm^3/h	6780	13330	7060
district heat	kW	12550	25820	15780
captured CO_2	Nm^3/h	6140	-	-
waste water	kg/h	-	9666	880
KPIs				
SN[b]	-	0.29	0.98	1.06
$\eta_{CGE,o}$	%	64.95	72.69	66.38
η_C	%	34.47	66.87	34.59
production costs				
$LCOP$ excl. taxes	€/MW h	74.88	121.25	75.56

[a] without electrolyzer
[b] upstream methanation

comparison. The low production costs result from the amount of concentrated CO_2, which creates additional revenues in the assumed scenario. The SER concept practically shows the same production costs and carbon utilization η_C at a slightly increased cold gas efficiency $\eta_{CGE,o}$. No CO_2 stream can be sold in this case. Nevertheless, almost the production costs of the DFB-Std variant 1 can be maintained because of the increased SNG and district heat amounts, the reduced electricity consumption, the simpler process layout, and the reduced equipment size. By adding additional H_2 to the process (DFB+H_2), the amount of SNG, district heat, and η_C is almost doubled. Furthermore, η_{CGE} increases to more than 72%. However, the definition of $\eta_{CGE,o}$ does not include electrolysis, which would lower $\eta_{CGE,o}$ to 63.3%, assuming an electrolyzer efficiency of 75% [31]. Large amounts of H_2 and water (about 10 t/h) are needed for this process, even when all the process water could be internally reused. The required chemical energy of H_2 amounts to 74 MW, which is in the same range as the chemical energy of the produced product gas. Thus, much higher production costs must be expected due to the large amounts and high price of H_2 in comparison to the produced SNG. Economically, the lack of a concentrated CO_2 stream exacerbates the situation, while an increased carbon utilization is favorable from a technical and ecological perspective. On the other hand, a pure oxygen stream would be available from electrolysis, which could create revenues or could be used as a gasification agent or within an OxySER process [160] in adapted concepts. However, these aspects are not treated within this thesis.

6.3 Implementation

Table 6.3 displays the main advantages and disadvantages of the three proposed process concepts as a decision basis. It incorporates the knowledge gained from the experimental investigations in Chapter 5 and the simulation studies in this chapter. Depending on the implementation scenario, the plant's location, the plant operator's goals, and the legal framework, the most suitable setup can be chosen considering this list.

Tab. 6.3: Advantages and disadvantages of the three proposed process concepts

concept	advantages	disadvantages
DFB-Std	– similar process proven on demonstration scale – cheapest option if CO_2 can be sold at spot market price – concentrated CO_2 stream with possibility for neg. emission via BECCS[a]	– CO_2 separation required – low carbon utilization – higher risk of catalyst deactivation through fouling due to low SN – steam addition to inlet of methanation reactor – least amount of SNG and district heat produced – economically unfavorable without CO_2 pricing
DFB+H_2	– adjustment of syngas composition to methanation requirements – doubling of η_C, SNG amount, and district heat – no CO_2 separation required – less risk of catalyst deactivation through fouling – no steam addition to inlet of methanation reactor	– high $LCOP$ due to high H_2 price and low SNG price – renewable H_2 required for ecologically viable concept – dynamic process behavior or buffer tanks required for fluctuating H_2 supply – large amounts of fresh water and electricity required for electrolysis – no usable CO_2 from an economic & ecological perspective
SER	– in-situ adjustment of product gas composition to methanation requirements – higher $\eta_{CGE,o}$ in comparison to DFB-Std concept – less risk of catalyst deactivation through fouling – no steam addition to inlet of methanation reactor – no CO_2 separation required – smaller units and less electrical power consumption – comparable $LCOP$ to DFB-Std route – economically preferred if no CO_2 is sold	– SER process industrially not proven – less stable operation in pilot plant – no increased η_C possible – exact tracking of product gas composition necessary to fulfill methanation requirements – no usable CO_2 from an economic & ecological perspective

[a] bioenergy carbon capture and storage

If the decision is made to roll out the technology and implement it into a country's energy system, a substantial contribution towards more sustainability could be achieved. Table 6.4 displays the implementation of SNG into three representative sectors of the Austrian energy system based on the DFB-Std reference case introduced in section 6.1. The results show that between 38%–57% of today's natural gas consumption of either sector could be replaced by SNG[4], which is equal to approximately 13.5 TW h in absolute numbers. Translated, this would mean that around 28 commercial-scale 100 MW_{th} plants could be erected if the full potential would be utilized. Additionally, a considerable amount of district heat would be available. From an ecological point of view, a CO_2 reduction potential of 12%–40% is calculated, depending on the considered sector.

Tab. 6.4: Comparison of possible implementation scenarios of SNG in the Austrian energy system, adapted from [125]

implementation scenario	natural gas demand[a]	substituted natural gas demand[b]	district heat	CO_2 reduction potential
SNG use in the energy sector	30.6 TW h	44%	6.7 TW h	39.4%
SNG use in the private and public sector (without mobility)	23.8 TW h	57%	5.1 TW h	40.5%
SNG use in industry	35.5 TW h	38%	7.3 TW h	12.3%

[a] current natural gas demand
[b] substitutable natural gas demand per sector, assuming a woody biomass potential of 75 PJ in 2050

The 13.5 TW h are opposed by an overall Austrian natural gas demand of about 90 TW h in 2021 [161] and an expected demand between 15–114 TW h in 2040, depending on the applied scenario [162]. Thus, 15% of the natural gas demand in 2021 or 12%–90% of the natural gas demand in 2040 could be replaced. Other studies have determined the potential of SNG from thermochemical processes in Austria ranging from 9 TW h to 42 TW h p.a. [81, 162, 163]. This study is within the lower range, resulting from the assumed woody biomass potential of 20.8 TW h (75 PJ) in 2050 (cf. [125]). This assumption excludes residual and waste materials because the implications on the process are not comprehensively studied in this work. If residual and waste materials would be considered as additional feedstock, each of the considered sector's natural gas consumption could be almost completely replaced, as **Paper V** shows. Of course, it needs to be taken into account that this is a theoretical consideration implying a maximum SNG usage scenario. Biomass is a valuable renewable carbon source and other products will be produced as well. Simultaneously, multiple other technologies are available to defossilize the three mentioned sectors. In the energy sector, RES, like wind and photovoltaics, as well as heat pumps and waste heat recovery for district heat production, will play an important role.

[4]Note that the numbers are meant as "either this sector or another sector" can be substituted, not all at once.

Similarly, heat pumps, solar thermal systems, and wood-fired boilers could provide the necessary heat in the public and private sectors. In industry, there is the possibility to switch to alternative production processes or provide high-temperature heat via increased waste heat recovery, H_2, or high-temperature heat pumps [125]. Nevertheless, gaseous energy carriers are forecasted to remain essential energy carriers in the future [5]. Especially peak-load coverage in the energy sector could be a valuable application with a substantial CO_2 reduction potential. Similarly, the provision of high-temperature heat in industrial processes lacks alternatives and could be an important application of SNG in the future.

Chapter 7

Conclusion & Outlook

The production of synthetic natural gas (*SNG*) from biomass presents a possibility to contribute to the defossilization of the energy system. Catalytic methanation processes have been applied to syngas from coal gasification for decades. Over the last two decades, the focus has shifted to converting biomass resources for a sustainable development in Europe. Dual fluidized bed (*DFB*) gasification has shown its capabilities to produce syngas and even SNG via catalytic methanation processes on a demonstration scale. Nevertheless, technological advances are necessary to allow a faster transformation to a sustainable future.

This work merged theoretical, experimental, and simulation-based investigations to develop fluidized bed methanation in combination with advanced DFB steam gasification further. Thermodynamic analyses were carried out to assess the impact of DFB gasification and sorption enhanced reforming (*SER*) under varying parameters on methanation. A full process chain, including gas cleaning units and a fluidized bed methanation reactor, was designed, set up, and investigated to demonstrate the production of SNG in combination with advanced DFB steam gasification, H_2 addition and SER. Simultaneously, impurities were tracked to gain more insight into the gas cleaning processes. Based on the acquired knowledge, simulation studies were carried out to evaluate advanced SNG production processes from a technical, economic, and ecological point of view. The conducted research allows the following conclusion to be drawn.

- Fluidized bed methanation is suitable for a single-stage, mid-temperature conversion of product gas to raw synthetic natural gas (*raw-SNG*) under nearly isothermal conditions and at nearly ambient pressure. Optimal reaction temperatures are between 320 and 360 °C, maximizing conversion.

- The prepared Ni/$\gamma-Al_2O_3$ catalyst proved to be well-suited for fluidized bed applications. No significant chemical deactivation or mechanical attrition was observed with the applied fluidized bed reactor.

- Investigations indicated that no water-gas shift (*WGS*) or olefine hydrogenation unit was necessary when applying fluidized bed methanation with the prepared catalyst in contrast to fixed-bed methanation.

- The gas grid specifications demand a CO limit of 0.1 mol.-%. This threshold level was found to be the most critical limitation, requiring a further conversion in a polishing reactor. If external H_2 is added or an SER product gas is methanated, the 10 mol-% H_2 or 2.5 mol-% CO_2 threshold can be limiting.

- The advanced process layout, utilizing unpressurized fluidized bed methanation and fixed-bed polishing, was shown to produce a higher-quality gas at slightly lower costs while reducing the requirements for the catalyst's activity due to the higher reaction temperature and significantly decreasing the electricity consumption by 17%–38%.

- From an economic point of view, SNG production can almost compete with the industrial price of fossil natural gas at 90 €/MW h in 2022, assuming revenues from the secondary products district heat and CO_2.

- SER, combined with fluidized bed methanation, was shown to be feasible and resulted in a more efficient process with fewer and smaller equipment. It should be applied due to its economic advantage, especially if no CO_2 can be sold as a secondary product.

- The utilization of external H_2 efficiently utilizes the valuable biomass carbon. About 2/3 of the biomass carbon can be transformed into CH_4 instead of 1/3. The efficient use of the sole renewable carbon source is highly desired from a technical and ecological perspective. However, H_2 costs are the main costs drivers. The H_2 costs would have to drop by 60% to make it economically competitive with the other concepts.

- SNG can significantly contribute to a greenhouse gas emission reduction presuming a sustainable use of biomass resources. Especially, the application for peak-load coverage in the energy sector or high-temperature heat provision in industry could lead to an emission reduction of 39% and 12%, respectively.

While this work provides some answers, more questions arise which need answering.

- An internally circulating fluidized bed (*ICFB*) reactor was designed and investigated. However, this work has not applied the internal circulation to methanation. The suggestions provided should be followed up for advanced methanation concepts.

- An advanced process layout was proposed and backed up by simulation. However, the experimental proof producing SNG according to the gas grid specifications is missing.
- The operational stability of the SER process should be increased and demonstrated on a larger scale. Additionally, the production of grid-feedable SNG via the SER process with the proposed methanation concept needs to be shown experimentally.
- H_2 addition in a hybrid concept requires more thought on how a dynamic operation could be integrated from a technical point of view. Furthermore, oxygen as a secondary product from electrolysis should be considered. Additionally, the production of grid-feedable SNG via the hybrid process with the proposed methanation concept needs to be shown experimentally.
- The mechanical and chemical stability of the catalyst was shown. However, longer-term experiments under standardized conditions and a dedicated test rig would provide more reliable results.
- Impurities were tracked throughout the process chain. However, gas cleaning of DFB product gas is still opaque considering the amount of substances involved. Fundamental correlations are missing and should be developed to provide an engineering basis for plant design.
- Residues and waste materials should be further investigated to strengthen the circular economy, reduce feedstock costs, and increase the biomass availability.
- The overall process is complex, and understanding the internal correlations is not trivial. Thus, advanced control, automation, and optimization strategies should be implemented for an efficient and cost-effective process.
- CH_4 is the simplest hydrocarbon foremost utilized as a combustion fuel. Furthermore, it has a comparatively low market value. Alternative products could be produced from syngas which have a higher market value and allow a material use of the biomass carbon.

In summary, this work suggests unpressurized fluidized bed methanation with an optimized catalyst and with fixed-bed polishing in combination with SER and advanced DFB gasification, resulting in technical and economic advantages (e.g. significantly reduced electricity consumption). It suggests the application of SNG in the industrial and energy sector, where alternatives are scarce in some applications and a significant greenhouse gas emission reduction could be achieved with the estimated additional biomass potential. The gained knowledge in this work supports the technology development during scale-up and incentivises research into these novel concepts, for

example, within a future "Reallabor" demonstration. Furthermore, it shows potential stakeholders that SNG can be economically competitive and ecologically beneficial, eventually supporting the transition towards a climate neutral energy system.

Bibliography

[1] UN General Assembly. *Transforming our world : the 2030 Agenda for Sustainable Development*. 2015. URL: https://www.refworld.org/docid/57b6e3e44.html (visited on 01/14/2024).

[2] United Nation Framework Convention on Climate Change. *The Paris Agreement*. 2016. URL: https://unfccc.int/documents/184656 (visited on 01/14/2024).

[3] United Nation Framework Convention on Climate Change. *COP28 Agreement Signals "Beginning of the End" of the Fossil Fuel Era*. 2023. URL: https://unfccc.int/news/cop28-agreement-signals-beginning-of-the-end-of-the-fossil-fuel-era (visited on 01/14/2024).

[4] IPCC. *Climate Change 2023: Synthesis Report: Contribution of Working Groups I, II and III to the Sixth Assessment Report of the Intergovernmental Panel on Climate Change*. Geneva, Switzerland, 2023. DOI: 10.59327/IPCC/AR6-9789291691647.

[5] IEA. *World Energy Outlook 2022*. Ed. by IEA. Paris, 2022. URL: https://www.iea.org/reports/world-energy-outlook-2022 (visited on 10/22/2023).

[6] S. Dunn. "Hydrogen futures: Toward a sustainable energy system". In: *International Journal of Hydrogen Energy* 27.3 (2002), pp. 235–264. DOI: 10.1016/S0360-3199(01)00131-8.

[7] T. J. Schildhauer and S. M. Biollaz, eds. *Synthetic Natural Gas from Coal, Dry Biomass, and Power-to-Gas Applications*. Hoboken, New Jersey: John Wiley & Sons, 2016.

[8] J. Kopyscinski, T. J. Schildhauer, and S. M. Biollaz. "Production of synthetic natural gas (SNG) from coal and dry biomass - A technology review from 1950 to 2009". In: *Fuel* 89.8 (2010), pp. 1763–1783. DOI: 10.1016/j.fuel.2010.01.027.

[9] IPCC. *Climate Change 2021 - The Physical Science Basis: Contribution of Working Group I to the Sixth Assessment Report of the Intergovernmental Panel on Climate Change*. United Kingdom and New York: Cambridge University Press, 2023. DOI: 10.1017/9781009157896.

[10] Austrian Federal Ministry for Agriculture, Forestry, Regions and Water Management. *Biogas aus Österreich: Erneuerbare-Gase-Gesetz geht in Begutachtung*. 2023. URL: https://info.bml.gv.at/themen/wald/wald-und-klima/erneuerbare-gase-gesetz-in-begutachtung.html (visited on 10/05/2023).

[11] J. Kopyscinski, T. J. Schildhauer, and S. M. A. Biollaz. "Methanation in a fluidized bed reactor with high initial CO partial pressure : Part I—Experimental investigation of hydrodynamics, mass transfer effects, and carbon deposition". In: *Chemical Engineering Science* 66.5 (2011), pp. 924–934. DOI: 10.1016/j.ces.2010.11.042.

[12] M. C. Seemann, T. J. Schildhauer, and S. M. A. Biollaz. "Fluidized Bed Methanation of Wood-Derived Producer Gas for the Production of Synthetic Natural Gas". In: *Industrial & Engineering Chemistry Research* 49.15 (2010), pp. 7034–7038. DOI: 10.1021/ie100510m.

[13] H. Thunman, M. Seemann, T. Berdugo Vilches, J. Maric, D. Pallares, H. Ström, G. Berndes, P. Knutsson, A. Larsson, C. Breitholtz, and O. Santos. "Advanced biofuel production via gasification – lessons learned from 200 man-years of research activity with Chalmers' research gasifier and the GoBiGas demonstration plant". In: *Energy Science and Engineering* 6.1 (2018), pp. 6–34. DOI: 10.1002/ese3.188.

[14] H. Hiller, R. Reimert, and H.-M. Stönner. "Gas Production, 1. Introduction". In: *Ullmann's encyclopedia of industrial chemistry*. Weinheim and Wiley online library: Wiley-VCH, 2010. DOI: 10.1002/14356007.a12_169.pub3.

[15] S. Rönsch and A. Ortwein. "Methanisierung von Synthesegasen - Grundlagen und Verfahrensentwicklungen". In: *Chemie Ingenieur Technik* 83.8 (2011), pp. 1200–1208. DOI: 10.1002/cite.201100013.

[16] P. Sabatier and Senderes J.B. "Direct hydrogenation of oxides of carbon in presence of various finely divided metals". In: *Comptes rendus de l'Académie des sciences* 134.1 (1902), pp. 689–691.

[17] S. Rönsch, J. Schneider, S. Matthischke, M. Schlüter, M. Götz, J. Lefebvre, P. Prabhakaran, and S. Bajohr. "Review on methanation—From fundamentals to current projects". In: *Fuel* 166 (2016), pp. 276–296. DOI: 10.1016/j.fuel.2015.10.111.

[18] S. Rönsch and M. Kaltschmitt. "Bio-SNG production — concepts and their assessment". In: *Biomass Conversion and Biorefinery* 2.4 (2012), pp. 285–296. DOI: 10.1007/s13399-012-0048-0.

[19] B. Lecker, L. Illi, A. Lemmer, and H. Oechsner. "Biological hydrogen methanation - A review". In: *Bioresource Technology* 245 (2017), pp. 1220–1228. DOI: 10.1016/j.biortech.2017.08.176.

[20] H. Hofbauer, M. Kaltschmitt, F. Keil, U. Neuling, and H. Wagner. "Vergasung in der Gasatmosphäre". In: *Energie aus Biomasse*. Ed. by M. Kaltschmitt, H. Hartmann, and H. Hofbauer. Berlin, Heidelberg: Springer Berlin Heidelberg, 2016, pp. 1059–1182. DOI: 10.1007/978-3-662-47438-9_13.

[21] S. Schwede, F. Bruchmann, E. Thorin, and M. Gerber. "Biological Syngas Methanation via Immobilized Methanogenic Archaea on Biochar". In: *Energy Procedia* 105 (2017), pp. 823–829. DOI: 10.1016/j.egypro.2017.03.396.

[22] F. Vogel. "Hydrothermale Verfahren". In: *Energie aus Biomasse*. Ed. by M. Kaltschmitt, H. Hartmann, and H. Hofbauer. Berlin, Heidelberg: Springer Berlin Heidelberg, 2016, pp. 1267–1337. DOI: 10.1007/978-3-662-47438-9_15.

[23] G. Peng, F. Vogel, D. Refardt, and C. Ludwig. "Catalytic Supercritical Water Gasification: Continuous Methanization of Chlorella vulgaris". In: *Industrial & Engineering Chemistry Research* 56.21 (2017), pp. 6256–6265. DOI: 10.1021/acs.iecr.7b00042.

[24] D. C. Elliott, G. G. Neuenschwander, T. R. Hart, R. S. Butner, A. H. Zacher, M. H. Engelhard, J. S. Young, and D. E. McCready. "Chemical Processing in High-Pressure Aqueous Environments. 7. Process Development for Catalytic Gasification of Wet Biomass Feedstocks". In: *Industrial & Engineering Chemistry Research* 43.9 (2004), pp. 1999–2004. DOI: 10.1021/ie034303o.

[25] A. Molino, F. Nanna, Y. Ding, B. Bikson, and G. Braccio. "Biomethane production by anaerobic digestion of organic waste". In: *Fuel* 103 (2013), pp. 1003–1009. DOI: 10.1016/j.fuel.2012.07.070.

[26] C. Da Costa Gomez. "Biogas as an energy option: an overview". In: *The Biogas Handbook*. Elsevier, 2013, pp. 1–16. DOI: 10.1533/9780857097415.1.

[27] M. Sposob, R. Wahid, and K. Fischer. "Ex-situ biological CO_2 methanation using trickle bed reactor: review and recent advances". In: *Reviews in Environmental Science and Bio/Technology* (2021). DOI: 10.1007/s11157-021-09589-7.

[28] M. A. Voelklein, D. Rusmanis, and J. D. Murphy. "Biological methanation: Strategies for in-situ and ex-situ upgrading in anaerobic digestion". In: *Applied Energy* 235 (2019), pp. 1061–1071. DOI: 10.1016/j.apenergy.2018.11.006.

[29] A. Bensmann, R. Hanke-Rauschenbach, R. Heyer, F. Kohrs, D. Benndorf, U. Reichl, and K. Sundmacher. "Biological methanation of hydrogen within biogas plants: A model-based feasibility study". In: *Applied Energy* 134 (2014), pp. 413–425. DOI: 10.1016/j.apenergy.2014.08.047.

[30] M. Götz, J. Lefebvre, F. Mörs, A. McDaniel Koch, F. Graf, S. Bajohr, R. Reimert, and T. Kolb. "Renewable Power-to-Gas: A technological and economic review". In: *Renewable Energy* 85 (2016), pp. 1371–1390. DOI: 10.1016/j.renene.2015.07.066.

[31] S. A. Grigoriev, V. N. Fateev, D. G. Bessarabov, and P. Millet. "Current status, research trends, and challenges in water electrolysis science and technology". In: *International Journal of Hydrogen Energy* 45.49 (2020), pp. 26036–26058. DOI: 10.1016/j.ijhydene.2020.03.109.

[32] D. Karatza, C. Konstantopoulos, S. Chianese, S. Diplas, P. Svec, E. Hristoforou, and D. Musmarra. "Hydrogen production through water splitting at low temperature over Fe_3O_4 pellet: Effects of electric power, magnetic field, and temperature". In: *Fuel Processing Technology* 211 (2021). DOI: 10.1016/j.fuproc.2020.106606.

[33] F. Safari and I. Dincer. "A review and comparative evaluation of thermochemical water splitting cycles for hydrogen production". In: *Energy Conversion and Management* 205 (2020). DOI: 10.1016/j.enconman.2019.112182.

[34] J. Castro, J. Leaver, and S. Pang. "Simulation and Techno-Economic Assessment of Hydrogen Production from Biomass Gasification-Based Processes: A Review". In: *Energies* 15.22 (2022). DOI: 10.3390/en15228455.

[35] T. Singh, A. Alhazmi, A. Mohammad, N. Srivastava, S. Haque, S. Sharma, R. Singh, T. Yoon, and V. K. Gupta. "Integrated biohydrogen production via lignocellulosic waste: Opportunity, challenges & future prospects". In: *Bioresource Technology* 338 (2021). DOI: 10.1016/j.biortech.2021.125511.

[36] A. Hauser, P. Wolf-Zoellner, S. Haag, S. Dettori, X. Tang, M. Mighani, I. Matino, C. Mocci, V. Colla, S. Kolb, M. Bampaou, K. Panopoulos, N. Kieberger, K. Rechberger, and J. Karl. "Valorizing Steelworks Gases by Coupling Novel Methane and Methanol Synthesis Reactors with an Economic Hybrid Model Predictive Controller". In: *Metals* 12.6 (2022). DOI: 10.3390/met12061023.

[37] S. Kleiber, A. Loder, M. Siebenhofer, A. Böhm, and S. Lux. "Direct Reduction of Siderite Ore Combined with Catalytic CO/CO_2 Hydrogenation to Methane and Methanol: A

Technology Concept". In: *Chemie Ingenieur Technik* 94.5 (2022), pp. 701–711. DOI: 10.1002/cite.202100189.

[38] A. Bartik, F. Benedikt, J. Fuchs, H. Hofbauer, and S. Müller. "Experimental investigation of hydrogen-intensified synthetic natural gas production via biomass gasification: a technical comparison of different production pathways". In: *Biomass Conversion and Biorefinery* (2023). DOI: 10.1007/s13399-023-04341-3.

[39] J. Witte, J. Settino, S. M. Biollaz, and T. J. Schildhauer. "Direct catalytic methanation of biogas—Part I: New insights into biomethane production using rate-based modelling and detailed process analysis". In: *Energy Conversion and Management* 171 (2018), pp. 750–768. DOI: 10.1016/j.enconman.2018.05.056.

[40] M. Gassner and F. Maréchal. "Thermo-economic optimisation of the integration of electrolysis in synthetic natural gas production from wood". In: *Energy* 33.2 (2008), pp. 189–198. DOI: 10.1016/j.energy.2007.09.010.

[41] C. H. Bartholomew. "Mechanisms of catalyst deactivation". In: *Applied Catalysis A: General* 212.1-2 (2001), pp. 17–60. DOI: 10.1016/S0926-860X(00)00843-7.

[42] A. Bartik, F. Benedikt, A. Lunzer, C. Walcher, S. Müller, and H. Hofbauer. "Thermodynamic investigation of SNG production based on dual fluidized bed gasification of biogenic residues". In: *Biomass Conversion and Biorefinery* 11 (2020), pp. 95–110. DOI: 10.1007/s13399-020-00910-y.

[43] F. Benedikt, M. Kuba, J. Christian, S. Müller, and H. Hofbauer. "Assessment of correlations between tar and product gas composition in dual fluidized bed steam gasification for online tar prediction". In: *Applied Energy* 238 (2019), pp. 1138–1149. DOI: 10.1016/j.apenergy.2019.01.181.

[44] J. Kopyscinski, M. C. Seemann, R. Moergeli, S. Biollaz, and T. J. Schildhauer. "Synthetic natural gas from wood: Reactions of ethylene in fluidised bed methanation". In: *Applied Catalysis A: General* 462-463 (2013), pp. 150–156. DOI: 10.1016/j.apcata.2013.04.038.

[45] J. Gao, Y. Wang, Y. Ping, D. Hu, G. Xu, and F. Su. "A thermodynamic analysis of methanation reactions of carbon oxides for the production of synthetic natural gas". In: *RSC Advances* 2.6 (2012), pp. 2358–2368. DOI: 10.1039/c2ra00632d.

[46] J. Li, L. Zhou, P. Li, Q. Zhu, J. Gao, F. Gu, and F. Su. "Enhanced fluidized bed methanation over a Ni/Al_2O_3 catalyst for production of synthetic natural gas". In: *Chemical Engineering Journal* 219 (2013), pp. 183–189. DOI: 10.1016/j.cej.2013.01.005.

[47] J. Kopyscinski, T. J. Schildhauer, and S. M. Biollaz. "Employing Catalyst Fluidization to Enable Carbon Management in the Synthetic Natural Gas Production from Biomass". In: *Chemical Engineering Technology* 32.3 (2009), pp. 343–347. DOI: 10.1002/ceat.200800413.

[48] V. Frick, J. Brellochs, and M. Specht. "Application of ternary diagrams in the design of methanation systems". In: *Fuel Processing Technology* 118 (2014), pp. 156–160. DOI: 10.1016/j.fuproc.2013.08.022.

[49] X. Bai, S. Wang, T. Sun, and S. Wang. "Influence of Operating Conditions on Carbon Deposition Over a Ni Catalyst for the Production of Synthetic Natural Gas (SNG) from Coal". In: *Catalysis Letters* 144 (2014), pp. 2157–2166. DOI: 10.1007/s10562-014-1379-1.

[50] M. Vannice. "The catalytic synthesis of hydrocarbons from H_2/CO mixtures over the group VIII metals: I. The specific activities and product distributions of supported metals". In: *Journal of Catalysis* 37.3 (1975), pp. 449–461. DOI: 10.1016/0021-9517(75)90181-5.

[51] G. A. Mills and F. W. Steffgen. "Catalytic Methanation". In: *Catalysis Reviews* 8.1 (1974), pp. 159–210. DOI: 10.1080/01614947408071860.

[52] I. Kuznecova and J. Gusca. "Property based ranking of CO and CO_2 methanation catalysts". In: *Energy Procedia* 128 (2017), pp. 255–260. DOI: 10.1016/j.egypro.2017.09.068.

[53] J. Ren, Y.-L. Liu, X.-Y. Zhao, and J.-P. Cao. "Methanation of syngas from biomass gasification: An overview". In: *International Journal of Hydrogen Energy* 45.7 (2020), pp. 4223–4243. DOI: 10.1016/j.ijhydene.2019.12.023.

[54] J. Gao, Q. Liu, F. Gu, B. Liu, Z. Zhong, and F. Su. "Recent advances in methanation catalysts for the production of synthetic natural gas". In: *RSC Advances* 5.29 (2015), pp. 22759–22776. DOI: 10.1039/C4RA16114A.

[55] P. Frontera, A. Macario, M. Ferraro, and P. L. Antonucci. "Supported catalysts for CO_2 methanation: A review". In: *Catalysts* 7.2 (2017), pp. 1–28. DOI: 10.3390/catal7020059.

[56] D. Hu, J. Gao, Y. Ping, L. Jia, P. Gunawan, Z. Zhong, G. Xu, F. Gu, and F. Su. "Enhanced Investigation of CO Methanation over Ni/Al_2O_3 Catalysts for Synthetic Natural Gas Production". In: *Industrial & Engineering Chemistry Research* 51.13 (2012), pp. 4875–4886. DOI: 10.1021/ie300049f.

[57] A. Kambolis, T. J. Schildhauer, and O. Kröcher. "CO Methanation for Synthetic Natural Gas Production". In: *Chimia* 69.10 (2015), pp. 608–613. DOI: 10.2533/chimia.2015.608.

[58] G. Zhang, T. Sun, J. Peng, S. Wang, and S. Wang. "A comparison of Ni/SiC and Ni/Al_2O_3 catalyzed total methanation for production of synthetic natural gas". In: *Applied Catalysis A: General* 462-463 (2013), pp. 75–81. DOI: 10.1016/j.apcata.2013.04.037.

[59] H. Zhu, R. Razzaq, C. Li, Y. Muhmmad, and S. Zhang. "Catalytic Methanation of Carbon Dioxide by Active Oxygen Material $Ce_xZr_{1-x}O_2$ Supported Ni−Co Bimetallic Nanocatalysts". In: *AIChE Journal* 59.7 (2013), pp. 2567–2576. DOI: 10.1002/aic.14026.

[60] S. Hwang, J. Lee, U. G. Hong, J. G. Seo, J. C. Jung, D. J. Koh, H. Lim, C. Byun, and I. K. Song. "Methane production from carbon monoxide and hydrogen over nickel–alumina xerogel catalyst: Effect of nickel content". In: *Journal of Industrial and Engineering Chemistry* 17.1 (2011), pp. 154–157. DOI: 10.1016/j.jiec.2010.12.015.

[61] J. Gao, C. Jia, J. Li, M. Zhang, F. Gu, G. Xu, Z. Zhong, and F. Su. "Ni/Al_2O_3 catalysts for CO methanation: Effect of Al_2O_3 supports calcined at different temperatures". In: *Journal of Energy Chemistry* 22.6 (2013), pp. 919–927. DOI: 10.1016/S2095-4956(14)60273-4.

[62] Y. H. Choi and W. Y. Lee. "Effect of Ni loading and calcination temperature on catalyst performance and catalyst deactivation of Ni/SiO_2 in the hydrodechlorination of 1,2–dichloropropane into propylene". In: *Catalysis Letters* 67.2/4 (2000), pp. 155–161. DOI: 10.1023/A:1019038110181.

[63] J. C. Schmid, F. Benedikt, J. Fuchs, A. M. Mauerhofer, S. Müller, and H. Hofbauer. "Syngas for biorefineries from thermochemical gasification of lignocellulosic fuels and residues—5 years' experience with an advanced dual fluidized bed gasifier design". In: *Biomass Conversion and Biorefinery* 11 (2021), pp. 2405–2442. DOI: 10.1007/s13399-019-00486-2.

[64] A. Molino, V. Larocca, S. Chianese, and D. Musmarra. "Biofuels production by biomass gasification: A review". In: *Energies* 11.4 (2018). DOI: 10.3390/en11040811.

[65] W. Boll, G. Hochgesand, C. Higman, E. Supp, P. Kalteier, W.-.-D. Müller, M. Kriebel, H. Schlichting, and H. Tanz. "Gas Production, 3. Gas Treating". In: *Ullmann's encyclopedia of industrial chemistry*. Weinheim and Wiley online library: Wiley-VCH, 2010. DOI: 10.1002/14356007.o12_o02.

[66] F. Feng, G. Song, J. Xiao, L. Shen, and S. V. Pisupati. "Carbon deposition on Ni-based catalyst with TiO_2 as additive during the syngas methanation process in a fluidized bed reactor". In: *Fuel* 235 (2019), pp. 85–91. DOI: 10.1016/j.fuel.2018.07.076.

[67] G. D. Weatherbee. "Hydrogenation of CO_2 on group VIII metals: II. Kinetics and mechanism of CO_2 hydrogenation on nickel". In: *Journal of Catalysis* 77.2 (1982), pp. 460–472. DOI: 10.1016/0021-9517(82)90186-5.

[68] J. Kopyscinski, T. J. Schildhauer, and S. M. A. Biollaz. "Methanation in a fluidized bed reactor with high initial CO partial pressure : Part II—Modeling and sensitivity study". In: *Chemical Engineering Science* 66.8 (2011), pp. 1612–1621. DOI: 10.1016/j.ces.2010.12.029.

[69] S. Rönsch, J. Köchermann, J. Schneider, and S. Matthischke. "Global Reaction Kinetics of CO and CO_2 Methanation for Dynamic Process Modeling". In: *Chemical Engineering & Technology* 39.2 (2016), pp. 208–218. DOI: 10.1002/ceat.201500327.

[70] L. Grossgasteiger. "Dynamic modeling and control of a fluidized bed methanation reactor". Master Thesis. Vienna: TU Wien, 2022. DOI: 10.34726/hss.2022.105021.

[71] J. M. Panek and J. Grasser. *Practical experience gained during the first twenty years of operation of the great plains gasification plant and implications for future projects*. Ed. by US Department of Energy-Office of Fossil Energy. Washington, 2006.

[72] T. J. Schildhauer and S. M. Biollaz. "Reactors for catalytic methanation in the conversion of biomass to synthetic natural gas (SNG)". In: *Chimia* 69.10 (2015), pp. 603–607. DOI: 10.2533/chimia.2015.603.

[73] P. Biegger, F. Kirchbacher, A. Roza Medved, M. Miltner, M. Lehner, and M. Harasek. "Development of honeycomb methanation catalyst and its application in power to gas systems". In: *Energies* 11.7 (2018), pp. 1–17. DOI: 10.3390/en11071679.

[74] Z. Liu, B. Chu, X. Zhai, Y. Jin, and Y. Cheng. "Total methanation of syngas to synthetic natural gas over Ni catalyst in a micro-channel reactor". In: *Fuel* 95 (2012), pp. 599–605. DOI: 10.1016/j.fuel.2011.12.045.

[75] O. Görke, P. Pfeifer, and K. Schubert. "Highly selective methanation by the use of a microchannel reactor". In: *Catalysis Today* 110.1-2 (2005), pp. 132–139. DOI: 10.1016/j.cattod.2005.09.009.

[76] D. Kunii and O. Levenspiel. *Fluidization engineering*. 2. ed. Butterworth-Heinemann series in chemical engineering. Boston: Butterworth-Heinemann, 1991.

[77] AlphaSYNT. *Erneuerbare Energieträger durch CO_2-Upcycling*. 2024. URL: https://alphasynt.ch/ (visited on 01/14/2024).

[78] M. Götz, S. Bajohr, F. Graf, R. Reimert, and T. Kolb. "Einsatz eines Blasensäulenreaktors zur Methansynthese". In: *Chemie Ingenieur Technik* 85.7 (2013), pp. 1146–1151. DOI: 10.1002/cite.201200212.

[79] J. Lefebvre, M. Götz, S. Bajohr, R. Reimert, and T. Kolb. "Improvement of three-phase methanation reactor performance for steady-state and transient operation". In: *Fuel Processing Technology* 132 (2015), pp. 83–90. DOI: 10.1016/j.fuproc.2014.10.040.

[80] M. Thema, T. Weidlich, M. Hörl, A. Bellack, F. Mörs, F. Hackl, M. Kohlmayer, J. Gleich, C. Stabenau, T. Trabold, M. Neubert, F. Ortloff, R. Brotsack, D. Schmack, H. Huber, et al. "Biological CO_2-Methanation: An Approach to Standardization". In: *Energies* 12.9 (2019), p. 1670. DOI: 10.3390/en12091670.

[81] H. Hofbauer, A. M. Mauerhofer, F. Benedikt, M. Hammerschmid, A. Bartik, M. Veress, R. Haas, M. Siebenhofer, and G. Resch. *Reallabor zur Herstellung von FT-Treibstoffen und SNG aus Biomasse und biogenen Reststoffen für die Land- und Forstwirtschaft*. Ed. by Bundesministerium für Landwirtschaft, Regionen und Tourismus. Vienna, 2020. URL: https://dafne.at/projekte/ftsng-reallabor (visited on 10/23/2023).

[82] V. Wilk. "Extending the range of feedstock of the dual fluidized bed gasification process towards residues and waste". Dissertation. Vienna: TU Wien, 2013. URL: http://katalog.ub.tuwien.ac.at/AC10774880.

[83] F. Benedikt, J. C. Schmid, J. Fuchs, A. M. Mauerhofer, S. Müller, and H. Hofbauer. "Fuel flexible gasification with an advanced 100 kW dual fluidized bed steam gasification pilot plant". In: *Energy* 164 (2018), pp. 329–343. DOI: 10.1016/j.energy.2018.08.146.

[84] F. Benedikt. "Fuel Flexible Advanced Dual Fluidized Bed Steam Gasification". Dissertation. Vienna: TU Wien, 2020. DOI: 10.34726/hss.2020.39988.

[85] A. M. Mauerhofer, S. Müller, F. Benedikt, J. Fuchs, A. Bartik, and H. Hofbauer. "CO_2 gasification of biogenic fuels in a dual fluidized bed reactor system". In: *Biomass Conversion and Biorefinery* 57.2 (2019), p. 460. DOI: 10.1007/s13399-019-00493-3.

[86] D. Schweitzer. "Experimentelle und simulative Untersuchung der Wasserdampfvergasung von Klärschlamm und weiteren biogenen Brennstoffen". Dissertation. Universität Stuttgart, 2018.

[87] J. C. Schmid, A. Bartik, F. Benedikt, A. M. Mauerhofer, J. Fuchs, E. Schanz, S. Reisinger, B. Nowak, F. Bühler, S. Müller, M. Fuchs, and H. Hofbauer. "Steam gasification of sewage sludge for synthesis processes". In: *Proceedings of the ICPS19-International Conference on Polygeneration Strategies*. 2019, pp. 45–53. DOI: 10.34726/45.

[88] J. C. Schmid, U. Wolfesberger, S. Koppatz, C. Pfeifer, and H. Hofbauer. "Variation of feedstock in a dual fluidized bed steam gasifier—influence on product gas, tar content, and composition". In: *Environmental Progress & Sustainable Energy* 31.2 (2012), pp. 205–215. DOI: 10.1002/ep.11607.

[89] A. M. Mauerhofer, J. Fuchs, S. Müller, F. Benedikt, J. C. Schmid, and H. Hofbauer. "CO_2 gasification in a dual fluidized bed reactor system: Impact on the product gas composition". In: *Fuel* 253 (2019), pp. 1605–1616. DOI: 10.1016/j.fuel.2019.04.168.

[90] A. M. Mauerhofer, S. Müller, A. Bartik, F. Benedikt, J. Fuchs, M. Hammerschmid, and H. Hofbauer. "Conversion of CO_2 during the DFB biomass gasification process". In: *Biomass Conversion and Biorefinery* 11.1 (2021), pp. 15–27. DOI: 10.1007/s13399-020-00822-x.

[91] M. Kuba, H. He, F. Kirnbauer, N. Skoglund, D. Boström, M. Öhman, and H. Hofbauer. "Mechanism of Layer Formation on Olivine Bed Particles in Industrial-Scale Dual Fluid Bed Gasification of Wood". In: *Energy & Fuels* 30.9 (2016), pp. 7410–7418. DOI: 10.1021/acs.energyfuels.6b01522.

[92] K. Fürsatz, J. Fuchs, F. Benedikt, M. Kuba, and H. Hofbauer. "Effect of biomass fuel ash and bed material on the product gas composition in DFB steam gasification". In: *Energy* 219 (2021). DOI: 10.1016/j.energy.2020.119650.

[93] F. Benedikt, J. Fuchs, J. C. Schmid, S. Müller, and H. Hofbauer. "Advanced dual fluidized bed steam gasification of wood and lignite with calcite as bed material". In: *Korean Journal of Chemical Engineering* 34.9 (2017), pp. 2548–2558. DOI: 10.1007/s11814-017-0141-y.

[94] U. Wolfesberger, I. Aigner, and H. Hofbauer. "Tar content and composition in producer gas of fluidized bed gasification of wood—Influence of temperature and pressure". In: *Environmental Progress & Sustainable Energy* 28.3 (2009), pp. 372–379. DOI: 10.1002/ep.10387.

[95] U. Wolfesberger-Schwabl. "Profiling tar behavior in dual fluidized bed biomass steam gasification". Dissertation. Vienna: TU Wien, 2013.

[96] J. C. Schmid. "Development of a novel dual fluidized bed gasification system for increased fuel flexibility". Dissertation. Vienna: TU Wien, 2014. DOI: 10.34726/hss.2014.25397.

[97] J. Fuchs, J. C. Schmid, S. Müller, and H. Hofbauer. "Dual fluidized bed gasification of biomass with selective carbon dioxide removal and limestone as bed material: A review". In: *Renewable and Sustainable Energy Reviews* 107 (2019), pp. 212–231. DOI: 10.1016/j.rser.2019.03.013.

[98] S. Hafner, M. Schmid, and G. Scheffknecht. "Parametric Study on the Adjustability of the Syngas Composition by Sorption-Enhanced Gasification in a Dual-Fluidized Bed Pilot Plant". In: *Energies* 14.2 (2021). DOI: 10.3390/en14020399.

[99] J. Fuchs, J. C. Schmid, F. Benedikt, S. Müller, H. Hofbauer, H. Stocker, N. Kieberger, and T. Bürgler. "The impact of bed material cycle rate on in-situ CO_2 removal for sorption enhanced reforming of different fuel types". In: *Energy* 162 (2018), pp. 35–44. DOI: 10.1016/j.energy.2018.07.199.

[100] N. Abdoulmoumine, S. Adhikari, A. Kulkarni, and S. Chattanathan. "A review on biomass gasification syngas cleanup". In: *Applied Energy* 155 (2015), pp. 294–307. DOI: 10.1016/j.apenergy.2015.05.095.

[101] S. Heyne, T. Liliedahl, and M. Marklund. *Biomass Gasification - A synthesis of technical barriers and current research issues for deployment at large scale*. Sweden, 2013. URL: https://www.osti.gov/etdeweb/biblio/22138974 (visited on 09/08/2023).

[102] P. Mondal, G. S. Dang, and M. O. Garg. "Syngas production through gasification and cleanup for downstream applications—Recent developments". In: *Fuel Processing Technology* 92.8 (2011), pp. 1395–1410. DOI: 10.1016/j.fuproc.2011.03.021.

[103] X. Meng, W. de Jong, R. Pal, and A. H. Verkooijen. "In bed and downstream hot gas desulphurization during solid fuel gasification: A review". In: *Fuel Processing Technology* 91.8 (2010), pp. 964–981. DOI: 10.1016/j.fuproc.2010.02.005.

[104] K. Liu, C. Song, and V. Subramani, eds. *Hydrogen and Syngas Production and Purification Technologies*. 1st ed. Hoboken, New Jersey: AIChE and John Wiley & Sons, 2010.

[105] R. Bardolf. "Optimierung eines Produktgaswäschers bei der Biomassedampfvergasung im Zweibettwirbelschichtverfahren". Dissertation. Vienna: TU Wien, 2017. DOI: 10.34726/hss.2017.36646.

[106] T. Pröll, I. G. Siefert, A. Friedl, and H. Hofbauer. "Removal of NH_3 from Biomass Gasification Producer Gas by Water Condensing in an Organic Solvent Scrubber". In: *Industrial & Engineering Chemistry Research* 44.5 (2005), pp. 1576–1584. DOI: 10.1021/ie049669v.

[107] P. Khakharia, A. Huizinga, C. Jurado Lopez, C. Sanchez Sanchez, F. de Miguel Mercader, T. J. H. Vlugt, and E. Goetheer. "Acid Wash Scrubbing as a Countermeasure for Ammonia Emissions from a Postcombustion CO_2 Capture Plant". In: *Industrial and Engineering Chemistry Research* 53.33 (2014), pp. 13195–13204. DOI: 10.1021/ie502045c.

[108] M. Asadullah. “Biomass gasification gas cleaning for downstream applications: A comparative critical review”. In: *Renewable and Sustainable Energy Reviews* 40 (2014), pp. 118–132. DOI: 10.1016/j.rser.2014.07.132.

[109] A. Larsson, I. Gunnarsson, and F. Tengberg. *The GoBiGas Project: Demonstration of the Production of Biomethane from Biomass via Gasification*. 2018. DOI: 10.13140/RG.2.2.27352.55043.

[110] B. Rehling. “Development of the 1MW Bio-SNG plant, evaluation on technological and economical aspects and upscaling considerations”. Dissertation. Vienna: TU Wien, 2012.

[111] H. Thunman, C. Gustavsson, A. Larsson, I. Gunnarsson, and F. Tengberg. “Economic assessment of advanced biofuel production via gasification using cost data from the GoBiGas plant”. In: *Energy Science and Engineering* 7.1 (2019), pp. 217–229. DOI: 10.1002/ese3.271.

[112] N. Meynet, Y. Kara, M. Maheut, M. Hervy, L. Brito, and J. Maistrello. “Numerical and experimental investigation of bed fluidization and heat transfer within a methanation reactor at demonstration scale”. In: *Thermal Science and Engineering Progress* 44 (2023). DOI: 10.1016/j.tsep.2023.102021.

[113] M. Hervy, J. Maistrello, L. Brito, M. Rizand, E. Basset, Y. Kara, and M. Maheut. “Power-to-gas: CO_2 methanation in a catalytic fluidized bed reactor at demonstration scale, experimental results and simulation”. In: *Journal of CO_2 Utilization* 50 (2021). DOI: 10.1016/j.jcou.2021.101610.

[114] ENGIE. *CMA CGM and ENGIE set to co-invest in the Salamander project, to produce second-generation biomethane*. 2022. URL: https://en.newsroom.engie.com/news/cma-cgm-and-engie-set-to-co-invest-in-the-salamander-project-to-produce-second-generation-biomethane-decd-314df.html (visited on 09/07/2023).

[115] ENGIE. *Green Gas: A world first for ENGIE!* 2020. URL: https://www.engie.com/en/news/gaya-energy-waste-gas-renewable (visited on 09/07/2023).

[116] A. Alamia, S. Òsk Gardarsdòttir, A. Larsson, F. Normann, and H. Thunman. “Efficiency Comparison of Large-Scale Standalone, Centralized, and Distributed Thermochemical Biorefineries”. In: *Energy Technology* 5.8 (2017), pp. 1435–1448. DOI: 10.1002/ente.201600719.

[117] K. Salbrechter and T. Schubert. “Combination of b-Fuels and e-Fuels—A Technological Feasibility Study”. In: *Energies* 14.17 (2021). DOI: 10.3390/en14175250.

[118] E. Giglio, G. Vitale, A. Lanzini, and M. Santarelli. "Integration between biomass gasification and high-temperature electrolysis for synthetic methane production". In: *Biomass and Bioenergy* 148 (2021). DOI: 10.1016/j.biombioe.2021.106017.

[119] J. M. Leimert, M. Neubert, P. Treiber, M. Dillig, and J. Karl. "Combining the Heatpipe Reformer technology with hydrogen-intensified methanation for production of synthetic natural gas". In: *Applied Energy* 217 (2018), pp. 37–46. DOI: 10.1016/j.apenergy.2018.02.127.

[120] J. Witte, A. Calbry-Muzyka, T. Wieseler, P. Hottinger, S. M. Biollaz, and T. J. Schildhauer. "Demonstrating direct methanation of real biogas in a fluidised bed reactor". In: *Applied Energy* 240 (2019), pp. 359–371. DOI: 10.1016/j.apenergy.2019.01.230.

[121] J. Brellochs. *Experimentelle Untersuchung und Prozess-Simulation der AER-Biomassevergasung zur Erzeugung eines regenerativen Erdgassubstitutes: Zugl.: Stuttgart, Univ. Diss., 2014*. Göttingen: Cuvillier, 2014.

[122] I. Martínez and M. C. Romano. "Flexible sorption enhanced gasification (SEG) of biomass for the production of synthetic natural gas (SNG) and liquid biofuels: Process assessment of stand-alone and power-to-gas plant schemes for SNG production". In: *Energy* 113 (2016), pp. 615–630. DOI: 10.1016/j.energy.2016.07.026.

[123] M. Veress. "Optimization of a process concept for the industrial production of Bio-SNG from low-grade fuels". Master Thesis. Vienna: TU Wien, 2020. DOI: 10.34726/hss.2020.63703.

[124] A. Bartik, J. Fuchs, G. Pacholik, K. Föttinger, H. Hofbauer, S. Müller, and F. Benedikt. "Experimental investigation on the methanation of hydrogen-rich syngas in a bubbling fluidized bed reactor utilizing an optimized catalyst". In: *Fuel Processing Technology* 237 (2022). DOI: 10.1016/j.fuproc.2022.107402.

[125] M. Hammerschmid, A. Bartik, F. Benedikt, M. Veress, S. Pratschner, S. Müller, and H. Hofbauer. "Economic and Ecological Impacts on the Integration of Biomass-Based SNG and FT Diesel in the Austrian Energy System". In: *Energies* 16.16 (2023). DOI: 10.3390/en16166097.

[126] P. Konstantin and M. Konstantin. *Praxisbuch Energiewirtschaft: Energieumwandlung, -transport und -beschaffung, Übertragungsnetzausbau und Kernenergieausstieg*. 5., aktualisierte Auflage. Berlin and Heidelberg: Springer Vieweg, 2023. DOI: 10.1007/978-3-662-67335-5.

[127] M. S. Peters and K. D. Timmerhaus. *Plant design and economics for chemical engineers*. 4. ed. McGraw-Hill chemical engineering series. New York: McGraw-Hill, 1991.

[128] Environment Agency Austria. *Berechnung von Treibhausgas (THG)-Emissionen verschiedener Energieträger*. Vienna, Austria, 2022. URL: https://secure.umweltbundesamt.at/co2mon/co2mon.html (visited on 10/02/2023).

[129] Environment Agency Germany. *ProBas - Prozessorientierte Basisdaten für Umweltmanagementsysteme*. Dessau-Roßlau, Germany, 2015. URL: https://www.probas.umweltbundesamt.de (visited on 10/03/2023).

[130] Internationales Institut für Nachhaltigkeitsanalysen und -strategien. *Globales Emissions-Modell Integrierter Systeme (GEMIS)*. Freiburg, Germany, 2018.

[131] A. M. Mauerhofer, J. C. Schmid, F. Benedikt, J. Fuchs, S. Müller, and H. Hofbauer. "Dual fluidized bed steam gasification: Change of product gas quality along the reactor height". In: *Energy* 173 (2019), pp. 1256–1272. DOI: 10.1016/j.energy.2019.02.025.

[132] J. Fuchs. "Process characteristics of sorption enhanced reforming in an advanced gasification system". Dissertation. Vienna: TU Wien, 2020. DOI: 10.34726/hss.2021.39987.

[133] A. Bartik, J. Fuchs, S. Müller, and H. Hofbauer. "Development of an internally circulating fluidized bed for catalytic methanation of syngas". In: *Proceedings of the 16. Minisymposium Verfahrenstechnik & 7. Partikelforum*. Ed. by C. Jordan. 2020, chapter MoV2–(04), 9 pages. DOI: 10.34726/566.

[134] H. Hofbauer. "Experimentelle Untersuchungen an einer zirkulierenden Wirbelschicht mit Zentralrohr". Dissertation. Vienna: TU Wien, 1982.

[135] J. R. Grace. *Handbook of Multiphase Systems*. Washington, D.C.: Hemisphere, 1982.

[136] Verfahrenstechnik und Chemieingenieurwesen, ed. *VDI-Wärmeatlas*. Berlin, Heidelberg: Springer Berlin Heidelberg, 2013. DOI: 10.1007/978-3-642-19981-3.

[137] A. Bartik, J. Fuchs, G. Pacholik, K. Föttinger, H. Hofbauer, S. Müller, and F. Benedikt. "Corrigendum to "Experimental investigation on the methanation of hydrogen-rich syngas in a bubbling fluidized bed reactor utilizing an optimized catalyst" [Fuel Processing Technology, Volume 237 (2022), 107402]". In: *Fuel Processing Technology* 252 (2023). DOI: 10.1016/j.fuproc.2023.107969.

[138] D. Cui, J. Liu, J. Yu, F. Su, and G. Xu. "Attrition-resistant Ni-Mg/Al_2O_3 catalyst for fluidized bed syngas methanation". In: *Catalysis Science and Technology* 5.6 (2015), pp. 3119–3129. DOI: 10.1039/c5cy00066a.

[139] Sasol Performance Chemicals. *PURALOX/CATALOX High-Purity Calcined Aluminas*. URL: https://www.sasolgermany.de/fileadmin/doc/alumina/Neu_2017/0372.SAS-BR-Inorganics_Puralox_Catalox_WEB.pdf (visited on 01/03/2022).

[140] D. Geldart. "Types of gas fluidization". In: *Powder Technology* 7.5 (1973), pp. 285–292. DOI: 10.1016/0032-5910(73)80037-3.

[141] J. Fuchs, J. C. Schmid, S. Müller, A. M. Mauerhofer, F. Benedikt, and H. Hofbauer. "The impact of gasification temperature on the process characteristics of sorption enhanced reforming of biomass". In: *Biomass Conversion and Biorefinery* 10 (2020), pp. 925–936. DOI: 10.1007/s13399-019-00439-9.

[142] R. Shirvani, A. Bartik, G. A. S. Alves, D. Garcia de Otazo Hernandez, S. Müller, K. Föttinger, and M. G. Steiger. "Nitrogen recovery from low-value biogenic feedstocks via steam gasification to methylotrophic yeast biomass". In: *Frontiers in Bioengineering and Biotechnology* 11 (2023). DOI: 10.3389/fbioe.2023.1179269.

[143] J. Loipersböck, M. Lenzi, R. Rauch, and H. Hofbauer. "Hydrogen production from biomass: The behavior of impurities over a CO shift unit and a biodiesel scrubber used as a gas treatment stage". In: *Korean Journal of Chemical Engineering* 34.8 (2017), pp. 2198–2203. DOI: 10.1007/s11814-017-0130-1.

[144] Österreichische Vereinigung für das Gas- und Wasserfach. *Richtlinie G B210 - Gasbeschaffenheit*. Ed. by ÖVGW. 2021.

[145] W. Terlouw, D. Peters, J. van Tilburg, M. Schimmel, T. Berg, J. Cihlar, G. Ur Rehman Mir, M. Spöttle, M. Staats, A. V. Leja-retta, M. Buseman, M. Schenkel, I. van Hoorn, C. Wassmer, E. Kamensek, et al. *Gas for Climate: The optimal role for gas in a net-zero emissions energy system*. Utrecht, Netherlands, 2019. URL: https://gasforclimate2050.eu/wp-content/uploads/2020/03/Navigant-Gas-for-Climate-The-optimal-role-for-gas-in-a-net-zero-emissions-energy-system-March-2019.pdf (visited on 10/23/2023).

[146] G. Jungmeier, L. Canella, J. Pucker-Singer, and M. Beermann. *Geschätzte Treibhausgasemissionen und Primärenergieverbrauch in der Lebenszyklusanalyse von Pkw-basierten Verkehrssystemen*. Graz, 2019.

[147] G. Jungmeier. *Umweltbilanz von E-Fuels – Vergleich mit anderen Treibstoffen im Lebenszyklus. Ö-1025 GEW/DGMK Onlinekonferenz „Innovative Energieversorgung"*. Graz, 2020. URL: https://www.wko.at/site/oegew/veranstaltungen/umweltbilanz-von-e-fuels.pdf (visited on 10/02/2023).

[148] G. T. Rochelle. "Conventional amine scrubbing for CO_2 capture". In: *Absorption-Based Post-combustion Capture of Carbon Dioxide*. Elsevier, 2016, pp. 35–67. DOI: 10.1016/B978-0-08-100514-9.00003-2.

[149] K. Li, W. Leigh, P. Feron, H. Yu, and M. Tade. "Systematic study of aqueous monoethanolamine (MEA)-based CO_2 capture process: Techno-economic assessment of the MEA process and its improvements". In: *Applied Energy* 165 (2016), pp. 648–659. DOI: 10.1016/j.apenergy.2015.12.109.

[150] A. Alamia, A. Larsson, C. Breitholtz, and H. Thunman. "Performance of large-scale biomass gasifiers in a biorefinery, a state-of-the-art reference". In: *International Journal of Energy Research* 41.14 (2017), pp. 2001–2019. DOI: 10.1002/er.3758.

[151] D. W. Green and M. Z. Southard. *Perry's Chemical Engineers' Handbook*. 9th edition. New York: McGraw Hill, 2019. URL: https://www.accessengineeringlibrary.com/content/book/9780071834087.

[152] K. H. Weber. *Engineering verfahrenstechnischer Anlagen: Praxishandbuch mit Checklisten und Beispielen*. 2., vollständig bearbeitete und aktualisierte Auflage. VDI-Buch. Berlin and Heidelberg: Springer Vieweg, 2016.

[153] S. Kolb, T. Plankenbühler, K. Hofmann, J. Bergerson, and J. Karl. "Life cycle greenhouse gas emissions of renewable gas technologies: A comparative review". In: *Renewable and Sustainable Energy Reviews* 146 (2021). DOI: 10.1016/j.rser.2021.111147.

[154] C. Cantuarias-Villessuzanne, B. Weinberger, L. Roses, A. Vignes, and J.-M. Brignon. "Social cost-benefit analysis of hydrogen mobility in Europe". In: *International Journal of Hydrogen Energy* 41.42 (2016), pp. 19304–19311. DOI: 10.1016/j.ijhydene.2016.07.213.

[155] National Renewable Energy Laboratory. *H2A: Hydrogen Analysis Production Models*. 2019. URL: https://www.nrel.gov/hydrogen/assets/docs/future-central-pem-electrolysis-version-nov20.xlsm (visited on 08/04/2023).

[156] E. Barbuzza, G. Buceti, A. Pozio, M. Santarelli, and S. Tosti. "Gasification of wood biomass with renewable hydrogen for the production of synthetic natural gas". In: *Fuel* 242 (2019), pp. 520–531. DOI: 10.1016/j.fuel.2019.01.079.

[157] F. Kirchbacher, M. Miltner, W. Wukovits, and M. Harasek. "Economic assessment of membrane-based power-to-gas processes for the European biogas market". In: *Renewable and Sustainable Energy Reviews* 112 (2019), pp. 338–352. DOI: 10.1016/j.rser.2019.05.057.

[158] D. Katla, M. Jurczyk, A. Skorek-Osikowska, and W. Uchman. "Analysis of the integrated system of electrolysis and methanation units for the production of synthetic natural gas (SNG)". In: *Energy* 237 (2021). DOI: 10.1016/j.energy.2021.121479.

[159] L. Stanger, A. Schirrer, F. Benedikt, A. Bartik, S. Jankovic, S. Müller, and M. Kozek. "Dynamic modeling of dual fluidized bed steam gasification for control design". In: *Energy* 265 (2023). DOI: 10.1016/j.energy.2022.126378.

[160] M. Hammerschmid, S. Müller, J. Fuchs, and H. Hofbauer. "Evaluation of biomass-based production of below zero emission reducing gas for the iron and steel industry". In: *Biomass Conversion and Biorefinery* 11.1 (2021), pp. 169–187. DOI: 10.1007/s13399-020-00939-z.

[161] Statistik Austria. *Energiebilanzen Österreich 1970-2021*. URL: https://www.statistik.at/statistiken/energie-und-umwelt/energie/energiebilanzen (visited on 08/07/2023).

[162] Baumann Martin, Fazeni-Fraisl Karin, Kienberger Thomas, Nagovnak Peter, Pauritsch Günter, Rosenfeld Daniel, Christoph Sejkora, and Tichler Robert. *Erneuerbares Gas in Österreich 2040: Quantitative Abschätzung von Nachfrage und Angebot*. Ed. by Bundesministerium für Klimaschutz, Umwelt, Energie, Mobilität, Innovation und Technologie. 2021. URL: https://www.bmk.gv.at/themen/energie/publikationen/erneuerbares-gas-2040.html (visited on 10/23/2023).

[163] C. Dißauer, B. Rehling, and C. Strasser. *Machbarkeitsuntersuchung Methan aus Biomasse*. 2019. (Visited on 10/23/2023).

List of Symbols

Symbol	Unit	Description
CDF	–	cumulative discount factor
$CEPCI_{base}$	–	chemical engineering plant cost index in base year
$CEPCI_{ref}$	–	chemical engineering plant cost index in 2019 or 2022
CO_2e_{red,sec_i}	%	CO_2 reduction potential of sector i
$C_{eq,base}$	€	equipment costs base case
$C_{eq,design}$	€	equipment costs design case
d_{SV}	µm	mean Sauter diameter
E	€	annual expenditures
E_{gas,sec_i}	$\frac{\text{TWh}}{\text{a}}$	annual substituted natural gas demand of sector i
CO_2e_{tot,sec_i}	$\frac{\text{kg}_{\text{CO}_2\text{e}}}{\text{a}}$	annual CO_2e emissions of sector i
FP_{NG}	$\frac{\text{kg}_{\text{CO}_2\text{e}}}{\text{kWh}}$	CO_2 footprint of natural gas
FP_{SNG}	$\frac{\text{kg}_{\text{CO}_2\text{e}}}{\text{kWh}}$	CO_2 footprint of SNG
$GHSV$	h^{-1}	gas hourly space velocity
i	–	interest rate
I_0	€	total capital investment costs
$LCOP$	$\frac{€}{\text{MWh}}$	levelized costs of products
$\dot{m}_{C,CH_4,SNG}$	$\frac{\text{kg}}{\text{h}}$	massflow of carbon in SNG
$\dot{m}_{C,GR,fuel}$	$\frac{\text{kg}}{\text{h}}$	massflow of carbon in the fuel to the GR
$M_{t,SNG}$	MWh	annual quantity of produced SNG
n	years	plant lifetime
$\dot{n}_j$	$\frac{\text{mol}}{\text{s}}$	molar flow of species j
N_j	–	number of carbon atoms in species j
$P_{CR,fuel}$	kW	chemical energy of the fuel to the CR
$P_{GR,fuel}$	kW	chemical energy of the fuel to the GR
P_{H_2}	kW	chemical energy of the additional hydrogen
P_{SNG}	kW	chemical energy of the SNG

Symbol	Unit	Description
P_{rawSNG}	kW	chemical energy of the raw-SNG
p_a	mbar	pressure in the annular region at the upper gap
p_d	mbar	pressure in the draft tube at the upper gap
$\dot{Q}_{loss}$	kW	calculated heat loss of the DFB pilot plant
$\dot{Q}_a$	$\frac{\mathrm{Nm^3}}{\mathrm{h}}$	volume flow to the annular region
$\dot{Q}_d$	$\frac{\mathrm{Nm^3}}{\mathrm{h}}$	volume flow to the draft tube
r	–	scaling factor
$R_{sec.prod.}$	€	annual revenues from secondary products
SN	–	stoichiometric number
S_{C2H6}	%	selectivity of C_2H_4 towards C_2H_6
S_{CO2}	%	selectivity of CO towards CO_2
S_a	$\frac{\mathrm{Nm^3}}{\mathrm{h}}$	gas slip between the draft tube and the annular region
S_{base}	suit. units	plant scale base case
S_d	$\frac{\mathrm{Nm^3}}{\mathrm{h}}$	gas slip between the annular region and the draft tube
S_{design}	suit. units	plant scale design case
u_a	$\frac{\mathrm{m}}{\mathrm{s}}$	superficial gas velocity in the annular region
u_d	$\frac{\mathrm{m}}{\mathrm{s}}$	superficial gas velocity in the draft tube
u_{mf}	$\frac{\mathrm{m}}{\mathrm{s}}$	minimum fluidization velocity
$WHSV$	$\frac{\mathrm{NL}}{\mathrm{g_{cat}\ h}}$	weight hourly space velocity
X_{CO}	%	carbon monoxide conversion
X_{CO_2}	%	carbon dioxide conversion
X_{H_2}	%	hydrogen conversion
y	–	molar fraction
Y_{CH_4}	%	methane yield
Z	–	installation factor
$\eta_{CGE,o}$	%	cold gas efficiency for industrial-scale concepts
$\eta^*_{CGE,o}$	%	cold gas efficiency for pilot-scale investigations
η_C	%	carbon utilization
ρ_b	$\frac{\mathrm{kg}}{\mathrm{m^3}}$	bulk density

List of Acronyms

AC activated carbon

BA bark

BECCS bioenergy carbon caputre and storage

BET Brunnauer-Emmett-Teller

BtG Biomass-to-Gas

CAD computer aided design

CDF cumulative discount factor

CEPCI chemical engineering plant cost index

CO_2e CO_2 equivalent

CR combustion reactor

DFB dual fluidized bed

FT Fischer-Tropsch

GCMS gas chromatography/mass spectroscopy

GR gasification reactor

HHV higher heating value

HTG hydrothermal gasification

ICFB internally circulating fluidized bed

IPCC Intergovernmental Panel on Climate Change

KPI key performance indicator

L limestone

LCOP levelized costs of products

LHV lower heating value

LI lignin

MEA monoethanolamine

MPC model predictive controller

NPV net present value

O olivine

ÖVGW Österreichische Vereinigung für das Gas- und Wasserfach

P&I piping and instrumentation

PDU process development unit

PFD process flow diagram

PtG Power-to-Gas

raw-SNG raw synthetic natural gas

RES renewable energy source

RME rapeseed methyl ester

RSC rapeseed cake

SER sorption enhanced reforming

SNG synthetic natural gas

SS sewage sludge

SW softwood

TEA techno-economic analysis

TPO temperature-programmed oxidation

TRL technology readiness level

TSA temperature swing adsorption

WGS water-gas shift

Appendix A

Simulation Parameters

In Table A.1 and Table A.2, the additional simulation parameters for the concepts introduced in section 6.2 are summarized. All other parameters are identical to the assumptions in section 6.1 (also see supplementary material of **Paper V** [125])

Tab. A.1: Relevant simulation parameters for the evaluation of alternative concepts in section 6.2

parameter	unit	value	reference
fluidized bed methanation reactor			
reaction temperature	°C	340	[38, 124]
reaction pressure	bar_a	1.05	
$WHSV$	$NL/(g_{cat}\,h)$	1.5	[38, 124]
steam content inlet[a]	vol.-%	15	
catalyst	-	Ni/Al_2O_3	
polishing reactor			
reaction temperature at exit	°C	360	
reaction pressure	bar_a	10	
$GHSV$	1/h	4000	
catalyst	-	Ni/Al_2O_3	

[a] only in case of DFB-Std variants

Tab. A.2: Additional simulation parameters for the SER concept in section 6.2.3, data taken from [121]

parameter	unit	stoichiometric number SN									
		1.31	1.18	1.09	1.04	1.00	0.97	0.93	0.87	0.81	0.72
PGY[a]	$Nm^3_{db}/kg_{fuel,daf}$	0.930	0.955	0.972	0.983	0.994	1.000	1.006	1.020	1.050	1.080
temp.	°C	685.0	690.0	695.0	697.5	700.0	701.0	702.5	705.0	710.0	715.0
H_2	$vol.-\%_{db}$	70.96	69.93	69.11	68.61	68.09	67.84	67.23	66.32	65.28	63.58
CO	$vol.-\%_{db}$	6.19	7.09	7.69	8.04	8.45	8.57	8.79	9.15	9.89	10.63
CO_2	$vol.-\%_{db}$	7.75	8.49	9.22	9.59	9.94	10.26	10.68	11.44	12.17	13.58
CH_4	$vol.-\%_{db}$	12.58	12.24	11.98	11.86	11.73	11.62	11.62	11.50	11.28	11.02
C_2H_4	$vol.-\%_{db}$	1.51	1.35	1.20	1.15	1.09	1.06	1.04	0.99	0.89	0.79
C_2H_6	$vol.-\%_{db}$	0.50	0.45	0.40	0.37	0.35	0.33	0.32	0.30	0.25	0.20
C_3H_8	$vol.-\%_{db}$	0.50	0.45	0.40	0.37	0.35	0.33	0.32	0.30	0.25	0.20

[a] product gas yield

Appendix B

Reactor Drawings

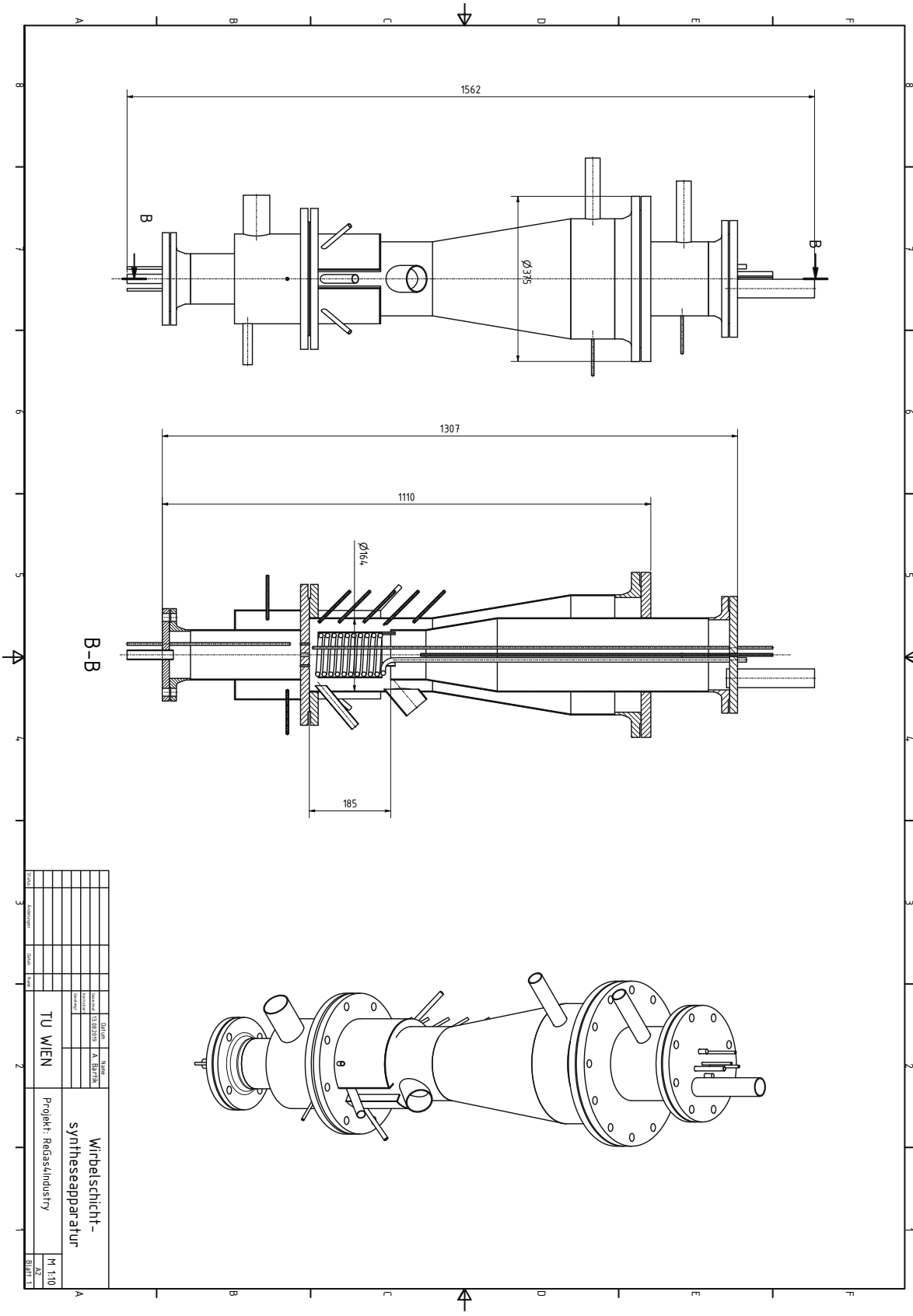

Fig. B.1: Drawing of the fluidized bed methanation reactor including main measurements

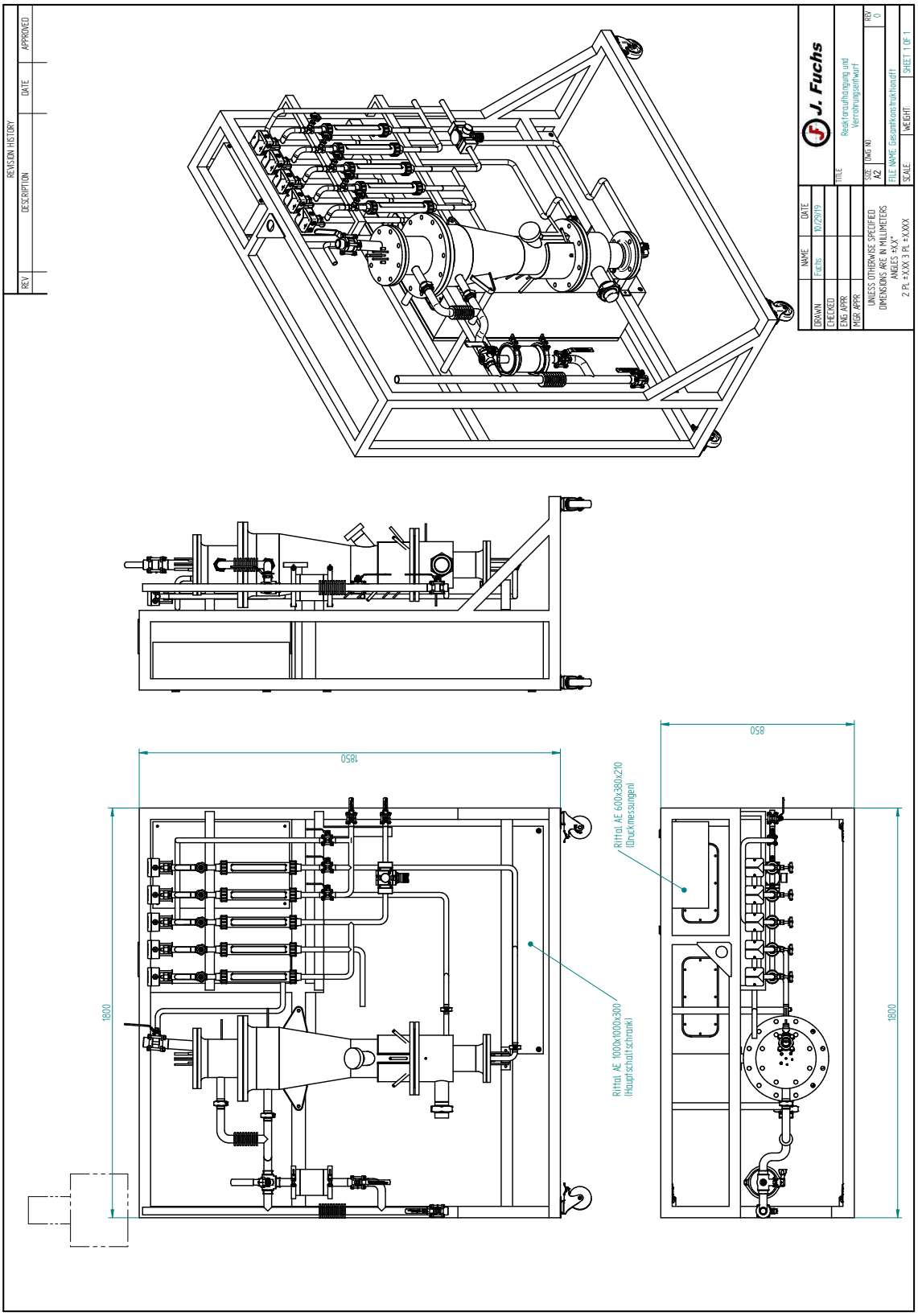

Fig. B.2: Drawing of the whole assembly including the fluidized bed methanation reactor and the mounting and auxiliary systems

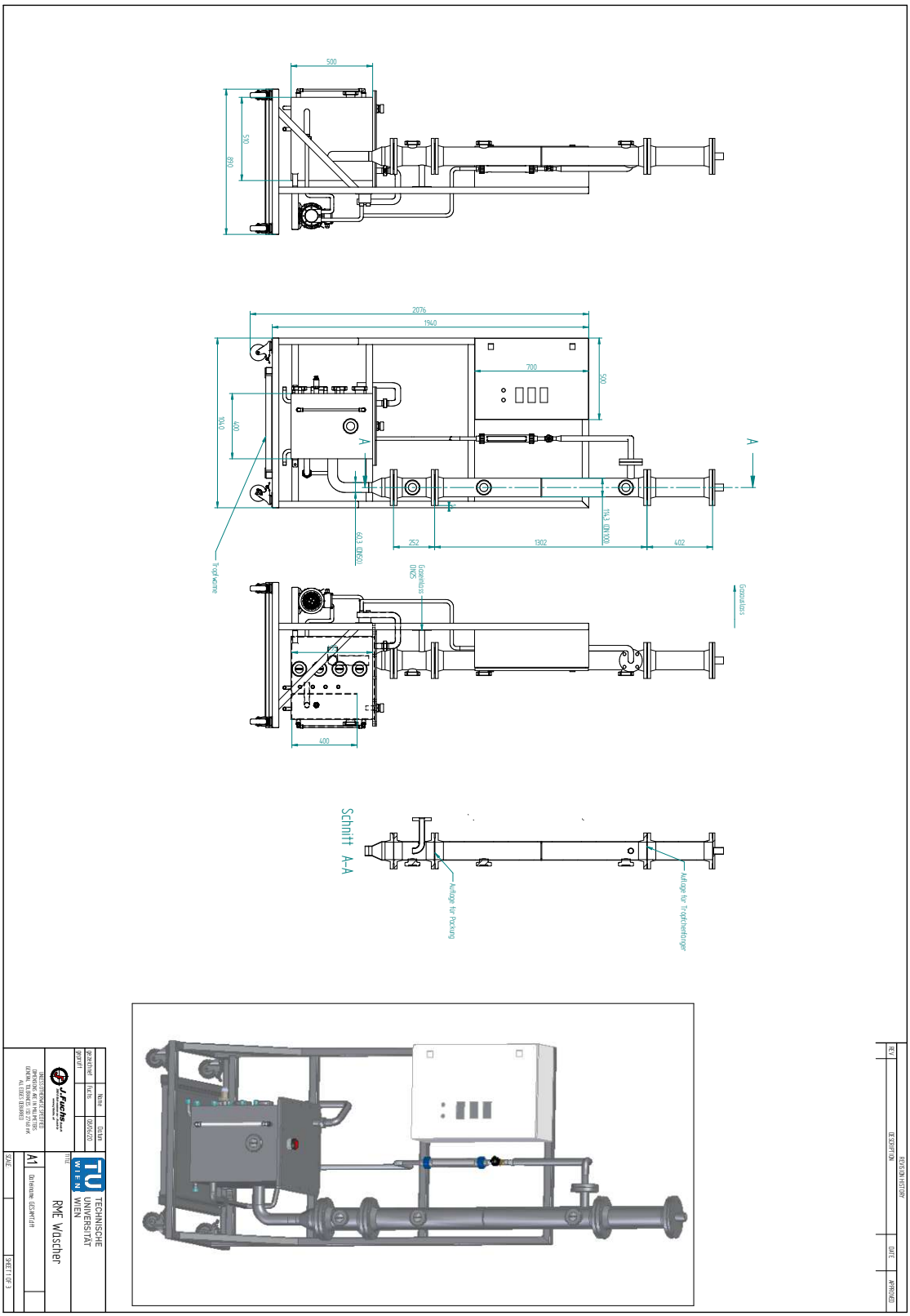

Fig. B.3: Drawing of the RME scrubber

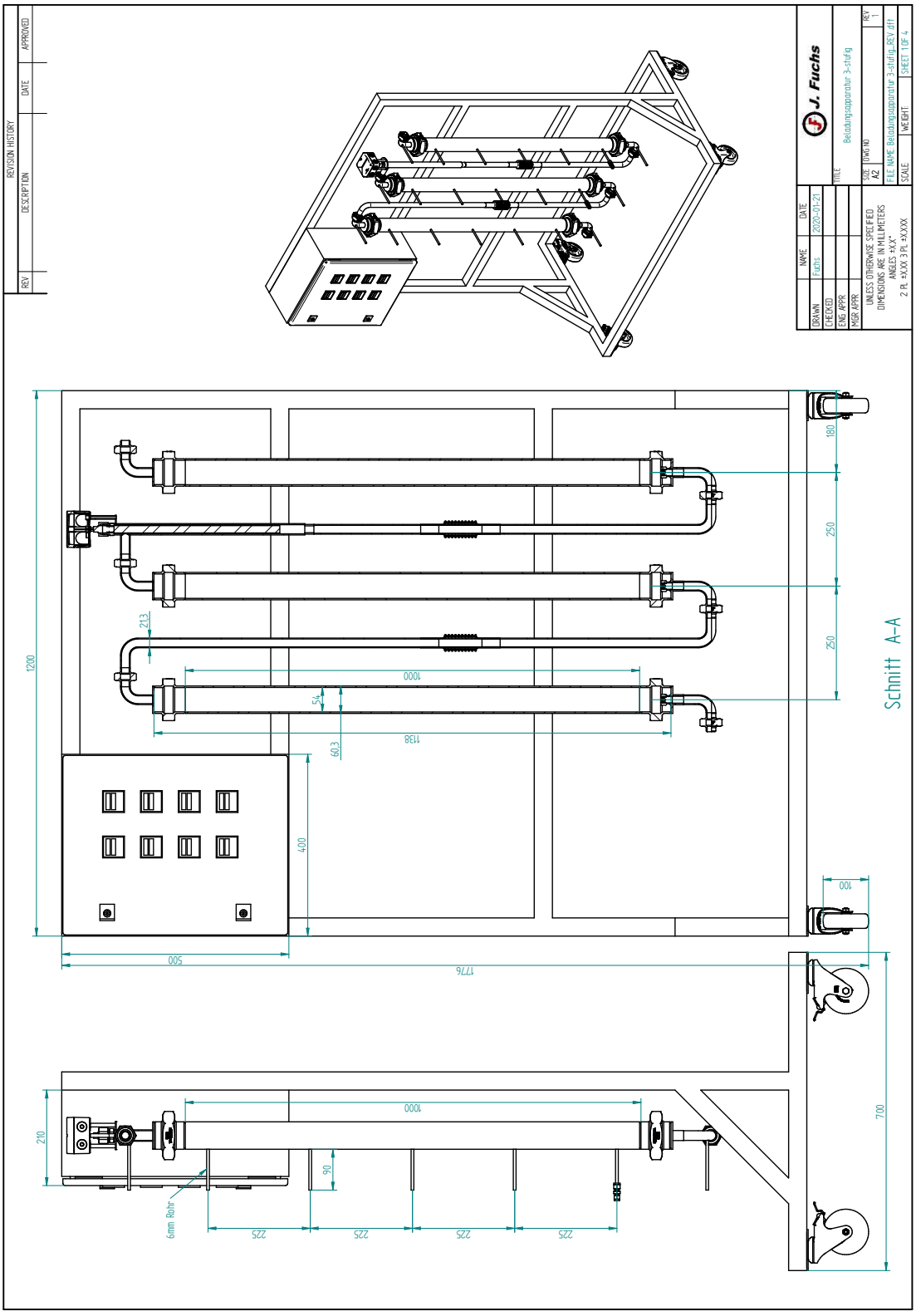

Fig. B.4: Drawing of the activated carbon adsorption beds, note that the setup was retrofitted in September 2023 replacing the screw fittings at the top and bottom of each column with flanges, installing a new gas distributor, and replacing the heating cartridge with a heating tape (not shown here)

Appendix C

Publications

C.1 Paper I

Thermodynamic investigation of SNG production based on dual fluidized bed gasification of biogenic residues

Bartik, A., Benedikt, F., Lunzer, A., Walcher, C., Müller, S., Hofbauer, H., *Biomass Conversion and Biorefinery*, **2020**, Vol. 11, pp. 95–110, https://doi.org/10.1007/s13399-020-00910-y.

Biomass Conversion and Biorefinery (2021) 11:95–110
https://doi.org/10.1007/s13399-020-00910-y

ORIGINAL ARTICLE

Thermodynamic investigation of SNG production based on dual fluidized bed gasification of biogenic residues

Alexander Bartik[1] · Florian Benedikt[1] · Andreas Lunzer[2] · Constantin Walcher[2] · Stefan Müller[1,2] · Hermann Hofbauer[1]

Received: 3 April 2020 / Revised: 8 July 2020 / Accepted: 23 July 2020 / Published online: 28 August 2020

Abstract

Natural gas is an important commodity in the European energy market. The gasification of biogenic residues and the further reaction to a methane-rich gas represent a promising concept for the production of synthetic natural gas on a fossil-free basis. This paper investigates the thermodynamics of methanation in a fluidized bed reactor for different product gas compositions of the dual fluidized bed gasification technology. The investigated product gases range from conventional steam gasification, over CO_2 gasification, to product gases from the sorption enhanced reforming process. All investigated product gases from conventional steam gasification show an understoichiometric composition and therefore require a proper handling of carbon depositions and a CO_2 separation unit downstream of the methanation reactor. The product gas from CO_2 gasification is considered disadvantageous for the investigated process, because it only exhibits a carbon utilization efficiency of 23%. Due to the high flexibility of the sorption enhanced reforming process, a nearly complete methanation of the carbonaceous species is possible without the need for a CO_2 separation step or the addition of steam upstream of the methanation reactor. Furthermore, the carbon utilization efficiency is found to be between 36 and 38%, similar to the results for conventional steam gasification. Temperature and pressure variations allow a thermodynamically optimized operation, which can increase the performance of the methanation and lower the extent of gas upgrading for grid feed-in. Additionally, if a higher hydrogen content in the natural gas grid would be allowed, the overall process chain could be further optimized and simplified.

Keywords Thermodynamics · Fluidized bed methanation · Synthetic natural gas · Dual fluidized bed gasification · Biogenic residues

1 Introduction

Increasing greenhouse gas emissions and the limited availability of primary energy carriers directed the energy policy of the European Union towards sustainable and innovative energy technologies [1]. Natural gas is one of the most important primary energy carriers in Europe, but its availability is heavily dependent on the non-European market. The production of synthetic natural gas (SNG) from biogenic residues offers a promising alternative to the utilization of fossil fuels and represents a novel concept to support the current energy strategy of the European Union [1, 2].

One possible process route is the dual fluidized bed (DFB) gasification, which allows the utilization of locally available residual biogenic or waste resources and offers possibilities for the production of highly valuable secondary energy carriers on a fossil-free basis. Wilk [3] and Benedikt et al. [4], for example, increased the fuel flexibility of the DFB process towards residues and waste for two generations of a 100 kW_{th} DFB gasifier at TU Wien, while Schweitzer [5] and Schmid et al. [6, 7] further extended the feedstock towards sewage sludge and manure. In addition, the combination of the DFB technology with sorption enhanced reforming (SER) enables the production of a nitrogen-free product gas with adjustable hydrogen to carbon monoxide or hydrogen to carbon dioxide contents [8]. Before the product gas from the DFB gasification process can be fed to the methanation unit, rigorous gas cleaning is required in order to protect the

✉ Alexander Bartik
alexander.bartik@tuwien.ac.at

[1] Institute of Chemical, Environmental and Bioscience Engineering, TU Wien, Getreidemarkt 9/166, 1060 Vienna, Austria

[2] Energy & Chemical Engineering GmbH, Waidhausenstraße 27/1/22, 1140 Vienna, Austria

downstream equipment and the methanation catalyst. Dust, tar, as well as sulfur and nitrogen containing compounds need to be removed. Gas cleaning is not further elaborated here, but in [9] a comprehensive overview over different gas cleaning strategies is provided. The exothermic methanation itself has been carried out in adiabatic or cooled fixed bed reactors, fluidized bed reactors, three-phase reactors, and structured reactors. The only commercially available reactor types thereof are adiabatic fixed bed reactors [10]. For this reactor type, many similar process concepts were developed mainly between the 1960s and the 1980s. All concepts consist of 2–7 adiabatic reactors with or without intermediate gas cooling and/or gas recycling. Two prominent representatives thereof are the TREMP and HICOM processes. Both utilize three adiabatic reactors with intermediate cooling and gas recycling. They are applied in various coal-to-SNG projects in China, whereas an adapted TREMP process is also installed in the biomass-to-SNG project GoBiGas in Sweden [11]. In general, this reactor type shows disadvantages in terms of heat management and resistance against carbon depositions on the catalyst. Especially, the heat evolution and therefore the temperature peaks in the adiabatic reactors necessitate a reactor cascade and increase the complexity of the process setup [11, 12]. Simultaneously to fixed beds, research activities concerning the development of fluidized beds as methanation reactors started [13]. One of the most prominent fluidized bed concepts is the COMFLUX process, which successfully demonstrated the production of 20 MW_{SNG} from coal. The 1 MW_{SNG} fluidized bed methanation unit connected to the DFB gasifier in Güssing on the other hand was developed by the Paul Scherrer Institut (PSI) and was the first demonstration of a biomass-to-SNG process on a large scale [10]. Fluidized beds can overcome the limitations imposed to fixed beds by their inherently good heat and mass transfer. This results in nearly isothermal operation conditions and an intrinsic catalyst regeneration [14]. However, high particle forces and therefore high attrition rates have prevented the commercialization of fluidized beds in catalytic methanation processes so far. Continued research work is thus put into the development of appropriate catalysts as reported in [15–17]. Other research groups focus on the development of structured reactors. The catalyst is dispersed on thermally highly conducting structures, thus reducing temperature hotspots. This concept, for example, was applied by the Engler-Bunte-Institut for the load-flexible methanation of gasifier product gas with additional hydrogen from electrolysis [12] or by Biegger et al. [18] for a power-to-gas (PtG) concept with a honeycomb methanation catalyst. The variety of reactor types also explains the wide range of operation conditions in the methanation reactor. Temperatures from 250 to 700 °C and pressures from 1 to 87 bar_a have been applied. From a thermodynamic point of view, the methanation is favored at low temperatures and high pressures. A more comprehensive comparison of different reactor concepts can be found in literature [10–13].

Depending on the composition of the raw-SNG after methanation, different gas upgrading steps might be necessary before the gas can be fed to the gas grid. In the case of DFB gasification and the consecutive catalytic methanation, the upgrading steps can include drying, CO_2 separation, and H_2 separation. Various kinds of CO_2 separation technologies have been proposed for this task. Heyne and Harvey [19] compared membranes, pressure swing adsorption (PSA), and chemical absorption with monoethanolamine and concluded that chemical absorption results in the highest cold gas efficiencies. Physical absorption is another method for the removal of CO_2. However, high pressures are usually required for these processes and Gassner and Maréchal [20] showed that it is the least favorable option for allothermal gasification processes compared with PSA and membrane technologies. For the separation of H_2, mainly membrane technologies are proposed [19–21]. However, to the best of our knowledge, no comparative study on H_2 separation technologies for the investigated process has been carried out so far.

In order to feed the generated gas into the Austrian gas grid, the feed-in regulations must be satisfied. In Austria, the limits for the most important accompanying substances are defined at 4 vol.-% for H_2 and 2 vol.-% for CO_2. Limitations for other trace substances and calorific properties are defined as well but are not relevant to this investigation. The values are standardized in [22, 23]. Interestingly, there is no specification mentioned for CO. This is due to the fact that the guidelines were developed for natural gas and later extended to biogas from biological methanation. Both sources do not contain CO and therefore this issue has not arisen. However, for the SNG production via the thermochemical pathway, a limit for the CO content would be necessary to ensure a high quality gas. This is an issue not only in Austria but also all around Europe, since no threshold levels are defined as summarized in [24]. Currently, the discussion focuses on an increased H_2 content in the natural gas grids all around Europe [25]. Studies have shown that up to 10 vol.-% of H_2 in the natural gas grid has no adverse effects on the grid and most applications [26, 27]. However, as long as this is not transferred to national or European law, the strict limits—as defined before—must be fulfilled. Therefore, an alternative is the generation of a CH_4/H_2 mixture, also referred to as hythane, which can be used as a substitute for natural gas directly in industrial applications without the need to feed it into the gas grid first [28].

In Güssing (Austria) and Gothenburg (Sweden), two plants for the conversion of woody biomass to SNG were operated on a large scale. Both concepts utilized a DFB gasification process but applied different gas cleaning and synthesis steps. In Gothenburg, an adapted four-step adiabatic fixed bed methanation process with intermediate cooling was used (TREMP process). Additionally, a water-gas shift reactor, a pre-methanation reactor, and an amine-based CO_2 separation

unit were installed upstream of the methanation reactors. The gasifier system was operated with a thermal fuel power of 32 MW_{th} and therefore was the largest DFB gasifier built so far. The DFB section was operated in total for 12,000 h with wood pellets and later with wood chips and forest residues as feedstock. During the operation, they identified some issues regarding the fuel feeding, the tar formation, and the product gas cooling [29]. Because of these problems, the SNG production periods were quite limited but nevertheless about 67 GWh of SNG was produced in total. From December 2017 to February 2018, they achieved the design goal and the installed capacity of 20 MW_{SNG} was reached. Chemical efficiencies for the production of SNG from 50 to 63% with wood pellets were reported. The carbon utilization efficiency was about 30%, which means that 30% of the carbon in the biomass is transferred to the SNG while the rest is exhausted mainly as CO_2 [30].

In contrast to this concept, the Güssing plant utilized a single fluidized bed methanation reactor and the amine-based CO_2 separation was performed downstream of the methanation reactor. Unlike the GoBiGas plant, a membrane for the separation of excess H_2 was required as the final gas-upgrading step. The 1 MW_{SNG} methanation section was mainly operated in 2009 and was the first plant to produce SNG from woody biomass on a demonstration scale. The gas was not injected into the gas grid but was stored in a compressed natural gas (CNG) tank. Nevertheless, the Austrian gas grid specifications were reached and SNG with about 95 vol.-% CH_4 and 3.8 vol.-% of N_2 in minor amounts of H_2, CO_2, CO, and C_2H_6 was produced. Additionally, a cold gas efficiency of 62% is reported for this process [31]. Because of the application of a fluidized bed methanation reactor the Güssing concept allowed a simpler process setup compared to GoBiGas. However, the Güssing setup was the first of its kind and was not optimized technically. The methanation section applied in Gothenburg on the other hand is commercially available and technically optimized to the specific requirements of the plant [10, 12].

Several other concepts follow the same goal to convert biogenic feedstock to SNG. Anaerobic digestion allows bacteria to convert non-woody biomass to biogas with approximately 60 vol.-% CH_4 and 40 vol.-% CO_2. This biogas can then be upgraded to SNG quality by removing the CO_2 and other minor impurities [32]. The same concept is applied to biogas from landfills or wastewater treatment plants where the biogas is produced naturally without the additional supply of feedstock [33].

Besides biological approaches, a significant amount of research is put into PtG concepts. The hydrogen produced via electrolysis can be utilized to methanate various kinds of carbon resources as the comprehensive review by Götz et al. [34] shows. One of these sources is the separated CO_2 from biogas plants, which can be upgraded to CH_4 by catalytic methanation instead of the simple exhaustion. One of the most prominent representatives of this technology is the Audi e-gas plant in Germany, which uses a molten salt cooled tube bundle reactor [10]. Besides the classical PtG concepts, also hybrid processes have been developed. For example, Witte et al. [35] directly upgraded the biogas to biomethane on a smaller scale in Switzerland by feeding it together with hydrogen to a bubbling fluidized bed reactor. Instead of the downstream catalytic methanation, Bensmann et al. [36] on the other hand proposed a direct introduction of the hydrogen into the biogas reactor which induced a biological methanation process. Other hybrid concepts add hydrogen to the product gas of a biomass gasification process in order to increase the hydrogen to carbon ratio and therefore increase the overall carbon utilization efficiency of the biomass-to-SNG process. Here, the DemoSNG project is mentioned, where this combination was experimentally tested with a honeycomb-type methanation reactor. It was shown that despite the fluctuating availability of the hydrogen, a continuous production of SNG was possible [37].

From a thermodynamic point of view, the main chemical species which are involved in the methanation reaction system are CH_4, H_2, CO, CO_2, and H_2O. The corresponding reaction equations are the CO methanation (Eq. 1),

$$CO + 3H_2 \rightleftharpoons CH_4 + H_2O \qquad \Delta H_R^{300} = -216\,\frac{kJ}{mol} \qquad (1)$$

the reverse water-gas shift reaction (Eq. 2), and

$$CO_2 + H_2 \rightleftharpoons CO + H_2O \qquad \Delta H_R^{300} = 39\,\frac{kJ}{mol} \qquad (2)$$

the CO_2 methanation (Eq. 3) which is a combination of Eq. 1 and Eq. 2.

$$CO_2 + 4H_2 \rightleftharpoons CH_4 + 2H_2O \qquad \Delta H_R^{300} = -177\,\frac{kJ}{mol} \qquad (3)$$

Additionally, the reaction enthalpies at 300 °C (ΔH_R^{300}) are given. Besides these species, the product gas of the DFB gasifier also contains hydrocarbons. As one of the main components, ethylene (C_2H_4) is identified and is thus included here [38]. The hydrogenation to methane is given in Eq. 4.

$$C_2H_4 + 2H_2 \rightarrow 2CH_4 \qquad \Delta H_R^{300} = -209\,\frac{kJ}{mol} \qquad (4)$$

A deactivation mechanism of the catalyst, which cannot be prevented by gas cleaning steps, is the formation of solid carbon on the catalyst. While adsorbed carbon on the catalyst surface is a necessary reaction intermediate during

methanation, the formation of stable deposits leads to catalyst fouling [39]. Thermodynamically, this deposition can be accounted for by the Boudouard reaction in Eq. 5.

$$2CO \rightleftharpoons CO_2 + C(s) \qquad \Delta H_R^{300} = -174 \frac{kJ}{mol} \tag{5}$$

The deposited surface carbon can also be hydrogenated to methane according to Eq. 6,

$$C(s) + 2H_2 \rightleftharpoons CH_4 \qquad \Delta H_R^{300} = -82.1 \frac{kJ}{mol} \tag{6}$$

or undergo gasification with steam as shown in Eq. 7 [40].

$$C(s) + H_2O \rightleftharpoons CO + H_2 \qquad \Delta H_R^{300} = 134 \frac{kJ}{mol} \tag{7}$$

These reactions show that increased amounts of H_2, H_2O, or CO_2 in the gasifier product gas might prevent the carbon deposition.

A different form of deposition occurs through the adsorption of hydrocarbons like C_2H_4 on the catalyst surface. Between 500 and 800 °C, the adsorption can lead to coke deposits [40]. In general, there is a large number of different forms and structural types of carbon or coke deposits which can occur at different temperature intervals in methanation processes [41].

If kinetic models are considered, all of the abovementioned reaction pathways have to be taken into consideration. The catalytic methanation of syngas is, however, mostly limited by heat transfer and not by kinetics under typical operating conditions. This limitation mostly applies for fixed bed reactors and thus multiple reactors with intermediate cooling are necessary in order to manage the heat released by the exothermic reactions [10]. Fluidized beds were shown to overcome this limitation and allow a low-temperature methanation in a single reactor step. The process was mainly found to be limited by the mass transfer between the bubble and the dense phase of the fluidized bed. Nevertheless, the gas composition is close to the thermodynamic equilibrium for temperatures down to 320 °C and kinetic limitations apply for lower temperatures as some studies confirm [17, 42, 43]. Additionally, the adjustment of the H_2/CO ratio of the feed gas to the required level of three can be directly carried out in the fluidized bed methanation reactor. Fixed bed applications usually require a separate water-gas shift reactor upstream of the methanation for this task [44, 45]. A thermodynamic calculation including the water-gas shift reaction thus provides a good estimation of the expected gas composition. Because of the broad variety of possible carbon species, deviations from the thermodynamic equilibrium for carbon depositions have to be expected [10]. Nevertheless, graphitic carbon has previously been used to elucidate this issue since kinetic models are often only valid for specific reaction conditions and catalysts [46].

Extensive studies have been performed on the thermodynamics of methanation. Bia et al. [39] used ternary diagrams to visualize the calculated boundaries of carbon formation under methanation conditions. Frick et al. [46] applied the same method but extended the investigation to different feed gas mixtures. They concluded that ternary diagrams are an appropriate tool for the design of methanation processes. Gao et al. [47] performed a systematic thermodynamic investigation on the methanation of CO and CO_2 under varying parameters like pressure, temperature, or the H_2/CO ratio. As a result, they give general indications on the effects of the parameter variations. Other research groups extended the modelling to a larger part of the process setup and used different modelling approaches. For example, Witte et al. [48] used rate-based modelling and investigated different combinations of methanation reactors and hydrogen membranes to upgrade biogas from biological digestion to biomethane. In order to upgrade the biogas, they proposed a PtG concept with renewable hydrogen via electrolysis. They concluded that, in order to reach the gas grid requirements, a combination of a bubbling fluidized bed reactor with a second-stage fixed bed methanation unit or a gas separation membrane are the technically and economically favorable options [49]. Neubert [50] proposed a similar two-stage methanation setup within the PtG concept. The first stage consists of a structured methanation reactor followed by an intermediate water condensation and a second-stage fixed bed reactor. Within his work, he elaborately used thermodynamic models and ternary diagrams to define the optimal CO_2 removal as well as steam and hydrogen addition in general. For the production of SNG from coal, Liu et al. [51] used thermodynamic calculations in Aspen Plus to find the most suitable process setup. They concluded that a circulating fluidized bed followed by a second-stage fixed bed methanation reactor poses the most promising concept. For small-scale air blown biomass gasifiers Vakalis et al. [52] thermodynamically modelled the methanation with additional hydrogen. They reached CH_4 concentrations of only 40 mol.-% because of the high N_2 concentrations inherent to the product gas of air-blown gasifiers. The modelling of a combination of the SER process with a TREMP methanation process was carried out in [53]. They reached cold gas efficiencies of 62% with this setup and about 60% when additional hydrogen from an electrolyzer was added. In [54], three different gasifier types were compared for the production of SNG with the conclusion that allothermal gasification systems, like the DFB system, result in the highest overall efficiencies. Rönsch et al. [11] give a comprehensive overview over many different modelling approaches for methanation reactors and SNG production plants. Depending on the scope of the study, the investigations range from detailed one-, two-, or three-dimensional methanation reactor models to flow sheet simulations of entire SNG process chains with zero-dimensional equilibrium models. However, no evaluation of

the results from the latest DFB gasifier design in terms of SNG production has been carried out. Furthermore, no detailed thermodynamic analysis of the SNG production from biogenic residues exists and no evaluation of the process in terms of the carbon utilization efficiency is reported.

In this paper, a thermodynamic model of a fluidized bed methanation reactor is developed and applied to specific feed gas mixtures, which have been obtained by experimental gasification test runs of different biogenic residues with a new generation of a 100 kW_{th} DFB gasifier at TU Wien. The chosen feed gas compositions for the methanation aim at covering the broad range of product gas compositions which can be produced by the DFB gasifier. The results show a detailed thermodynamic analysis of the raw-SNG gas compositions and key values for different feed gas mixtures and varying operation conditions like temperature and pressure. These results are discussed and evaluated in terms of their suitability for a feed-in into the natural gas grid. Because of the different process setups regarding the CO_2 separation unit in Güssing and Gothenburg, the placement of the CO_2 separation unit upstream or downstream of the methanation reactor is discussed as well.

2 Concept and methodology

In order to calculate the thermodynamic equilibrium, only four of the seven reaction equations (Eq. 1 to Eq. 7) need to be considered. Otherwise, the system would be overdetermined, because only four equations are linearly independent of each other. For example, the CO_2 methanation reaction can be seen as the reversed water-gas shift reaction followed by the CO methanation.

Thermodynamic calculations were performed with HSC Chemistry 6 and MATLAB. HSC Chemistry is a commercially available software tool for thermodynamic calculations and contains a database with thermodynamic property data. It calculates the thermodynamic equilibrium concentrations with the Gibbs free energy minimization method. For the purpose of this work, a MATLAB-based program for the thermodynamic equilibrium calculations was developed. This program calculates the thermodynamic equilibrium based on the temperature dependent thermodynamic property data from HSC Chemistry. The solution was obtained by numerically solving the equilibrium constant expressions for each reaction equation. The equilibrium concentrations were then automatically plotted over temperature and pressure. The model was validated by comparing the calculated results on a random basis to results obtained with HSC Chemistry. This comparison showed that the model is highly accurate.

Figure 1 visualizes the modelling approach with a basic flowsheet. In the DFB gasification process, the feedstock is converted to the gasifier product gas. The validated results for a multitude of experimental test runs in a 100 kW_{th} DFB gasifier at TU Wien have already been published elsewhere (see Sect. 3) and are used as a basis for the modelling of the methanation in this study. In the gas cleaning section, impurities like dust, tar, as well as sulfur and nitrogen containing contaminants are removed. The gas cleaning is not included in the model because it does not influence the thermodynamic calculations of the methanation. Therefore, the gas cleaning is treated as a black box which removes all impurities except ethylene. Ethylene was found to be the main hydrocarbon in the gasifier product gas besides CH_4 which is not removed by conventional gas cleaning steps like scrubbers or activated carbon filters. Besides ethylene, also hydrocarbons like benzene, toluene, xylene, or naphthalene are often not completely removed [55–57]. In this investigation, they are neglected because the concentrations are comparably low. After the gas cleaning, the gasifier product gas is fed to the methanation unit. Here, the thermodynamic model is applied and the conversion of the feed gas to raw-SNG is calculated. Since the raw-SNG does not fulfill the requirements of the gas grid, the necessary gas upgrading steps are also discussed but not modelled. Optionally, the CO_2 separation can be carried out as shown in Fig. 1 or as part of the raw-SNG upgrading after the methanation reactor. The standard setup in this investigation is the downstream CO_2 separation as part of the raw-SNG upgrading. However, also the upstream CO_2 separation as indicated in Fig. 1 is discussed.

The main focus of this investigation is a low-temperature methanation (300 °C) at ambient pressure. These parameter settings result from the current efforts on the scientific investigation of a novel bench-scale fluidized bed methanation setup for the given parameters. As the DFB gasification process also operates at ambient pressure an additional energy input for compression is avoided. This bench-scale methanation setup has been designed and built at TU Wien and is currently in the commissioning phase. Nevertheless, also a temperature variation from 200 to 500 °C and a pressure range from 1 to 10 bar_a are investigated. While thermodynamic calculations are in general independent of the reactor design, the validity of the underlying assumptions is nevertheless defined by the process-related circumstances. In this study, this translates to the following assumptions: (i) the water-gas shift reaction takes place simultaneously to the methanation reactions in one reactor without a need for a prior adjustment of the H_2/CO ratio, (ii) C_2H_4 is hydrogenated to methane, and (iii) despite the high exothermicity of the reactions, a low-temperature methanation (e.g. 300 °C) is possible in one reactor. These assumptions are only valid for fluidized bed methanation but would not be valid for fixed bed methanation as reported in literature [10, 44, 45, 58]. Graphite is chosen as the prevailing carbon species, since Frick et al. [46] found that

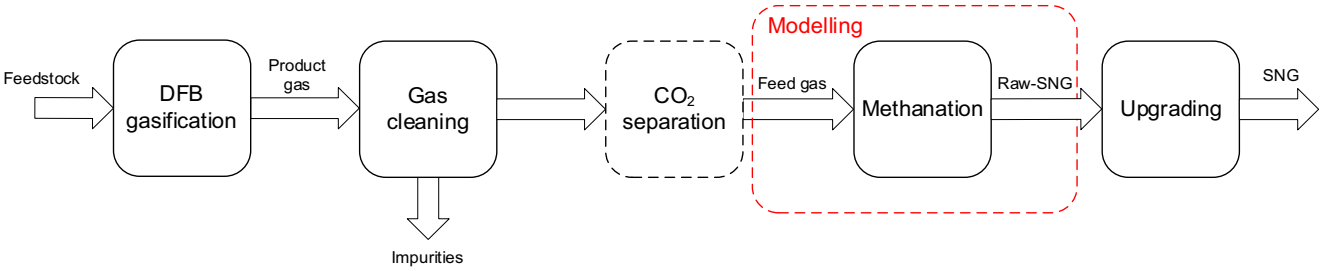

Fig. 1 SNG production flowsheet via the DFB gasification route; the highlighted area defines the modelled part of the process in this study

the Gibbs free energy is lower than for amorphous carbon and is thus preferentially formed.

In order to classify the feed gas composition, the stoichiometric number (*SN*) is defined in Eq. 8.

$$SN = \frac{y_{H_2}}{3\,y_{CO} + 4\,y_{CO_2} + 2\,y_{C_2H_4}} \tag{8}$$

SN gives the ratio between the molar fraction of H_2 (y_{H_2}) to the molar fractions of the carbonaceous species in the feed gas which react to CH_4. If *SN* is equal to 1, there is a stoichiometric amount of H_2 available according to Eqs. 1, 3, and 4. Because the regarded pressures in this study are relatively low, an ideal gas behavior is assumed and molar fractions are thus equal to volume fractions. The definition of *SN* is not unambiguous, because the chemical equilibrium is influenced by all available species and therefore also by CH_4 and H_2O. Nevertheless, it allows an approximate classification of the feed gas mixture. Typical product gases from the DFB gasification of biogenic feedstock show similar CH_4 concentrations; moreover H_2O concentrations in the feed gases are assumed 0. The latter is attributed to the required gas cleaning which is conventionally carried out at low temperatures [59]. If similar CH_4 concentrations and a water-free feed gas are assumed, the implementation of *SN* is justified.

Additionally, the CH_4 yield (Y_{CH_4}) is defined in Eq. 9. It describes how much of the carbon in the feed gas is converted to CH_4.

$$Y_{CH_4} = \frac{\dot{n}_{CH_4,eq}}{\sum_i N_i\,\dot{n}_{i,feed}} \times 100 \tag{9}$$

The carbon yield (Y_C) in Eq. 10 is a measure for carbon deposition.

$$Y_C = \frac{\dot{n}_{C,eq}}{\sum_i N_i\,\dot{n}_{i,feed}} \times 100 \tag{10}$$

Index *i* refers to the carbonaceous species in the feed (*i* = CH_4, CO, CO_2, C_2H_4), and N_i is the number of carbon atoms in species *i*.

The CO conversion (X_{CO}) in Eq. 11 gives the amount of CO which is converted during the reaction.

$$X_{CO} = \frac{\dot{n}_{CO,feed} - \dot{n}_{CO,eq}}{\dot{n}_{CO,feed}} \times 100 \tag{11}$$

Analogously to Eq. 11, the CO_2 conversion (X_{CO_2}) is defined in Eq. 12.

$$X_{CO_2} = \frac{\dot{n}_{CO_2,feed} - \dot{n}_{CO_2,eq}}{\dot{n}_{CO_2,feed}} \times 100 \tag{12}$$

In order to assess the performance of the overall process, the carbon utilization efficiency (η_C) is introduced (Eq. 13). It sets the amount of carbon in the methane of the raw-SNG ($\dot{n}_{CH4,eq}$) in relation to the amount of carbon which is introduced to the process via the feedstock ($\dot{n}_{C,feedstock}$). If CO_2 is used as gasification agent, the amount of carbon in the gasification agent must be considered as well ($\dot{n}_{C,gasif}$). The carbon utilization efficiency illustrates how much of the carbon is valorized as CH_4 in the SNG and how much is "lost" mainly as CO_2.

$$\eta_C = \frac{\dot{n}_{CH4,eq}}{\dot{n}_{C,feedstock} + \dot{n}_{C,gasif}} = \eta_{C,DFB} \times Y_{CH4} \tag{13}$$

An analogous way to calculate the carbon utilization efficiency is by the multiplication of the carbon utilization efficiency over the DFB gasifier ($\eta_{C,DFB}$) and the methane yield in the methanation section (Y_{CH4}). In this paper, $\eta_{C,DFB}$ is calculated from the validated results of test runs with the 100 kW_{th} DFB gasifier at TU Wien. This value is therefore only valid for this gasifier. An extrapolation of $\eta_{C,DFB}$ to large-scale gasifiers is not recommended since the internal energy and mass balances might differ. In this small-scale gasifier, the high heat losses are balanced by the addition of heating oil in the combustion section of the DFB process which is not the case for large-scale plants. Large-scale gasifiers exhibit much lower heat losses, but, depending on the feedstock, a partial recycling of product gas to the combustion section might still

be necessary. The recycled amount of product gas is not available for methanation. This factor cannot be considered in the calculation, and the shown results therefore need to be seen as a maximum.

Additionally, the minimum amount of steam (H_2O_{feed}), which needs to be added upstream of the methanation reactor to prevent carbon formation, is introduced. In order to calculate H_2O_{feed}, every investigated reaction condition with each feed gas is checked for the possibility of carbon formation. If carbon formation is possible, the water content in the feed gas is incrementally increased until the thermodynamic possibility for carbon formation yields 0. At this point, H_2O_{feed} can be obtained. Furthermore, gas cleaning is not within the scope of this study and the feed gas mixtures for the methanation are assumed free of impurities and other minor components. Besides, kinetics or heat and mass transfer phenomena are not considered.

3 Results and discussion

Table 1 shows the investigated feed gas compositions for the methanation derived from DFB gasification. In the upper part of the table, the operational parameters of the DFB gasification process are shown. All displayed feed gas compositions are obtained with a new generation 100 kW_{th} DFB gasifier at TU Wien. The DFB process is not elaborated in this study and further information can be found in literature [4, 7, 8, 56, 60, 61]. The lower part of Table 1 depicts the gas compositions which are derived from the DFB gasification process and are in further consequence used as the feed gas compositions for the methanation process. All feed gases are assumed to be free of H_2O. Feed gas no. 1 shows a typical SER product gas with a high hydrogen content. Limestone (L) is used as bed material, and bark (BA) is chosen as feedstock. Feed gas no. 2–no. 4 present product gases from conventional gasification. With feed gas no. 2, the same fuel and bed material as with feed gas no. 1 is used but the gasification temperature is higher which results in lower H_2 and higher CO and CO_2 contents. For feed gas no. 3, lignin (LI) is used as fuel and olivine (O) as bed material. Sewage sludge (SS) and an olivine/limestone mixture (O/L) are the basis for feed gas no. 4, which results in low H_2 and high CO_2 contents. For feed gas no. 5, a CO_2/H_2O mixture is used as gasification agent and rapeseed cake (RSC) and O as fuel and bed material, respectively. This results in even lower H_2 and high CO and CO_2 concentrations. Feed gas no. 6 shows a temperature variation for SER gasification. This is included to demonstrate the adaptability of the DFB gasification process to the requirements of the methanation process (cf. Fig. 6). Data for this variation is only available for softwood (SW) as feedstock.

In Fig. 2, the results of the chemical equilibrium calculations at 300 °C and 1 bar_a are shown for feed gas nos. 1–5. The volume fractions of the dry gas components after the methanation (referred to as raw-SNG) and the water content of the raw-SNG ($H_2O_{raw\text{-}SNG}$) as well as the minimum required water content in the feed gas in order to prevent carbon deposition (H_2O_{feed}) are depicted.

Additionally, Table 2 lists some key figures as defined in Eqs. 8–12 complementary to the results in Fig. 2. In Fig. 2a and the left part of Table 2 (without H_2O_{feed}), the results for a water-free feed gas are displayed. Figure 2b and the right part of Table 2 (with H_2O_{feed}) display the results with steam addition to the feed gases in order to prevent carbon formation. C_2H_4 is not depicted in any of the figures, because it is

Table 1 Investigated feed gases

DFB parameters	Unit	Feed gas number					
		1	2	3	4	5	6
Source	–	[8]	[4]	[56]	[7]	[60]	[61]
Gasification agent	–	H_2O	H_2O	H_2O	H_2O	CO_2/H_2O[a]	H_2O
Feedstock	–	BA	BA	LI	SS	RSC	SW
Bed material	–	L	L	O	O/L[b]	O	L
Gasification temperature	°C	625	761	789	800	840	582–797
Combustion temperature	°C	820	998	945	945	938	830–1041
Feed gas composition to methanation (water-free feed)							
H_2	vol.-%	68.3	51.1	42.6	35.6	25.8	71.1–47.6
CO	vol.-%	6.5	17.9	21.2	13.7	32.1	7.3–21.6
CO_2	vol.-%	8.9	22.4	21.8	36.5	33.7	4.1–23
CH_4	vol.-%	14.5	8.0	12.0	11.7	7.3	17.4–8.8
C_2H_4	vol.-%	1.9	0.6	2.4	2.5	1.1	1.9–0.5

[a] CO_2/H_2O = 68/32 vol.-%

[b] O/L = 80/20 wt.-%

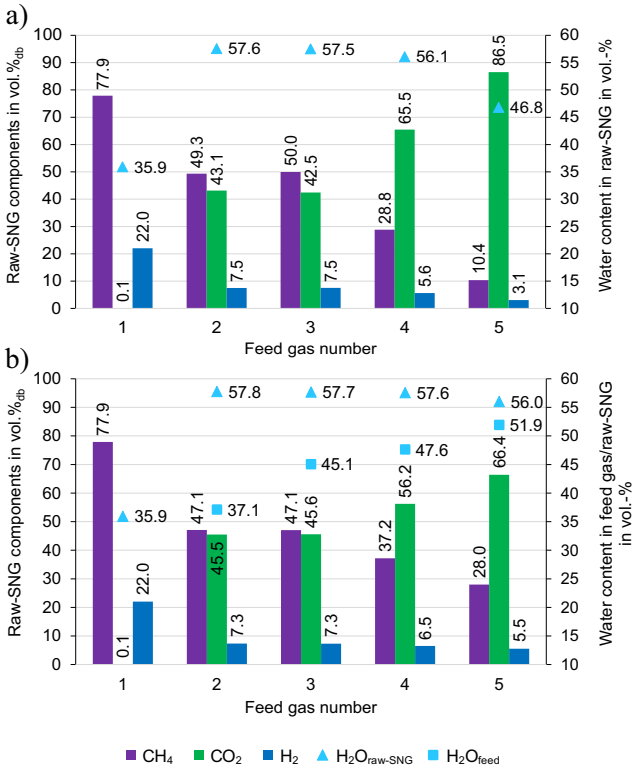

Fig. 2 Raw-SNG gas composition for feed gas nos. 1–5 at 1 bar_a and 300 °C. **a** Water-free feed gas. **b** Feed gas with steam addition to prevent carbon deposition

completely converted under all investigated conditions. CO is also not shown in Fig. 2 because it is almost entirely converted (see Table 2) and only trace amounts remain in the raw-SNG. The feed gases are displayed in descending order for *SN* in Fig. 2 as well as in Table 2. This results in a decreasing trend for CH_4 and H_2 and an increasing trend for CO_2 in the raw-SNG. Analogously, the methane yield and the CO_2 conversion drop significantly with understoichiometric feed gases.

A closer look at the results for the water-free feed gases reveal that the SER feed gas (feed gas no. 1) allows an almost complete conversion of CO and CO_2 to CH_4. Thus, no CO_2 separation is necessary. In addition, no carbon formation is thermodynamically expected. However, 22 vol.-$\%_{db}$ of H_2 is still in the raw-SNG and needs to be separated below 4 vol.-% before grid feed-in according to the Austrian regulations [22, 23]. Feed gas nos. 2–5 result in a lower CH_4 content and a higher CO_2 content. The CO conversion is almost complete even though *SN* is well below one for feed gas nos. 2–5. This is possible because thermodynamically the feed-CO is rather converted to solid carbon than left unreacted in the raw-SNG. This results in severe carbon depositions with a carbon yield as high as 54.5%. More than half of the carbon in the feed would be deposited on the catalyst. This deposition would result in a high loss of carbon and deactivate the catalyst. Therefore, feed gas nos. 2–5 should not be introduced into the methanation reactor without a previous steam addition. Thus, in Fig. 2b and the right part of Table 2, the results with the addition of steam to the feed gas are depicted. The amount of steam added corresponds to the minimum amount needed to prevent carbon formation. For feed gas no. 1, no steam addition is necessary and therefore the results are the same as in Fig. 2a. All other feed gases require steam addition in a range of 37 to 52 vol.-%. The raw-SNG for these feed gases therefore shows a different composition compared with the water-free feed gases. For feed gas nos. 2 and 3, about half the raw-SNG consists of CH_4, the rest is CO_2 and H_2. For feed gas nos. 4 and 5, CO_2 constitutes the main component in the raw-SNG with a CH_4 yield of approximately 40% and 30%, respectively. All four gas compositions require the separation of both CO_2 and H_2 before grid feed-in, even if the less stringent limitation of 10 vol.-% H_2 is applied. Compared with the results of the dry feed gases, the CH_4 yield is slightly increased but the CO_2 conversion is significantly lowered. All four gases show a negative CO_2 conversion, which implies that more moles of CO_2 are produced than consumed during the reaction. The influence of the steam addition on the reactions can be pictured as follows: The water-gas shift reaction (Eq. 2) proceeds towards CO_2 and H_2. This way, more H_2 is available for the methanation of CO and less CO needs to be methanated because it is shifted towards CO_2. The additional H_2 is used to hydrogenate the solid carbon. From this point of view, it also becomes apparent that the CO_2 conversion is less compared with the results of the water-free feed or even negative. There are of course many ways to illustrate this effect. The reaction pathway is only important for the consideration

Table 2 Key figure results of the equilibrium calculations

Parameter	Unit	Feed gas number (without H_2O_{feed})					Feed gas number (with H_2O_{feed})				
		1	2	3	4	5	1	2	3	4	5
SN	-	1.16	0.35	0.27	0.19	0.11	1.16	0.35	0.27	0.19	0.11
Y_{CH_4}	%	99.9	28.2	24.6	14.4	5.2	99.9	50.8	49.2	39.8	29.6
Y_C	%	0	47.2	54.5	52.8	50.9	0	0	0	0	0
X_{CO}	%	100	99.9	99.9	99.8	99.9	100	99.8	99.8	99.6	99.8
X_{CO_2}	%	99.7	45.6	42.7	39.9	2.2	99.7	− 8.5	− 34.9	− 10.3	− 57.1

of kinetic effects and does not influence the thermodynamic equilibrium. Table 2 shows that the CO conversion remains almost complete for all feed gases. Nevertheless, the CO_2 methanation is found to be kinetically inhibited even for very low CO concentrations [62]. For feed gas no. 1, only 7 $ppm_{v,db}$ of CO remain in the raw-SNG in the thermodynamic equilibrium. At least 600–700 $ppm_{v,db}$ need to be expected for feed gas nos. 2–5. As long as there are no regulations on the allowed CO content, no statement about the grid feed-in can be made. The authors recommend a threshold value for CO if the production of SNG via the thermochemical pathway is further pursued at industrial scale.

3.1 Investigation of the sewage sludge product gas

In the following section, a more in-depth discussion of the feed gas derived from SS gasification follows (feed gas no. 4). Because of the expected carbon deposition for this feed gas composition, H_2O should be added if a long catalyst lifetime and a high conversion efficiency are aimed at. This was already discussed in the previous section. Hence, Fig. 3 depicts the raw-SNG gas composition after the addition of steam for a temperature variation from 200 to 500 °C and pressures of 1, 5, and 10 bar_a (Fig. 3b). The amount of steam added corresponds to the minimum amount needed to prevent carbon deposition. This minimum volume fraction of H_2O in the feed gas (H_2O_{feed}) as well as Y_{CH_4} is also displayed (Fig. 3a). With increasing temperature, less CH_4 and CO_2 and more CO and H_2 are present. Accordingly, the CH_4 yield decreases from 41 to 26% with increasing temperature at 1 bar_a. H_2O_{feed} decreases from 55 to 40 vol.-% within the displayed temperature range. Nevertheless, the methanation is preferred at low temperatures from a thermodynamic point of view if the additionally required steam is not seen as the decisive factor. Especially, the low methane yield and the strongly rising CO content at higher temperatures make low-temperature methanation attractive. Pressure only has a significant influence on the gas composition at higher temperatures. At 500 °C, Y_{CH_4} can be substantially elevated and the H_2 content significantly lowered if the pressure is increased to 5 bar_a. A further pressurization only allows a minor improvement of Y_{CH_4} but still reduces the H_2 content by 5 percentage points. At 200 °C, Y_{CH_4} is almost constant for all pressures. For H_2O_{feed}, hardly any influence of pressure can be observed.

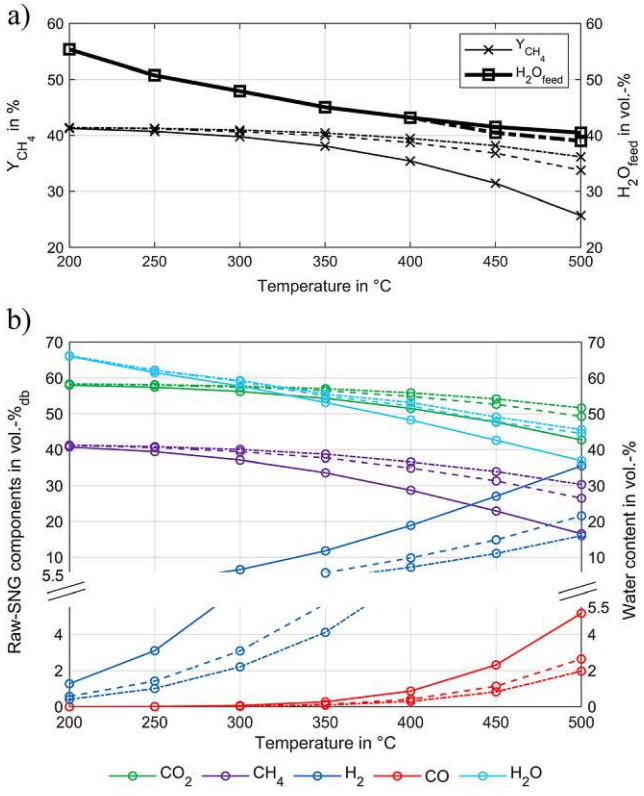

Fig. 3 Temperature and pressure variation for feed gas no. 4 in the thermodynamic equilibrium: 1 bar_a (full line), 5 bar_a (dashed line), and 10 bar_a (dash-dotted line). **a** CH_4 yield and feed water content. **b** Raw-SNG gas composition

In general, this feed gas shows a rather unfavorable composition for methanation. The stoichiometric number is far below 1, and the CO_2 content in the feed gas is even higher than the H_2 content. For grid feed-in, the CO_2 needs to be separated from the raw-SNG. A maximum of only 2 vol.-% is allowed. A H_2 content below the allowed threshold level of 4 vol.-% after CO_2 separation and without an additional H_2 separation unit could be achieved by increasing the pressure at 260 °C to 5 bar_a or at 280 °C to 10 bar_a. If the stringent feed-in specification of the natural gas grid is loosened and 10 vol.-% H2 is allowed in the future, the methanation can be performed at 350 °C at 10 bara, 320 °C at 5 bara, or 270 °C at 1 bara. Even though there is only a slight influence of pressure on the gas composition at these temperatures, a small increase can nevertheless enable the grid feed-in without an H2 separation unit. This is especially interesting if 10 vol.-% of H2 would be allow in the gas grid because the reaction temperature would be in a range where catalysts were found to be kinetically active. If the desired commodity is hythane, only CO2 separation is necessary and the discussion concerning the H2 content and the pressurization can be neglected.

3.2 Investigation of the feed gases with upstream CO_2 separation

Firstly, the upstream CO_2 separation is discussed with the sewage sludge product gas (feed gas no. 4) in detail before the discussion is extended to all other investigated feed gas compositions. In Fig. 4, the equilibrium calculations for feed gas no. 4 in a temperature range from 200 to 500 °C and pressures of 1, 5, and 10 bar_a are shown. In contrast to Fig. 3, the CO_2 separation is done upstream of the methanation reactor as demonstrated in the GoBiGas project in

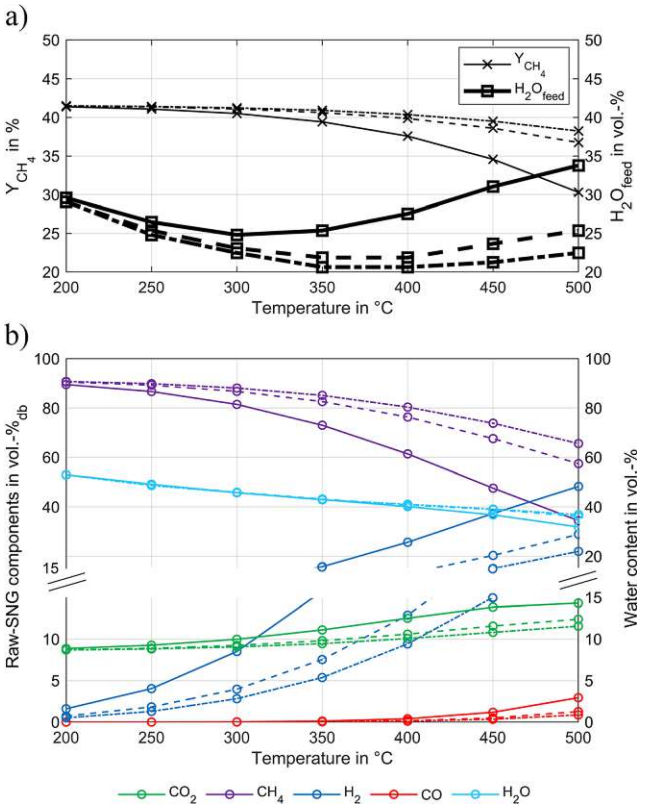

Fig. 4 Temperature and pressure variation for feed gas no. 4 in the thermodynamic equilibrium with CO_2 separation upstream of the methanation: 1 bar_a (full line), 5 bar_a (dashed line), and 10 bar_a (dash-dotted line). **a** CH_4 yield and feed water content. **b** Raw-SNG gas composition

Gothenburg. The feed gas to the methanation is therefore free of CO_2. In order to enable a fair comparison to Fig. 3, the calculation of the methane yield includes the CO_2 separation step in this case. A comparison between Figs. 3 and 4 reveals that Y_{CH_4} is slightly increased, whereas the required amount of steam in the feed is substantially lowered. The lower amount of steam in the feed could lead to a more energy-efficient process because less steam needs to be provided to the methanation reactor. Interestingly, at higher temperatures, H_2O_{feed} increases again and the pressure sensitivity is much more pronounced in comparison. The H_2 content is a little higher and the CO content slightly lower (e.g., 250 $ppm_{v,db}$ compared with 667 $ppm_{v,db}$ at 300 °C and 1 bar_a) comparing CO_2 separation upstream and downstream of the methanation reactor. The CO_2 content is in a range of 9 to 15 vol.-$\%_{db}$, which implies that CO_2 is formed during the reaction. The CO_2 content as well as the higher H_2 and lower CO content in the raw-SNG can be explained by the water-gas shift reaction (Eq. 2) which is shifted towards CO_2 and H_2 due to the missing CO_2 and the understoichiometric H_2/CO ratio in the feed. In this case, the CO_2 needs to be separated again, which requires a second CO_2 separation unit. The same applies for feed gas nos. 2, 3, and 5. These feed gases also have a H_2/CO ratio below 3, and therefore CO_2 is formed during the reaction in an order that it exceeds the limit of 2 vol.-% for all investigated operation conditions. Hence, a simple process setup with a single CO_2 separation step upstream of the methanation reactor does not suffice for a single stage methanation when understoichiometric feed gases, like feed gas nos. 2–5, are introduced to the methanation reactor. Two possible arrangement results are as follows: (i) The CO_2 separation unit is placed downstream of the methanation reactor. The resulting disadvantage is the slightly lower methane yield, as shown above, and a higher gas volume flow through the methanation reactor because of the surplus CO_2. The latter increases the capital expenditures (CAPEX) of the methanation reactor. On the other hand, the strong volume contraction during methanation reduces the gas flow through the CO_2 separation unit which in turn reduces the CAPEX. (ii) A CO_2 separation unit is placed upstream and downstream of the methanation reactor. The methane yield is slightly higher and the gas flow through the methanation is lower. The disadvantages in this case are the increased CAPEX for the second CO_2 separation step and the increased heat flux in the methanation reactor due to the missing ballast gas. Hence, the second option does not seem to be favorable because of the additionally required process unit in the case of a single stage fluidized bed methanation with the investigated understoichiometric feed gases (feed gas nos. 2–5). For the SER feed gases (feed gas no. 1 and no. 6), the CO_2 separation can be neglected completely if the right operating conditions are chosen as is explained below. For a multistage process, like GoBiGas, the upstream CO_2 removal is nevertheless justified. The water-gas shift reaction is carried out in a separate reactor followed by the CO_2 separation unit, both upstream of the methanation reactors. This way, the production of CO_2 and surplus H_2 in the methanation section can be suppressed and no further gas upgrading besides drying is necessary.

3.3 Investigation of the SER product gas

Feed gas no. 1 is a typical SER product gas with a high H_2 content. The *SN* is greater than 1, which allows a practically complete methanation of the carbonaceous species (CO + CO_2 + C_2H_4) at temperatures up to 300 °C with a CH_4 yield of nearly 100% (Fig. 5).

Pressure only has a significant influence on the gas composition at higher temperatures. With pressurization, the decreasing trend of CH_4 and the increasing trends of H_2, CO, and CO_2 at higher temperatures can be counteracted. In addition, above 440 °C at 1 bar_a carbon formation is thermodynamically possible. As is shown in Fig. 5a, H_2O needs to be added in this small operating window. At higher pressures, the steam addition can be prevented. Below 300 °C, there is practically no influence of pressure or temperature on the gas composition. In this case, methanation around 300 °C and

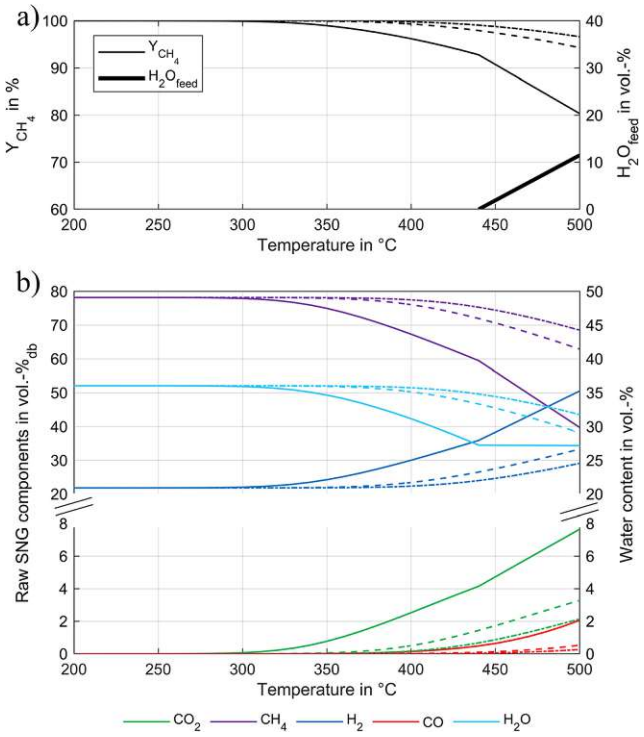

Fig. 5 Temperature and pressure variation for feed gas no. 1 in the thermodynamic equilibrium: 1 bar_a (full line), 5 bar_a (dashed line), and 10 bar_a (dash-dotted line). **a** CH_4 yield and feed water content. **b** Raw-SNG gas composition

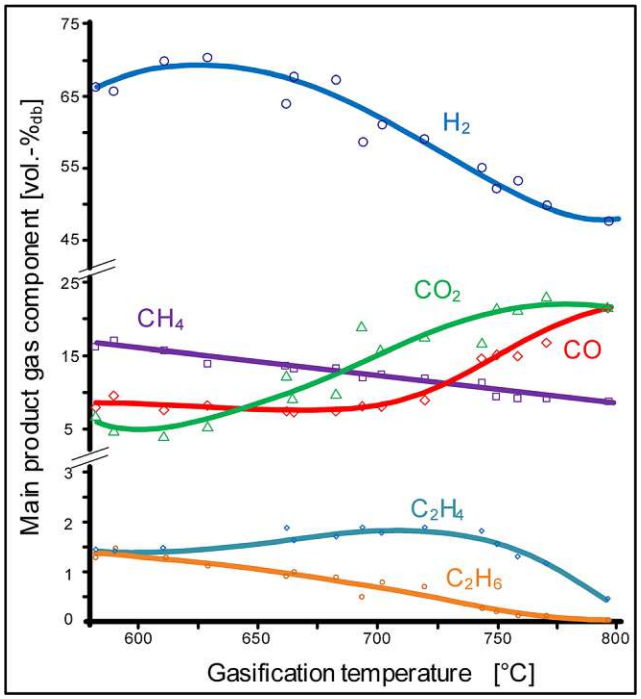

Fig. 6 Product gas composition over gasification temperature for the 100 kW_{th} DFB gasifier at TU Wien for softwood and olivine as fuel and bed material, respectively (from [61])

1 bar_a shows a favorable raw-SNG composition without the need of compression. Lower temperatures would not improve the gas composition but increase the challenge of employing an active catalyst. For grid feed-in, only H_2 would need to be separated from the raw-SNG. For the application as hythane on the other hand, no further upgrading step is necessary except water condensation.

3.4 Investigation of variable product gas compositions of the SER process

Fuchs et al. [61] already described the adaptability of the SER process with regard to the product gas composition. In Fig. 6, the evolution of the product gas components over the gasification temperature of the 100 kW_{th} DFB gasifier at TU Wien is depicted. The product gas can be adjusted to the required feed gas for methanation by varying the gasification temperature. However, this also adds an additional parameter to the modelling of the methanation reactions. The range for the gas components, the temperatures, the used bed material, and the fuel is already listed in Table 1 (feed gas no. 6).

Figure 7 displays the composition of the raw-SNG in the thermodynamic equilibrium for all data points of Fig. 6 over *SN*. Temperature and pressure are again set to 300 °C and 1 bar_a respectively, for the methanation process. In order to assess the carbon formation, Y_C is given. There is a decreasing trend for CO_2, H_2O, and the amount of carbon formed for an increasing *SN*. CH_4 has a maximum at a *SN* slightly above 1. At the same point, carbon formation declines to 0 and the small incline in H_2 turns into a sharp increase for higher *SN*. CO is only present in trace amounts (0.14–614 $ppm_{v,db}$) and is not displayed here. From a thermodynamic point of view, the feed gas with a *SN* of 1.09 results in a raw-SNG with the most favorable composition for the methanation at 300 °C and 1 bar_a. A *SN* of 1.09 corresponds to a gasification temperature of about 680 °C. The associated compositions for the feed gas and the raw-SNG as well as the key figures are depicted in Table 3. Both CO and CO_2 are almost completely converted and therefore no CO_2 separation step is necessary. Compared with feed gas no. 1 the H_2 content is lower but for grid feed-in the H_2 still needs to be separated. A pressure increase to 4 bar_a lowers the H_2 content below 10 vol.-%, and the raw-SNG could be directly utilized as SNG without further purification if the loosened H_2 restriction in the gas grid is assumed. This would be an economic improvement because no H_2 separation step is necessary. Additionally, the CH_4 yield and the CO_2 conversion increase and the CO content decreases. The according raw-SNG composition and the key figures at 4 bar_a and 300 °C are also displayed in Table 3. Different operation conditions of the methanation might favor other feed gas compositions from Fig. 6 and vice versa. In order to find the most suitable feed gas composition for deviating methanation conditions, reiterations of the thermodynamic equilibrium calculations would have to be carried out.

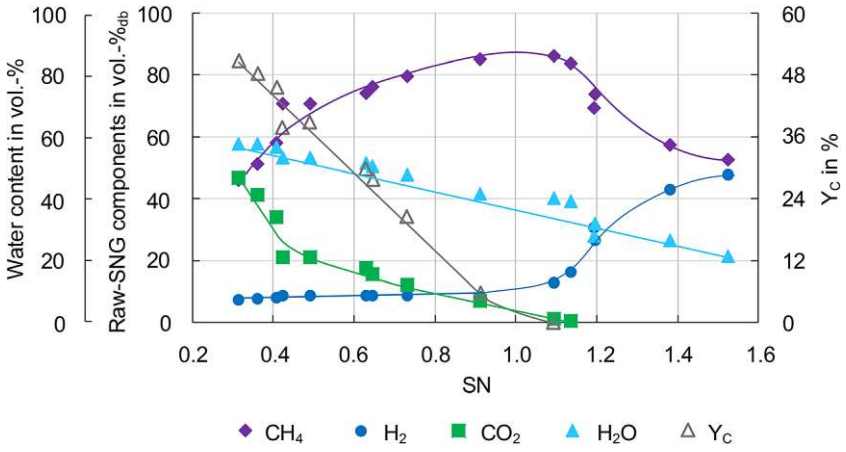

Fig. 7 Raw-SNG gas composition and Y_C over *SN* at 300 °C and 1 bar_a for the feed gas compositions according to Fig. 6 in the thermodynamic equilibrium

3.5 Comparison of all investigated feed gases with the carbon utilization efficiency

Table 4 compares the investigated feed gases (feed gas nos. 1–6) by means of the carbon utilization efficiencies (η_C, $\eta_{C,DFB}$) as well as the H_2 and CO_2 contents in the raw-SNG at 300 °C and 1 bar_a. η_C is the highest for the product gas from the gasification of LI (feed gas no. 3) and the lowest for the product gas from the CO_2 gasification of RSC (feed gas no. 5). All other values for η_C are in a similar range between 34.6 and 37.9%. The comparison of η_C and $\eta_{C,DFB}$ reveals that the carbon utilization for the SER product gases (feed gas no. 1 and 6) is governed by the carbon utilization in the DFB system. The excess carbon (in the form of CO_2), which is still in the raw-SNG in case of conventional gasification (like feed gas nos. 2–4), is already removed within the SER process by the increased transport of carbon from the fuel to the flue gas. This results in a low $\eta_{C,DFB}$ but a similar value for η_C compared with feed gas nos. 2 and 4 because nearly a complete carbon utilization is achieved in the methanation section. Additionally, no CO_2 separation step is required as the possibility to adjust the stoichiometric number *SN* is inherent to the process. Further savings result from the fact that no steam addition to the feed gas is necessary and the fact that the composition of the feed gas can be adjusted (cf. Fig. 6). Despite the high flexibility, a H_2 separation is nevertheless required under current regulations. If 10 vol.-% of H_2 would be allowed, the SER process seems economically advantageous because neither a CO_2 nor a H_2 separation unit or a steam addition to the feed gas is required under the right process conditions (e.g. feed gas no. 6 at 300 °C and 4 bar_a). The CO_2 separation alone was estimated to account for 13–22% of the total fixed capital investment costs of a biomass-to-SNG plant [19].

The highest η_C is reached with feed gas no. 3, which originates from the gasification of lignin with olivine as bed material. The high η_C results from the high value for $\eta_{C,DFB}$. Almost 93% of the carbon in the fuel is relocated to the gasifier product gas. The lowest η_C results from feed gas no. 5, which originates from the gasification of rapeseed cake with olivine as bed material and a CO_2/H_2O mixture as gasification agent. The gasification with a CO_2 admixture to the

Table 3 Feed gas and raw-SNG composition and key figures for the feed gas with a *SN* of 1.09 at 300 °C and 1 bar_a as well as 300 °C and 4 bar_a in the thermodynamic equilibrium

Parameter	Unit	Feed gas	Raw-SNG at 1 bar_a	Raw-SNG at 4 bar_a
CH_4	vol.-$\%_{db}$	13.3	86.1	90.0
H_2	vol.-$\%_{db}$	67.8	12.8	9.8
CO	vol.-$\%_{db}$	7.3	0.005	0.0008
CO_2	vol.-$\%_{db}$	9.8	1.1	0.2
C_2H_4	vol.-$\%_{db}$	1.7	0	0
H_2O	vol.-%	0	40.2	41.6
Y_{CH_4}	%	-	98.8	99.7
Y_C	%	-	0	0
X_{CO}	%	-	100	100
X_{CO_2}	%	-	95.8	99.1

Table 4 Comparison of the carbon utilization efficiencies and the H_2 and CO_2 contents in the raw-SNG for feed gas nos. 1–6 at 300 °C and 1 bar_a

Parameter	Unit	Feed gas number					
		1	2	3	4	5	6
$\eta_{C,\ DFB}$	%	36.5	72.8	92.6	86.9	78.0	38.4
η_C	%	36.5	37.0	47.0	34.6	23.1	37.9
H_2 content	vol.-$\%_{db}$	22.0	7.3	7.3	6.5	5.5	12.8
CO_2 content	vol.-$\%_{db}$	0.1	45.5	45.6	56.2	66.4	1.1

gasification agent therefore cannot be used advantageously for the production of SNG if no external hydrogen is provided. For feed gas nos. 2–5, a CO_2 separation and a H_2 separation is required. If the 10 vol.-% H_2 threshold is applied, the H_2 separation can be avoided (e.g. feed gas no. 4 at 320 °C and 5 bar_a). Even the 4 vol.-% H_2 threshold can be met if the operation conditions are adapted (e.g. feed gas no. 4 at 280 °C and 10 bar_a), but kinetic effects at these low temperatures most likely need to be considered. For these feed gases (feed gas nos. 2–5), the carbon utilization efficiency can be increased by the addition of H_2 from external sources (e.g. electrolysis) which allows the methanation of the leftover CO_2. From a technical and ecological point of view, the addition is advantageous since η_C can be maximized. The availability and the expenditures for the additional hydrogen on the other hand need to be eyed critically. In this paper, this concept is not discussed any further but some relevant studies were already referred above [50, 52].

In general, the calculated results are in good agreement with literature values. The GoBiGas plant reached a η_C of about 30%, which is slightly lower as most of the calculated values. The slightly lower values seem justified, since this study is based on thermodynamic calculations and therefore the results need to be seen as maximum values. The gasification section of the GoBiGas plant reached a $\eta_{C,DFB}$ of about 70% as can be calculated from the results in [63]. This value is similar to feed gas no. 2 but lower compared with all other feed gases. The discrepancy possibly arises from the small scale and good performance of the pilot plant as well as the difficult scalability of the carbon utilization efficiency as explained in the methodology section. Taking the results from the modelling study of Heyne and Harvey [19], a η_C of 35% can be calculated, which is very close to the calculated values in this paper. Also, the raw-SNG composition with 45 vol.-$\%_{db}$ of CH_4, 47 vol.-$\%_{db}$ of CO_2, and 4 vol.-$\%_{db}$ of H_2 is close to the calculated values. Similar values were also reported by Gassner et al. [64] who calculated a raw-SNG composition with 45 vol.-$\%_{db}$ CH_4, 45 vol.-$\%_{db}$ CO_2, and 6 vol.-$\%_{db}$ H_2. Both studies assumed similar operating conditions at approximately 300 °C and 1 bar_a. Experimentally, Seemann et al. [58] confirmed a similar raw-SNG composition. They reconstructed the feed gas composition of the Güssing gasifier and reached slightly lower CH_4 concentrations at approximately 40 vol.-$\%_{db}$ CH_4, 47 vol.-$\%_{db}$ CO_2, and 4 vol.-$\%_{db}$ H_2. The 1 MW_{SNG} methanation plant in Güssing, however, could not meet the 4 vol.-% threshold, and a two-stage membrane separation process was necessary, whereas in Gothenburg, no H_2 separation unit was required [10, 31].

4 Conclusion and outlook

In this work, the suitability of various product gases from the 100 kW_{th} DFB gasifier for methanation in a fluidized bed reactor was evaluated from a thermodynamic point of view. It was shown that a complete methanation of CO and CO_2 is only possible for SER product gases. For all other presented product gases, only the methanation of CO is possible, whereas CO_2 might even constitute the main raw-SNG component. Additionally, gases from conventional steam gasification or gasification with CO_2 admixture to the gasification agent (H_2O + CO_2) are subject to carbon depositions in the methanation reactor. Therefore, up to 55 vol.-% of H_2O needs to be added to the feed gas for a stable operation. Furthermore, the influence of different operation conditions of the methanation on the raw-SNG composition was visualized. By the careful choice of operation conditions, energy savings and/or less effort for further gas upgrading can be accomplished. A comparison between upstream and downstream CO_2 separation revealed that only a downstream CO_2 separation results in the required SNG quality if a single fluidized bed methanation reactor with understoichiometric feed gases is utilized. A further investigation of the SER product gases revealed that it is also possible to adapt the gasification process to suit certain methanation conditions. A SER product gas with a stoichiometric number of 1.09, which corresponds to a gasification temperature of 680 °C, was shown to be the most suitable feed gas for methanation. No CO_2 separation step and no H_2O addition to the feed gas was necessary, which clearly indicated an economic advantage. However, under current regulations, a H_2 separation unit could not be avoided for the raw-SNG from the SER product gas. An increase of the allowed H_2 content in the natural gas grid to 10 vol.-% would therefore increase the degrees of freedom of the whole system. In turn, this would result in improved operating points, which would simplify the overall process and reduce costs. This would apply for all investigated feed gases, but especially the SER process would benefit from these loosened restrictions. For example, the SER product gas (feed gas no. 6) could be methanated at 300 °C and 4 bar_a to gas grid quality without a CO_2 or H_2 separation step nor a H_2O addition to the feed gas.

A comparison of the carbon utilization efficiencies revealed that the gasification of lignin resulted in the highest

overall value of 47%. Apart from one exception, all other values including the SER product gases range between 34.6 and 37.9%. Only if CO_2 is added to the gasification agent, the carbon utilization factor drops to 23%. The addition of H_2 from an external source would allow a much more efficient conversion of the carbon, but the availability and the economic implications would need to be considered.

It should be noted that all investigations in this paper are based on thermodynamic equilibrium calculations. Catalyst poisoning due to insufficient gas cleaning, kinetic limitations concerning carbon deposition, methanation of CO_2, the high feed water content, or low temperatures as well as possible heat or mass transfer limitations necessitate experimental investigations. These issues are subject of further investigations with the bench-scale fluidized bed methanation setup at TU Wien.

Funding information Open access funding provided by TU Wien (TUW). This work is part of the research project ReGas4Industry (871732) and receives financial support from the research program "Energieforschung" funded by the Austrian Climate and Energy Fund.

Abbreviations *BA,* bark; *bar_a,* bar absolute; *C,* carbon; *CNG,* compressed natural gas; *db,* dry basis; *DFB,* dual fluidized bed; *eq,* equilibrium; *feed,* in the feed gas; *gasif,* in the gasification agent; ΔH_R^{300}, molar reaction enthalpy at 300 °C; *H_2O_{feed},* volume fraction of H_2O in the feed in vol.-%; *L,* limestone; *LI,* lignin; *O,* olivine; *N_i,* number of carbon atoms in species *i*; $\dot{n}_i$, molar flow of species *i* in mol/s; *η_C,* overall carbon utilization efficiency; *$\eta_{C,\ DFB}$,* carbon utilization efficiency over the DFB gasifier; *O/L ,* olivine/limestone mixture; *PSA,* pressure swing adsorption; *PSI,* Paul Scherrer Institute; *PtG,* power-to-gas; *raw-SNG,* raw synthetic natural gas after methanation/before gas upgrading; *RSC,* rapeseed cake; *SER,* sorption enhanced reforming; *SN,* stoichiometric number; *SNG,* synthetic natural gas; *SS,* sewage sludge; *SW,* softwood; *v,* volumetric; *vol.-%,* volumetric percent; *wt.-%,* weight percent; *X_{CO},* carbon monoxide conversion in %; X_{CO_2}, carbon dioxide conversion in %; *Y_C,* carbon yield in %; Y_{CH_4}, methane yield in %; *y_i,* molar fraction of species *i*

References

1. European Commission (2018) Directive (EU) 2018/2001 of the European Parliament and of the Council of 11 December 2018 on the promotion of the use of energy from renewable sources. Off J Eur Union L 328/82:128
2. International Energy Agency (2018) Gas 2018: analysis and forecasts to 2023. IEA. https://www.iea.org/reports/gas-2018. Accessed 29 March 2020
3. Wilk V (2013) Extending the range of feedstock of the dual fluidized bed gasification process towards residues and waste. Dissertation, TU Wien
4. Benedikt F, Schmid JC, Fuchs J, Mauerhofer AM, Müller S, Hofbauer H et al (2018) Fuel flexible gasification with an advanced 100 kW dual fluidized bed steam gasification pilot plant. Energy 164:329–343. https://doi.org/10.1016/j.energy.2018.08.146
5. Schweitzer D, Gredinger A, Schmid M, Waizmann G, Beirow M, Spörl R, Scheffknecht G (2018) Steam gasification of wood pellets, sewage sludge and manure: gasification performance and concentration of impurities. Biomass Bioenergy 111:308–319. https://doi.org/10.1016/j.biombioe.2017.02.002
6. Schmid JC, Wolfesberger U, Koppatz S, Pfeifer C, Hofbauer H (2012) Variation of feedstock in a dual fluidized bed steam gasifier-influence on product gas, tar content, and composition. Environ Prog Sustain Energy 31(2):205–215. https://doi.org/10.1002/ep.11607
7. Schmid JC, Bartik A, Benedikt F, Mauerhofer AM, Fuchs J, Schanz E, Reisinger S, Nowak B, Bühler F, Müller S, Fuchs M, Hofbauer H (2019) Steam gasification of sewage sludge for synthesis processes. In: Hofbauer H (ed) Proceedings of the ICPS 19, Vienna, pp 45-53
8. Fuchs J, Schmid JC, Müller S, Hofbauer H (2019) Dual fluidized bed gasification of biomass with selective carbon dioxide removal and limestone as bed material: a review. Renew Sust Energ Rev 107:212–231. https://doi.org/10.1016/j.rser.2019.03.013
9. Asadullah M (2014) Biomass gasification gas cleaning for downstream applications: a comparative critical review 40:118–132. https://doi.org/10.1016/j.rser.2014.07.132
10. Schildhauer TJ, Biollaz SMA (2016) Synthetic natural gas from coal, dry biomass, and power-to-gas applications. John Wiley & Sons, Hoboken
11. Rönsch S, Schneider J, Matthischke S, Schlüter M, Götz M, Lefebvre J, Prabhakaran P, Bajohr S (2016) Review on methanation – from fundamentals to current projects. Fuel 166:276–296. https://doi.org/10.1016/j.fuel.2015.10.111
12. Schildhauer TJ, Biollaz SMA (2015) Reactors for catalytic methanation in the conversion of biomass to synthetic natural gas (SNG). Chimia 69(10):603–607. https://doi.org/10.2533/chimia.2015.603
13. Kopyscinski J, Schildhauer TJ, Biollaz SMA (2010) Production of synthetic natural gas (SNG) from coal and dry biomass - a technology review from 1950 to 2009. Fuel 89(8):1763–1783. https://doi.org/10.1016/j.fuel.2010.01.027
14. Seemann MC, Schildhauer TJ, Biollaz SMA, Stucki S, Wokaun A (2006) The regenerative effect of catalyst fluidization under methanation conditions. Appl Catal A Gen 313(1):14–21. https://doi.org/10.1016/j.apcata.2006.06.048
15. Liu B, Ji S (2013) Comparative study of fluidized-bed and fixed-bed reactor for syngas methanation over Ni-W/TiO_2-SiO_2 catalyst. J Energy Chem 22(5):740–746. https://doi.org/10.1016/S2095-4956(13)60098-4
16. Liu J, Shen W, Cui D, Yu J, Su F, Xu G (2013) Syngas methanation for substitute natural gas over Ni–Mg/Al_2O_3 catalyst in fixed and fluidized bed reactors. Catal Commun 38:35–39. https://doi.org/10.1016/j.catcom.2013.04.014
17. Li J, Zhou L, Li P, Zhu Q, Gao J, Gu F, Su F (2013) Enhanced fluidized bed methanation over a Ni/Al_2O_3 catalyst for production of synthetic natural gas. Chem Eng J 219:183–189. https://doi.org/10.1016/j.cej.2013.01.005
18. Biegger P, Kirchbacher F, Medved A, Miltner M, Lehner M, Harasek M (2018) Development of honeycomb methanation catalyst and its application in power to gas systems. Energies 11(7):1679. https://doi.org/10.3390/en11071679

19. Heyne S, Harvey S (2014) Impact of choice of CO_2 separation technology on thermo-economic performance of Bio-SNG production processes. Int J Energy Res 38(3):299–318. https://doi.org/10.1002/er.3038
20. Gassner M, Maréchal F (2012) Thermo-economic optimisation of the polygeneration of synthetic natural gas (SNG), power and heat from lignocellulosic biomass by gasification and methanation. Energy Environ Sci 5(2):5768. https://doi.org/10.1039/c1ee02867g
21. Rönsch S, Kaltschmitt M (2012) Bio-SNG production — concepts and their assessment. Biomass Conv Biorefin 2(4):285–296. https://doi.org/10.1007/s13399-012-0048-0
22. Österreichische Vereinigung für das Gas- und Wasserfach (2001) Richtlinie G 31: 2001-05 Erdgas in Österreich-Gasbeschaffenheit. ÖVGW. Accessed 29 March 2020
23. Österreichische Vereinigung für das Gas- und Wasserfach (2011) Richtlinie G B220: 2011-11 Regeneratives Gase – Biogas. ÖVGW. Accessed 29 March 2020
24. Thema M, Weidlich T, Hörl M, Bellack A, Mörs F, Hackl F, Kohlmayer M, Gleich J, Stabenau C, Trabold T, Neubert M, Ortloff F, Brotsack R, Schmack D, Huber H, Hafenbradl D, Karl J, Sterner M (2019) Biological CO_2-methanation: an approach to standardization. Energies 12(9):1670. https://doi.org/10.3390/en12091670
25. European Committee for Standardization (2018) Gas infrastructure-quality of gas-group H German Version (EN 16726:2015+A1:2018)
26. European Commitee for Standardization (2016) Natural gas and biomethane for use in transport and biomethane for injection in the natural gas network - part 1: specifications for biomethane for injection in the natural gas network German Version (EN 16723–1:2016)
27. Judd R, Pinchbeck D (2016) Hydrogen admixture to the natural gas grid. Compend Hydrog Energy 4:165–192. https://doi.org/10.1016/B978-1-78242-364-5.00008-7
28. Kraussler M, Schindler P, Hofbauer H (2017) An experimental approach aiming the production of a gas mixture composed of hydrogen and methane from biomass as natural gas substitute in industrial applications. Bioresour Technol 237:39–46. https://doi.org/10.1016/j.biortech.2017.03.040
29. Thunman H, Seemann M, Berdugo Vilches T, Maric J, Pallares D, Ström H, Berndes G, Knutsson P, Larsson A, Breitholtz C, Santos O (2018) Advanced biofuel production via gasification - lessons learned from 200 man-years of research activity with Chalmers' research gasifier and the GoBiGas demonstration plant. Energy Sci Eng 6(1):6–34. https://doi.org/10.1002/ese3.188
30. Larsson A, Gunnarsson I, Tengberg F (2018) The GoBiGas Project. Demonstration of the production of biomethane from biomass via gasification. Technical Report
31. Rehling B (2012) Development of the 1 MW Bio-SNG plant, evaluation on technological and economical aspects and upscaling considerations. Dissertation, TU Wien
32. Molino A, Nanna F, Ding Y, Bikson B, Braccio G (2013) Biomethane production by anaerobic digestion of organic waste. Fuel 103:1003–1009. https://doi.org/10.1016/j.fuel.2012.07.070
33. Rasi S (2009) Biogas composition and upgrading to biomethane. Dissertation, University of Jyväskyla
34. Götz M, Lefebvre J, Mörs F, McDaniel Koch A, Graf F, Bajohr S, Reimert R, Kolb T (2016) Renewable power-to-gas: a technological and economic review. Renew Energy 85:1371–1390. https://doi.org/10.1016/j.renene.2015.07.066
35. Witte J, Calbry-Muzyka A, Wieseler T, Hottinger P, Biollaz SMA, Schildhauer TJ (2019) Demonstrating direct methanation of real biogas in a fluidised bed reactor. Appl Energy 240:359–371. https://doi.org/10.1016/j.apenergy.2019.01.230
36. Bensmann A, Hanke-Rauschenbach R, Heyer R, Kohrs F, Benndorf D, Reichl U, Sundmacher K (2014) Biological methanation of hydrogen within biogas plants: a model-based feasibility study. Appl Energy 134:413–425. https://doi.org/10.1016/j.apenergy.2014.08.047
37. Bajohr S, Schollenberger D, Buchholz D, Weinfurtner T, Götz M (2014) Kopplung der PtG-Technologie mit thermochemischer Biomassevergasung: Das KIC-Projekt "DemoSNG". gwf - Gas|Erdgas (155): 470–475
38. Benedikt F, Kuba M, Christian J, Müller S, Hofbauer H (2019) Assessment of correlations between tar and product gas composition in dual fluidized bed steam gasification for online tar prediction. Appl Energy 238:1138–1149. https://doi.org/10.1016/j.apenergy.2019.01.181
39. Bai X, Wang S, Sun T, Wang S (2014) Influence of operating conditions on carbon deposition over a Ni catalyst for the production of synthetic natural gas (SNG) from coal. Catal Lett 144:2157–2166. https://doi.org/10.1007/s10562-014-1379-1
40. Kambolis A, Schildhauer TJ, Kröcher O (2015) CO methanation for synthetic natural gas production. Chimia 69(10):608–613. https://doi.org/10.2533/chimia.2015.608
41. Bartholomew CH (2001) Mechanisms of catalyst deactivation. Appl Catal A Gen 212(1–2):17–60. https://doi.org/10.1016/S0926-860X(00)00843-7
42. Kopyscinski J, Schildhauer TJ, Biollaz SMA (2011) Methanation in a fluidized bed reactor with high initial CO partial pressure : part I — experimental investigation of hydrodynamics, mass transfer effects, and carbon deposition. Chem Eng Sci 66(5):924–934. https://doi.org/10.1016/j.ces.2010.11.042
43. Kopyscinski J, Schildhauer TJ, Biollaz SMA (2009) Employing catalyst fluidization to enable carbon management in the synthetic natural gas production from biomass. Chem Eng Technol 32(3):343–347. https://doi.org/10.1002/ceat.200800413
44. Lommerzheim W, Flockenhaus C (1978) One stage combined shift-conversion and partial methanation process for upgrading synthesis gas to pipeline quality. In: American Gas Association (ed) Proceedings of the Tenth Synthetic Pipeline Gas Symposium, Chicago, pp 439–451
45. Seemann M (2007) Methanation of biosyngas in a fluidized bed reactor: development of a one-step synthesis process, featuring simultaneous methanation, watergas shift and low temperature tar reforming. Dissertation, ETH Zurich
46. Frick V, Brellochs J, Specht M (2014) Application of ternary diagrams in the design of methanation systems. Fuel Process Technol 118:156–160. https://doi.org/10.1016/j.fuproc.2013.08.022
47. Gao J, Wang Y, Ping Y, Hu D, Xu G, Su F (2012) A thermodynamic analysis of methanation reactions of carbon oxides for the production of synthetic natural gas. RSC Adv 2:2358–2368. https://doi.org/10.1039/c2ra00632d
48. Witte J, Settino J, Biollaz SMA, Schildhauer T (2018) Direct catalytic methanation of biogas – part I: new insights into biomethane production using rate-based modelling and detailed process analysis. Energy Convers Manag 171:750–768. https://doi.org/10.1016/j.enconman.2018.05.056
49. Witte J, Kunz A, Biollaz SMA, Schildhauer T (2018) Direct catalytic methanation of biogas – part II: techno-economic process assessment and feasibility reflections. Energy Convers Manag 178:26–43. https://doi.org/10.1016/j.enconman.2018.09.079
50. Neubert M (2019) Catalytic methanation for small- and mid-scale SNG production. Dissertation, Friedrich-Alexander-Universität
51. Liu J, Cui D, Yao C, Yu J, Su F, Xu G (2016) Syngas methanation in fluidized bed for an advanced two-stage process of SNG production. Fuel Process Technol 141:130–137. https://doi.org/10.1016/j.fuproc.2015.03.016
52. Vakalis S, Malamis D, Moustakas K (2018) Thermodynamic modelling of an onsite methanation reactor for upgrading producer gas from commercial small scale biomass gasifiers. J Environ

Manag 216:145–152. https://doi.org/10.1016/j.jenvman.2017.06.044
53. Martínez I, Romano MC (2016) Flexible sorption enhanced gasification (SEG) of biomass for the production of synthetic natural gas (SNG) and liquid biofuels: process assessment of stand-alone and power-to-gas plant schemes for SNG production. Energy 113:615–630. https://doi.org/10.1016/j.energy.2016.07.026
54. van der Meijden CM, Veringa HJ, Rabou LPLM (2010) The production of synthetic natural gas (SNG): a comparison of three wood gasification systems for energy balance and overall efficiency. Biomass Bioenergy 34(3):302–311. https://doi.org/10.1016/j.biombioe.2009.11.001
55. Nakamura S, Kitano S, Yoshikawa K (2016) Biomass gasification process with the tar removal technologies utilizing bio-oil scrubber and char bed. Appl Energy 170:186–192. https://doi.org/10.1016/j.apenergy.2016.02.113
56. Schmid JC, Benedikt F, Fuchs J, Mauerhofer AM, Müller S, Hofbauer H (2019) Syngas for biorefineries from thermochemical gasification of lignocellulosic fuels and residues - 5 years' experience with an advanced dual fluidized bed gasifier design. Biomass Convers Biorefin (2019). https://doi.org/10.1007/s13399-019-00486-2
57. Loipersböck J, Lenzi M, Rauch R, Hofbauer H (2017) Hydrogen production from biomass: the behavior of impurities over a CO shift unit and a biodiesel scrubber used as a gas treatment stage. Korean J Chem Eng 34(8):2198–2203. https://doi.org/10.1007/s11814-017-0130-1
58. Seemann MC, Schildhauer TJ, Biollaz SMA (2010) Fluidized bed methanation of wood-derived producer gas for the production of synthetic natural gas. Ind Eng Chem Res 49(15):7034–7038. https://doi.org/10.1021/ie100510m
59. Abdoulmoumine N, Adhikari S, Kulkarni A, Chattanathan S (2015) A review on biomass gasification syngas cleanup. Appl Energy 155:294–307. https://doi.org/10.1016/j.apenergy.2015.05.095
60. Mauerhofer AM, Müller S, Benedikt F, Fuchs J, Bartik A, Hofbauer H (2019) CO_2 gasification of biogenic fuels in a dual fluidized bed reactor system. Biomass Convers Biorefin. https://doi.org/10.1007/s13399-019-00493-3
61. Fuchs J, Schmid JC, Müller S, Mauerhofer AM, Benedikt F, Hofbauer H (2019) The impact of gasification temperature on the process characteristics of sorption enhanced reforming of biomass. Biomass Convers Biorefin. https://doi.org/10.1007/s13399-019-00439-9
62. Van Herwijnen T, Van Doesburg H., De Jong W.A. (1973) Kinetics of the methanation of CO and CO_2 on a nickel catalyst. J Catal 28(3):391–402. https://doi.org/10.1016/0021-9517(73)90132-2
63. Karlbrink M (2015) An evaluation of the performance of the GoBiGas gasification process. Master Thesis, Chalmers University of Technology
64. Gassner M, Baciocchi R, Maréchal F, Mazzotti M (2009) Integrated design of a gas separation system for the upgrade of crude SNG with membranes. Chem Eng Process Process Intensif 48(9):1391–1404. https://doi.org/10.1016/j.cep.2009.07.002

C.2 Paper II

Development of an internally circulating fluidized bed for catalytic methanation of syngas

Bartik, A., Fuchs, J., Müller, S., Hofbauer, H., in Proceedings of the 16th Minisymposium Verfahrenstechnik, September 21st–22nd, **2020**, TU Wien, Vienna, https://doi.org/10.34726/566.

Development of an internally circulating fluidized bed for catalytic methanation of syngas

Alexander Bartik[1*], Josef Fuchs[1], Stefan Müller[1], Hermann Hofbauer[1]

[1] Institute of Chemical, Environmental and Bioscience Engineering, TU Wien, Austria
*Corresponding Author, alexander.bartik@tuwien.ac.at

Keywords: Internally circulating fluidized bed, Catalytic methanation, Reactor design, Fluid dynamics

Abstract

In this work, an internally circulating fluidized bed reactor was proposed and designed for the catalytic methanation of syngas from the 100 kW_{th} dual fluidized bed gasification reactor at TU Wien. Additionally, first fluid dynamic investigations were carried out in order to determine characteristic pressures and the gas slip in the internally circulating fluidized bed. The results from the design of the reactor showed that a volume contraction in the reactor between 30-50% and a heat generation between 0.16 to 0.25 kW per kW of exit gas need to be considered in the thermodynamic equilibrium for a low temperature methanation process at 300 °C and 1 bar_a. Further technical and economic considerations resulted in the design of a fluidized bed with an outer diameter of 164 mm, which corresponds to a maximum feed gas volume flow of 6 m^3_{stp}/h and a maximum chemical energy of 15 kW in the exit gas for the chosen catalyst properties. The fluid dynamic investigations with an inert bed material showed that there is a clear correlation between the pressure difference between the draft tube and the annular region and the fluidization ratio. Additionally, the gas slip was shown to increase with a higher fluidization ratio as well as higher absolute fluidization velocities. Furthermore, the gas slip from the annular region to the draft tube was shown to be by an order of magnitude higher than the gas slip from the draft tube to the annular region.

Introduction

The global energy system clearly shows a transition from solid energy carriers via liquids to gaseous energy carriers. This trend can be observed throughout historical data and is also predicted for centuries to come [1]. Besides the mere transition from solids to gases, there is also a transition from fossil fuels towards renewable energy resources taking place today. Synthetic natural gas (SNG) is one possible energy carrier which combines both trends and therefore shows a relevant potential for the implementation in future energy systems [2].

The Biomass-to-Gas (BtG) route is a viable concept for the production of valuable secondary energy carriers, like SNG, on a fossil-free basis. A possible process route within the BtG concepts is the dual fluidized bed (DFB) gasification and the consecutive upgrading to SNG. The upgrading steps consist of a gas cleaning section, the catalytic methanation process itself and the purification of the methane-rich gas (raw-SNG) in order to fulfill the feed-in requirements of the natural gas grid. Within this process chain, there are still some technical and economical challenges which must be addressed in order to make this process competitive [3]–[5]. Some recent investigations already focus on the implementation of the process chain in different industrial settings to extend the fields of application and improve the economic performance. In [6], for example, the process is utilized in an integrated hot metal production plant to replace the natural gas demand which is currently covered with fossil natural gas. Another study investigated the production of SNG from sewage sludge as feedstock. The results showed that the process can be economically competitive due to the negative purchase price of sewage sludge [7].

In this work, the focus lies on the design of the methanation reactor where the highly exothermic methanation reactions take place. The most important equations describing the ongoing processes are the CO-methanation reaction,

$$CO + 3H_2 \rightleftharpoons CH_4 + H_2O \qquad \Delta H_R^{300} = -216\,\frac{kJ}{mol} \quad (1)$$

the reverse water gas shift reaction, and

$$CO_2 + H_2 \rightleftharpoons CO + H_2O \qquad \Delta H_R^{300} = 39\,\frac{kJ}{mol} \quad (2)$$

the CO_2-methanation reaction, which is implicitly defined by the linear combination of Eq.(1) and (2) [8].

$$CO_2 + 4H_2 \rightleftharpoons CH_4 + 2H_2O \qquad \Delta H_R^{300} = -177\,\frac{kJ}{mol} \quad (3)$$

Besides these species, the product gas of the DFB gasifier also contains higher hydrocarbons like ethylene (C_2H_4). The hydrogenation of C_2H_4 to methane can be written as:

$$C_2H_4 + 2H_2 \rightarrow 2CH_4 \qquad \Delta H_R^{300} = -209\,\frac{kJ}{mol} \quad (4)$$

There are more reaction equations which can be considered in a methanation process, but are irrelevant for the purpose of this paper. A more detailed thermodynamic analysis for this process route can be found in [9].

Commercially, only adiabatic fixed bed reactors are available today. This type of reactor is chosen because of the low construction effort for a single reactor and the low mechanical stress on the catalyst. However, there are some major drawbacks as well. Because of the highly exothermic methanation reactions, a reactor cascade with intermediate gas cooling and most of the time also product gas recycle is necessary. This in term increases the complexity of the overall process setup. In addition, the risk for catalyst deactivation by carbon depositions and/or coke formation is high. For these reasons, alternative reactor concepts have been investigated. Cooled fixed bed reactors, fluidized bed reactors, three-phase reactors and structured reactors have been proposed for this purpose. This variety of reactor concepts also lead to a wide range of reaction conditions. 250 °C to 700 °C and 1 bar_a to 87 bar_a have been applied. Every reactor concept benefits from certain advantages but also shows disadvantages compared to adiabatic fixed beds. Fluidized bed reactors, for example, distinguish themselves by the improved heat and mass transfer. Therefore, nearly isothermal operation conditions and a high conversion close to the thermodynamic equilibrium even at lower temperatures are possible. Also, the risk for catalyst deactivation by coke formation is reduced and no separate water gas shift reactor prior to the methanation is necessary. All of the above points allow a shorter gas cleaning section

and reduce the number of required methanation reactors to a minimum. However, a drawback of the fluidized bed methanation reactor is the high mechanical stress on the catalyst. More information on the different reactor types can be found in [8], [10]–[12].

There are two large-scale projects for the conversion of woody biomass to SNG based on the DFB gasification technology. The GoBiGas project (Gothenburg, Sweden) produced 20 MW_{SNG} from the product gas of a DFB gasifier and utilized the commercially available TREMP process from Haldor Topsøe with 4 adiabatic methanation reactors with intermediate cooling and product gas recycling at a pressure of 16 bar_a. Together with the gas cleaning, the gas pretreatment and the gas upgrading, 16 main process steps are implemented in this plant. The second large-scale project was the 1 MW_{SNG} plant in Güssing, Austria. This plant utilized a single fluidized bed methanation reactor and 10 main process steps were necessary for the production of SNG from the product gas of the DFB gasifier. The operating conditions in the reactor were about 380 °C and 1 bar_a [8], [13].

Some investigations have already been performed on fluidized bed methanation in small lab-scale test rigs. These investigations mainly focus on the assessment of the catalyst performance in fluidized beds with only a few millimeters in diameter [14], [15]. Other investigations in somewhat larger bubbling fluidized bed reactors, with a diameter of about 50 mm, were conducted by the Paul Scherrer Institute (PSI). Extensive studies on kinetics, carbon depositions and mass transfer phenomena were carried out. All investigations utilized a bubbling fluidized bed but hardly any considerations to the reactor design are mentioned [16]–[18]. Other studies propose advanced two-stage methanation processes with a fluidized bed methanation reactor as the first stage and a fixed bed reactor as the second stage. However, these process setups were only theoretically proposed but have not been experimentally investigated so far [19], [20]. Neubert on the other hand already carried out experiments in a two-stage methanation process with intermediate water condensation including a structured reactor as the first stage and a fixed bed reactor as the second stage and reached to required gas quality for grid feed-in in Germany [21].

In this paper an internally circulating fluidized bed (ICFB) methanation reactor for improved heat and mass transfer is proposed and designed. Additionally, first results of fluid dynamic investigations of the ICFB are presented. The reactor concept is developed for the purpose of investigating the methanation process with bottled gases on the one hand and with 'live gas' from the 100 kW_{th} DFB gasifier at TU Wien on the other hand.

Concept and methodology

Design

ICFB's have been studied and applied to various processes in the past and today. Because of the possibility to split the reactor in different reaction zones, it is used in coal and biomass gasification processes, for example. The development of the DFB technology at TU Wien is also based on an ICFB and has been optimized over the last three decades [22], [23].

The ICFB reactor usually consists of one reactor with two separated fluidized beds and/or reaction zones, which are connected by the circulation of the solid material between the two zones. One possibility to separate the fluidized beds is by the insertion of a draft tube, which divides the reactor into an inner cylindrical fluidized bed and an outer annular fluidized bed. A schematic diagram of such an ICFB is shown in Fig. 1. By the independently controllable gas supply to each fluidized bed, it is possible to create a circulation between the two zones. For example, if there is a higher fluidization velocity inside the draft tube than in the annular region, the solids will rise in the draft tube and traverse downwards in the outer fluidized bed (green arrows in Fig. 1). ICFB's with draft tube mainly distinguish themselves by the fluid velocity in the draft tube. If the velocity is low, such that the particles are not carried out of the fluidized bed, the result are two interconnected bubbling fluidized beds and the solid circulation works on the principle of an airlift pump. If the fluid velocity in the draft tube is well above the point of entrainment (u_{se}, se=significant entrainment), the particles are carried out of the draft tube and flow back into the outer zone by the widening of the reactor above the draft tube. This type is called fast internally circulating fluidized bed (FICFB). Besides this definition, ICFB's can be distinguished by the type of the gas distributor or by the type of connection between the two reactor zones [24]–[27].

The proposed reactor concept is designed according to the following design parameters. The minimum fluidization velocity (u_{mf}) (Eq. 5) and u_{se} (Eq. 6) are calculated according to Grace [28] and Bi and Grace [29], respectively.

$$u_{mf} = \frac{\mu}{\rho_g \, d_{SV}} \left(\sqrt{27.2^2 + 0.0408 \, Ar} - 27.2 \right) \tag{5}$$

$$u_{se} = \frac{\mu}{\rho_g \, d_{SV}} \, 1.53 \, Ar^{0.5} \tag{6}$$

Where Ar is the Archimedes number.

$$Ar = \frac{d_{SV}^3 \, \rho_g \, (\rho_p - \rho_g) \, g}{\mu^2} \tag{7}$$

In order to calculate these parameters, gas properties like the dynamic viscosity μ and the density ρ_g must be known under the prevailing reaction conditions. For this reason, a model in the process simulation software IPSEpro was implemented. In this software, the property data for all required substances are implemented. These substances are H_2, CO, CO_2, CH_4, H_2O, N_2 and C_2H_4. Besides the property data of the gases, also the property data of the solid bed material must be defined. The defined bed material has a Sauter diameter of $d_{SV} = 165 \; \mu m$ and a particle density of $\rho_p = 2000 \; kg/m^3$. These values resemble the Ni/Al_2O_3-catalyst, which was synthesized especially for the utilization in a fluidized bed. Another useful definition for the characterization of the two fluidized beds is the superficial velocity in relationship to u_{mf}. This relationship can be defined for both the inner (u_d/u_{mf}, i.e. draft tube) and the outer (u_a/u_{mf}, i.e. annular region) fluidized bed. Division of these two values leads to the fluidization ratio,

$$fluidization \; ratio = \frac{u_d/u_{mf}}{u_a/u_{mf}} = \frac{u_d}{u_a} \tag{8}$$

which characterizes the circulation between the fluidized beds. Furthermore, the reaction conditions in the design case are set to 300 °C and 1 bar_a. The low temperature is possible because of the superiority of the fluidized bed in terms of heat management. It allows a high conversion and thus a methane-rich gas in a single reactor unit. Atmospheric pressure is chosen because the DFB gasification process works under ambient pressure and the energy, which is required for the pressurization of the feed gas, is omitted. Additionally, thermodynamic calculations reveal that there is only a mild influence of pressure on the gas composition

especially at low temperatures [9]. The temperature of the feed gas at the inlet to the reactor is set to 250 °C.

For the design of the fluidized bed, it is important to consider the chemical reactions taking place in the reactor. Not only the gas composition changes during the methanation process, but also the volume contracts (see Eq. 1,3 and 4). In the case of methanation it has been reported that the reaction kinetics are fast and the thermodynamic equilibrium can be approached within the first few millimeters of the reactor height [30]. Both statements justify the use of the exit gas composition/properties and volume flow in the thermodynamic equilibrium for the fluid dynamic calculations of the fluidized bed. Four typical feed gas compositions were used for the design of the reactor.

- a stoichiometric mixture of H_2 and CO_2 (H_2:CO_2 = 4:1).
- a stoichiometric mixture of H_2 and CO (H_2:CO = 3:1).
- a typical product gas composition from the DFB steam gasification with wood as fuel and olivine as bed material (typ. product gas) [23].
- a typical product gas composition from the sorption enhanced reforming process (SER) [31].

Fluid dynamic investigations

In order to characterize the fluid dynamic behavior of the ICFB cold flow experiments are carried out. The investigations focus on the determination of the pressure difference between the draft tube and the annular region of the ICFB as well as the gas slip between the two regions. As bed material quartz sand with similar properties as the catalyst is used. It characterizes as a Geldart group B material with a Sauter diameter of $d_{SV} = 143\,\mu m$ and a particle density of $\rho_p = 2600\ kg/m^3$. Fig. 1 shows the location of the pressure measurements. In order to obtain the pressure difference in the upper gap the pressure in the annular region (p_a) is subtracted from the pressure in the draft tube (p_d). This difference is an indication for the circulation of the bed material between the two regions as stated in [24]. The measurements are carried out with Kalinsky DS2 pressure transmitters. The gas slip on the other hand has an influence on the superficial velocity in the fluidized beds as well as on the gas compositions. The latter is important if two different feed gas streams are introduced to the two fluidized bed regions. This would be the case if, for example, an advanced two-stage methanation process in one reactor is investigated. In this case, the feed gas could be introduced to the draft tube and the exit gas of the draft tube then could be recycled to the annular region with a partial water condensation in between. The gas slip can be determined by introducing a tracer gas to one of the fluidized beds and measuring the concentration of the tracer gas after the draft tube (y_d), the annular region (y_a) and in the inlet stream (y_i). In our case, the tracer gas was CO_2 and its concentration was measured with an Emerson NGA 2000 gas analyzer module. A CO_2 mass balance then leads to Eq. 9 and Eq. 10 for the gas slip from the draft tube to the annular region (S_a) and vice versa (S_d).

$$S_d = \dot{Q}_d \frac{y_i - y_d}{y_d} \tag{9}$$

$$S_a = \dot{Q}_d y_a \frac{y_d - y_i}{y_d(y_d - y_a)} + \dot{Q}_a y_a \frac{1}{y_d - y_a} \tag{10}$$

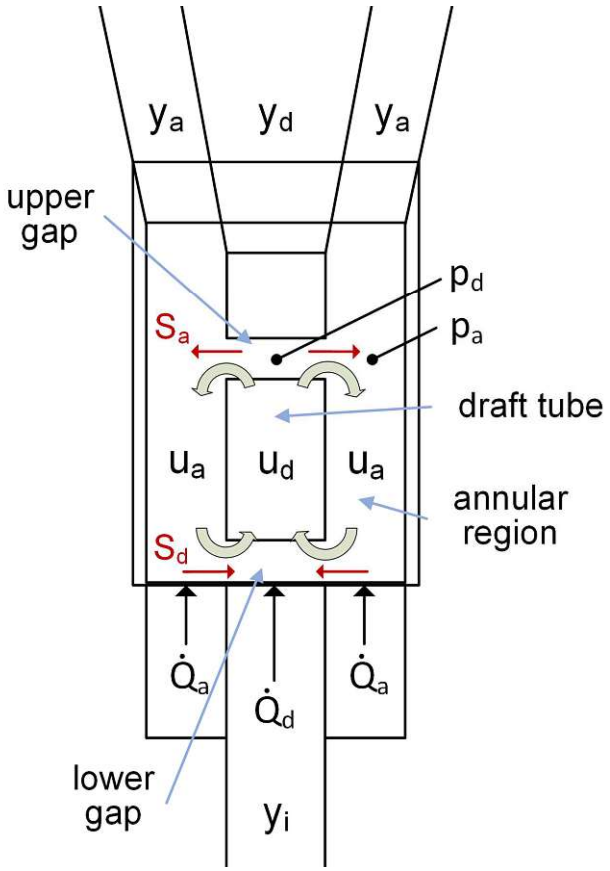

Figure 1: Schematic diagram of the ICFB reactor with bed material circulation (green arrows) and the direction of the gas slip (red arrows)

$\dot{Q}_d$ and $\dot{Q}_a$ denote the set volume flows to the draft tube and the annular region, respectively. All variables are also graphically represented in Fig. 1 and additionally also the direction of the gas slip is denoted with red arrows. The assumption that the gas slip to the draft tube (S_d) mainly takes place in the lower gap was experimentally confirmed in preliminary tests, while the assumption that the gas slip to the annular region (S_a) mainly takes place in the upper gap was shown to be a valid approximation in [24].

Results

Design

In Fig. 2a and Fig. 2b the feed gas composition and the equilibrium exit gas composition, respectively, are displayed for the four reference cases. The H_2:CO_2 feed gas mixture leads to an exit gas which consists mostly of CH_4 and H_2O. The latter can be easily condensed after the reactor but needs to be considered for the fluid dynamic design. The high water content can be explained by Eq. 3. It shows that two moles of H_2O are formed per mole of CO_2. The H_2:CO feed gas mixture shows a similar result, but with a higher CH_4 and a lower water content. For the typical product gas, the high CO_2 content is - besides CH_4 and H_2O - a relevant component for the fluid dynamic calculation. This is due to the understoichiometric hydrogen to carbon ratio of this feed gas. The SER product gas on the other hand produces an exit gas with a similar composition as the H_2:CO feed gas mixture. The CO in the feed gas is almost completely converted for all feed gases. In Fig. 2c the corresponding excess heat released by the exothermic reactions and the volume contraction for each feed gas mixture is depicted. The volume contraction is given in percent of the feed gas volume. The highest contraction takes place with the H_2:CO feed gas. The volume of the exit gas reduces to almost 50%

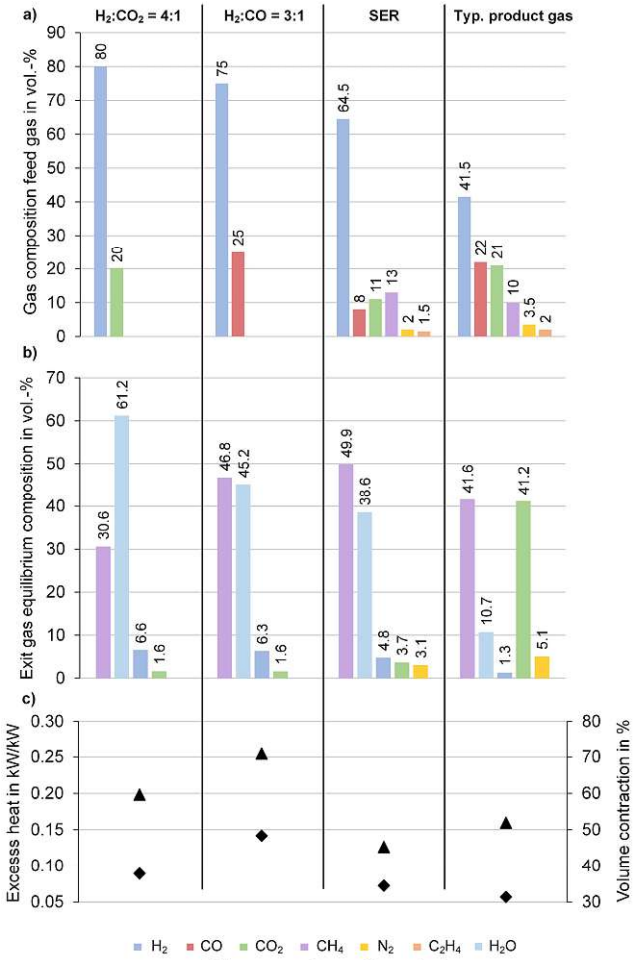

Figure 2: Gas compositions used for the design of the fluidized bed reactor: a) feed gas composition, b) exit gas composition according to the thermodynamic equlibrium at 300 °C and 1 bar_a, c) heat dissipation and volume contraction during the conversion of the feed gas to the exit gas

of the volume of the feed gas. The excess heat on the left axis indicates how much heat is released by the exothermic reactions and therefore needs to be removed by the reactor cooling to ensure an isothermal operation. It is given in kW per kW of chemical energy of the exit gas. The H_2:CO mixture leads to the highest amount of produced heat with about 0.25 kW/kW.

With this knowledge, it is possible to calculate the fluid dynamic parameters and in further consequence determine the plant size and the plant design. The calculation is done by varying the size parameters of the fluidized beds and checking the required volume flows and the fluidization ratio. Based on this iteration a decision for a plant size is made. Consequently, the results for these size parameters are shown. The diameter of the inner fluidized bed is 80 mm and the diameter of the annular fluidized bed is 164 mm. The decision for this size is based on the following limitations: i) the amount of gas in the feed must be covered by gas cylinders and is therefore limited because of economic considerations, ii) the excessive heat must be manageable in the reactor, iii) the amount of product gas from the 100 kW_{th} pilot plant must be sufficient (typically 20-30 Nm^3/h on a dry basis), iv) the size of the fluidized beds should not be below a certain scale limit in order to have a representative size for further upscaling considerations. Table 1 shows the results of this calculation. u_{mf} and u_{se} as

Table 1: U_{mf} and U_{se} as well as calculation results for the four investigated feed gas compositions and three different fluidization ratios

Parameter	Unit	Gas compositions			
		H_2:CO_2 = 4:1	H_2:CO = 3:1	SER	Typ. prod. gas
U_{mf}	cm/s	2.0	2.03	1.98	1.68
U_{se}	cm/s	464	468	454	358
$U_d/U_a = 5/2$					
Volume flow feed	Nm^3/h	2.76	3.36	2.59	2.08
Excess heat	kW	1.1	2.14	1.1	0.96
Chem. Energy exit gas	kW	5.54	8.41	8.64	6.02
$U_d/U_a = 10/3$					
Volume flow feed	Nm^3/h	4.82	**5.88**	4.53	3.66
Excess heat	kW	1.92	**3.74**	1.91	1.68
Chem. Energy exit gas	kW	9.68	14.7	**15.1**	10.53
$U_d = U_{se}, U_a = 0$					
Volume flow feed	Nm^3/h	63.6	77.1	59.1	44.3
Excess heat	kW	25.35	49	25	20.3
Chem. Energy exit gas	kW	127.8	193	197	127.4

well as the chosen fluidization ratios, the required volume flows of the feed gas, the excess heat, which is produced by the exothermic reactions, and the chemical energy of the exit gas (i.e. the raw-SNG) are listed for the four previously defined feed gas compositions. The fluidization ratio of 5/2 represents the standard design case and the fluidization ratio of 10/3 the maximum design case. The resulting maximum values are displayed in bold numbers. The maximum volume flow of 5.88 Nm^3/h of feed gas for the

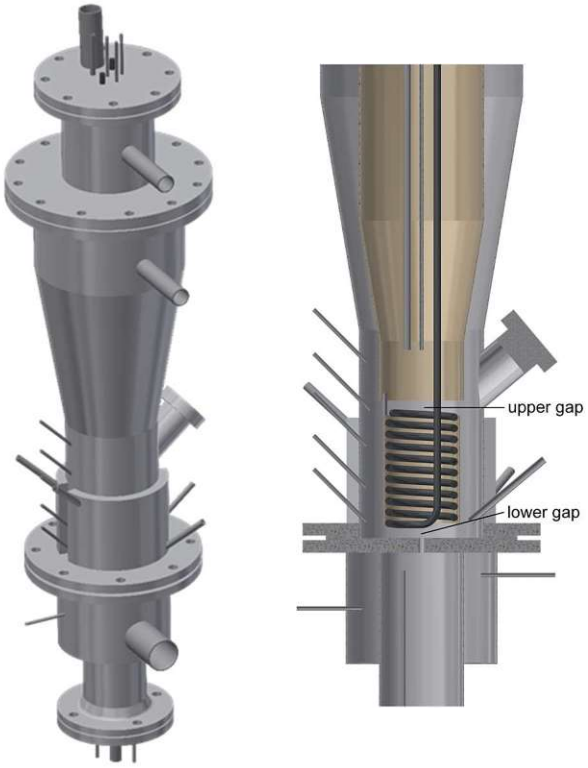

Figure 3: 3D-CAD drawing of the ICFB reactor: isometric view of the whole reactor (left), sectional view of the lower reactor part (right)

H_2:CO mixture can be covered from gas cylinders. This list also shows that the reactor cooling must dissipate a maximum of 3.74 kW. In the last section of the table, values

for the design of a FICFB are given. In this case, the velocity in the draft tube is equal to u_{se}. The resulting volume flows and the excess heat are by an order of magnitude higher than in the previous cases. This volume flow can neither be covered by gas cylinders nor by the DFB pilot plant. Vice versa, if the volume flows are reduced to a manageable level, the reactor diameter is considered too small for a representative operation. Therefore, the design and construction of a FICFB is not expedient in this case.

Based on these calculations a 3D-CAD drawing of the ICFB reactor is created. The left picture in Fig. 3 shows the complete reactor from the outside. The lowest part of the drawing shows the two windboxes, which allow an individual gas flow to the two fluidized beds. The flange above the windbox incorporates the gas distributor, which is in this case made of 22 pneumatic silencers. This flange connects to the actual reactor zone where the reaction takes place. Above the reaction zone are two conical freeboards – one for the annular fluidized bed and one for the draft tube. The gas streams then leave the reactor by two separate pipes.

In the right part of Fig. 3, a section view of the lower reactor part is shown. The bed material is fluidized and the reaction takes place in the depicted area above the gas distributor. In order to manage the heat released by the exothermic reactions, the draft tube is cooled by an air perfused coil. Below and above the draft tube the gap for the bed material circulation can be seen (upper gap and lower gap). A cooling jacket on the outside of the reactor additionally cools the annular part of the ICFB with air. The air crisscrosses several times in the cooling jacket before it is exhausted. The exiting raw-SNG can be separately withdrawn from the reactor through the inner pipe and the outer conical annular region.

Subsequently a P&I diagram of the whole process setup is drafted based on the results from the calculations and the 3D-CAD drawing (Fig. 4). All temperature, pressure, gas volume flow and gas measurement points are displayed in the flowchart. The plant is equipped with a maximum of 10 pressure and 29 temperature measurement points. Also, 5 gas measurement points for the measurement of the gas

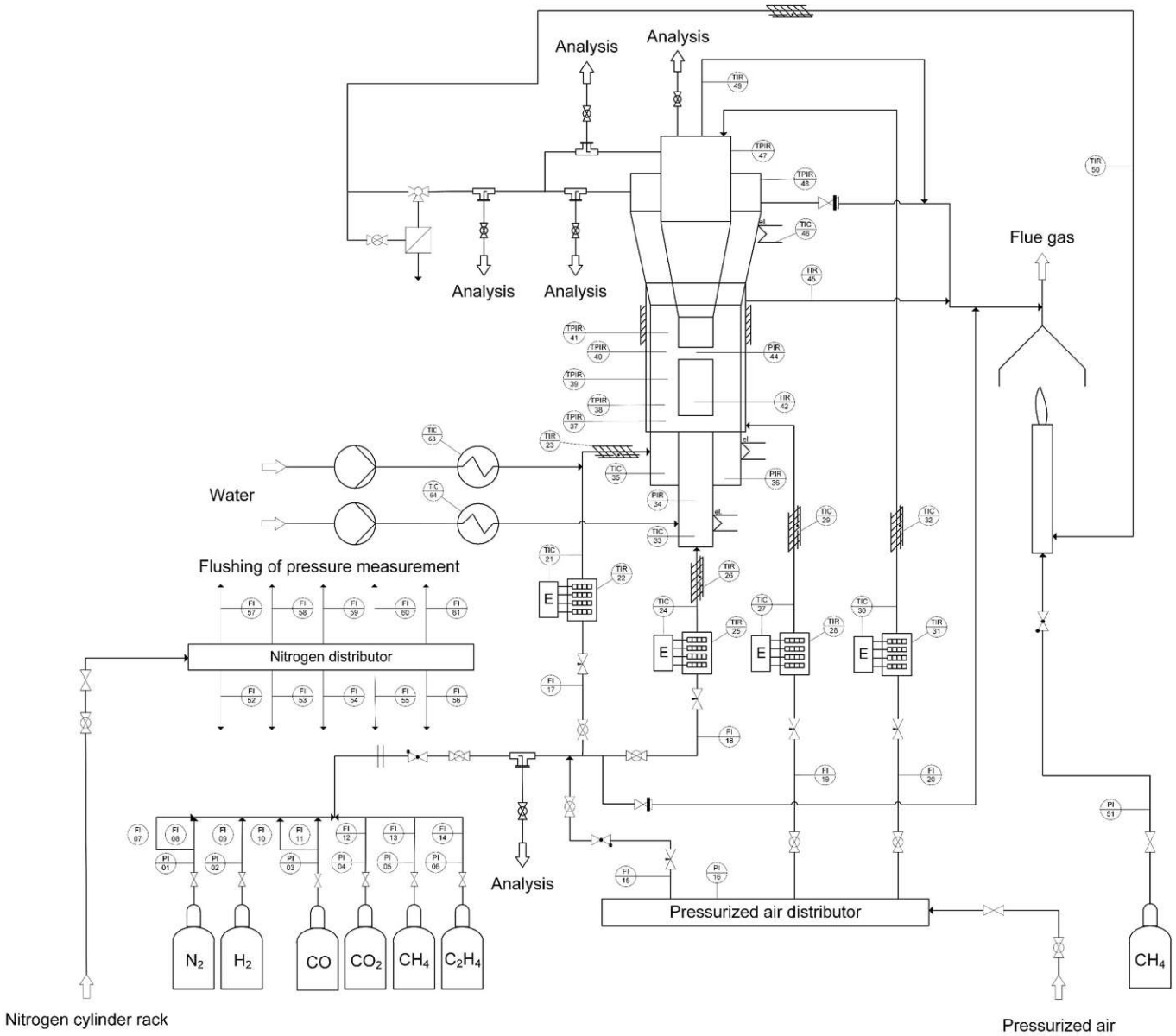

Figure 4: P&I flowchart of the process setup

The various small pipes coming off of the reactor are used for the installation of temperature sensors as well as connection points for pressure or gas measurements.

composition with online measuring devices are included (denoted by 'Analysis' in the flowchart). All pressure measurement points are flushed with a small amount of nitrogen to protect the pressure transmitters and to clear the pipes from reacting gases and bed material. In the bottom left corner of the flowchart, the gas cylinders are depicted. The volume flows of the single gas components are controlled by variable area flow meters (also called rotameters) with an integrated needle valve. The mixed gas is then split up into two streams in order to supply the gas flow to the draft tube and the annular fluidized bed. Again, rotameters are used to set the split ratio between the two regions. The composition of the mixed feed gas can be verified at the point marked with 'Analysis'. Afterwards the feed gas streams are preheated to 250 °C (design case) by electrical heating cartridges. Additionally, heating tapes are used to equalize the heat losses in the pipes from the heating cartridges to the reactor. In the reactor itself, temperature, pressure and gas measurement points are installed over the height of the annular fluidized bed in order to obtain axial profiles. In the draft tube the measurement is carried out by vertically moveable pipes which also yield axial profiles. At the two exits of the reactor, the composition of the two gas streams from the draft tube and the annular zone can be measured separately. These two gas streams are then mixed and the gas composition can be measured again. Afterwards, the gas flows through a filter stuffed with glass wool. The plant parts after the reactor are also equipped with heating tapes in order to prevent water condensation. A bypass allows changing the filter material during operation, if any problems should arise. The exit gas is then directed to a natural gas operated torch where the raw-SNG is burnt. Eventually, the flue gases are ventilated through a chimney. At the bottom center of the flowchart the pressurized air supply for the reactor cooling is depicted. Again, rotameters with a needle valve control the volume flow of the cooling air. For the plant start-up phase, the air can be preheated the same way the feed gas is preheated. The cooling air leaving the reactor is also ventilated through the chimney. In order to enable the water-gas shift reaction, water vapor can be dosed individually to the two fluidized beds. Additionally, the installation of two safety valves ensure a safe operation of the plant.

The shown configuration in Fig. 4 is designed and constructed for the operation with gas cylinders and 'live-gas' from the DFB pilot plant at TU Wien. The latter case is not shown in the flowchart. Regarding the construction of the plant, there is, however, no change necessary. The flowchart also shows that the separate exit gases from the draft tube and the annular zone are merged together after the reactor. This can be easily adapted for the investigation of a two-stage methanation process. The exit gas from the annular zone can be recirculated to the draft tube by the installation of a recirculation pipe as well as a blower. Additionally, a partial water condensation in the recirculation pathway can be installed. Both measures possibly allow an enhanced conversion of the feed gas to methane.

In Fig. 5, a picture of the bench-scale ICFB methanation setup at TU Wien is shown. The picture shows the plant without insulation and without heating tapes. On the right, the connection points to the gas cylinders and the pressurized air are located. Here, also the rotameters for the feed gas splitting and the cooling air are shown. On the left middle the actual ICFB reactor is placed. The exhaust gas pathway follows to the left of the reactor. The pressure transmitters and the electrical installations are located on the back of the plant in the control cabinet. Each of the 4 heating cartridges has an installed electrical power of 1.2 kW. Together with the heating tapes and the water evaporators, the plant has a maximum installed electrical power of about 11.5 kW.

Figure 5: Picture of the bench-scale methanation setup at TU Wien

Fluid dynamic investigations

In Fig. 6 the pressure difference in the upper gap between the draft tube and the annular region is shown over the fluidization ratio u_d/u_a. In the P&I flowchart, the corresponding pressure measurement points are PIR44 and PIR40. The graph shows that the pressure difference increases with an increasing fluidization ratio. With a high accuracy, this relationship is shown to be of a quadratic nature and can be seen as an indication for the bed material circulation rate. Additionally, also the absolute fluidization velocities influence the pressure difference. I.e. a higher u_a and therefore also a higher u_d lead to a higher pressure difference at a constant fluidization ratio. These results are in accordance with [24], who also found that the pressure difference gives an indication for the bed material circulation rate.

Fig. 7 shows the gas slip from the draft tube to the annular region (S_a) in Nm^3/h over the fluidization ratio u_d/u_a for different fluidization velocities (u_a=1.5-3.9u_{mf}) and two different sand filling levels. In Fig. 7a, the sand completely

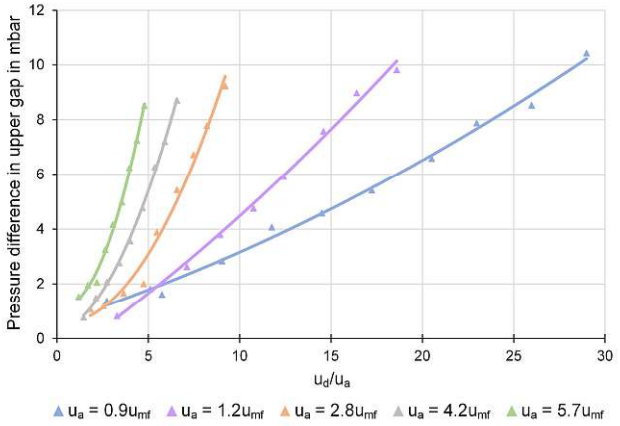

Figure 6: Pressure difference in the upper gap over the fluidization ratio

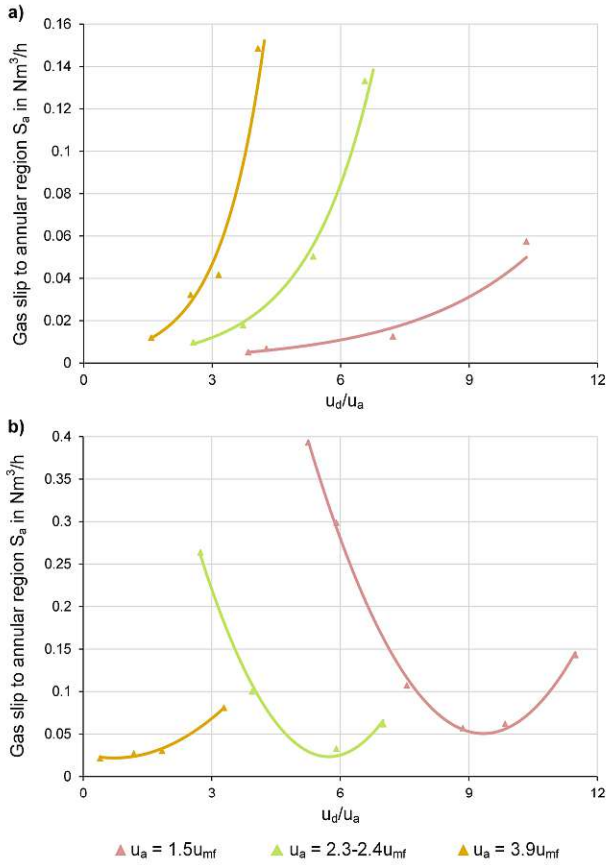

Figure 7: Gas slip to the annular region (S_a) over the fluidization ratio for different u_a: a) sand covers the upper gap completely, b) sand covers the upper gap only partially

covers the upper gap even when the reactor is not fluidized, while in Fig. 7b the upper gap is not completely covered with sand as long as the reactor is not fluidized.

The results for the fully covered gap in Fig. 7a show a steep incline of the gas slip with a rising u_d/u_a. The rising gas slip is in accordance with the increasing pressure difference in the upper gap (cf. Fig. 6). This increased pressure leads to a higher bed material circulation rate and simultaneously also pushes the gas from the draft tube to the annular region. Besides the influence of the fluidization ratio, also the absolute fluidization velocities determine the gas slip to a large extent. Like the pressure difference, higher fluidization velocities lead to a higher gas slip. Between $5*10^{-3}$ and 0.15 Nm^3/h, which is equal to a relative gas slip between 0.4 to 5 % of $\dot{Q}_d$, slip to the annular region. In Fig. 7b on the contrary, the only partially covered upper gap leads to a much higher gas slip compared to the fully covered gap, because the gas is able to flow from the draft tube to the annular region without resistance from the bed material. With an increasing fluidization ratio (for $u_a=1.5u_{mf}$ and $u_a=2.4u_{mf}$), the gas slip decreases because the bed material expands further and therefore also the gap closes gradually. At a certain fluidization ratio, the gap is fully closed and the gas slip increases again with higher fluidization ratios. If the absolute fluidization velocities are high enough in order to cover the gap even at low fluidization ratios (e.g. $u_a=3.9u_{mf}$), the course of the curve is similar to the curves in Fig. 7a.

The gas slip from the annular region to the draft tube S_d does not show such a clear correlation with the fluidization ratio as S_a. Nevertheless, it could be shown that S_d ranges between 0.1 and 0.76 Nm^3/h, which is equal to a relative gas slip between 4 to 43% of $\dot{Q}_a$. Hence, S_d is almost an order of magnitude higher than S_a and thus has a significant impact on the fluidization velocity and the gas composition in the draft tube. These results are again in accordance with Hofbauer [24] who also found that S_d is much higher than S_a.

Conclusion and Outlook

In this work, an ICFB has been proposed and designed for the optimized catalytic methanation of syngas from the DFB gasification process. Additionally, first results from fluid dynamic investigations in the ICFB have been presented. The application of a fluidized bed shows advantages in terms of heat management, conversion efficiencies and the prevention of catalyst fouling by coke depositions. Additionally, the whole process setup of the BtG process route is simplified. This work has shown, that the design of an ICFB for catalytic methanation requires careful thermodynamic modelling (Fig. 1). Besides the different gas compositions and properties, also the volume contraction of the gas during methanation must be considered. Additionally, the heat evolution by the exothermic reactions must be modelled in order to design a suitable cooling system to ensure an isothermal operation of the fluidized bed. The consideration of different operating conditions has been used to determine the plant size and point out the limits of a technical and economical operation (Table 1). These considerations have resulted in a novel reactor design for the production of maximum 15 kW of raw-SNG from about 6 Nm^3/h of syngas. Additionally, fluid dynamic investigations have shown that the pressure difference in the upper gap between the draft tube and the annular region is proportionate to the fluidization ratio and most likely also to the bed material circulation rate. The determination of the gas slip between the two fluidized beds has also shown a clear correlation with the fluidization ratio. A completely covered upper gap has been shown to be essential for a minimal gas slip. Simultaneously, the gas slip from the annular region to the draft tube has been found to be by an order of magnitude higher than the gas slip from the draft tube to the annular region. Further investigations concerning the fluid dynamics should focus on the determination of the gas slip from the annular region to the draft tube and on the quantification of the bed material circulation rate. With respect to the actual methanation, the designed ICFB reactor will be used to investigate the methanation reactions with syngas from gas cylinders. Additionally, the plant will be integrated into the whole BtG process chain, where it is connected to the 100 kW_{th} DFB pilot plant and a gas cleaning section in order to demonstrate 'live-gas' methanation.

Acronyms

BtG	biomass-to-gas
CAD	computer aided design
DFB	dual fluidized bed
FICFB	fast internally circulating fluidized bed
ICFB	internally circulating fluidized bed
SER	sorption enhanced reforming
SNG	synthetic natural gas

Symbols

Ar	Archimedes number
d_{SV}	Sauter diameter in μm

u_a	superficial velocity in the annular fluidized bed in cm/s
u_d	superficial velocity in the draft tube in cm/s
u_{mf}	minimum fluidization velocity in cm/s
u_{se}	velocity where significant entrainment occurs (= fast fluidized bed) in cm/s
μ	dynamic viscosity in Pas
ρ_g	density of the gas in kg/m^3
ρ_p	particle density in kg/m^3
S_a	gas slip from the draft tube to the annular region in Nm^3/h
S_d	Gas slip from the annular region to the draft tube in Nm^3/h
$\dot{Q}_a$	volume flow to annular region in Nm^3/h
$\dot{Q}_d$	volume flow to annular region in Nm^3/h
y_a	volume fraction of CO_2 above the annular fluidized bed
y_d	volume fraction of CO_2 above the draft tube
y_i	volume fraction of CO_2 in the feed gas

Acknowledgement

This work is part of the research project ReGas4Industry (871732) and receives financial support from the research program "Energieforschung" funded by the Austrian Climate and Energy Fund.

References

[1] S. Dunn, "Hydrogen futures: Toward a sustainable energy system," Int. J. Hydrogen Energy, vol. 27, no. 3, pp. 235–264, 2002.
[2] European Commission, "Directive (EU) 2018/2001 of the European Parliament and of the Council of 11 December 2018 on the promotion of the use of energy from renewable sources," Off. J. Eur. Union, vol. L 328/82, no. December, p. 128, 2018.
[3] D. Hornbachner, G. Hutter, and D. Moor, "Biogas-Netzeinspeisung - Rechtliche, wirtschaftliche und technische Voraussetzungen in Österreich," 2005.
[4] A. Larsson, I. Gunnarsson, and F. Tengberg, "The GoBiGas Project - Demonstration of the Production of Biomethane from Biomass via Gasification", Technical Report, 2018.
[5] J. Karstensson, A. Eliasson, and A. Kronander, "Feasibility study for gasification of biomass for synthetic natural gas (SNG) production," 2015. doi: 10.13140/RG.2.1.4321.6245
[6] S. Müller, L. Theiss, B. Fleiß, M. Hammerschmid, J. Fuchs, S. Penthor, D.C. Rosenfeld, M. Lehner and H. Hofbauer, "Dual Fluidized Bed Based Technologies for Carbon Dioxide Reduction – Example Hot Metal Production", accepted for publication in Biomass Conv. Bioref., 2020
[7] M. Veress, A. Bartik, F. Benedikt, M. Hammerschmid, J. Fuchs, S. Müller and H. Hofbauer, "Development and techno.economic evaluation of an optimized concept for industrial bio-SNG production from sewage sludge", Proceedings of the 28th European Biomass Conference, 2020
[8] T. J. Schildhauer and S. M. A. Biollaz, Synthetic Natural Gas from Coal, Dry Biomass, and Power-to-Gas Applications. Hoboken: John Wiley & Sons, 2016.
[9] A. Bartik, F. Benedikt, A. Lunzer, C. Walcher, S. Müller, and H. Hofbauer, "Thermodynamic Investigation of SNG Production Based on Dual Fluidized Bed Gasification of Biogenic Residues", Biomass Conv. Bioref., 2020. doi: 10.1007/s13399-020-00910-y
[10] J. Kopyscinski, T. J. Schildhauer, and S. M. A. Biollaz, "Production of synthetic natural gas (SNG) from coal and dry biomass - A technology review from 1950 to 2009," Fuel, vol. 89, no. 8, pp. 1763–1783, 2010. doi: 10.1016/j.fuel.2010.01.027
[11] T. J. Schildhauer and S. M. A. Biollaz, "Reactors for catalytic methanation in the conversion of biomass to synthetic natural gas (SNG)," Chimia, vol. 69, no. 10, pp. 603–607, 2015. doi: 10.2533/chimia.2015.603
[12] S. Rönsch et al., "Review on methanation – From fundamentals to current projects," Fuel, vol. 166, pp. 276–296, 2016. doi: 10.1016/j.fuel.2015.10.111
[13] B. Rehling, "Development of the 1MW Bio-SNG plant , evaluation on technological and economical aspects and upscaling considerations," Dissertation, 2012.
[14] J. Li et al., "Enhanced fluidized bed methanation over a Ni/Al2O3 catalyst for production of synthetic natural gas," Chem. Eng. J., vol. 219, pp. 183–189, 2013. doi: 10.1016/j.cej.2013.01.005
[15] B. Liu and S. Ji, "Comparative study of fluidized-bed and fixed-bed reactor for syngas methanation over Ni-W/TiO2-SiO2 catalyst," J. Energy Chem., vol. 22, no. 5, pp. 740–746, 2013. doi: 10.1016/S2095-4956(13)60098-4
[16] J. Kopyscinski, T. J. Schildhauer, and S. M. A. Biollaz, "Fluidized-bed methanation: Interaction between kinetics and mass transfer," Ind. Eng. Chem. Res., vol. 50, no. 5, pp. 2781–2790, 2011. doi: 10.1021/ie100629k
[17] M. C. Seemann, T. J. Schildhauer, S. M. A. Biollaz, S. Stucki, and A. Wokaun, "The regenerative effect of catalyst fluidization under methanation conditions," Appl. Catal. A Gen., vol. 313, no. 1–2, pp. 14–21, 2006. doi: 10.1016/j.apcata.2006.06.048
[18] M. C. Seemann, T. J. Schildhauer, and S. M. A. Biollaz, "Erratum: Fluidized bed methanation of wood-derived producer gas for the production of synthetic natural gas", Ind. Eng. Chem. Res., vol. 49, no. 15, p. 7034-7038, 2010. doi: 10.1021/ie100510m
[19] J. Liu, D. Cui, C. Yao, J. Yu, F. Su, and G. Xu, "Syngas methanation in fluidized bed for an advanced two-stage process of SNG production," Fuel Process. Technol., vol. 141, pp. 130–137, 2016. doi: 10.1016/j.fuproc.2015.03.016
[20] J. Witte, J. Settino, S. M. A. Biollaz, and T. J. Schildhauer, "Direct catalytic methanation of biogas – Part I: New insights into biomethane production using rate-based modelling and detailed process analysis," Energy Convers. Manag., vol. 171, no. December 2017, pp. 750–768, 2018. doi: 10.1016/j.enconman.2018.05.056
[21] M. Neubert, "Catalytic methanation for small- and mid-scale SNG production," Friedrich-Alexander Universität Erlangen-Nürnberg, Dissertation, 2019.
[22] H. Hofbauer, "Energy from Biomass via Gasification in Güssing," in Biomass Power for the World: Transformations to Effective Use, W. van Swaaij, S. Kersten, and W. Palz, Eds. Pan Stanford, 2015.
[23] J. C. Schmid, F. Benedikt, J. Fuchs, A. M. Mauerhofer, S. Müller, and H. Hofbauer, "Syngas for biorefineries from thermochemical gasification of lignocellulosic fuels and residues - 5 years' experience with an advanced dual fluidized bed gasifier design," Biomass Conv. Bioref., 2019. doi: 10.1007/s13399-019-00486-2

[24] H. Hofbauer, “Experimentelle Untersuchungen an einer zirkulierenden Wirbelschicht mit Zentralrohr,” TU Wien, Dissertation, 1982.
[25] B. J. Milne, F. Berruti, L. A. Behie, and T. J. W. De Bruijn, “The internally circulating fluidized bed (ICFB): A novel solution to gas bypassing in spouted beds,” Can. J. Chem. Eng., vol. 70, no. 5, pp. 910–915, 1992. doi: 10.1002/cjce.5450700512
[26] J. M. Lee, Y. J. Kim, and S. D. Kim, “Catalytic coal gasification in an internally circulating fluidized bed reactor with draft tube,” Appl. Therm. Eng., vol. 18, no. 11, pp. 1013–1024, 1998. doi: 10.1016/S1359-4311(98)00039-8
[27] Y. J. Kim, J. M. Lee, and S. D. Kim, “Bed With Draught Tube,” vol. 76, no. 11, pp. 1067–1073, 1997. doi: 10.1016/S0016-2361(97)00112-9
[28] J. R. Grace, Handbook of Multiphase Systems. Washington, D.C.: Hemisphere, 1982.
[29] H. T. Bi and J. R. Grace, “Effect of measurement method on the velocities used to demarcate the onset of turbulent fluidization,” Chem. Eng. J. Biochem. Eng. J., vol. 57, no. 3, pp. 261–271, 1995. doi: 10.1016/0923-0467(94)02875-B
[30] J. Kopyscinski, T. J. Schildhauer, and S. M. A. Biollaz, “Methanation in a fluidized bed reactor with high initial CO partial pressure : Part I — Experimental investigation of hydrodynamics , mass transfer effects , and carbon deposition,” Chem. Eng. Sci., vol. 66, no. 5, pp. 924–934, 2011. doi: 10.1016/j.ces.2010.11.042
[31] J. Fuchs, J. C. Schmid, S. Müller, and H. Hofbauer, “Dual fluidized bed gasification of biomass with selective carbon dioxide removal and limestone as bed material: A review,” Renew. Sustain. Energy Rev., vol. 107, no. November 2018, pp. 212–231, 2019. doi: 10.1016/j.rser.2019.03.013

C.3 Paper III

Experimental investigation on the methanation of hydrogen-rich syngas in a bubbling fluidized bed reactor utilizing an optimized catalyst

Bartik, A., Fuchs, J., Pacholik, G., Föttinger, K., Hofbauer, H., Müller, S., Benedikt, F.,
Fuel Processing Technology, **2022**, Vol. 237, 107402,
https://doi.org/10.1016/j.fuproc.2022.107402.

Fuel Processing Technology 237 (2022) 107402

Contents lists available at ScienceDirect

Fuel Processing Technology

journal homepage: www.elsevier.com/locate/fuproc

Experimental investigation on the methanation of hydrogen-rich syngas in a bubbling fluidized bed reactor utilizing an optimized catalyst

Alexander Bartik [a,*], Josef Fuchs [a], Gernot Pacholik [b], Karin Föttinger [b], Hermann Hofbauer [a], Stefan Müller [a], Florian Benedikt [a]

[a] Institute of Chemical, Environmental and Bioscience Engineering, TU Wien, Getreidemarkt 9/166, 1060 Vienna, Austria
[b] Institute of Materials Chemistry, TU Wien, Getreidemarkt 9, 1060 Vienna, Austria

ARTICLE INFO

Keywords:
Catalytic fluidized bed methanation
Catalyst preparation
Sustainable and renewable synthetic natural gas
Dual fluidized bed steam gasification
Sorption enhanced reforming

ABSTRACT

Catalytic methanation processes allow the production of natural gas substitutes on a sustainable and renewable basis. This study investigates the catalytic methanation of syngas from dual fluidized bed steam gasification of biomass in an innovative bubbling fluidized bed methanation reactor with an optimized catalyst. Syngas from conventional gasification and a novel combination with syngas from sorption enhanced reforming were investigated. The applied fluidized bed reactor allowed an almost isothermal operation with optimal reaction temperatures between 320 °C–360 °C. Simultaneously, no chemical deactivation or mechanical attrition during 200 h of operation indicates a high long-term stability of the catalyst. The methane concentration downstream the methanation reactor increased from 43 to 74 vol.-%$_{db}$ through the methanation of a hydrogen-rich syngas produced via sorption enhanced reforming. Simultaneously, the methane yield is doubled to 95% and the hydrogen, carbon monoxide and carbon dioxide conversions are improved. Furthermore, it could be shown that a CO_2 content below 1 vol.-%$_{db}$ is feasible in the (raw) synthetic natural gas, allowing grid injection without CO_2 separation. The results indicate that sorption enhanced reforming in combination with an optimized fluidized bed methanation can lead to technical and economic improvements in sustainable synthetic natural gas production.

1. Introduction

Many industrial high-temperature processes and domestic residences rely on the supply of natural gas as an energy carrier [1,2]. However, the targets formulated by the European Commission will require a substantial reduction in the use of fossil fuels in the future [3]. The conversion of biogenic feedstock to renewable synthetic natural gas (SNG) offers the possibility of producing a chemically and physically almost identical gas that can be transported in the already existing gas distribution infrastructure and utilized with already established end-use technologies [4].

Catalytic methanation processes have been studied and developed for more than 100 years since Sabatier and Senders first discovered that noble metals catalyze methanation reactions. In the 1970s and 1980s, the primary focus lay on the conversion of coal to SNG. Due to the rising awareness of climate change and the urgent need to reduce GHG emissions, renewable alternatives for SNG production have been developed. Biomass-to-Gas (BtG) as well as Power-to-Gas (PtG) routes gained importance [4,5]. Besides catalytic methanation concepts, biological methanation approaches attract more and more attention [6,7]. Today, various process concepts exist that aim at an optimized production of SNG. One possible production route is the dual fluidized bed (DFB) gasification of woody biomass or waste materials and consecutive fluidized bed methanation. A primary advantage of the DFB process is that it produces a nitrogen-free syngas that is well suited for downstream synthesis processes. At TU Wien, a 100 kW_{th} advanced DFB pilot plant has been developed and extensively investigated [8]. The investigations show that the new design allows the utilization of various waste resources and significantly impacts the quality of the syngas, which in turn affects the downstream synthesis processes [9,10]. However, due to the typical composition of woody biomass, the production of a stoichiometric syngas for methanation with a H_2/CO ratio of three is impracticable and thus further measures must be taken. Sorption enhanced reforming (SER) is an alternative operation mode of the advanced DFB process, where the stoichiometric ratio of H_2 to CO and CO_2 is influenced and can be adapted to the needs of the downstream synthesis process. Fuchs et al. showed that both the gasification temperature [11] and the

* Corresponding author.
E-mail address: alexander.bartik@tuwien.ac.at (A. Bartik).

https://doi.org/10.1016/j.fuproc.2022.107402
Received 8 May 2022; Received in revised form 23 June 2022; Accepted 1 July 2022
Available online 12 August 2022

Nomenclature

BtG	Biomass-to-Gas
BET model	Brunauer-Emmett-Teller model
DFB	Dual fluidized bed
GHG	Greenhouse gas
KPI	Key performance indicators
P&I diagram	piping and instrumentation diagram
PtG	Power-to-Gas
raw-SNG	raw synthetic natural gas after methanation/before upgrading
SER	sorption enhanced reforming
SN	stoichiometric number of the feed gas
SNG	synthetic natural gas
TPO	temperature-programmed oxidation
TPR	temperature-programmed reduction
WHSV	weight hourly space velocity in Nl/g h
db	dry basis
d_{SV}	mean Sauter diameter in μm
feed	in the feed gas to the methanation reactor
ΔH_R^0	reaction enthalpy at standard conditions in kJ/mol
$\dot{n}_i$	molar flow of species *i* in mol/s
N_i	number of carbon atoms in species *i*
out	in the outlet of the methanation reactor
S_{CO_2}	selectivity of CO towards CO_2 in %
$S_{C_2H_4}$	selectivity of C_2H_6 towards C_2H_4 in %
u_{mf}	minimum fluidization velocity
X_{CO}	carbon monoxide conversion in %
X_{CO_2}	carbon dioxide conversion in %
X_{H_2}	hydrogen conversion in %
Y_{CH_4}	methane yield in %
y_i	molar fraction of species *i*
ρ_b	bulk density in kg/m^3

bed material circulation rate [12] have a major impact on the gas composition. By utilizing this syngas in the methanation reactor, it is theoretically possible to produce grid feedable SNG without the need for a CO_2 separation unit [13]. So far, the investigations on the suitability of these syngases (advanced DFB and SER) for methanation have only been of theoretical nature [13–15]. In a modelling approach, both Bartik et al. [13] and Brellochs [14] state optimal gasification temperatures in the range of 680 °C–700 °C for the production of SNG via SER. Since these studies are of theoretical nature, an objective of this work is the experimental investigation and evaluation of syngas from the advanced DFB pilot plant in a fluidized bed methanation unit. The fluidized bed methanation unit is designed to allow an isothermal operation of the methanation process through internal particle circulation while not disturbing the bubble formation and the gas/solid contact. A more detailed description of the reactor is shown in Section 2.1. Since the DFB and the SER processes are not part of the experimental investigations in this study, literature is referred to [8,9,16–21].

During catalytic methanation, H_2 and CO react to CH_4 and H_2O according to Eq. 1. The water-gas shift reaction (Eq. 2) leads to the formation of CO_2 and H_2 if the syngas shows a low H_2/CO ratio. Vice versa, if the syngas shows an overstoichiometric composition, CO_2 and H_2 react via the reversed water-gas shift reaction and form CH_4 and H_2O in combination with Eq. 1.

$$CO + 3H_2 \rightleftharpoons CH_4 + H_2O \qquad \Delta H_R^0 = -206\frac{kJ}{mol} \tag{1}$$

$$CO + H_2O \rightleftharpoons CO_2 + H_2 \qquad \Delta H_R^0 = -41\frac{kJ}{mol} \tag{2}$$

Especially for syngas with a low H_2/CO ratio, the Boudouard reaction (Eq. 3) plays an important role. Carbon may form on the catalyst surface and block or infiltrate active reaction sites [22].

$$2CO \rightleftharpoons CO_2 + C(s) \qquad \Delta H_R^0 = -172\frac{kJ}{mol} \tag{3}$$

Other species often found in the syngas of the DFB or SER process are hydrocarbons like ethylene (C_2H_4). Ethylene can be hydrogenated to ethane (C_2H_6) (Eq. 4) and further to methane (Eq. 5) but can also lead to coke deposits on the catalyst [23]. The behavior of ethylene very much depends on the applied conditions and the type of reactor [24].

$$C_2H_4 + H_2 \rightarrow C_2H_6 \qquad \Delta H_R^0 = -137\frac{kJ}{mol} \tag{4}$$

$$C_2H_4 + 2H_2 \rightarrow 2CH_4 \qquad \Delta H_R^0 = -202\frac{kJ}{mol} \tag{5}$$

All these reaction equations are highly exothermic, and large quantities of heat need to be removed. For this purpose, reactor concepts have been developed to cope with this issue [25]. Fluidized beds are known for their high heat and mass transfer capabilities due to the movement of the particles [26]. Hence, fluidized beds have been under investigation for catalytic methanation processes since 1950, as a review by Kopyscinski describes in detail [4]. The Paul Scherrer Institute recently picked up on the developments and investigated the fluidized methanation process more closely. They applied spatially resolved concentration and temperature measurements along the height of the catalytic bed. The results show that the particle movement leads to an in-situ regeneration of the catalyst particles and therefore reduces the risk for carbon depositions even in the presence of ethylene [24,27]. Furthermore, they concluded that the mass transfer between the bubble phase and the dense phase is a limiting factor in the upper part of the bed [28]. Seemann et al. [29] utilized a 10 kW fluidized bed reactor and demonstrated the conversion of syngas from the 8 MW DFB plant in Güssing. They reached around 40 vol.-% CH_4 for a period of 200 h until a sulfur breakthrough was detected. Witte et al. [30] applied the same reactor setup to convert biogas from a digester with hydrogen to SNG and showed a stable long-term operation for >1000 h. On a larger scale, Hervy et al. [31] demonstrated CO_2 methanation in a 400 kW fluidized bed methanation reactor. They proved that a high conversion efficiency could be maintained despite temperature and load variations.

Despite these advantages, fluidized beds impose mechanical stress on catalyst particles. Thus, the development of an attrition-resistant catalyst with a proper fluidization behavior is necessary, which has not been considered or documented in the investigations mentioned above. In general, a significant amount of research has been put into the development of methanation catalysts, as some reviews show [32,33]. However, only a few investigations focus on the application in fluidized beds or the use of α-Al_2O_3 as catalyst support. Typically, γ-Al_2O_3 is used because of its high surface area and the highly dispersed metal particles, while α-Al_2O_3 is often disregarded because of its low surface area and weak metal-support interaction [33]. For fluidized bed applications, Cui et al. [34] added different binders to improve the attrition resistance of the produced catalyst and found that acidic silica sol showed the highest resistance. Other investigations proved the superiority of fluidized beds over fixed beds in terms of conversion rates and coking resistance in small lab-scale test rigs [35,36]. However, a holistic approach, considering the catalytic activity in combination with an optimal fluidization behavior in a representative fluidized bed reactor scale, seems to be missing.

This work investigates the catalytic methanation process in a 10 kW bubbling fluidized bed methanation reactor utilizing an optimized

catalyst for fluidized bed applications. In contrast to the commonly used γ-Al_2O_3, an attrition-resistant α-Al_2O_3 with a high specific surface area and improved fluidization properties is utilized. Besides the determination of the reactor and catalyst performance, the proposed concept is applied to systematically investigate the methanation of premixed gases imitating syngas from the advanced DFB pilot plant. The goal is to demonstrate that (raw) SNG production via SER and fluidized bed methanation with a tailored catalyst can lead to an optimized process chain with technical and economic advantages.

2. Materials and methods

2.1. Fluidized bed methanation reactor setup

Fig. 1 shows a 3D-CAD drawing of the fluidized bed reactor setup designed for the catalytic methanation of syngas. The reactor consists of two separate reaction zones operated in the bubbling fluidization regime. Both zones can be fluidized individually via two separate wind boxes. The gas distributor consists of nozzles, which provide the necessary pressure drop for uniform gas distribution. Both reaction zones are cooled individually to manage the heat released by the exothermic reaction. An air perfused coil cools the inner reaction zone, while a cooling jacket is used to cool the annular reaction zone. Thus, an isothermal operation of the methanation reactor is ensured. At the same time, the fluidization in the two reaction zones is not disturbed by internals. The catalyst, however, can move freely between the zones through the 'upper gap' and the 'lower gap' as denoted in Fig. 1. More information on the reactor setup is documented in [37].

Fig. 2 shows a simplified piping and instrumentation (P&I) diagram of the reactor setup. In the lower-left part of the diagram, the gases (N_2/H_2/CO/CO_2/CH_4/C_2H_4) are withdrawn from gas cylinders and premixed according to the volume flow set by valves and rotameters. After splitting and preheating, the gas stream enters the wind boxes. Here, water vapor can be added if the syngas composition requires so. The reaction zones are equipped with thermocouples type K to measure the axial temperature distribution along the reactor height. The gas outlet is equipped with a particle filter and downstream the raw-SNG is burnt in a flare. The gas compositions of the syngas input and the raw-SNG output are analyzed online, as described in section 2.3.

2.2. Catalyst preparation

The catalyst contained 20 wt.-% NiO and 2 wt.-% MgO and was produced in 6 batches, following the preparation method of Hu et al. [38]. The reagents used for this are listed in the supplementary material (chapter A). Nickel nitrate hexahydrate and magnesium nitrate hexahydrate were dissolved (approx. 300 ml) in water and afterward the support was added. The solution was heated and stirred until the excess water was evaporated. The powder was dried overnight at 120 °C and calcined for 4 h at 500 °C with a heating ramp of 5 °C/min. The used support was a Puralox SCCa-150/200 α-Al_2O_3 from SASOL, which is in particular designed for fluidized bed applications and thus exhibits a high level of attrition resistance. Despite the high calcination temperatures typical for α-Al_2O_3, the material is reported to have a high surface area [39].

2.3. Catalyst characterization & measurement system

A MicrotracBEL Catalyst Analyzer Belcat-II was used for the temperature-programmed reduction (TPR) and the pulse chemisorption measurements of CO and H_2 on the catalyst sample. N_2 physisorption was performed in a Micromeritics ASAP 2020 Serial # 1455 for the measurement of the surface area using the BET model. To determine possible carbon depositions on the catalyst, temperature-programmed oxidation (TPO) experiments were carried out. More information on the experimental measurement procedure can be found in the supplementary material (chapter B).

The particle size distribution and the Sauter diameter (d_{SV}) of the catalyst are determined with a Malvern Instruments Mastersizer 2000 laser diffraction particle size analyzer. A Rosemount NGA 2000 gas analyzer is used to measure H_2, CO, CO_2 and CH_4 concentrations in the feed gas and the raw-SNG. Another NGA 2000 module with a low measurement range (< 5000 ppm_v) is used for the reliable detection of low CO concentrations in the raw-SNG. Additionally, a Perkin Elmer ARNEL – Clarus 500 gas chromatograph (GC) detects ethane (C_2H_6), ethylene (C_2H_4), acetylene (C_2H_2), propane (C_3H_8), and nitrogen (N_2) quantitatively. Higher hydrocarbons (C_3+) are qualitatively detected. Furthermore, the GC redundantly measures the CO, CO_2, and CH_4 concentrations, which are included in the data evaluation.

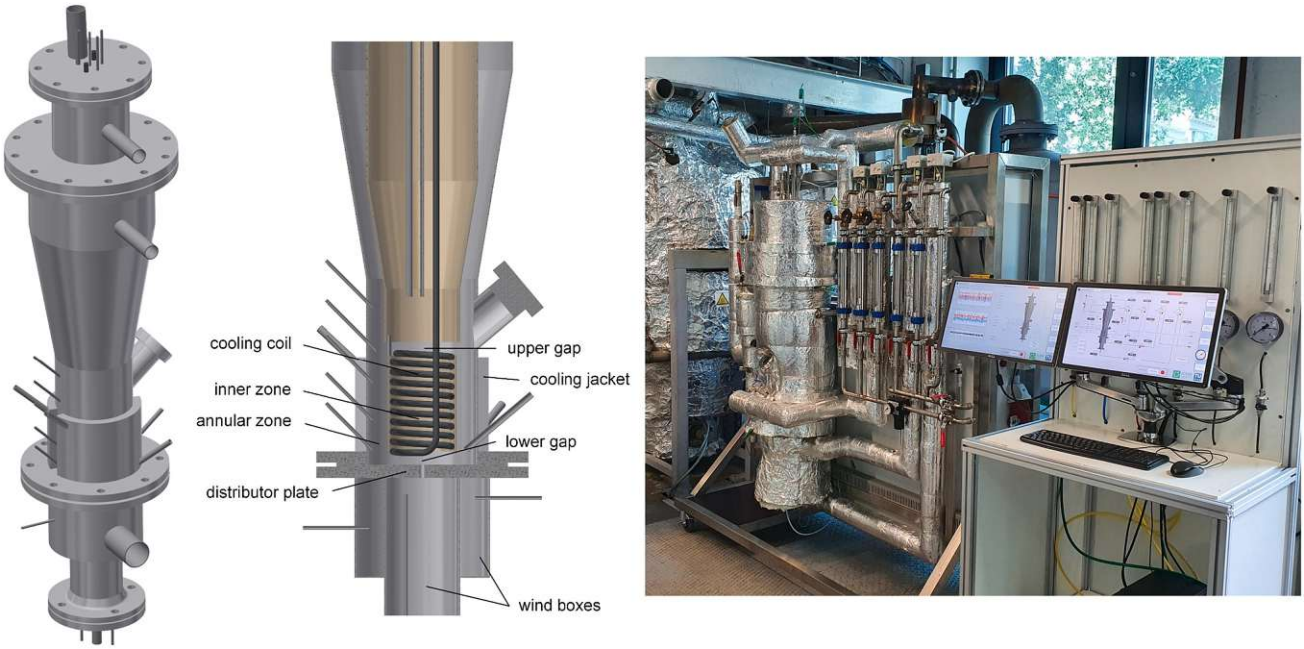

Fig. 1. 3D-CAD drawing (left) and picture (right) of the fluidized bed reactor.

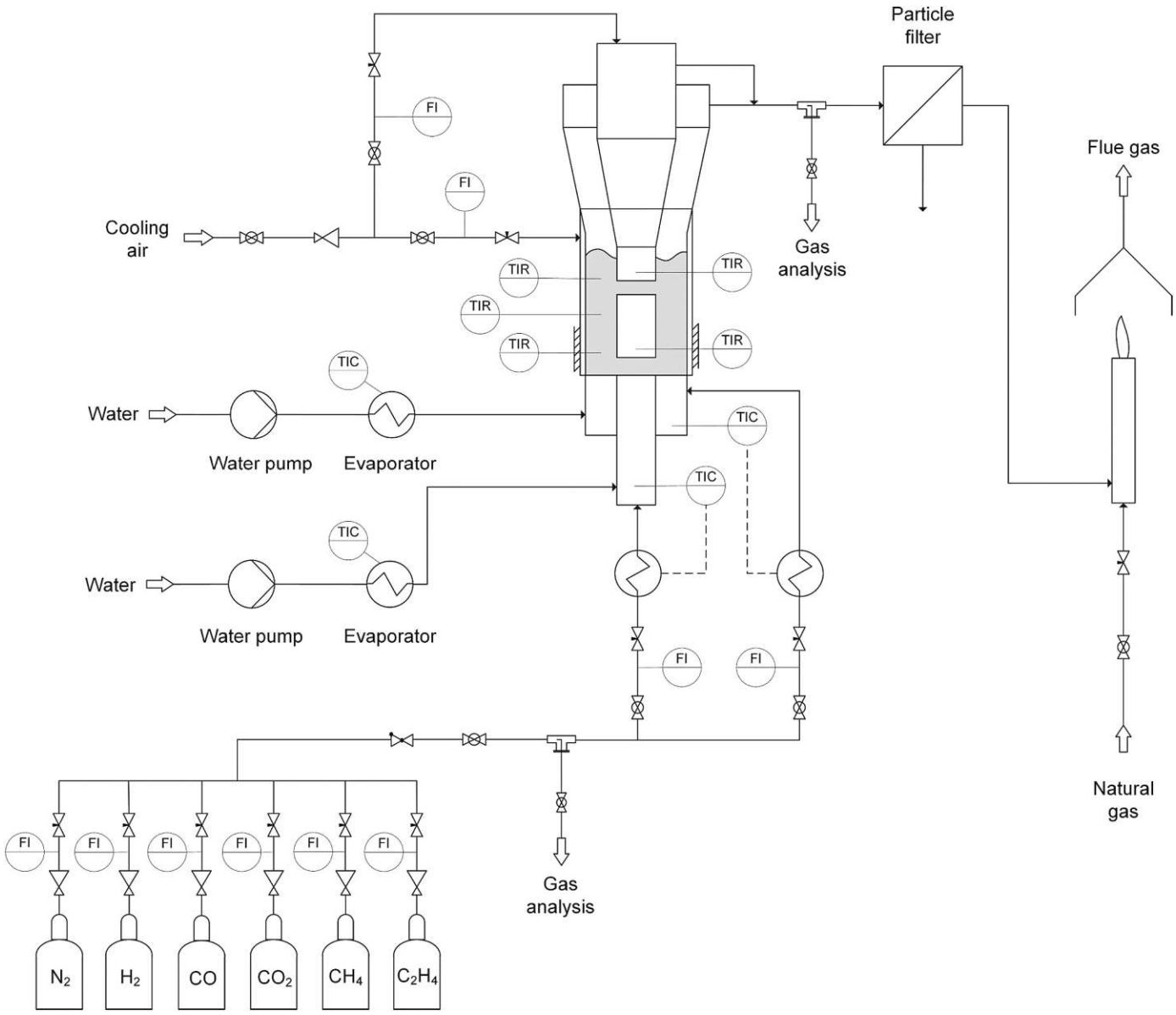

Fig. 2. Simplified P&I diagram of the fluidized bed reactor setup.

2.4. Experimental conditions

For the fluidized bed methanation experiments, 1.6 kg of the prepared Ni/α-Al_2O_3 catalyst and 1.5 kg of the unimpregnated α-Al_2O_3 support were used in the reactor. This amounts to an unfluidized bed height of about 20 cm. The catalyst was heated up at a rate of approximately 3 °C/min and reduced at 500 °C for 6 h in a 9:1 volume-based hydrogen to nitrogen atmosphere.

For the purpose of this investigation, the gas velocity and the mean temperature in the inner and the annular reaction zone were kept equal to each other for all experiments. Furthermore, the gas preheating temperature was set to 250 °C, and the pressure was equal to ambient conditions for all experiments. All temperatures given in section 3 are mean values computed from two measurements in the inner reaction zone and three measurements in the annular reaction zone, as indicated in Fig. 2.

The following syngas compositions are tested:

- Stoichiometric H_2/CO syngas for the determination of the catalyst and reactor performance (H_2/CO).
- Typical DFB syngas composition from the 100 kW_{th} advanced DFB pilot plant (DFB).
- The flexible SER syngas composition from the 100 kW_{th} advanced DFB pilot plant (SER).

Table 1 lists the gas compositions for these cases. The exact compositions of the SER syngases are given in the supplementary material (chapter C), following the work of Fuchs et al. [11]. Additionally, the parameter variations carried out for each gas composition are depicted. A variation of the C_2H_4 content was investigated because the syngas of the advanced DFB gasifier exhibits varying concentrations depending on factors such as temperature, bed material, and type of biomass [40]. Because of the different gas compositions and reaction conditions, the fluidization number varies between 1.8 and 7.8 u_{mf}. Especially the variation of the weight hourly space velocity (WHSV) results in the most pronounced influence on the fluidization number.

2.5. Process simulation & key performance indicators

All gas analysis measurements are validated by the calculation of

Table 1
Syngas compositions and parameter variations tested in the fluidized bed methanation reactor.

Syngas composition			
	H_2/CO	DFB [8,9]	SER [11,21]
H_2 [vol.-%$_{db}$]	75	42.3	54.6–70.8
CO [vol.-%$_{db}$]	25	23.1	7.4–14.8
CO_2 [vol.-%$_{db}$]	–	21.9	4.6–17.2
CH_4 [vol.-%$_{db}$]	–	10.4	11.4–17.1
C_2H_4 [vol.-%$_{db}$]	–	2.4	1.2–2
Parameter variation in the methanation reactor			
Temperature [°C]	280–420	280–400	360
WHSV [Nl/g h]	0.8–1.5	1–1.5	1.5
H_2O [vol.-%]	–	0–40	–
C_2H_4 [vol.-%$_{db}$]	–	1.1–3.2	–

mass and energy balances around the reactor. For this purpose, a mathematical model of the reactor is created in the process simulation tool IPSEpro. In addition to the mass and energy balances, the model also calculates the fluid dynamic properties of the fluidized bed as well as the key performance indicators (KPI's) defined in Eqs. 6–12. All presented results in this paper reflect the balanced solution obtained from IPSEpro and not the direct measurement values.

The methane yield (Y_{CH_4}) is calculated according to Eq. 6, where $\dot{n}$ is the molar flow of species i and N is the number of carbon atoms in the respective gas component in the feed gas (*feed*) and the raw-SNG (*out*). Eqs. 7, 8, and 9 define the CO conversion (X_{CO}), the CO_2 conversion (X_{CO_2}) and the H_2 conversion (X_{H_2}), respectively.

$$Y_{CH_4} = \frac{\dot{n}_{CH_4,out}}{\sum_i N_i \dot{n}_{i,feed}} * 100 \quad (6)$$

$$X_{CO} = \frac{\dot{n}_{CO,feed} - \dot{n}_{CO,out}}{\dot{n}_{CO,feed}} * 100 \quad (7)$$

$$X_{CO_2} = \frac{\dot{n}_{CO_2,feed} - \dot{n}_{CO_2,out}}{\dot{n}_{CO_2,feed}} * 100 \quad (8)$$

$$X_{H_2} = \frac{\dot{n}_{H_2,feed} - \dot{n}_{H_2,out}}{\dot{n}_{H_2,feed}} * 100 \quad (9)$$

Eqs. 10 and 11 show the calculation of the CO_2 selectivity (S_{CO_2}) and the C_2H_6 selectivity ($S_{C_2H_6}$), respectively. Eq. 10 is based on the assumption that CO_2 is only formed from CO via the water-gas shift reaction (Eq. 2). The C_2H_6 selectivity only considers the formation of C_2H_6 via the hydrogenation of C_2H_4 (Eq. 4). However, the catalyst also shows a slight selectivity of CO towards C_2H_6 under certain reaction conditions. Therefore, the C_2H_6 selectivity is only depicted if the formation via CO does not occur.

$$S_{CO_2} = \frac{\dot{n}_{CO_2,out} - \dot{n}_{CO_2,feed}}{\dot{n}_{CO,feed} - \dot{n}_{CO,out}} * 100 \quad (10)$$

$$S_{C_2H_6} = \frac{\dot{n}_{C_2H_6,out}}{\dot{n}_{C_2H_4,feed} - \dot{n}_{C_2H_4,out}} * 100 \quad (11)$$

The stoichiometric number (*SN*) is calculated according to Eq. 12. It assesses the stoichiometry of the feed gas for methanation according to the reaction equations Eqs. 1, 2 and 5.

$$SN = \frac{y_{H_2}}{3\, y_{CO} + 4\, y_{CO_2} + 2\, y_{C_2H_4}} \quad (12)$$

3. Results and discussion

3.1. Catalyst and reactor performance

3.1.1. Catalyst properties

Table 2 gives an overview of the properties of the α-Al_2O_3 support and the prepared NiO/α-Al_2O_3 catalyst. From a fluid dynamic point of view, both can be classified as group B particles close to the transition area to group A, according to Geldart [41]. The Sauter diameter (d_{SV}) and the bulk density (ρ_b) increase through the impregnation of the support with NiO. Nevertheless, the uniform and narrow particle size distribution of the support is maintained. 99% of the particles are sized between 80 and 280 μm (cf. Fig. 4). Since the particles are also approximately spherical, they are deemed well suited for an optimal fluidization behavior [26]. Additionally, a very high BET surface area was measured for the support, despite literature reports, which attribute Al_2O_3 in the alpha configuration a rather low surface area due to the high calcination temperature. Liu et al. [42] for example, achieved a surface area of 44 m^2/g, while other supports exhibit values around 10 m^2/g [43,44]. By impregnating the support with nickel, the surface area is reduced by about 22%, most likely through the blockage of pores with NiO particles [43]. Nevertheless, the resulting catalyst shows a very high surface area at around 140 m^2/g, which is even in the range of commonly used γ-Al_2O_3-based catalysts [28,38]. The average Ni particle size at 37 nm is in the upper part of the spectrum but within the expected range. The somewhat larger Ni particles may result from a weaker catalyst/support interaction and the preparation conditions [43].

Fig. 3 illustrates the H_2 consumption during the TPR of the catalyst. Two main reduction temperatures at 595 °C and 766 °C were identified. The hydrogen uptake was 1.5 mmol/g and 0.34 mmol/g for the first and the second peak, respectively. The lower temperature can be assigned to a less strongly bounded NiO on Al_2O_3 and the NiO that is reduced at 766 °C to Ni-aluminate spinels. MgO is known to be responsible for a higher amount of NiO being present in the form that is easier to reduce. MgO was not likely to be reduced under these conditions [45]. Additionally, the Al_2O_3 in the alpha configuration leads to less strongly bound NiO, which lowers the reduction temperature [43]. The H_2 consumption per Ni atom was approximately 0.7, indicating a core-shell structure of Ni, where the core was still oxidized and only the shell atoms were in metallic form after reduction.

In order to further evaluate the performance of the catalyst, the mechanical and chemical stability was evaluated. Fig. 4 (left) depicts the particle size distribution and the mean Sauter diameter (d_{SV}) of the fresh and the used catalyst. No significant attrition of the catalyst was detected during approximately 200 h of operation under fluidized bed conditions. The narrow and uniform particle size distribution of the fresh catalyst could be maintained. Only a slightly smaller Sauter diameter was measured for the used catalyst. The deviation is, however, too small to state significant attrition of the catalyst. On the one hand the measurement accuracy is lower than the deviation and on the other hand the reduction of the catalyst is not accounted for since the fresh catalyst was in the original, oxidized state when the measurement was performed. The measurement accuracy is deemed suitable for the statement of no significant attrition, especially considering the relatively high number of operating hours. For a finite statement, even longer-term

Table 2
Measured properties of the Al_2O_3 support and the prepared NiO/α-Al_2O_3 catalyst.

Parameter	α-Al_2O_3	NiO/α-Al_2O_3
Geldart group	B	B
d_{SV} [μm]	140	150
ρ_b [kg/m^3]	787	902
BET surface area [m^2/g]	183	142
Ni surface area [m^2/g]	–	2.8
Ni mean particle size [nm]	–	37

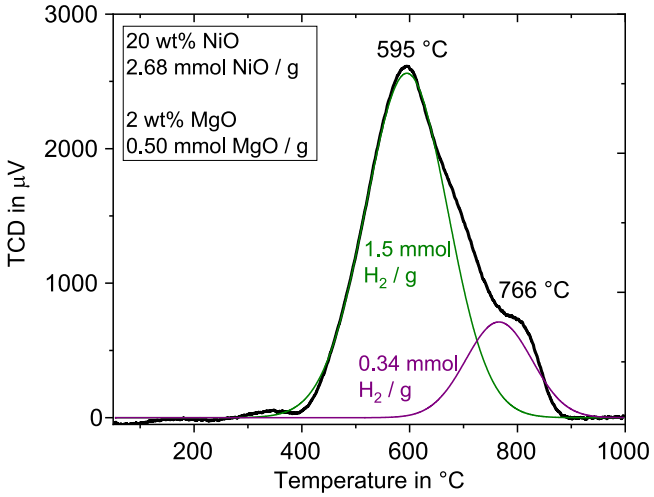

Fig. 3. TPR of Ni/α-Al_2O_3 with the quantification of the hydrogen consumption per species and the molar amount of NiO and MgO per gram of the catalyst.

experiments could show if relevant attrition occurs. Furthermore, no chemical deactivation of the catalyst occurred during the methanation experiments over a period of approximately 100 h. The chemical stability was determined by repeatedly carrying out methanation experiments under the same process conditions and comparing the raw-SNG gas composition (see supplementary material chapter B). Nevertheless, some carbon deposition was found on the catalyst by performing TPO analysis of the used catalyst (Fig. 4 right). The TPO curve suggests that only very little amounts of carbon were deposited on the catalyst. Furthermore, the CO_2 peak at around 350 °C suggests amorphous carbon, which is rather weakly bound [46]. In general, literature reports under fixed bed conditions indicate that larger Ni particles on α-Al_2O_3 are more stable and active over time than smaller particles on low-temperature calcined supports [43].

3.1.2. Temperature and space velocity variation for CO-methanation at stoichiometric conditions

In this section, the performance of the catalyst and the reactor is investigated by carrying out stoichiometric H_2/CO methanation experiments. Fig. 5 shows the raw-SNG composition for varying temperatures and WHSV's in comparison to the maximum thermodynamic values (dotted lines). There is a clear influence of both parameters visible. At high temperatures, the experimental values approach the thermodynamic equilibrium independent of the applied WHSV. However, a small deviation remains, which is attributed to the back-mixing behavior of fluidized beds. Additionally, the results also confirm the findings of Kopyscinski et al. [28], who describe that the mass transfer between the bubble phase and the dense emulsion phase is a limiting factor. Above the surface of the fluidized bed, less reacted gas of the bubble phase mixes with gas from the dense emulsion phase, which overall results in a below-maximum conversion. At lower temperatures, kinetic limitations take over and lead to a pronounced deviation from the thermodynamic equilibrium. Thus, also the WHSV has a greater influence on the gas composition. The maximum CH_4 content of 76.5 vol.-%$_{db}$ is reached at a temperature of 320 °C and a WHSV of 0.8 Nl/g h. At the same time, the H_2 and CO contents are minimal at 18.9 vol.-%$_{db}$ and 400 ppm$_{db}$, respectively. Accordingly, the maxima and minima shift towards higher temperatures for higher WHSV, following the kinetic limitation. CO_2 is produced via the water-gas shift reaction (Eq. 2), yielding around 5 to 8 vol.-%$_{db}$. Additionally, the amount of CO_2 is higher and the CO_2 selectivity increases from around 6 to 8% with a higher WHSV. Both assertions indicate that the catalyst is very active towards the water-gas shift reaction (Eq. 2). Furthermore, the catalyst shows a slight selectivity of CO towards ethane below 330 °C. Up to 0.6 vol.-%$_{db}$ ethane were detected.

During the experiments, the temperature distribution along the height of the catalytic bed is monitored to determine the isothermal operation capabilities of the reactor. Since the stoichiometric H_2/CO methanation yields the highest specific heat amount compared to the other investigated gas compositions, the maximum temperature gradients also occur in this case. A maximum gradient of 10 °C was measured at 280 °C and 1 Nl/g h. In general, the gradient is much lower. Especially at temperatures above 320 °C a deviation of only around 2 °C was measured. Thus, an isothermal operation with the applied reactor and catalyst combination was shown to be feasible and the thermal stress on the catalyst is kept at a minimum. An additional particle mixing by induced solid circulation due to different fluidization velocities in the inner and annular reaction zones was not needed.

3.2. Methanation of hydrogen-rich syngas

In this section, typical DFB and SER syngas compositions from the advanced 100 kW_{th} DFB pilot plant at TU Wien are investigated in the fluidized bed methanation reactor. The utilized syngas compositions are defined in Table 1 and the figure headings. The exact syngas compositions for the SER methanation experiments are listed in the supplementary material (chapter C).

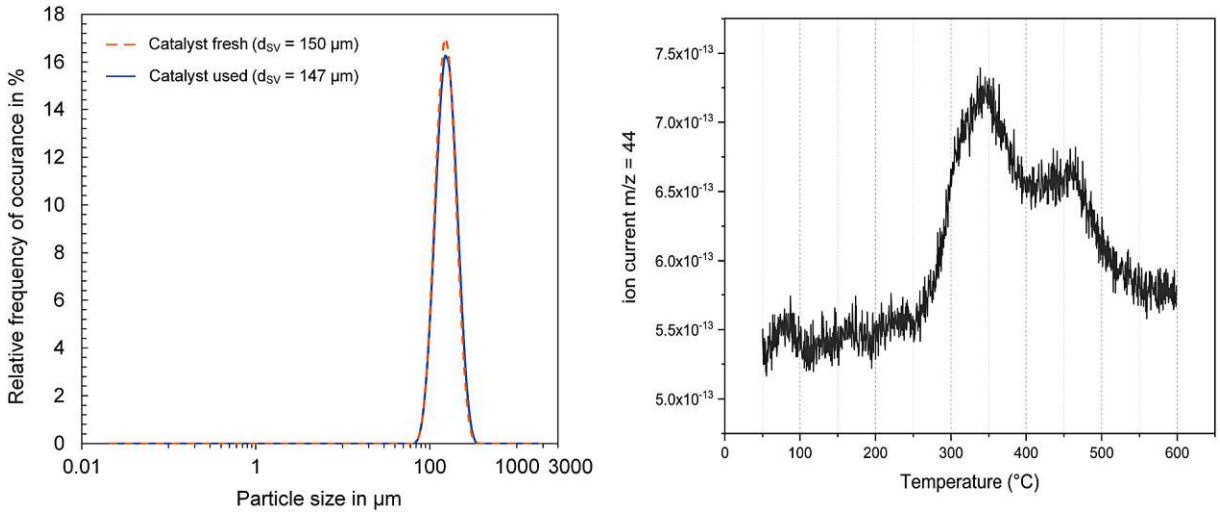

Fig. 4. Comparison of the particle size distribution of the fresh and the used catalyst (left) and TPO of the used catalyst (right).

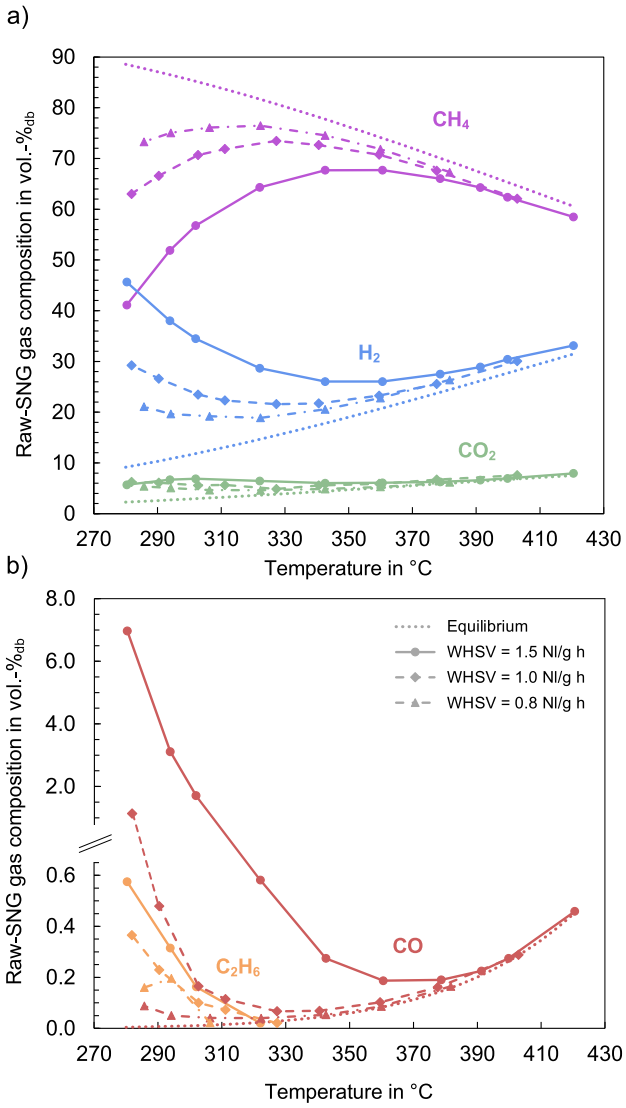

Fig. 5. Experimentally determined raw-SNG composition for stoichiometric H_2/CO methanation (75/25 vol.-%) as a function of reaction temperature and WHSV and raw-SNG composition in the thermodynamic equilibrium (dotted lines), a) CH_4, H_2 and CO_2 concentrations, b) CO and C_2H_6 concentrations.

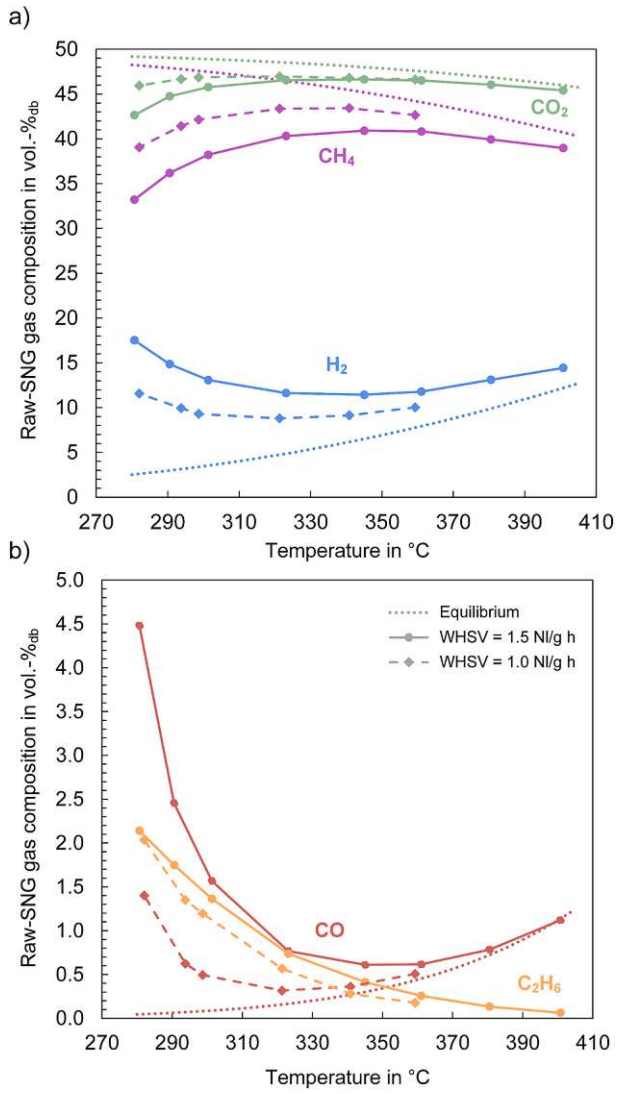

Fig. 6. Experimentally determined raw-SNG composition for a typical DFB syngas as a function of reaction temperature and WHSV and raw-SNG composition in the thermodynamic equilibrium (dotted lines), a) CH_4, H_2 and CO_2 concentrations, b) CO and C_2H_6 concentrations; feed gas composition: H_2 = 42.3%, CO = 23.1%, CO_2 = 21.9%, CH_4 = 10.4%, C_2H_4 = 2.4%.

3.2.1. *DFB syngas methanation*

Fig. 6 shows the raw-SNG composition for varying temperatures and WHSV's in comparison to the maximum thermodynamic values (dotted lines). Because of the understoichiometric composition of the DFB syngas (SN = 0.26), 20 vol.-% water vapor was added to the syngas. Both the added water vapor and the water produced through the methanation reaction (Eq. 1) lead to a shift of the gas (Eq. 2) and the production of CO_2. Together with the CO_2 already present in the syngas, it is the component with the highest concentration in the raw-SNG. A maximum CH_4 concentration of 43.4 vol.-%$_{db}$ and a minimum H_2 and CO concentration of 8.8 vol.-%$_{db}$ and 0.32 vol.-%$_{db}$, respectively, was measured at a temperature of 320 °C and a WHSV of 1 Nl/g h. Similar to Fig. 5, there is an influence of temperature and WHSV visible on the gas composition. At higher temperatures and lower WHSV's, the thermodynamic equilibrium is approached. However, the influence of both parameters is less pronounced compared to the stoichiometric CO methanation experiments. Between 300 and 400 °C, the CH_4 concentration only varies by 2.7 vol.-%$_{db}$ at 1.5 Nl/g h. Interestingly, the CO_2 and CO concentrations at high temperatures are closer to the thermodynamic equilibrium than the CH_4 and H_2 concentrations. Again, this could indicate that the water-gas shift reaction is favored over the methanation reaction, as Kopyscinski et al. already discussed in [24,28] for a different nickel catalyst. However, at low temperatures, Kopyscinski et al. [47] state that the water-gas shift reaction is negligible. This does not seem to be the case for the investigated catalyst since the CO_2 concentrations are especially high at low temperatures. Ethylene was also added to the feed gas and is fully converted to ethane and other components like methane. The concentration of ethane strongly depends on the temperature and, to a lesser extent, on the WHSV.

Fig. 7 visualizes the C_2H_6 selectivity ($S_{C_2H_6}$) and the CO_2 selectivity (S_{CO_2}). At temperatures around 400 °C, almost no ethane is formed, whereas at a temperature of 280 °C the C_2H_6 selectivity is as high as 65%. Additionally, a lower WHSV leads to a lower selectivity. This shows that the reaction of ethane to methane is kinetically inhibited at lower temperatures, whereas the conversion of ethylene is complete for all applied conditions. On the other hand, the concentration of ethylene in the syngas does not seem to have any influence on the C_2H_6 selectivity. At 360 °C, the same selectivities were achieved for all investigated concentrations. The course of the C_2H_6 selectivity over temperature agrees very well with the results published by Kopyscinski et al. [24],

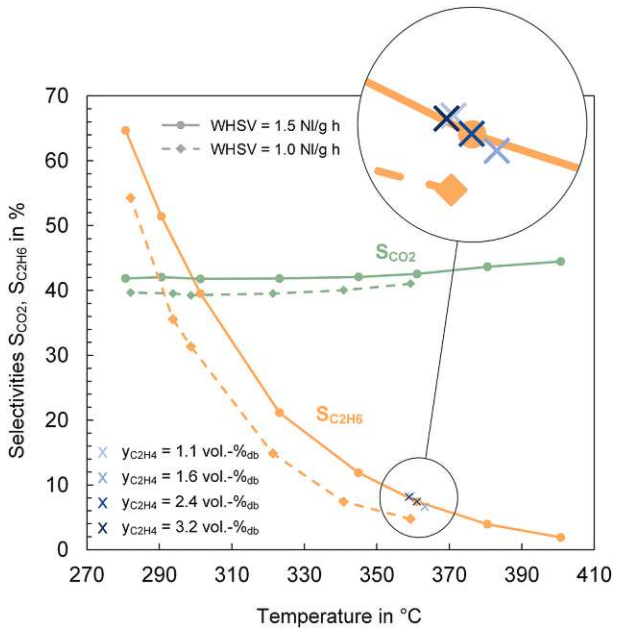

Fig. 7. Ethane selectivity ($S_{C_2H_6}$) as a function of reaction temperature, WHSV, and syngas ethylene concentration as well as carbon dioxide selectivity (S_{CO_2}) as a function of reaction temperature and WHSV for a typical DFB syngas.

who found similar C_2H_6 selectivities even though they used a catalyst with 50 wt.-% NiO and a syngas composition with higher CO and C_2H_4 contents. However, above 350 °C, their C_2H_6 selectivity approaches zero, whereas Fig. 7 still shows some selectivity.

Furthermore, the measurement data shows that no other hydrocarbons are formed under the applied reaction conditions. Reference experiments without ethylene in the syngas also show that CO is not selective towards C_2H_6 over the whole temperature range for a typical DFB syngas (see supplementary material chapter D). This is in contrast to the stoichiometric H_2/CO methanation experiments in Fig. 5 where CO shows some selectivity towards C_2H_6. Both the added steam and the understoichiometric composition of the syngas can be responsible for the suppression of ethane formation from CO. In general, the formation of ethane to a certain amount is desirable because of the higher energy density and increased heating value of the resulting SNG. This, in turn, increases the leeway for fulfilling the specifications of the gas grid, since the minimum required heating value can be reached more easily. However, ethane and other hydrocarbons usually present in the DFB syngas can lead to coke formation. Even though this issue is less pronounced in fluidized beds, it can still lead to a coverage of the catalyst surface with carbon species and deactivation of the catalyst [48,49]. Carbon deposition is, however, strongly influenced by the reaction temperature and low temperatures (<380 °C) were found to suppress carbon formation to a large extent [24]. Within this work, carbon deposition was detected after an operation period of 100 h under different operating conditions. However, the deposited carbon did not lead to a deactivation of the catalyst (also see section 3.1.1). A more detailed investigation under specified conditions would be required to allow a final statement concerning this topic.

A look at the CO_2 selectivity shows that it is relatively constant over the investigated temperature range, which is again in agreement with [24]. For higher temperatures only a minor increase can be observed. A lower WHSV decreases the CO_2 selectivity as is the case for the stoichiometric H_2/CO methanation in section 3.1.2. This is explained by the fact that the methanation reactions gain importance at lower WHSV and lead to an increased CO conversion to CH_4. The higher CO_2 concentrations for lower WHSV in Fig. 6 are therefore attributed to dilution effects.

The feed water content was set to 20 vol.-% to prevent carbon depositions and was chosen according to thermodynamic consideration as well as literature values. However, the amount of water also shows an influence on the raw-SNG composition since it is a reaction product of the methanation reactions but an educt of the water-gas shift reaction. Accordingly, the CH_4 and CO concentrations decrease with increasing water content, while the H_2 concentration and the CO_2 selectivity increase as experiments (see supplementary material chapter D) and Kopyscinski et al. [24] confirm. Additionally, higher water concentrations can lead to a hydrothermal deactivation of the catalyst, which involves grain growth of the catalytic phase, especially at higher temperatures [22]. Therefore, an optimization of the feed water content depends on the reaction conditions, the syngas composition, and the catalyst and is a tradeoff between the raw-SNG composition and catalyst deactivation. In this work, no further investigations on the hydrothermal deactivation were carried out.

3.2.2. SER syngas methanation

Syngas from the SER process is very flexible in its composition, which can be taken advantage of in methanation processes. Fig. 8 depicts the raw-SNG composition over the stoichiometric number SN (Eq. 12) of the syngas at a methanation temperature of 360 °C and a WHSV of 1.5 Nl/g h. Additionally, the thermodynamic values are given (dotted lines). The syngas compositions range from widely understoichiometric to overstoichiometric compositions (SN = 0.4–1.6). Accordingly, also the raw-SNG composition changes with SN. In general, the experimentally determined values follow the course of the thermodynamic prediction well. For a high SN, the distance to the thermodynamic equilibrium decreases further, due to the diminishing amounts of CO and CO_2, which need to be methanated, despite the constant WHSV. Furthermore, the CO_2 concentration is very close to the thermodynamic equilibrium, which again indicates a preference of the catalyst towards the water-gas shift reaction. The highest methane concentrations are found for an almost stoichiometric composition containing 71 vol.-%db CH_4. A lower SN leads to an excess of CO_2 and higher CO concentrations but to a lower H_2 content. In this case, not enough H_2 is available to convert the CO_2 in the syngas. On the other hand, a higher SN and therefore a higher H_2 partial pressure in the syngas allows an almost complete conversion of CO_2 and CO. No CO_2 separation unit for the upgrading of the raw-SNG is necessary in this case. This is true for a SN $\geq$ 1.2 under the considered reaction conditions. However, excessive amounts of hydrogen are left in the raw-SNG, which need to be separated or recirculated before grid feeding. Hydrogen separation is necessary for all investigated compositions, since the limit of 10 vol.-%db according to the regulations [50] was not reached. Ethylene is again fully converted, but a certain amount remains as ethane in the raw-SNG.

Fig. 9 depicts the key figures Y_{CH_4}, X_{CO}, X_{CO_2}, X_{H_2}, and $S_{C_2H_6}$ over SN for the methanation of the SER syngas. Y_{CH_4}, X_{CO}, and X_{CO_2} increase with a higher SN and reach almost 100%. The H_2 conversion, on the other hand, decreases from left to right. Especially when looking at the CO_2 conversion, the effect of the different syngas compositions becomes evident. While the CO_2 conversion is almost zero on the left side of the diagram, it is nearly complete for the highest depicted SN. Overall, the performance improvement is most pronounced on the left side of the diagram, i.e., when increasing SN from 0.4 to 1. Higher SN lead to a lower increase of the key figures at the expense of a more pronounced decline in H_2 conversion. In other words, the driving force for the reaction decreases. Interestingly, the ethane selectivity is relatively constant over the whole SN range even though the syngas composition varies considerably. Only a slight decrease is observed towards higher SN.

3.3. Comparison of DFB and SER syngas methanation

This chapter compares the raw-SNG composition (Fig. 10 left) and

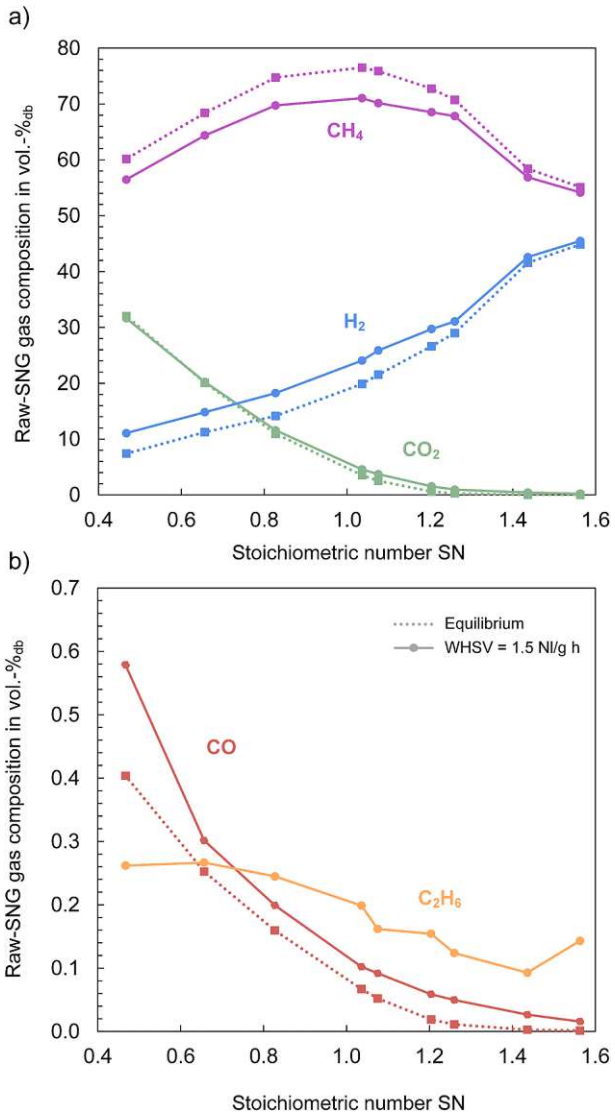

Fig. 8. Experimentally determined raw-SNG composition and raw-SNG composition in the thermodynamic equilibrium (dotted lines) for different SER syngas compositions as a function of the stoichiometric number SN at 360 °C and a WHSV of 1.5 Nl/g h, a) CH_4, H_2 and CO_2 concentrations, b) CO and C_2H_6 concentrations; feed gas composition: H_2 = 54.6–70.8%, CO = 7.4–14.8%, CO_2 = 4.6–17.2%, CH_4 = 11.4–17.1%, C_2H_4 = 1.2–2%.

the key figures (Fig. 10 right) of the DFB and SER syngas methanation experiments. The two displayed datasets were recorded under the same reaction conditions at 360 °C and a WHSV of 1 Nl/g h with a SN of 1.05 for the SER syngas. The CH_4 content increases by more than 30 percentage points by utilizing the SER syngas, while the CO and CO_2 concentrations decrease to low levels. However, the residual H_2 content more than doubles. This is not because of a lower H_2 conversion but due to the dilution of the DFB raw-SNG with CO_2. After CO_2 separation, the residual H_2 concentrations are in a similar range. Nevertheless, both raw-SNG gases require an H_2 and CO_2 separation unit before grid feeding under the considered reaction conditions. On the contrary, the residual CO concentration of the SER raw-SNG is within the limit of 0.1 mol.-% according to the regulations [50], whereas a further reduction for the DFB raw-SNG is required. In general, the SER raw-SNG is much closer to the specifications of the gas grid and an injection to the gas grid is possible without CO or CO_2 separation, as Fig. 8 shows.

Thermodynamic investigations predict that grid feeding even without H_2, CO and CO_2 separation is theoretically possible under the

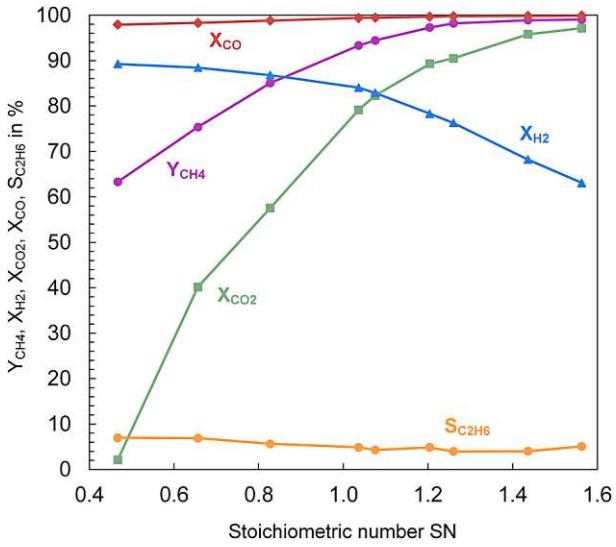

Fig. 9. CH_4 yield, H_2 conversion, CO conversion, CO_2 conversion and C_2H_6 selectivity as a function of the stoichiometric number at 360 °C and a WHSV of 1.5 Nl/g h.

right process conditions. This includes a further reduction of reaction temperature and a pressurized application. For the depicted, slightly overstoichiometric composition, this could be thermodynamically achieved at around 300 °C and 4 bar_a [13]. Alternatively, a two-stage methanation process could be applied, as some theoretical considerations show [51].

Fig. 10 (right) displays the key figures defined in Eqs. 6–9 and 11. The SER syngas methanation allows a doubling of the CH_4 yield and a substantial amount of CO_2 conversion. Simultaneously, the H_2 and CO conversions are slightly increased as well. The DFB syngas, on the other hand, leads to the production of additional CO_2 through the shift of the gas via the water-gas shift reaction. However, the ethane selectivity is lower in the case of the SER syngas. This is attributed to the high H_2 partial pressure of the SER syngas, which influences the selectivity to some extent (cf. Fig. 9).

Overall, it is necessary to look at the performance of the whole process chain and not only at the methanation itself. The methanation KPI's are much more favorable for the SER syngas. However, this should not create the illusion that the performance of the whole process from biomass to SNG is more favorable as well. The high methane yield for the SER syngas methanation is only possible because of the different process characteristics of the SER and the DFB operation modes of the gasifier. Therefore, a comparison of the whole process chain is necessary.

3.4. Summary

This study shows experimental results of syngas methanation in a fluidized bed methanation reactor. The main focus points are the development and testing of a stable catalyst for fluidized beds, the methanation reactor design and the detailed investigation of the fluidized bed methanation process characteristics through parameter variations. Furthermore, optimized process concepts are investigated through the methanation of flexible syngas compositions from the advanced dual fluidized bed technology.

The following results can be summarized:

(i) The synthesized catalyst performs well in terms of avoidance of mechanical attrition and chemical deactivation and, therefore, maintaining a proper fluidization behavior. No significant mechanical attrition and chemical deactivation of the catalyst was detected during 200 h under fluidized bed conditions and 100 h

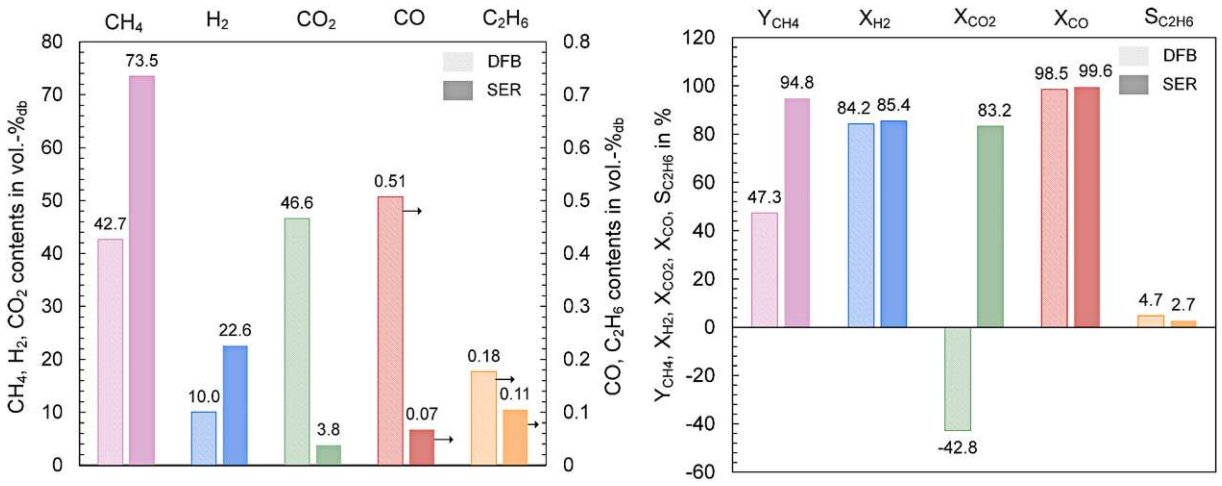

Fig. 10. Comparison of the raw-SNG composition (left) and the key figures (right) of the DFB (hatched) and the SER (filled) syngas methanation experiments at 360 °C and a WHSV of 1 Nl/g h.

under methanation conditions. Simultaneously, the catalyst showed a sufficient catalytic activity and selectivity towards the methanation reactions. The results were achieved by utilizing a highly porous and inert α-Al_2O_3 as support.

(ii) The reactor design, in combination with the dilution of the catalyst with support material, allowed an isothermal operation of the process with temperature gradients as low as 2 °C. Between 280 °C and 420 °C, a clear transition between thermodynamic and kinetic limitations could be observed. The optimal tradeoff between these limitations was found to be in a temperature range between 320 and 360 °C.

(iii) A maximum of 43 vol.-%$_{db}$ CH_4 was reached through the methanation of a typical syngas composition from the advanced 100 kW DFB gasification pilot plant. Because of the under-stoichiometric composition of the syngas from the DFB process, CO_2 was produced through the water-gas shift reaction and constituted the main component in the raw-SNG.

(iv) Under all conditions, a full conversion of ethylene to ethane and other components was shown. At low temperatures, kinetic limitations favored the production of ethane while higher temperatures allowed a complete conversion to other components. Neither the ethylene concentration in the syngas nor the syngas composition (DFB or SER) showed a significant influence on the selectivity of ethylene towards ethane.

(v) The SER syngas methanation was shown to yield a much more favorable composition for grid feeding and higher methane yields, while simultaneously improving the H_2, CO and CO_2 conversions, compared to DFB syngas methanation. A maximum CH_4 content of 73 vol.-%$_{db}$ could be reached, which represents an increase of 30 vol.-%$_{db}$ compared to DFB syngas methanation.

(vi) An almost complete conversion of CO and CO_2 was achieved through the methanation of an overstoichiometric SER syngas (SN $\geq$ 1.2), allowing grid feeding without the need for an expensive CO_2 separation unit. Hydrogen separation and recirculation is, however, necessary under the investigated reaction conditions.

4. Conclusion and outlook

In this work, the catalytic methanation of syngas from the advanced DFB technology was experimentally investigated, combining a bubbling fluidized bed methanation reactor with an optimized methanation catalyst for fluidized bed applications. Fluidized bed reactors can be advantageously applied to SNG production because of the high heat and mass transfer capabilities. This leads to several advantages compared to the commercially utilized fixed bed methanation reactors, provided that the catalyst shows a proper fluidization behavior.

To this end, the following conclusions and recommendations can be drawn from the conducted experiments:

(i) α-Al_2O_3 was shown to be a viable catalyst support for methanation reactions. Especially in fluidized bed applications, it could be advantageously used as an alternative to the commonly utilized γ-Al_2O_3 because of the high mechanical and chemical stability and a proper fluidization behavior of the prepared catalyst.

(ii) The stress on the catalyst was minimized due to nearly isothermal operating conditions. This is a result of the special reactor design and the dilution of the catalyst with inert support material.

Additionally, the fluidized bed methanation reactor and the synthesized catalyst were applied to the methanation of syngas from advanced DFB gasification and the SER process. The SER process allows the production of syngas with a suitable stoichiometric ratio of H_2 to CO and CO_2, yielding the following conclusions for fluidized bed methanation:

(iii) The SER process in combination with fluidized bed methanation could lead to an improved and more cost-effective route for SNG production. No separation of excessive CO_2 or CO from the raw-SNG is required for grid-feeding when selecting a suitable syngas composition. Compared to conventional DFB steam gasification, the methane yield is doubled (up to 95%) and the H_2, CO and CO_2 conversions are improved. Especially if no external hydrogen is available, the direct methanation of SER syngas could lead to a simpler and more efficient process route for SNG production.

For a full comparison of the DFB and SER syngas methanation, further investigations on the optimal process conditions and the performance of the whole process chain are necessary. Additionally, the long-term mechanical and chemical stability of the catalyst should be examined.

CRediT authorship contribution statement

Alexander Bartik: Conceptualization, Methodology, Investigation, Writing – review & editing, Visualization. **Josef Fuchs:** Methodology, Validation, Writing – review & editing. **Gernot Pacholik:** Investigation, Writing – review & editing. **Karin Föttinger:** Validation, Writing – review & editing, Supervision. **Hermann Hofbauer:** Conceptualization, Writing – review & editing, Supervision, Project administration,

Funding acquisition. **Stefan Müller:** Validation, Writing – review & editing, Supervision, Funding acquisition. **Florian Benedikt:** Conceptualization, Methodology, Writing – review & editing, Supervision, Project administration, Funding acquisition.

Declaration of Competing Interest

The authors declare that they have no known competing financial interests or personal relationships that could have appeared to influence the work reported in this paper.

Acknowledgment

This study was carried out within the doctoral college CO_2Refinery at TU Wien. It is also part of the research project ReGas4Industry (871732) and receives financial support from the research program "Energieforschung" funded by the Austrian Climate and Energy Fund. Furthermore, the authors would like to thank Jonas Hauser for the technical assistance, Wolfgang Ipsmiller for the assistance and rental of the particle size analyzer, Johannes Schmid for the support during the conceptualization of the reactor and SASOL for the supply of the catalyst support. The authors acknowledge TU Wien Bibliothek for financial support through its Open Access Funding Programme.

Appendix A. Supplementary data

Supplementary data to this article can be found online at https://doi.org/10.1016/j.fuproc.2022.107402.

References

[1] Eurostat, Energy balance flow for European Union (27 countries) 2020 [Online]. Available, https://ec.europa.eu/eurostat/cache/sankey/energy/sankey.html, 2022. accessed: Apr. 19.
[2] S. Lechtenböhmer, L.J. Nilsson, M. Åhman, C. Schneider, Decarbonising the energy intensive basic materials industry through electrification – Implications for future EU electricity demand, Energy 115 (2016) 1623–1631, https://doi.org/10.1016/j.energy.2016.07.110.
[3] European Commission, Directive (EU) 2018/2001 of the European Parliament and of the Council of 11 December 2018 on the promotion of the use of energy from renewable sources, Off. J. the Eur. Union L 328/82, December (2018) 128 [Online]. Available: https://eur-lex.europa.eu/legal-content/EN/TXT/PDF/?uri=CELEX:32018L2001&from=EN. (Accessed 20 April 2022).
[4] J. Kopyscinski, T.J. Schildhauer, S.M. Biollaz, Production of synthetic natural gas (SNG) from coal and dry biomass - a technology review from 1950 to 2009, Fuel 89 (8) (2010) 1763–1783, https://doi.org/10.1016/j.fuel.2010.01.027.
[5] S. Rönsch, J. Schneider, S. Matthischke, M. Schlüter, M. Götz, J. Lefebvre, P. Prabhakaran, S. Bajohr, Review on methanation – from fundamentals to current projects, Fuel 166 (2016) 276–296, https://doi.org/10.1016/j.fuel.2015.10.111.
[6] B. Lecker, L. Illi, A. Lemmer, H. Oechsner, Biological hydrogen methanation - a review, Bioresour. Technol. 245 (Pt A) (2017) 1220–1228, https://doi.org/10.1016/j.biortech.2017.08.176.
[7] M. Sposob, R. Wahid, K. Fischer, Ex-situ biological CO_2 methanation using trickle bed reactor: review and recent advances, Rev. Environ. Sci. Biotechnol. (2021), https://doi.org/10.1007/s11157-021-09589-7.
[8] J.C. Schmid, F. Benedikt, J. Fuchs, A.M. Mauerhofer, S. Müller, H. Hofbauer, Syngas for biorefineries from thermochemical gasification of lignocellulosic fuels and residues - 5 years' experience with an advanced dual fluidized bed gasifier design, Biomass Conv. Biorefine. (2019), https://doi.org/10.1007/s13399-019-00486-2.
[9] F. Benedikt, Fuel Flexible Advanced Dual Fluidized Bed Steam Gasification, Dissertation, Institute of Chemical, Environmental, and Bioscience Engineering, TU Wien, Vienna, 2020, https://doi.org/10.34726/hss.2020.39988.
[10] A.M. Mauerhofer, J.C. Schmid, F. Benedikt, J. Fuchs, S. Müller, H. Hofbauer, Dual fluidized bed steam gasification: Change of product gas quality along the reactor height, Energy 173 (2019) 1256–1272, https://doi.org/10.1016/j.energy.2019.02.025.
[11] J. Fuchs, J.C. Schmid, S. Müller, A.M. Mauerhofer, F. Benedikt, H. Hofbauer, The impact of gasification temperature on the process characteristics of sorption-enhanced reforming of biomass, Biomass Conv. Biorefine. (2019), https://doi.org/10.1007/s13399-019-00439-9.
[12] J. Fuchs, J.C. Schmid, F. Benedikt, S. Müller, H. Hofbauer, H. Stocker, N. Kieberger, T. Bürgler, The impact of bed material cycle rate on in-situ CO_2 removal for sorption enhanced reforming of different fuel types, Energy 162 (2018) 35–44, https://doi.org/10.1016/j.energy.2018.07.199.
[13] A. Bartik, F. Benedikt, A. Lunzer, C. Walcher, S. Müller, H. Hofbauer, Thermodynamic investigation of SNG production based on dual fluidized bed gasification of biogenic residues, Biomass Conv. Bioref. 11 (2020) 95–110, https://doi.org/10.1007/s13399-020-00910-y.
[14] J. Brellochs, Experimentelle Untersuchung und Prozess-Simulation der AER-Biomassevergasung zur Erzeugung eines regenerativen Erdgassubstitutes, Dissertation, Universität Stuttgart, 1st ed., Cuvillier, Göttingen, 2014. ISBN: 9783954048830, https://cuvillier.de/de/shop/publications/6859.
[15] I. Martínez, M.C. Romano, Flexible sorption enhanced gasification (SEG) of biomass for the production of synthetic natural gas (SNG) and liquid biofuels: Process assessment of stand-alone and power-to-gas plant schemes for SNG production, Energy 113 (2016) 615–630, https://doi.org/10.1016/j.energy.2016.07.026.
[16] J. Fuchs, J.C. Schmid, S. Müller, H. Hofbauer, Dual fluidized bed gasification of biomass with selective carbon dioxide removal and limestone as bed material: a review, Renew. Sust. Energ. Rev. 107 (2018) (2019) 212–231, https://doi.org/10.1016/j.rser.2019.03.013.
[17] J.C. Schmid, Development of a novel dual fluidized bed gasification system for increased fuel flexibility, Dissertation, Institute of Chemical, Environmental, and Bioscience Engineering, TU Wien, Vienna, 2014, https://doi.org/10.34726/hss.2014.25397.
[18] S. Hafner, M. Schmid, G. Scheffknecht, Parametric study on the adjustability of the syngas composition by sorption-enhanced gasification in a dual-fluidized bed pilot plant, Energies 14 (2) (2021) 399, https://doi.org/10.3390/en14020399.
[19] J. Fuchs, Process characteristics of sorption enhanced reforming in an advanced gasification system, Dissertation, Institute of Chemical, Environmental, and Bioscience Engineering, TU Wien, Vienna, 2020, https://doi.org/10.34726/hss.2021.39987.
[20] J. Karl, T. Pröll, Steam gasification of biomass in dual fluidized bed gasifiers: a review, Renew. Sust. Energ. Rev. 98 (2018) 64–78, https://doi.org/10.1016/j.rser.2018.09.010.
[21] S. Müller, J. Fuchs, J.C. Schmid, F. Benedikt, H. Hofbauer, Experimental development of sorption enhanced reforming by the use of an advanced gasification test plant, Int. J. Hydrog. Energy 42 (50) (2017) 29694–29707, https://doi.org/10.1016/j.ijhydene.2017.10.119.
[22] C.H. Bartholomew, Mechanisms of catalyst deactivation, Appl. Catal. A Gen. 212 (1–2) (2001) 17–60, https://doi.org/10.1016/S0926-860X(00)00843-7.
[23] A. Kambolis, T.J. Schildhauer, O. Kröcher, CO methanation for synthetic natural gas, Production 69 (10) (2015) 608–613, https://doi.org/10.2533/chimia.2015.608.
[24] J. Kopyscinski, M.C. Seemann, R. Moergeli, S. Biollaz, T.J. Schildhauer, Synthetic natural gas from wood: reactions of ethylene in fluidised bed methanation, Appl. Catal. A Gen. 462-463 (2013) 150–156, https://doi.org/10.1016/j.apcata.2013.04.038.
[25] T.J. Schildhauer, S.M. Biollaz, Synthetic Natural Gas from Coal, Dry Biomass, and Power-to-Gas Applications, John Wiley & Sons, Hoboken, 2016, https://doi.org/10.1002/9781119191339.
[26] D. Kunii, O. Levenspiel, Fluidization Engineering, 2nd ed., Butterworth-Heinemann, Boston, 1991. ISBN: 0-409-90233-0.
[27] J. Kopyscinski, T.J. Schildhauer, S.M. Biollaz, Employing Catalyst Fluidization to Enable Carbon Management in the Synthetic Natural Gas Production from Biomass no. 3, 2009, pp. 343–347, https://doi.org/10.1002/ceat.200800413.
[28] J. Kopyscinski, T.J. Schildhauer, S.M.A. Biollaz, Methanation in a fluidized bed reactor with high initial CO partial pressure: part I — experimental investigation of hydrodynamics mass transfer effects and carbon deposition, Chem. Eng. Sci. 66 (5) (2011) 924–934, https://doi.org/10.1016/j.ces.2010.11.042.
[29] M.C. Seemann, T.J. Schildhauer, S.M.A. Biollaz, Fluidized bed methanation of wood-derived producer gas for the production of synthetic natural gas, Ind. Eng. Chem. Res. 49 (15) (2010) 7034–7038, https://doi.org/10.1021/ie100510m.
[30] J. Witte, A. Calbry-Muzyka, T. Wieseler, P. Hottinger, S.M. Biollaz, T. J. Schildhauer, Demonstrating direct methanation of real biogas in a fluidised bed reactor, Appl. Energy 240 (September 2018) (2019) 359–371, https://doi.org/10.1016/j.apenergy.2019.01.230.
[31] M. Hervy, J. Maistrello, L. Brito, M. Rizand, E. Basset, Y. Kara, M. Maheut, Power-to-gas: CO_2 methanation in a catalytic fluidized bed reactor at demonstration scale, experimental results and simulation, J. CO_2 Util. 50 (2021), 101610, https://doi.org/10.1016/j.jcou.2021.101610.
[32] J. Ren, Y.-L. Liu, X.-Y. Zhao, J.-P. Cao, Methanation of syngas from biomass gasification: an overview, Int. J. Hydrog. Energy 45 (7) (2020) 4223–4243, https://doi.org/10.1016/j.ijhydene.2019.12.023.
[33] J. Gao, Q. Liu, F. Gu, B. Liu, Z. Zhong, F. Su, Recent advances in methanation catalysts for the production of synthetic natural gas, RSC Adv. 5 (29) (2015) 22759–22776, https://doi.org/10.1039/C4RA16114A.
[34] D. Cui, J. Liu, J. Yu, F. Su, G. Xu, Attrition-resistant Ni-Mg/Al_2O_3 catalyst for fluidized bed syngas methanation, Catal. Sci. Technol. 5 (6) (2015) 3119–3129, https://doi.org/10.1039/c5cy00066a.
[35] J. Li, L. Zhou, P. Li, Q. Zhu, J. Gao, F. Gu, F. Su, Enhanced fluidized bed methanation over a Ni/Al_2O_3 catalyst for production of synthetic natural gas, Chem. Eng. J. 219 (2013) 183–189, https://doi.org/10.1016/j.cej.2013.01.005.
[36] B. Liu, S. Ji, Comparative study of fluidized-bed and fixed-bed reactor for syngas methanation over Ni-W/TiO_2-SiO_2 catalyst, J. Energy Chem. 22 (5) (2013) 740–746, https://doi.org/10.1016/S2095-4956(13)60098-4.
[37] A. Bartik, J. Fuchs, S. Müller, H. Hofbauer, Development of an internally circulating fluidized bed for catalytic methanation of syngas, in: C. Jordan (Ed.), Proceedings of the 16th Minisymposium Verfahrenstechnik and 7th Partikelforum, TU Wien, Sept. 21/22, 2020, https://doi.org/10.34726/566.
[38] D. Hu, J. Gao, Y. Ping, L. Jia, P. Gunawan, Z. Zhong, G. Xu, F. Gu, F. Su, Enhanced investigation of CO methanation over Ni/Al_2O_3 catalysts for synthetic natural gas

production, Ind. Eng. Chem. Res. 51 (13) (2012) 4875–4886, https://doi.org/10.1021/ie300049f.
[39] Sasol Performance Chemicals, PURALOX/CATALOX High-Purity Calcined Aluminas [Online]. Available, https://www.sasolgermany.de/fileadmin/doc/alumina/Neu_2017/0372.SAS-BR-Inorganics_Puralox_Catalox_WEB.pdf, 2022. accessed: Apr. 20.
[40] F. Benedikt, M. Kuba, J. Christian, S. Müller, H. Hofbauer, Assessment of correlations between tar and product gas composition in dual fluidized bed steam gasification for online tar prediction, Appl. Energy 238 (December 2018) (2020) 1138–1149, https://doi.org/10.1016/j.apenergy.2019.01.181.
[41] D. Geldart, Types of gas fluidization, Powder Technol. 7 (5) (1973) 285–292, https://doi.org/10.1016/0032-5910(73)80037-3.
[42] Y. Liu, J. Gao, Q. Liu, F. Gu, X. Lu, L. Jia, G. Xu, Z. Zhong, F. Su, Preparation of high-surface-area Ni/α-Al_2O_3 catalysts for improved CO methanation, RSC Adv. 5 (10) (2015) 7539–7546, https://doi.org/10.1039/c4ra13634a.
[43] J. Gao, C. Jia, J. Li, M. Zhang, F. Gu, G. Xu, Z. Zhong, F. Su, Ni/Al_2O_3 catalysts for CO methanation: effect of Al_2O_3 supports calcined at different temperatures, J. Energy Chem. 22 (6) (2013) 919–927, https://doi.org/10.1016/S2095-4956(14)60273-4.
[44] J. Gao, C. Jia, M. Zhang, F. Gu, G. Xu, F. Su, Effect of nickel nanoparticle size in Ni/α-Al_2O_3 on CO methanation reaction for the production of synthetic natural gas, Catal. Sci. Technol. 3 (8) (2013) 2009, https://doi.org/10.1039/c3cy00139c.
[45] M. SanchezSanchez, R. Navarro, J. Fierro, Ethanol steam reforming over Ni/M_xO_y-Al_2O_3 (M=Ce, La, Zr and Mg) catalysts: Influence of support on the hydrogen production, Int. J. Hydrog. Energy 32 (10–11) (2007) 1462–1471, https://doi.org/10.1016/j.ijhydene.2006.10.025.
[46] A. Wolfbeisser, O. Sophiphun, J. Bernardi, J. Wittayakun, K. Föttinger, G. Rupprechter, Methane dry reforming over ceria-zirconia supported Ni catalysts, Catal. Today 277 (2016) 234–245, https://doi.org/10.1016/j.cattod.2016.04.025.
[47] J. Kopyscinski, T.J. Schildhauer, F. Vogel, S.M.A. Biollaz, A. Wokaun, Applying spatially resolved concentration and temperature measurements in a catalytic plate reactor for the kinetic study of CO methanation, J. Catal. 271 (2) (2010) 262–279, https://doi.org/10.1016/j.jcat.2010.02.008.
[48] M.C. Seemann, T.J. Schildhauer, S.M. Biollaz, S. Stucki, A. Wokaun, The regenerative effect of catalyst fluidization under methanation conditions, Appl. Catal. A Gen. 313 (1–2) (2006) 14–21, https://doi.org/10.1016/j.apcata.2006.06.048.
[49] I. Czekaj, F. Loviat, F. Raimondi, J. Wambach, S. Biollaz, A. Wokaun, Characterization of surface processes at the Ni-based catalyst during the methanation of biomass-derived synthesis gas: X-ray photoelectron spectroscopy (XPS), Appl. Catal. A Gen. 329 (2007) 68–78, https://doi.org/10.1016/j.apcata.2007.06.027.
[50] Österreichische Vereinigung für das Gas-und Wasserfach, Richtlinie G B210 - Gasbeschaffenheit, 2021. https://portal.ovgw.at/pls/f?p=101:203::::RP,203:P203_ID,P203_FROM_PAGE_ID:1075524,202.
[51] J. Witte, A. Kunz, S.M. Biollaz, T.J. Schildhauer, Direct catalytic methanation of biogas – part II: techno-economic process assessment and feasibility reflections, Energy Convers. Manag. 178 (September) (2018) 26–43, https://doi.org/10.1016/j.enconman.2018.09.079.

Fuel Processing Technology 252 (2023) 107969

Contents lists available at ScienceDirect

Fuel Processing Technology

journal homepage: www.elsevier.com/locate/fuproc

Corrigendum to "Experimental investigation on the methanation of hydrogen-rich syngas in a bubbling fluidized bed reactor utilizing an optimized catalyst" [Fuel Processing Technology, Volume 237 (2022), 107402]

Alexander Bartik [a,*], Josef Fuchs [a], Gernot Pacholik [b], Karin Föttinger [b], Hermann Hofbauer [a], Stefan Müller [a], Florian Benedikt [a]

[a] Institute of Chemical, Environmental and Bioscience Engineering, TU Wien, Getreidemarkt 9/166, 1060 Vienna, Austria
[b] Institute of Materials Chemistry, TU Wien, Getreidemarkt 9, 1060 Vienna, Austria

The authors regret that a declaration error occurred in the above-mentioned article. The catalyst support material was wrongly declared as α-Al_2O_3. Instead, the Puralox SCCa-150/200 Al_2O_3 support material from SASOL shows a γ/δ crystal phase structure.

The authors would like to apologise for any inconvenience caused.

DOI of original article: https://doi.org/10.1016/j.fuproc.2022.107402.
* Corresponding author.
E-mail address: alexander.bartik@tuwien.ac.at (A. Bartik).

https://doi.org/10.1016/j.fuproc.2023.107969

Available online 23 September 2023

C.4 Paper IV

Experimental investigation of hydrogen-intensified synthetic natural gas production via biomass gasification: a technical comparison of different production pathways

Bartik, A., Benedikt, F., Fuchs, J., Hofbauer, H., Müller, S., *Biomass Conversion and Biorefinery*, **2023**, article in press, https://doi.org/10.1007/s13399-023-04341-3.

Biomass Conversion and Biorefinery
https://doi.org/10.1007/s13399-023-04341-3

ORIGINAL ARTICLE

Experimental investigation of hydrogen-intensified synthetic natural gas production via biomass gasification: a technical comparison of different production pathways

Alexander Bartik[1] · Florian Benedikt[1] · Josef Fuchs[1] · Hermann Hofbauer[1] · Stefan Müller[1]

Received: 10 March 2023 / Revised: 5 May 2023 / Accepted: 11 May 2023

Abstract

A sustainable and secure energy supply requires alternative concepts for energy generation. Utilizing biomass to produce synthetic natural gas (SNG) allows the synthesis of a currently widely used energy carrier on a renewable basis. The additional integration of hydrogen increases the carbon utilization of the biomass. This study experimentally investigates and compares the production of raw-SNG in three novel process chain configurations combining the advanced dual fluidized bed (DFB) gasification technology, gas cleaning units, and a fluidized bed methanation reactor. The three process chains comprise the direct methanation of DFB product gas, a hybrid route with hydrogen addition to the DFB product gas, and the methanation of a hydrogen-enriched product gas generated through DFB gasification with in situ CO_2 removal (SER process). The direct methanation of the DFB product gas yielded a raw-SNG CH_4 content of 40 vol.-%$_{db}$ at 360 °C and atmospheric pressure conditions. Through the integration of external hydrogen in a hybrid process, the carbon utilization of the biomass could be increased from 37% to around 70% at an unchanged cold gas efficiency of 58–59%. Via the SER process, a high raw-SNG CH_4 content of 70 vol.-%$_{db}$ was achieved at an increased cold gas efficiency of 66% without the need for external hydrogen. Finally, a comparison points out the main advantages of the process configurations and provides a decision basis for novel SNG production pathways.

Keywords Sustainable and renewable synthetic natural gas · Advanced dual fluidized bed steam gasification · Sorption enhanced reforming · Fluidized bed methanation · Hydrogen integration · Experimental investigation in pilot scale

Nomenclature

CR	Combustion reactor
DFB	Dual fluidized bed
FICFB	Fast internally circulating fluidized bed
GCMS	Gas chromatography linked with a mass spectrometer
GR	Gasification reactor
feed	In the feed gas to the methanation reactor
KPI	Key performance indicator
out	In the outlet of the methanation reactor
raw-SNG	Raw synthetic natural gas after methanation/before upgrading
RME	Rapeseed methyl ester
SNG	Synthetic natural gas
SER	Sorption enhanced reforming
WHSV	Weight hourly space velocity in Nl/(g_{cat} h)
$\dot{n}_i$	Molar flow of species i in mol/s
N_i	Number of carbon atoms in species i
$\dot{m}_{C,CH_4,RawSNG}$	Amount of carbon in CH_4 in the raw-SNG in kg/h
$\dot{m}_{C,GR,fuel}$	Amount of carbon in the fuel to the GR in kg/h
$\dot{m}_{GR,fuel,daf}$	Amount of dry and ash-free fuel to the GR in kg/h
$\dot{m}_{H_2O,GR,fuel}$	Amount of water to the GR through the fuel in kg/h
$\dot{m}_{steam,GR}$	Amount of steam to the GR through the gasification agent in kg/h
$P_{CR,fuel}$	Chemical energy of the fuel to the CR in kW
$P_{GR,fuel}$	Chemical energy of the fuel to the GR in kW

✉ Alexander Bartik
alexander.bartik@tuwien.ac.at

[1] Institute of Chemical, Environmental and Bioscience Engineering, TU Wien, Getreidemarkt 9/166, 1060 Vienna, Austria

Published online: 26 May 2023

P_{H_2}	Chemical energy of the external hydrogen in kW
P_{PG}	Chemical energy of the product gas in kW
P_{RawSNG}	Chemical energy of the raw-SNG in kW
$\dot{Q}_{loss,DFB}$	Heat losses of the DFB system in kW
SN	Stoichiometric number of the feed gas
U	Superficial gas velocity
U_{mf}	Minimum fluidization velocity
X_{CO}	Carbon monoxide conversion in %
X_{CO_2}	Carbon dioxide conversion in %
X_{H_2}	Hydrogen conversion in %
Y_{CH_4}	Methane yield in %
y_i	Molar fraction of species i
φ_{SF}	Steam-to-fuel ratio
$\eta_{CG,o,DFB}$	Overall cold gas efficiency of the DFB system in %
$\eta_{CG,o}$	Overall cold gas efficiency of the full process chain in %
η_C	Carbon utilization efficiency in %

1 Introduction

The replacement of fossil fuels by renewable energy carriers and the respective production pathways are crucial in mitigating climate change and securing the independence of energy imports within the European Union. Synthetic natural gas (SNG) from renewable resources, as well as biogas from fermentation, has the potential to contribute to these goals, especially considering the limited time frame to accomplish the transformation [1].

Over the last two decades, biological and catalytic SNG production technologies from renewable resources have been developed. The two main strategies for the catalytic production of SNG are as follows: (i) the utilization of biogenic feedstock via a thermochemical pathway and (ii) the utilization of renewable electricity via an electrochemical pathway together with biogenic carbon dioxide [2, 3]. Both routes have been demonstrated on a large scale, e.g., the 32 MW_{th} GoBiGas SNG plant in Gothenburg, Sweden [4] or the 6 MW_{el} Power-to-Gas plant in Werlte, Germany [5]. The latter produces SNG through the hydrogenation of biogenic carbon dioxide in a molten salt-cooled tube bundle reactor. An alkaline electrolysis provides the necessary hydrogen, and the carbon dioxide is separated through amine scrubbing from a nearby biogas plant. The GoBiGas plant, on the other hand, produces SNG through dual fluidized bed (DFB) gasification of woody biomass and consecutive gas cleaning and catalytic conversion to methane in a fixed bed reactor cascade. A generic flow sheet of such a process chain is depicted in Fig. 1a. In the DFB gasification system, the biogenic feedstock is converted to a product gas, typically

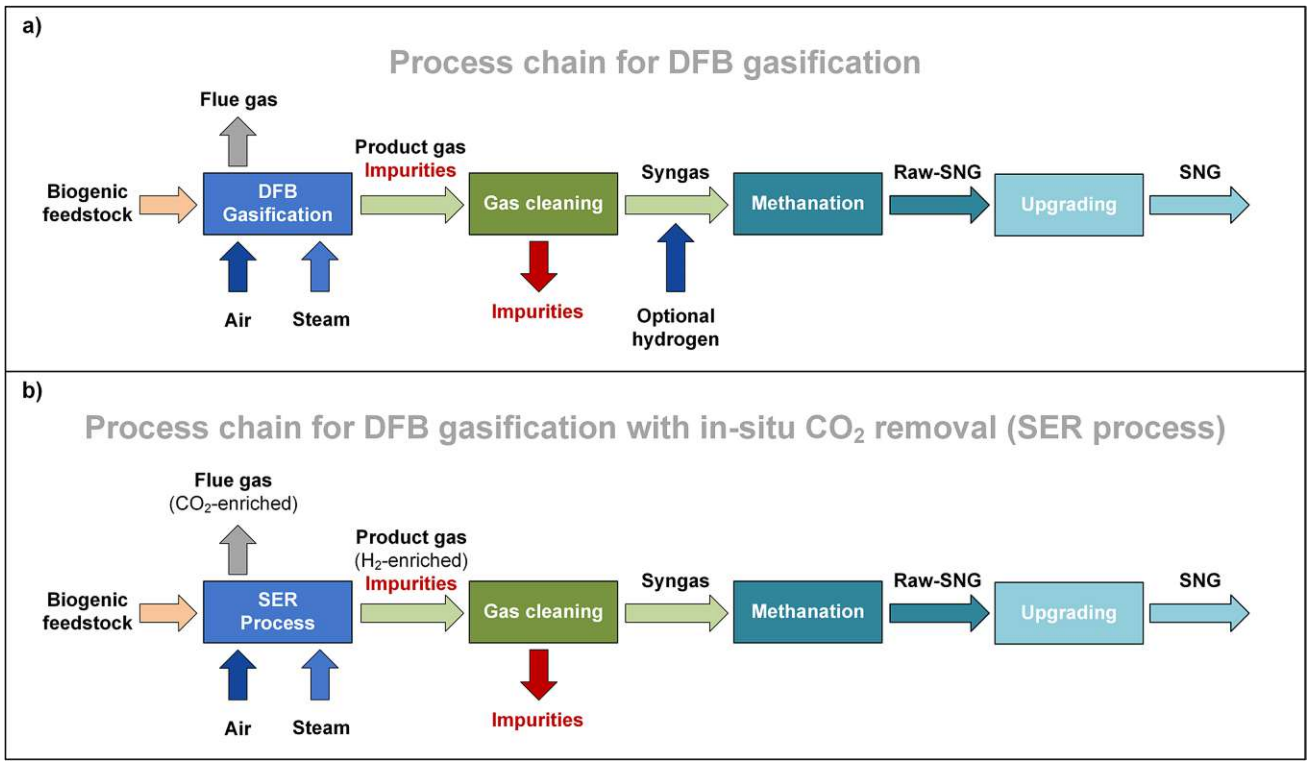

Fig. 1 Basic process layouts of two SNG production processes based on DFB gasification: **a** DFB gasification with optional hydrogen addition to the syngas, **b** DFB gasification with in-situ CO_2 removal (SER process)

utilizing steam as a gasification agent. Depending on the type and quality of the feedstock, a certain amount of impurities must be removed from the product gas to protect the methanation catalyst from poisoning and deactivation and achieve the necessary gas quality for the respective application. The cleaned product gas or syngas is then catalytically converted to raw-SNG in the methanation section. Depending on the applied concept, an upgrading of the raw-SNG is necessary to fulfill the national feed-in regulations of the natural gas grid. The upgrading might comprise gas drying, carbon dioxide, and hydrogen separation [6].

The necessity for carbon dioxide, or carbon separation in general, arises from the typical composition of woody biomass. On average, the elemental composition can be written as $CH_{1.44}O_{0.66}$ [7]. For the hydrogenation of the main carbon-containing species in the syngas, namely carbon monoxide and carbon dioxide, a molar ratio of three and four, respectively, is required. Due to this discrepancy, only limited utilization of biogenic carbon can be achieved. For example, the GoBiGas plant reports a carbon utilization factor of around 30% [8]. An interesting way to increase carbon utilization is the combination of the thermochemical conversion technology with power-to-gas by adding hydrogen before the methanation reactor (optional hydrogen), as indicated in Fig. 1a. This hybrid approach improves the production of SNG from a technical and ecological point of view. However, the integration of hydrogen production is generally a cost driver that influences the process' competitiveness [9, 10]. Moreover, hydrogen must not originate from fossil resources for an ecologically viable concept. Therefore, various renewable hydrogen production methods are currently under investigation. The most widely discussed and matured technology is water electrolysis [11]. However, there is a multitude of other technologies utilizing thermal, electrical, photonic, or biochemical energy to convert water or biomass to hydrogen [12]. Some examples are electrical or thermochemical water splitting [13, 14], biomass gasification [15], and dark or photo-fermentation of biogenic materials [16].

To avoid any additional hydrogen production, a modified DFB gasification process can be applied: The so-called sorption enhanced reforming (SER) process [17] allows for the in situ adaptation of the product gas composition towards high hydrogen contents via in situ CO_2 removal in the DFB gasification system (Fig. 1b). This way, the product gas composition can be matched to the requirements of the methanation section. Bartik et al. [18] and Brellochs [19] showed on a theoretical basis that potentially no CO_2 separation would be required for upgrading the raw-SNG to the gas grid requirements. Experimentally, the methanation of typical SER product gases was shown by Bartik et al. [20] in a fluidized bed reactor and by Gómez et al. [21] in two-fixed bed methanation reactors utilizing synthetically premixed gases. However, there seems to be no experimental investigation of the whole process chain, including gasification, gas cleaning, and methanation.

The hybrid route with optional hydrogen addition (Fig. 1a) was already proposed on a theoretical basis by Gassner and Maréchal [9] in 2008. Alamia et al. [22] simulated the integration of hydrogen to an optimized GoBiGas plant and calculated cold gas efficiencies between 70 and 73% for SNG production. Some experimental investigations were carried out by Salbrechter and Schubert [23]. They performed methanation experiments in fixed-bed reactors with varying hydrogen contents in the premixed syngas. They argue that a substoichiometric hydrogen addition leads to a good trade-off between electrolysis capacity and the overall efficiency, which they calculated at 60% for a large-scale plant. However, around 17 vol.-% of CO_2 is still in the raw-SNG and needs to be separated before grid injection. Multiple alternative concepts for the integration of hydrogen in the SNG production process have been proposed. For example, Menin et al. [24] modeled a combination of biomass steam gasification, alkaline water electrolysis, and biological methanation in a trickle-bed reactor and calculated a cold gas efficiency of 50.6%. Giglio et al. [25] conceptualized a catalytic methanation process in isothermal reactors in combination with solid oxide electrolysis and oxygen/steam-blown gasification and calculated cold gas efficiencies as high as 71.7%. From an experimental point of view, Leimert et al. [26] combined the heatpipe reformer gasification technology with a polytropic fixed bed methanation reactor and demonstrated the production of raw-SNG with additional hydrogen. However, due to limitations in the methanation reactor, the residual H_2 and CO_2 concentrations in the raw-SNG were quite high. Another demonstration of a hybrid process concept was shown by Witte et al. [27]. They directly upgraded biogas in a fluidized bed methanation reactor with external hydrogen over more than 1000 h with an average methane yield of 96%. Other researchers have modeled the hydrogen addition to syngas to produce other fuels and chemicals like dimethyl ether [28] and methanol [29]. Industrial process gases are also an interesting carbon source for a further hydrogenation to methane. For example, off-gases from steelworks can be utilized for methane synthesis with additional hydrogen [30]. In the case of direct iron ore reduction with hydrogen, the off-gas already consists of a considerable amount of hydrogen, which can be utilized as the reducing agent for a consecutive methanation reaction [31]. However, for the hybrid route investigated in this study, no experimental investigations connecting DFB gasification with fluidized bed methanation and hydrogen addition seem to be available.

In this study, we investigate several novel process chains for the production of raw-SNG from woody biomass on a pilot scale. At TU Wien, a 100 kW_{th} advanced DFB pilot plant converting woody biomass to product gas is coupled

with gas cleaning units and a 10 kW_{th} fluidized bed methanation reactor to produce raw-SNG. Figure 2 (left) depicts the basic principle of the DFB gasification process. In the gasification reactor (GR), the biogenic feedstock is converted to a product gas containing mainly H_2, CO, CO_2, and CH_4 with steam as a gasification agent. Due to the allothermal operation of the GR, a nearly nitrogen-free product gas is obtained. However, impurities, like tars and nitrogen- and sulfur-containing species, might need to be removed in the gas cleaning section, depending on the quality of the feedstock. The GR is coupled with a combustion reactor (CR) through a solid circulation loop. In the CR, ungasified char is combusted with air to heat up the bed material. Since the CR is operated as a fast fluidized bed, the hot bed material is transported back to the GR, where it sustains the endothermic gasification process. Via the usage of limestone as bed material and suitable temperature levels in the reactors, the in situ removal of CO_2 from the gasification reactor can be facilitated (Fig. 2 (right)). At comparably low temperatures of 600 to 700 °C in the GR, $CaCO_3$ is formed out of CaO and gaseous CO_2. The removal of gaseous CO_2 from the product gas stimulates the water–gas-shift reaction and leads to an increased hydrogen content (up to 70 vol.-$\%_{db}$). The captured CO_2 is transported to the CR as $CaCO_3$ together with the bed material and char. At elevated temperatures in the CR, the $CaCO_3$ is calcined. Thus, gaseous CO_2 is released again in the CR, and CaO is formed out of $CaCO_3$. Two main parameters which allow the targeted adjustment of the product gas composition are the gasification temperature and the bed material cycle rate [17]. More information on the DFB process and the overall process chain can be found in Sect. 2 and is also reported in literature [32–34].

The aim of this work is the demonstration of raw-SNG production through advanced DFB gasification, gas cleaning, and fluidized bed methanation. The novelty lies in the investigation of multiple novel process configurations on a pilot scale regarding gas compositions, conversions, yields, and efficiencies. Furthermore, extensive analytical measurements show the whereabouts and quantities of impurities over the entire SNG process chains. The investigations include three configurations, namely

(a) DFB gasification and direct methanation of the DFB product gas (DFB-Std)
(b) DFB gasification with external hydrogen addition to the product gas and methanation of the hydrogen-enriched product gas (DFB + H_2)
(c) DFB gasification with in-situ CO_2 removal (SER process) and direct methanation of the hydrogen-enriched product gas without external hydrogen addition (SER)

Finally, a comparison of the three configurations shows the advantages and disadvantages of the respective process chains and therefore helps determine a suitable process depending on the defined goals.

2 Materials and methods

2.1 Complete process chain

Figure 3 shows a basic flowsheet of the process chain for raw-SNG production at TU Wien. The main units are

- A 100 kW_{th} advanced DFB gasification reactor
- A biodiesel (rapeseed methyl ester (RME)) scrubber
- Activated carbon and zinc oxide (ZnO) adsorber beds
- And a 10 kW_{th} fluidized bed methanation reactor

The left part of the diagram depicts the fuel-feeding system. Three fuel hoppers are available to feed the feedstock via screws into the lower GR. The generated product

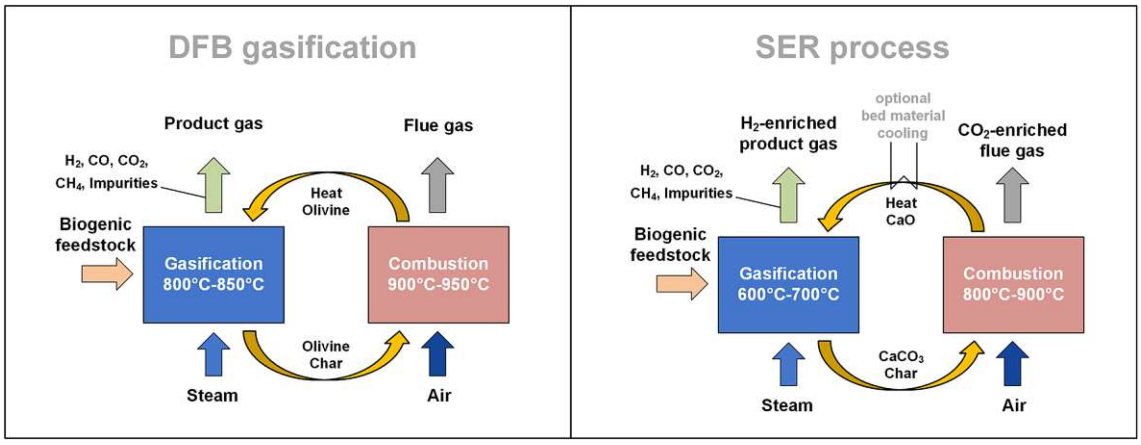

Fig. 2 Basic principle of DFB gasification (left) and DFB gasification with in situ CO_2 removal (SER process) (right)

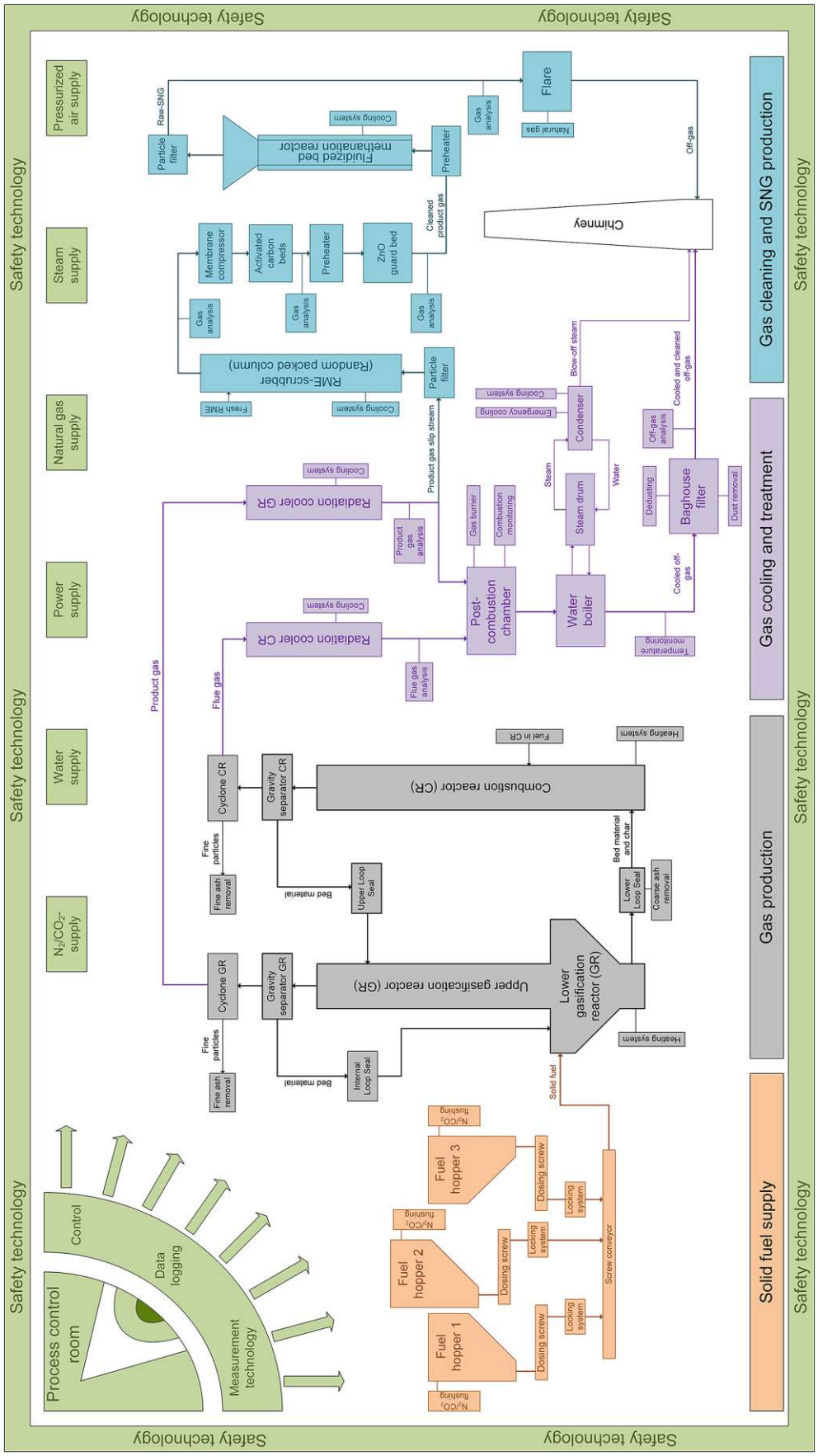

Fig. 3 Basic flow sheet of the SNG process chain at TU Wien

gas further reacts in the upper GR and leaves the DFB system after particle separation in a gravity separator and a cyclone. After passing through a radiation cooler, a partial flow of the product gas is directed toward the SNG process chain. The unutilized part of the product gas is burnt in a post-combustion chamber together with the flue gas from the CR. Before the off-gas is vented to the atmosphere, the gas is cooled in a boiler, and dust is separated in a baghouse filter.

The partial product gas flow directed to the SNG process chain is cleaned in a filter stuffed with glass wool and enters the RME scrubber. The following membrane compressor is used as a blower to set the required volume flow for the methanation reactor. Since the process chain is operated at almost atmospheric pressure, no significant pressure increase is desired. To further remove impurities from the product gas stream, the gas passes through two activated carbon beds and a ZnO bed at elevated temperatures. The preheated gas then enters the fluidized bed methanation reactor, where the syngas is converted to raw-SNG. A glass wool filter holds back potentially carried-out catalyst particles and a natural gas–operated flare is used to burn the raw-SNG downstream of the gas analysis measurements. Auxiliary systems, like process media supply, measurement technology, a process control system, and safety measures, accompany the main process chain. In Sects. 2.2–2.4, a more detailed description of the single process units follows.

2.2 100 kWth advanced dual fluidized bed pilot plant

The advanced DFB pilot plant at TU Wien is a further development of industrially realized DFB gasification plants. Figure 4 shows pictures of the pilot plant (left) and a schematic drawing of the reactor concept (right) [33]. Here, a more detailed drawing of the constructional design of the reactor is depicted, compared to the basic principle of the DFB system in Figs. 2 and 3. The same reactor is used for DFB gasification and the SER process. Feedstock enters the lower GR through a fuel-feeding screw above the top of the bed (on-bed feeding). In the lower GR, the pyrolytic decomposition and gasification of the solid feedstock take place. The CR is designed as a fast fluidized bed, where parts of the unconverted feedstock combust together with additional fuel (fuel to CR). Both reactors are connected via loop seals, enabling bed material circulation between the reactors. The novelty of the advanced concept mainly lies in the implementation of an upper gasification reactor and gravity separators. The upper GR is designed as a counter-current column with local constrictions, which increases the gas–solid contact time and the turbulence between the bed material and the upward-flowing product gas. Gravity separators ensure a gentle gas–solid separation and allow the utilization of soft bed materials like limestone. An internal loop seal allows the recirculation of particles within the upper and lower

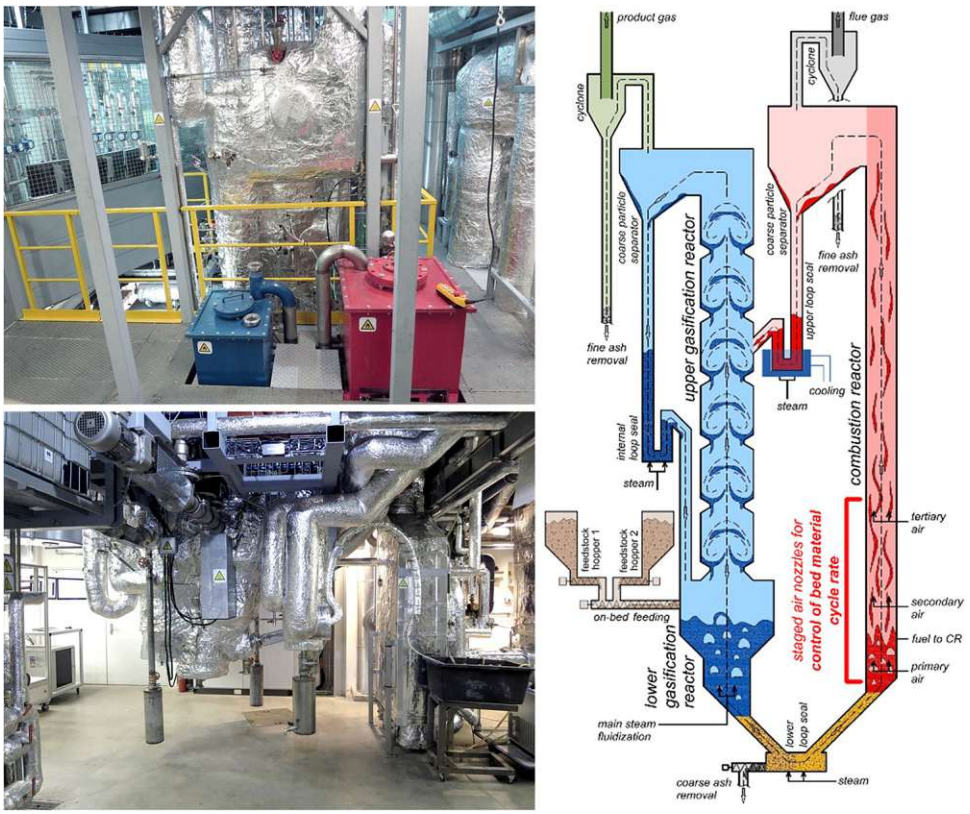

Fig. 4 Photos of the 100 kW_{th} advanced DFB pilot plant at TU Wien (left) and schematic drawing of the reactor design (right) [33]

GR. To reach a suitable temperature spread between CR and GR for the SER process, a loop seal cooling is installed additionally. Furthermore, the bed material cycle rate can be influenced by staged air nozzles in the CR. By leaving the total amount of air introduced into the CR constant, but shifting the partial amounts at a specific height, an efficient control of the bed material cycle rate is possible (primary air, secondary air, tertiary air). A detailed description of the design is documented by Schmid [33]. A detailed analysis of DFB gasification and SER is not within the scope of this paper since the mechanisms of these gasification processes are well documented in the literature [17, 32, 34].

Olivine is commonly used as bed material for DFB gasification. It is a magnesium-iron-silicate-based mineral that forms a calcium-rich layer on the surface of the particles through the interaction with the fuel ash and thus promotes its catalytic activity [35]. Therefore, limestone has been extensively investigated as an alternative, catalytically highly active bed material [36]. In this investigation, a 80/20 wt.-% olivine/limestone mixture is used as bed material for the DFB gasification and pure limestone for the SER process to enable the in-situ CO_2 removal. Softwood pellets with quality class A1 according to ISO 17225–2 are used as feedstock for the test runs. Table 1 shows the results of the ultimate and proximate analysis of the softwood pellets. The pellets show low water and ash contents as well as low amounts of sulfur and chlorine and high ash melting temperatures. These high-quality pellets were used in all test runs as a reference fuel for a fair comparison of the different process configurations. The compositions of the bed materials are listed in the supplementary material.

Table 1 Ultimate and proximate analyses of softwood pellets

Parameter	Softwood pellets
Water content (wt.-%)	7.2
Ash content (wt.-$\%_{db}$)	0.2
Carbon (wt.-$\%_{daf}$)	50.8
Hydrogen (wt.-$\%_{daf}$)	5.9
Nitrogen (wt.-$\%_{daf}$)	0.2
Sulfur (wt.-$\%_{daf}$)	0.005
Chlorine (wt.-$\%_{daf}$)	0.005
Oxygen[a] (wt.-$\%_{daf}$)	43.1
Volatile matter (wt.-$\%_{daf}$)	85.6
LHV (MJ/kg_{db})	18.9
Ash deformation temp. (°C)	1330
Ash flow temp. (°C)	1440

[a]Calculated by difference to 100 wt.-$\%_{daf}$

2.3 Gas cleaning

Ni catalysts are prone to deactivation through impurities in the product gas. Thus, it is crucial to implement a sufficient gas-cleaning strategy to protect the catalyst from poisoning and coke formation. To this end, a particle filter, an RME scrubber, activated carbon beds, and a ZnO guard bed are installed (Fig. 5). The particle filter is a simple glass wool stuffed cylinder that holds back dust particles resulting from bed material attrition, fuel ash, and unconverted biomass char. The RME scrubber is designed as a randomly packed column with a diameter of 0.1 m, a demister, and a connected phase separator. In the counter-current column, tar components are condensed and dissolved in the RME. Furthermore, steam condenses and water-soluble substances like NH_3 and HCl dissolve in the water phase. In the phase separator, a division occurs into a water phase, an emulsion phase, and an RME phase. The RME phase is recirculated to the scrubber, while the water and emulsion phases are withdrawn periodically. The scrubber is designed for an operating temperature between 10 and 50 °C. A cryostat provides the necessary cooling power. Fixed-bed adsorption in two activated carbon beds is performed to reduce tar components that have not been separated in the scrubber and to adsorb sulfur compounds. A Desorex K 43 and an Oxorbon K40 J from Donau Carbon are used for this purpose. A ZnO guard bed serves as protection against a breakthrough of sulfur compounds (especially H_2S) and is operated at temperatures between 300 and 350 °C.

Fig. 5 Photo of the RME scrubber (left) and the activated carbon beds (right)

2.4 Fluidized bed methanation setup

Figure 6 depicts a 3D-CAD drawing of the reactor (left) and a picture of the fluidized bed methanation setup (right) at TU Wien. The reactor is designed for an SNG output of 10 kW_{th} and utilizes 1.5 kg of a self-prepared 20 wt.-% NiO/Al_2O_3 catalyst with a mean particle size of 150 µm and 1.6 kg of unimpregnated Al_2O_3. Because of the catalyst dilution, the full capacity of the reactor is not used, and the SNG output is reduced to about 5 kW for the presented experiments. The reactor is separated into two individually fluidized reaction zones operated in the bubbling fluidized bed regime. The heat released by the exothermic methanation reactions is handled with an air-cooled coil and a jacket. Water vapor can be added to the preheated syngas streams to avoid carbon depositions on the catalyst. Alternatively, hydrogen from gas cylinders can be added to the syngas prior to the methanation reactor. The gas composition can be analyzed either downstream of the hydrogen addition or in the raw-SNG downstream of the methanation reactor. A programmable logic controller records all measured temperatures, pressures, and gas analysis measurements and controls the heating tapes and cartridges. Further information on the reactor concept and the catalyst is documented in [20].

2.5 Measurement equipment

The overall process chain is equipped with more than 130 temperature and 80 pressure measurement points. Additionally, 27 gas analysis channels allow the simultaneous logging of the product gas, flue gas, and raw-SNG compositions with Rosemount NGA-2000 modules. In the product gas and the raw-SNG, the H_2, CO, CO_2, CH_4, and O_2 concentrations are measured. A PerkinElmer ARNEL – Clarus 500 gas chromatograph additionally measures ethylene, ethane, propane, and nitrogen concentrations every 12 min. Additionally, CO_2, CO, and CH_4 concentrations are redundantly measured as well. Tar sampling is performed with adapted standardized equipment, following the tar protocol (DIN CEN/TS 15,439). Single tar components are measured by gas chromatography linked with a mass spectrometer (GCMS). NH_3 is detected through wet chemical analysis with similar sampling equipment and sulfuric acid as a solvent. A more detailed description of the tar and NH_3 measurement procedure at the 100 kW_{th} pilot plant is documented in [37]. Sample bags are used for the offline measurement of H_2S with a second PerkinElmer ARNEL – Clarus 500 gas chromatograph.

2.6 Process simulation and key performance indicators

The process simulation tool IPSEpro is used to validate the measurement values by calculation of mass and energy balances and key performance indicators (KPIs). To this end, the whole process chain is modeled and set up in IPSEpro. The measured temperatures, pressures, and gas compositions in the single process units are the basis for the simulation. Furthermore, measured mass flows of the biomass input, the gasification and fluidization agent, the combustion air, the product gas and flue gas amounts, and the syngas amount in the SNG chain are used. Due to this over-specified equation system, the results in this paper represent the balanced solution from process simulation and not the raw measurement values (except where explicitly stated). Therefore, single test runs are evaluated, and no repetitions are carried out.

An important operating parameter of the DFB gasification plant is the steam-to-fuel ratio (φ_{SF}) (Eq. 1). It is defined as the amount of steam and the amount of fuel water in relation to the amount of dry and ash-free fuel introduced to the GR.

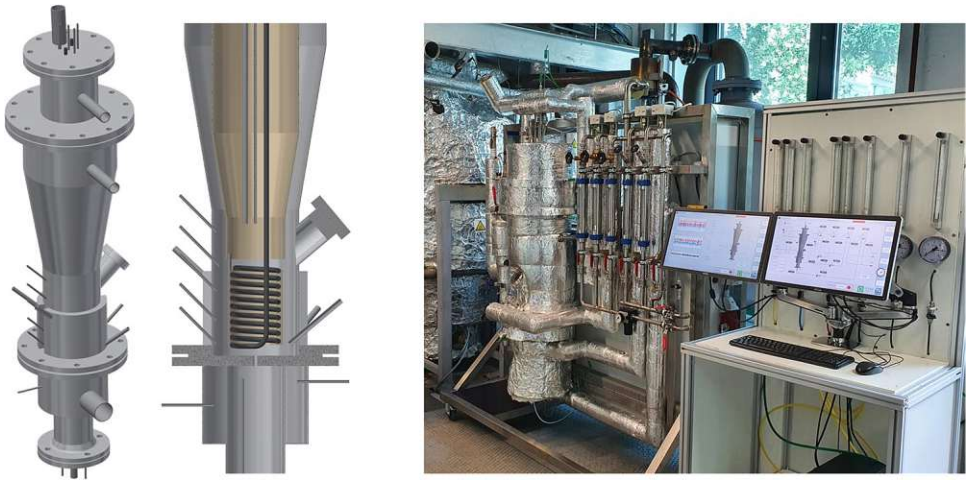

Fig. 6 3D-CAD drawing of the fluidized bed methanation reactor (left) and photo of the setup at TU Wien (right)

$$\varphi_{SF} = \frac{\dot{m}_{steam,GR} + \dot{m}_{H_2O,GR,fuel}}{\dot{m}_{GR,fuel,daf}} \quad (1)$$

Equation 2 shows the definition of the overall cold gas efficiency for the DFB system ($\eta_{CG,o,DFB}$). It relates the chemical energy of the product gas based on the lower heating value with the chemical energy of the fuel introduced to the GR as well as the additional fuel introduced to the CR. The relatively high heat losses of the pilot plant compared to industrial-sized gasification plants are subtracted in this equation.

$$\eta_{CG,o,DFB} = \frac{P_{PG}}{P_{GR,fuel} + P_{CR,fuel} - \dot{Q}_{loss,DFB}} * 100 \quad (2)$$

Important KPIs concerning the methanation section are displayed in Eqs. 3–7. The methane yield (Y_{CH_4}) is calculated according to Eq. 3, where $\dot{n}$ is the molar flow, and N is the number of carbon atoms in the respective gas component in the feed gas (*feed*) and the raw-SNG (*out*). Equations 4, 5, and 6 define the CO conversion (X_{CO}), the CO_2 conversion (X_{CO_2}), and the H_2 conversion (X_{H_2}), respectively.

$$Y_{CH_4} = \frac{\dot{n}_{CH_4,out}}{\sum_i N_i \dot{n}_{i,feed}} * 100 \quad (3)$$

$$X_{CO} = \frac{\dot{n}_{CO,feed} - \dot{n}_{CO,out}}{\dot{n}_{CO,feed}} * 100 \quad (4)$$

$$X_{CO_2} = \frac{\dot{n}_{CO_2,feed} - \dot{n}_{CO_2,out}}{\dot{n}_{CO_2,feed}} * 100 \quad (5)$$

$$X_{H_2} = \frac{\dot{n}_{H_2,feed} - \dot{n}_{H_2,out}}{\dot{n}_{H_2,feed}} * 100 \quad (6)$$

The stoichiometric number (SN) (Eq. 7) evaluates the product gas in terms of its stoichiometry for methanation. It relates the hydrogen content to the content of carbonaceous species to be methanated according to the corresponding reaction equations.

$$SN = \frac{y_{H_2}}{3y_{CO} + 4y_{CO_2} + 2y_{C_2H_4}} \quad (7)$$

The overall process chain is evaluated through the overall cold gas efficiency ($\eta_{CG,o}$) according to Eq. 8. It relates the chemical energy of the raw-SNG to the chemical energy of the fuel input to the GR and the CR minus heat losses (equal to Eq. 2) plus the chemical energy introduced through the external hydrogen addition.

$$\eta_{CG,o} = \frac{P_{RawSNG}}{P_{GR,fuel} + P_{CR,fuel} - \dot{Q}_{loss,DFB} + P_{H_2}} * 100 \quad (8)$$

Equation 9 shows the carbon utilization efficiency (η_C), which assesses the amount of carbon in the CH_4 of the raw-SNG compared to the amount of carbon introduced via the fuel in the GR.

$$\eta_C = \frac{\dot{m}_{C,CH_4,RawSNG}}{\dot{m}_{C,GR,fuel}} * 100 \quad (9)$$

3 Results and discussion

3.1 Operating parameters of the different process configurations

Table 2 summarizes the main operating conditions for the DFB gasification and SER process chains. Since the hydrogen addition (DFB + H_2) was carried out during the same steady-state gasification operating point as the direct methanation of the DFB product gas (DFB-Std), the operating conditions of the DFB gasification and gas cleaning parts are valid for both configurations (Sects. 3.2 and 3.3).

In general, all units are operated around atmospheric pressure. The mean temperature in the lower GR is a mean value of 7 thermocouples placed along the height of the bubbling fluidized bed. The temperature in the upper GR is the temperature where hot bed material from the CR re-enters the gasification reactor from the upper loop seal. In the CR, the given temperature is a mean value of the temperature where oil is introduced (cf. Figure 4, fuel to CR) and the temperature at the exit of the CR. Both the GR and the CR temperatures are lower in the case of the SER process to enable in situ CO_2 removal. The high additional fuel input power to the CR for DFB gasification results from the relatively high gasification temperatures and the high heat losses of the 100 kW_{th} DFB pilot plant. A much lower amount for the SER process is sufficient because of the lower operating temperatures. A steam-to-fuel ratio of 0.8–0.95 is typical for this pilot plant [32]. It is based on the amount of steam required to drive the gasification reactions and the amount of steam required to fluidize the bed material. The RME scrubber was operated at a temperature of 18 °C and 36 °C with a relatively high solvent-to-gas ratio in both cases, typical for laboratory-sized columns [38]. The higher scrubber temperature for the SER process results from the higher steam content in the product gas and therefore increased water condensation enthalpy in the scrubber. The activated carbon adsorbers are operated at a slightly

Table 2 Operating parameters of the DFB gasification and SER process configurations

Parameter	DFB gasification	SER process
DFB gasifier		
Bed material mixture (wt.-%)	80/20 olivine/limestone mixture	100 limestone
Feedstock	Softwood pellets	Softwood pellets
Mean temperature lower GR (°C)	836	681
Temperature upper GR (°C)	962	778
Mean temperature CR (°C)	1015	880
Fuel input GR (kW)	91	96
Fuel input CR (kW)	52	13
φ_{SF} ($kg_{H2O}/kg_{fuel,daf}$)	0.80	0.95
Gas cleaning		
Particle filter temperature (°C)	258	252
Scrubber gas exit temperature (°C)	18	36
Scrubber solvent to gas ratio (kg_{RME}/kg_{PG})	127	152
Activated carbon bed 1 temperature (°C)	51	50
Activated carbon bed 2 temperature (°C)	51	50
ZnO guard bed temperature (°C)	351	325
Methanation		
WHSV (Nl/g_{cat} h)	1.3	1
Mean reaction temperature (°C)	361	342
H_2O input concentration (vol.-%)	25	5.7
Raw-SNG output (kW)	4.1	5.6
Fluidization number (U/U_{mf})	5.9	3.7

elevated temperature at about 50 °C and the ZnO guard bed at about 325–350 °C to enable sufficient kinetic activity. In the fluidized bed methanation reactor, the mean temperature is set to the temperature where the CH_4 content is maximized. The mean value is computed from 5 thermocouples which are laterally and radially distributed in the catalytic bed (see [20]). For the methanation of the DFB product gas, the optimal temperature is around 360 °C, and for the SER process around 340 °C. In order to prevent carbon depositions on the catalyst, water vapor is added to the feed gas of the methanation reactor for the direct methanation of the DFB product gas. The amount is a trade-off between thermodynamic considerations and the resulting gas composition. Water is a reaction product of the Sabatier reaction and therefore influences the raw-SNG gas composition. A lower feed water content would increase the methane content in the raw-SNG and vice versa, as was shown in [20] and [39]. However, a lower feed water content might increase the carbon depositions and reduce the lifetime of the catalyst. Consequently, determining an optimal water content is a multi-objective optimization problem and thus not trivial to answer. In the case of the SER process, no additional water vapor was added to the feed gas of the methanation reactor since the hydrogen contents are considerably higher and the risk for carbon deposition is lower. Another parameter for the fluidized bed methanation reactor is the fluidization number. The reactor is operated in the bubbling fluidized bed regime with a fluidization number between 3.7 and 6 U/U_{mf}, where U is the superficial gas velocity and U_{mf} is the minimum fluidization velocity.

3.2 Direct methanation of the DFB product gas (DFB-Std)

This section shows the results of the full process chain for the direct methanation of the DFB product gas without external hydrogen addition. Figure 7 depicts the raw gas analysis values for the main components of the product gas of the DFB gasifier (top) and the raw-SNG (bottom) on a dry and nitrogen-free basis over time. Nitrogen is excluded because it results from flushing the fuel hoppers and the pressure measurement points, while hardly any nitrogen is expected from the fuel in the case of softwood pellets. Investigations not depicted in the current study showed that CO_2 can be used as a flushing agent, which reduces the nitrogen content in the product gas close to zero. Both the product gas and the raw-SNG compositions show a stable trend over the displayed 8.5 h. The excluded parts of the diagram are mainly caused by the maintenance of the gas measurement equipment, while the process itself remains in a steady state (see temperature trends in the supplementary material). Other excluded parts in the

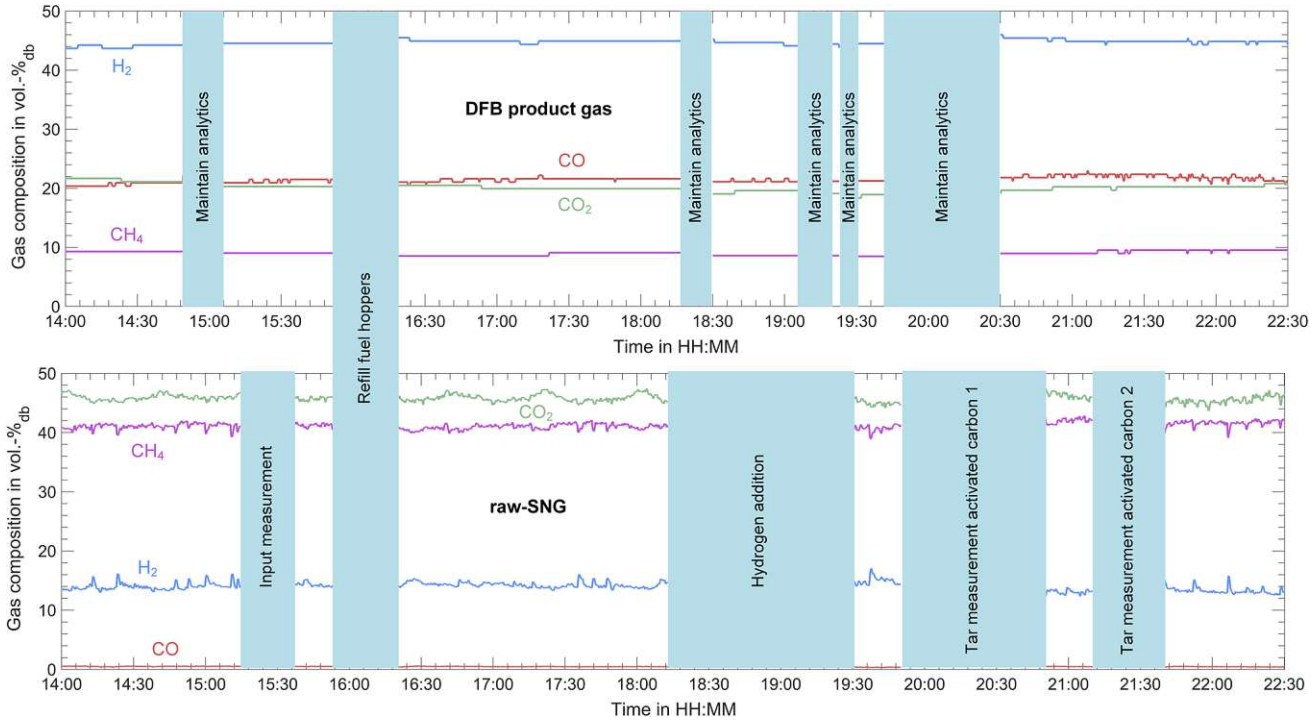

Fig. 7 Raw measurement values of the DFB product gas composition (top) and the raw-SNG composition (bottom) on a dry and nitrogen-free basis over time

raw-SNG measurement were caused by parameter variations, measuring the input gas to the methanation reactor, and tar measurements after the activated carbon filters. The latter causes a reduction in volume flow to the methanation reactor. The only interruption of the process was caused by refilling the fuel hoppers. The product gas has a comparably high hydrogen content, which is attributed to the limestone in the bed material and the relatively high gasification temperatures. Similar values were reported by Schmid et al. [32] for the 100 kW_{th} DFB pilot plant. In the raw-SNG, CO_2 constitutes the main component, followed by CH_4. Residual H_2 also remains in the raw-SNG, while CO is almost completely converted. For process simulation and the mean values of the parameters in Table 2, the time frame between 16:30 and 22:30 is evaluated. Prior to that, the process is not fully in a steady state, as the CO concentration in the product gas and the temperatures in the GR show.

Figure 8a depicts the evolution of temperature and pressure (top) and gas compositions (bottom) at different positions along the process chain (stream numbers 1–12) for the validated steady-state operation between 16:30 and 22:30. Each displayed stream number can be allocated to a certain point in the process chain according to the process flow diagram in Fig. 8b). The illustration of the gas composition is divided into two sections: from stream 1–8, the evolution of impurities such as BTEX, GCMS tar, NH_3, and H_2S are depicted, while for stream 9–12, the evolution of the main gas components (H_2, CO_2, CO, CH_4) and the water content is displayed. The illustration of impurities and main gas components for the other stream numbers is omitted because the gas composition does not change there. Furthermore, the impurity concentrations are displayed on a logarithmic scale, where the minimum value on the axis indicates that the lower detection limit is reached (bdl = below detection limit, see supplementary material for quantification of limits). Actual measurement values are indicated by marks and the corresponding measured value.

The product gas leaves the DFB system (no. 1) at 838 °C and is cooled in the radiation cooler. At this point (no. 2), gas measurements are taken. H_2S concentrations are quite low because of the high quality of the fuel and agree well with reported values [32]. GCMS tar concentrations are also low because of the high gasification temperatures and the limestone share in the bed material. The components and concentrations of the GCMS tar are listed in the supplementary material. BTEX amounts to the highest share of impurities in the product gas at roughly 4000 $ppm_{v,db}$. For all BTEX measurements, the sum is only comprised of benzene and toluene since ethylbenzene and xylene were below the detection limits. The main gas composition is also measured at this point. Since the dry main gas composition does not change, the values at stream no. 10 can be taken, where the main gas composition is redundantly measured.

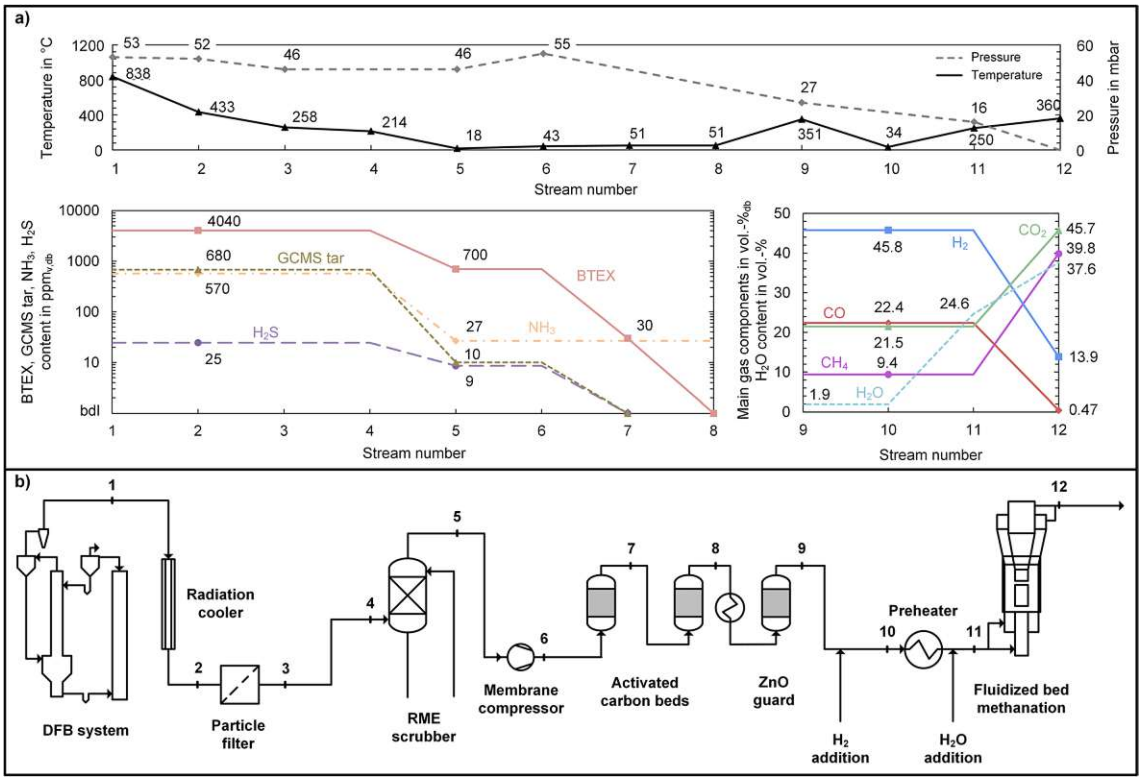

Fig. 8 Process conditions over the whole process chain during the direct methanation of the DFB product gas: **a** evolution of temperature, pressure (top), and concentration of impurities and main gas components (bottom), **b** process flow diagram with stream numbers, see supplementary material for detection limits

In the particle filter, dust and char particles are removed at around 260 °C before the gas enters the RME scrubber at a slightly lower temperature due to heat losses (no. 4). Entering the scrubber at this temperature level ensures that no tar components condensate in the particle filter or the piping. The gas leaves the scrubber at 18 °C with a reduced amount of impurities (no. 5). Especially GCMS tar concentrations are reduced by a large margin through condensation and dissolution in the RME (98.5% separation efficiency). Naphthalene, which makes up two-thirds of the GCMS tar concentration, is removed below the detection limit. NH_3 is a water-soluble molecule and is also efficiently removed (95% separation efficiency) in the scrubber through dissolution in the condensed water vapor. Assuming water saturation at the exit of the scrubber leads to a calculated water content of 1.9 vol.-% (see stream no. 9). BTEX components are reduced by 83%. Because benzene has a lower boiling point than toluene, the remaining BTEX sum mainly consists of benzene, while toluene is almost completely removed. The high separation efficiencies in the scrubber are attributed to the relatively low operating temperatures (18 °C) and the high solvent-to-gas ratio. Literature reports a substantial variation of separation efficiencies in the RME scrubber based on the applied operating conditions. Laboratory-sized columns operated at a high solvent-to-gas ratio and at temperatures below 10 °C report almost complete NH_3 [40] and tar [38] separation efficiencies. At an industrial scale, operating temperatures are usually higher due to technical limitations and economic considerations, which considerably limit the separation efficiencies [37, 38]. Furthermore, the H_2S concentration is reduced in the scrubber as well.

The membrane compressor is used to set the required volume flow and to overcome pressure losses throughout the process chain—no pressurized operation is intended. Since the DFB system is operated at a slight overpressure of around 50 mbar, the membrane compressor only increases the pressure marginally (no. 6). The activated carbon beds further reduce the concentrations of the impurities and are operated at around 50 °C. GCMS tar and H_2S concentrations are reduced below the detection limit in the first bed (no. 7). However, 30 $ppm_{v,db}$ of toluene is still measured after the first bed and removed below the detection limit in the second bed (no. 8). NH_3 has not been measured after the activated carbon beds and is assumed to pass through unaffected. Since no H_2S breakthrough was detected, the ZnO guard bed only acts as an additional security layer. A temperature reduction after the ZnO guard bed (no. 10) and a consecutive preheating (no. 11) is required because of the volume flow measurement

with a gas meter in this particular case. In an industrial plant, the sensible heat after the ZnO guard bed could be directly utilized as preheating for the methanation reactor. After the preheater, steam is added to the syngas at 250 °C (no. 11) to shift the gas in the methanation reactor towards H_2. In the methanation reactor, syngas is converted to raw-SNG (no. 12). A methane content of about 40 vol.-$\%_{db}$ is achieved. The high CO_2 content is a result of the water–gas shift reaction and the substoichiometric product gas composition (concerning SN), which leads to the production of CO_2 in the methanation reactor. For the same reason, and because of thermodynamic and kinetic limitations, residual H_2 remains in the raw-SNG, while CO is almost completely converted.

Seemann et al. [41] achieved similar results applying fluidized bed methanation of a partial product gas flow from the DFB gasifier in Güssing, Austria. They operated the fluidized bed reactor at 385 °C and 3 bar_a at 4.5 Nl/g_{cat} h with a commercial 50 wt.-% Ni/γ-Al_2O_3 catalyst. However, the product gas composition from the DFB gasifier in Güssing differs from the advanced DFB pilot plant. The DFB Güssing product gas shows a lower H_2 and CO_2 content and a higher CO content, which leads to an overall lower stoichiometric number. Because of the deviating product gas composition and different operating conditions, their raw-SNG shows a slightly higher CH_4 content and an increased CO_2 content, while the H_2 content is lower. Especially a pressurized operation, which could be performed in this case, in combination with the lower stoichiometric number, allows a suppression of the H_2 content in the raw-SNG. On the other hand, a pressurized application requires compression energy and pressure vessels according to the pressurized equipment directive.

3.3 Methanation of the DFB product gas with external hydrogen addition (DFB + H_2)

This section shows the results of the product gas methanation with external hydrogen addition. Hydrogen addition was performed during the same steady-state gasification experiment already presented in Sect. 3.1. Therefore, only the results of the methanation part are discussed. Table 3 lists the main operating parameters for two different operating points. The operating points differ in terms of the amount of hydrogen added to the product gas before methanation, which is represented by the stoichiometric number (SN = 0.91 and SN = 1.04). Through the additional hydrogen amount, the WHSV and the fluidization number in the methanation reactor increase compared to the direct methanation of the product gas and the raw-SNG output approximately doubles. The reaction temperature and pressure are kept constant at approximately 360 °C and 1 bar_a, respectively. Because of the high hydrogen content and the roughly stoichiometric composition, no additional steam is added to the feed gas of the methanation reactor.

Table 3 Operating parameters of the methanation reactor

Parameter	SN = 0.91	SN = 1.04
WHSV (Nl/g_{cat} h)	1.8	2.0
Mean reaction temperature (°C)	358	364
Raw-SNG output (kW)	7.6	8.4
Fluidization number (U/U_{mf})	6.2	6.9
H_2 addition (vol.-%)[a]	91	111
Water addition (vol.-%)	0	0

[a]In vol.-% of the amount of syngas upstream H_2 addition

Figure 9 depicts the evolution of the gas composition over stream nos. 9–12 for the two different operating points. Figure 9a shows the operating point with less hydrogen (SN = 0.91). Between stream nos. 9 and 10, hydrogen is added to the product gas, which increases the hydrogen content to 72 vol.-$\%_{db}$ and dilutes the other gas components. The raw-SNG after the methanation reactor (stream no. 12) consists mainly of methane as well as a significant amount

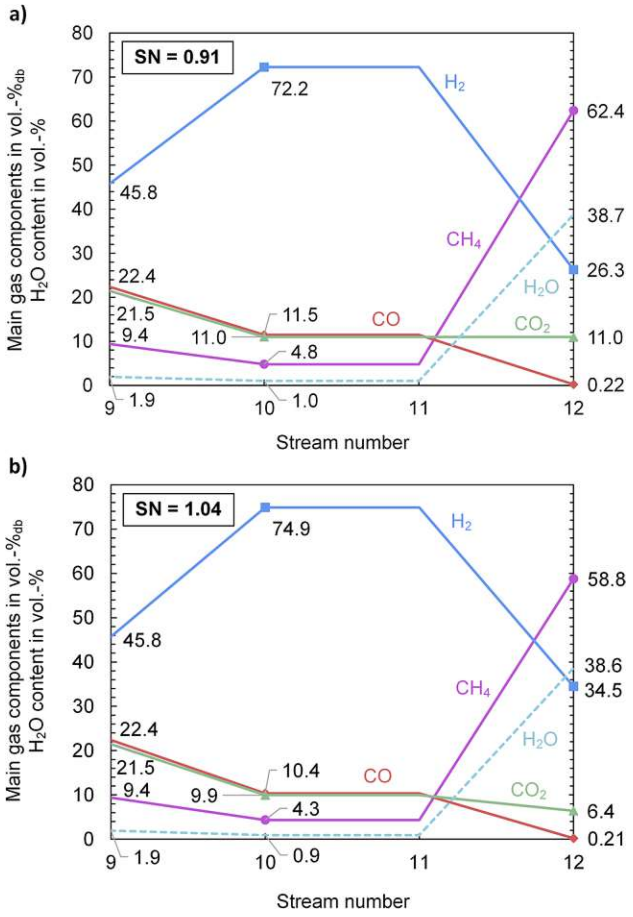

Fig. 9 Evolution of main gas components over the methanation reactor (stream nos. 9–12) for DFB + H_2: **a** SN = 0.91, **b** SN = 1.04

of residual hydrogen and carbon dioxide. Coincidentally, the volume percentage of CO_2 remains the same before and after methanation because of the volume contraction during the reaction. A CO_2 conversion nevertheless takes place, as Fig. 10 elucidates. Carbon monoxide, on the other hand, is converted to a large extent.

Figure 9b shows the operating point with a higher amount of hydrogen added (SN = 1.04). In comparison, this leads to lower methane and higher residual hydrogen contents compared to SN = 0.91. Carbon dioxide is further reduced, while the residual CO content remains almost unaffected.

3.4 Direct methanation of the SER product gas

The SER process allows an adaption of the product gas composition towards higher hydrogen contents via in situ CO_2 removal, as explained in Fig. 2 (right). No additional hydrogen was added to the product gas. Figure 10 depicts the raw gas analysis values for the main components of the SER product gas (top) and the raw-SNG (bottom) on a dry and nitrogen-free basis. The gas compositions show constant mean values over the displayed 105 min but increased instabilities on a lower time scale compared to DFB gasification. An H_2 content of about 60 vol.-$\%_{db}$ could be reached in the product gas, whereas the CO and CO_2 concentrations are lowered to around 11 vol.-$\%_{db}$ compared to DFB-Std. CH_4 is somewhat increased to around 13 vol.-$\%_{db}$ because of the reduced product gas volume flow due to the CO_2 removal. Hence, the product gas composition is much closer to the requirements of the methanation reactions without the need for additional hydrogen compared to the product gas of DFB gasification. Therefore, also the CH_4 content in the raw-SNG is elevated to around 70 vol.-$\%_{db}$, the rest being residual contents of H_2 and CO_2. Only trace amounts of CO remain in the raw-SNG.

To track the temperatures, pressures, gas compositions, and impurity concentrations, Fig. 11 depicts the via mass and energy balancing validated data at different positions along the SER process chain in analogy to Fig. 8. Because of the SER operation mode of the gasifier, the temperatures at the exit of the gasifier, and therefore after the radiation cooler, are lower (stream nos. 1 and 2). GCMS tar and BTEX concentrations differ from the DFB gasification process chain because of the catalytically active bed material on the one hand and the lower gasification temperatures on the other hand. The GCMS tar components and concentrations are again listed in the supplementary material. Despite using the same softwood pellets in the DFB gasification and the SER process chains, the NH_3 concentration is higher for the latter. This is because of the lower gasification temperatures plus the in situ CO_2 removal and thus a lower volume flow of dry product gas from the gasifier in the case of the SER process. In the filter and entry to the RME scrubber, temperatures are similar to the DFB gasification. However, the

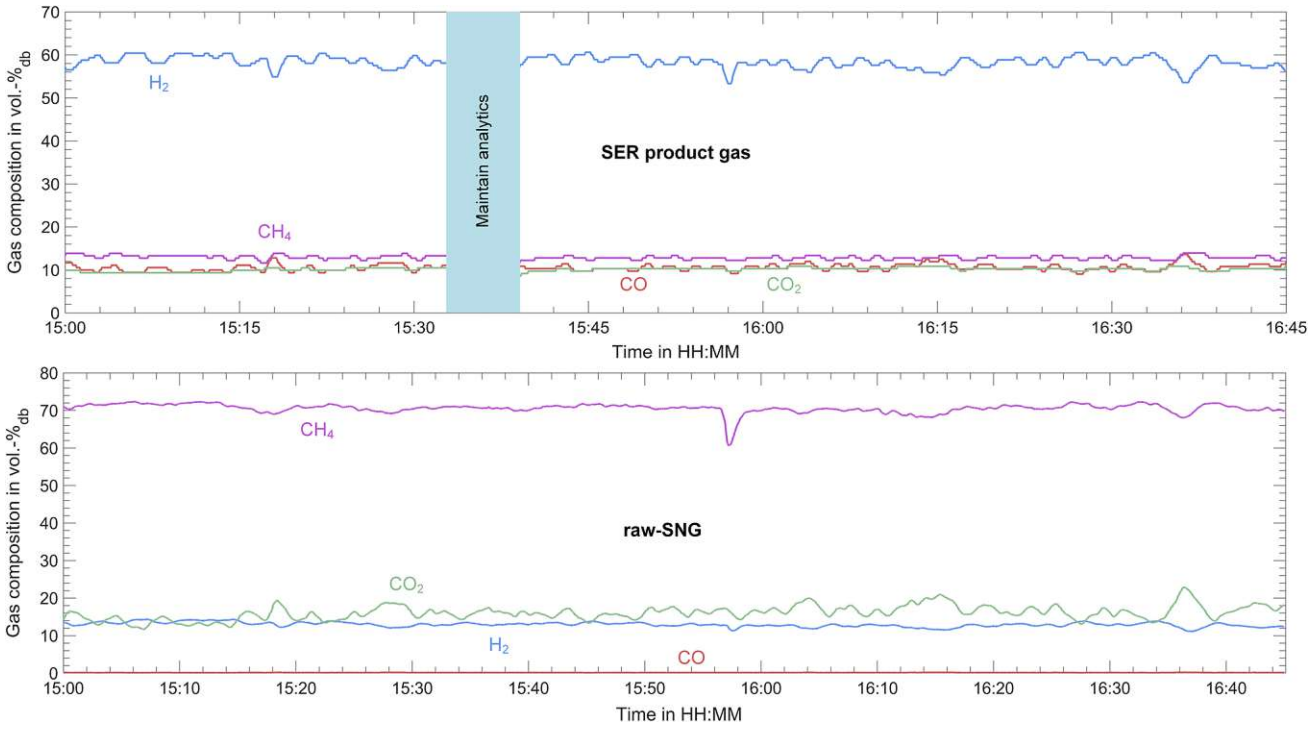

Fig. 10 Raw measurement values of the SER product gas composition (top) and the raw-SNG composition (bottom) on a dry and nitrogen-free basis over time

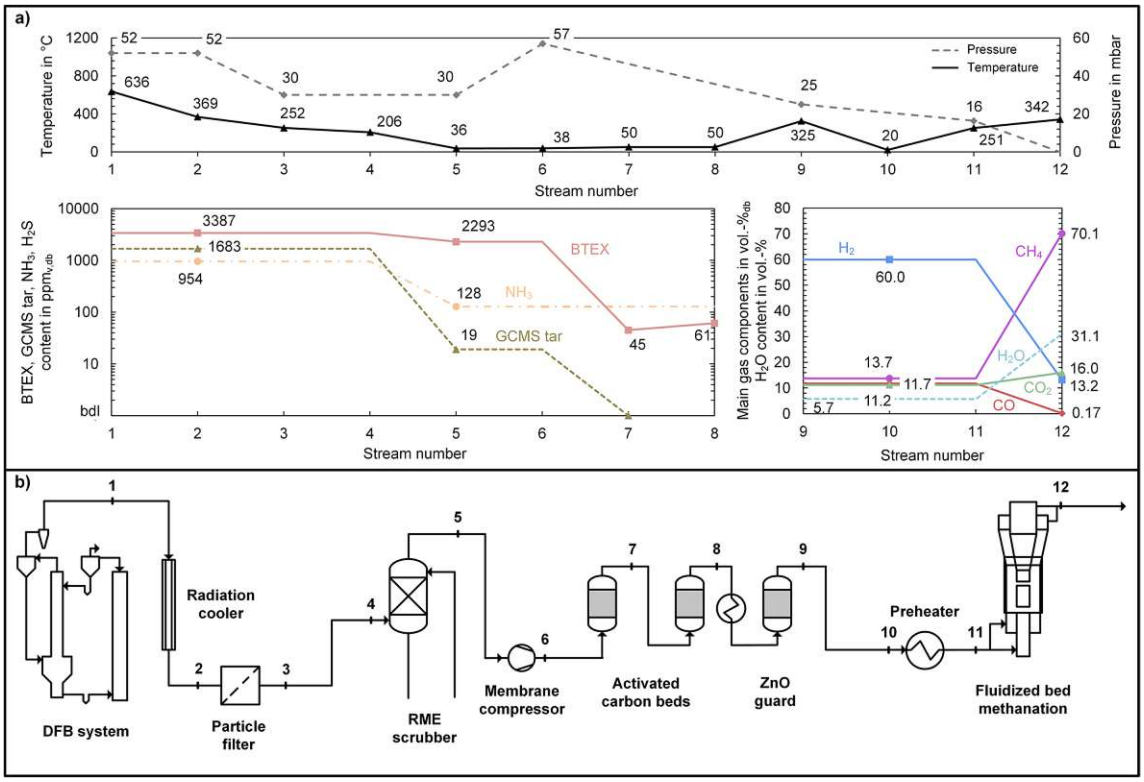

Fig. 11 Process conditions over the whole process chain during the direct methanation of the SER product gas: **a** evolution of temperature, pressure (top), and concentration of impurities and main gas components (bottom), **b** process flow diagram with stream numbers, see supplementary material for detection limits

exit temperature of the RME scrubber (no. 5) is elevated to 36 °C due to the increased steam content in the product gas for the SER process and thus a higher condensation enthalpy. At a constant cooling power of the scrubber, this leads to an elevated exit temperature and thus a higher residual water content in the scrubbed product gas. GCMS tars, BTEX and NH_3 are again reduced in the scrubber. However, the increased operating temperature of the scrubber leads to a reduced separation efficiency of BTEX and NH_3 at 32% and 87%, respectively. The separation efficiency of GCMS tar is unaffected by the increased operating temperature. In the activated carbon adsorbers, residual GCMS tar components are removed and BTEX concentrations are further reduced. However, no full removal of BTEX was possible in this case. Toluene was detected after the first and the second activated carbon bed (nos. 7 and 8). The DFB gasification process chain already showed a breakthrough of toluene through the first activated carbon bed. For the SER process chain, the increased water vapor content in the scrubbed product gas might have further lowered the adsorption capacities of the activated carbon. The increase of the toluene concentration from the first to the second bed might even indicate the desorption of toluene. In the methanation reactor, the syngas (no. 10) is converted to raw-SNG (no. 12) after preheating (no. 11). A high methane content of 70 vol.-$\%_{db}$ is reached while the H_2 concentration drops to 16 vol.-$\%_{db}$ and only 0.17 vol.-$\%_{db}$ of CO remains. Part of the CO_2 is also converted, but the concentration actually increases because of the volume reduction of the methanation reactions.

3.5 Comparison of the process chains

For a comparison of the different process chain configurations, the raw-SNG gas composition (Fig. 12a)) and the KPIs of the methanation reactor (Fig. 12b)) are displayed. A substantial increase in methane content and a decrease in carbon dioxide content result from the externally added hydrogen (DFB + H_2) and the methanation of the SER product gas (SER). Concurrently, the methane yield and the CO_2 conversion increase. While the highest methane content is reached for the substoichiometric SER product gas (SN = 0.71), the methane yield is higher for DFB + H_2 because of the higher SN. The lower methane content for SN = 0.91 and SN = 1.04 results from the dilution with a higher amount of residual hydrogen. In the case of the DFB-Std process chain (SN = 0.30), CO_2 is produced from CO and H_2O through the water–gas shift reaction in the methanation reactor. With hydrogen addition and the SER product gas, CO_2 is actually

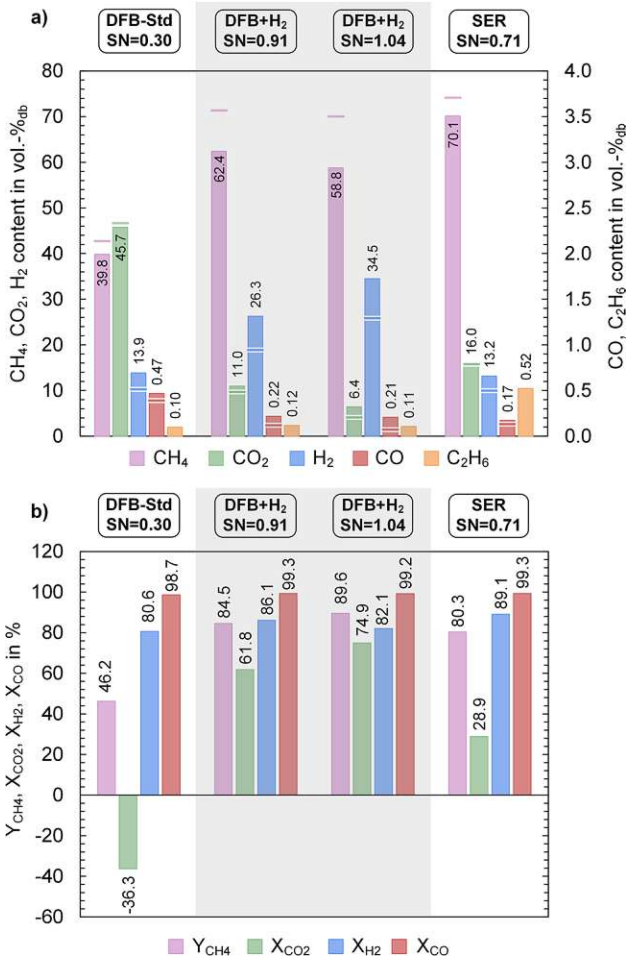

Fig. 12 Comparison of the three operating points: **a** raw-SNG composition, **b** KPIs of the methanation reactor

converted. The higher the amount of hydrogen at the inlet of the methanation reactor, the higher the CO_2 conversion. Residual hydrogen contents in the raw-SNG increase with an increasing amount of hydrogen in the syngas. Hydrogen conversion is, however, higher for the SER configuration, followed by SN = 0.91 and SN = 1.04. DFB-Std operation yields the lowest hydrogen conversion because the added steam to the product gas shifts the raw-SNG towards H_2 and CO_2 according to the water–gas shift reaction. CO is almost completely converted for all operating points. Nevertheless, the DFB + H_2 and SER process chains allow a further reduction of the CO content and a slight increase in CO conversion. Some ethane is detected in the raw-SNG, which results from the conversion of ethylene to ethane and possibly the ethane in the product gas itself. The ethane content in the raw-SNG is similar for all three DFB gasification operating points but higher for the SER configuration because of the higher ethylene content in the SER product gas.

Figure 12a additionally depicts the theoretical composition of the raw-SNG in the thermodynamic equilibrium, denoted by horizontal bars. In the case of DFB-Std and SER product gas methanation, the measured composition is close to the thermodynamic limit. For the two DFB + H_2 operating points, a larger deviation from the maximum values can be seen. Especially methane and hydrogen contents deviate from thermodynamic predictions, and a further conversion would have been theoretically possible. In this case, the higher WHSV and, therefore, a lower residence time resulting from hydrogen addition most likely lead to a kinetic limitation of the reaction. In general, the results agree very well with investigations carried out with synthetically premixed syngases in the same methanation reactor [20]. In general, the raw-SNG compositions of the DFB + H_2 and SER process configurations are much closer to the requirements of the natural gas grid. However, a further conversion of H_2, CO_2, and CO would still be necessary. This could be achieved at lower reaction temperatures or a pressurized operation. Theoretical calculations show that adapted operating conditions can lead to a grid-feedable SNG for the SER [18, 19] and the DFB + H_2 [22] configurations. Excessive separated hydrogen, e.g., via membrane separation, could be recirculated to the inlet of the methanation reactor. Alternatively, a second-stage methanation reactor with intermediate water condensation could also enhance conversion rates to reach grid specifications. This possibility was already shown for biogas upgrading to SNG with additional hydrogen [42].

For the performance of the methanation reactor alone, it is unimportant how the adjustment of the syngas towards high H_2 contents is achieved. The main influencing parameter is the SN at the inlet of the methanation reactor and, to some extent, the changing WHSV due to H_2 addition. However, the performance of the whole process chain depends very much on the origin of the syngas. Therefore, to compare the KPIs of the whole process chain, Fig. 13 depicts the overall cold gas efficiency ($\eta_{CG,o}$) and the carbon utilization efficiency (η_C). Interestingly, $\eta_{CG,o}$ is very similar for the DFB-Std and the DFB + H_2 operating points at 58 to 59%. Large-scale industrial plants, like GoBiGas and Güssing, report similar values at a maximum of 62–63% [8, 43]. However, a fair comparison is hardly possible. On the one hand, large-scale gasifiers perform at a higher cold gas efficiency than the pilot-scale plant at TU Wien. On the other hand, upgrading the raw-SNG to grid-feedable SNG is experimentally not investigated in this paper. This would reduce the cold gas efficiency, even if the excessive hydrogen is recirculated to the feed of the methanation reactor. For the SER process configuration, on the other hand, a higher cold gas efficiency results from this setup. Compared to DFB gasification, the gasification and combustion temperatures for SER are lower, and more char is available for combustion. Therefore, the amount of additional fuel needed in the combustion reactor is much lower, increasing the overall cold gas efficiency. Brellochs [19] calculates an overall cold gas efficiency of

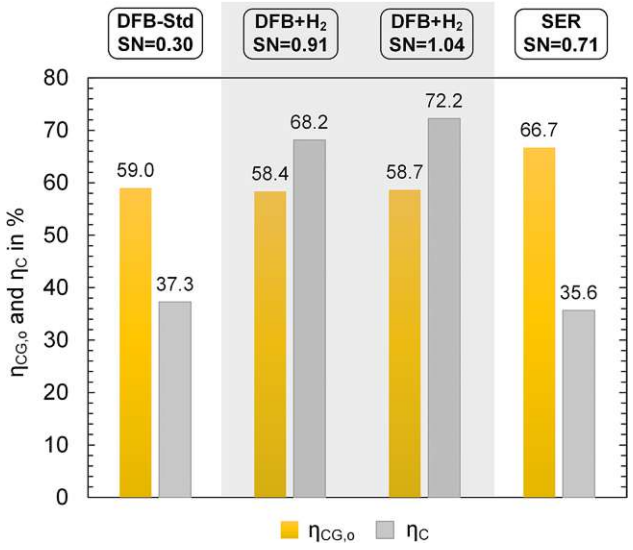

Fig. 13 Comparison of the KPIs of the overall process chain for the three operating points

67.5% for a 10 MW_{th} SNG plant based on a process simulation of the SER process, which is close to the calculated 66.7% in this study. For the DFB + H_2 process, simulations carried out by Gassner and Maréchal [9] and Alamia et al. [22] result in values between 67 and 73%. These values are considerably higher than in this study, which is a result of the limited conversion in the methanation reactor. Furthermore, the same limited comparability between small and large-scale installations remains, as discussed above.

The carbon utilization efficiency at 37% for the DFB-Std product gas methanation is within the expected range following theoretical considerations [18]. Larsson et al. [8] state a somewhat lower η_C at around 30% for the large-scale GoBiGas plant. This can be explained by the product gas recirculation to the combustion reactor to compensate for the heat demand in the gasifier in large-scale plants, which is not carried out at pilot scale. The SER process configuration shows a similar, slightly lower η_C. Most of the carbon is lost through char combustion and the calcination of $CaCO_3$ in the CR of the DFB system. The carbon in the $CaCO_3$ needs to be sacrificed to achieve a H_2-enriched product gas through the CO_2 removal in the GR. Some carbon is also lost through the remaining CO_2 in the raw-SNG and the separated tar in the scrubber.

Through the addition of hydrogen, a significant increase of η_C to roughly 70% is possible. More hydrogen addition (SN = 1.04) leads to a higher carbon utilization than less hydrogen addition (SN = 0.91), which was already indicated by the methane yield in Fig. 12. The remaining carbon is again lost through char combustion in the CR and to some extent through the remaining CO_2 in the raw-SNG and the separated tar in the scrubber.

In this study, the investigations were carried out with softwood pellets as a comparable reference fuel for all process configurations. However, the type and quality of biomass can have a major impact on the product gas quality and thus on the required gas cleaning and the raw-SNG composition. For example, Schmid et al. [32] and Schweitzer et al. [44] show that different fuels like bark, hazelnut shells, sugar cane bagasse, or sewage sludge have an impact on the product gas composition and on the concentration of impurities in particular. Residual materials typically exhibit higher concentrations of nitrogen and sulfur-containing compounds which necessitates a more rigorous gas cleaning section. The impact of different fuels on the raw-SNG composition is, for example, discussed by Bartik et al. [18]. Besides the feedstock, water is another important resource for the process. Steam is required as a gasification and fluidization agent in the GR and for the production of H_2 through electrolysis. Nevertheless, the overall water consumption of the process can be kept to a minimum through process integration. For large-scale applications, the separated water phase from the RME scrubber can be reused as a gasification agent. Similarly, the water fraction resulting from condensation and gas drying during the upgrading of raw-SNG can be reused within the process. However, a more detailed insight into different feedstocks and the water balance would go beyond the scope of this paper.

Overall, the comparison reveals the strengths and weaknesses of the different process configurations. As a decision basis, Table 4 lists a summary of the main advantages and disadvantages of the three process configurations.

4 Conclusions

In this work, advanced process chains for raw-SNG production were experimentally investigated and compared on a pilot scale and measured analytical values were validated with the aid of process simulation. A 100 kW_{th} advanced DFB gasification reactor was coupled with gas cleaning units and a 10 kW_{th} fluidized bed methanation reactor. External hydrogen addition allowed the investigation of hybrid SNG production process chains with increased carbon utilization. DFB gasification with in situ CO_2 removal (SER process) in combination with methanation was investigated as another novel process configuration. It allowed an adaption of the product gas composition to the needs of the methanation process without the use of external hydrogen. Additionally, extensive analytical measurements allowed the tracking and quantification of impurities over the whole process chain.

The following conclusions can be drawn:

Table 4 Advantages and disadvantages of the investigated process configurations

Process configuration	Advantages	Disadvantages
DFB-Std	- Stable steady-state operation - Similar large-scale operation demonstrated [43]	- High CO_2 contents in raw-SNG (upgrading effort) - Unsuitable product gas composition for methanation - Risk of catalyst aging through carbon deposition - Steam addition to inlet of methanation reactor
DFB + H_2	- Flexible adjustment of syngas composition through H_2 addition - Doubling of carbon utilization and thus doubling of SNG amount - Less risk of catalyst aging through carbon deposition due to SN adjustment - No steam addition at inlet of methanation reactor necessary - Possibly less effort for gas upgrading required	- Costs for hydrogen production - Increase in overall system complexity due to additional process units - Renewable electricity required for ecological viable concept - Potentially fluctuating H_2 supply increases requirements on dynamic process behavior
SER	- In situ adjustment of product gas composition through SER process without the need for external hydrogen addition - Higher overall cold gas efficiency for this setup - Less risk of methanation catalyst aging through carbon deposition due to SN adjustment - No steam addition at inlet of methanation reactor necessary - Possibly less effort for gas upgrading required - Less volume flow due to in-situ CO_2 removal and thus smaller units and less electrical power consumption	- SER process not yet demonstrated on a large-scale - No increase in carbon utilization possible

(i) A stable steady-state operation of the advanced DFB gasifier in combination with the SNG process chain was demonstrated (DFB-Std). A product gas with 46 vol.-% H_2 is converted to a raw-SNG with around 40 vol.-% CH_4 with an overall cold gas efficiency of 59% without external hydrogen addition.

(ii) The incorporation of external hydrogen (DFB + H_2) allowed a more efficient utilization of the biomass carbon. With a carbon utilization efficiency of about 70%, almost twice the amount of carbon is utilized for methane production compared to the DFB-Std process chain, while the cold gas efficiency remains practically the same. Simultaneously, the H_2, CO, and CO_2 conversions are improved despite the higher WHSV compared to the DFB-Std process chain.

(iii) The SER process can be applied advantageously to catalytic methanation as an alternative to hydrogen addition or the DFB-Std process chain. It allows the adjustment of the product gas composition towards high hydrogen contents suitable for methanation without the technical limits and additional expenses of external hydrogen addition. Additionally, SNG production is feasible at a higher overall cold gas efficiency, while the carbon utilization is similar to the DFB-Std process chain.

(iv) Low concentrations of impurities in the product gas through the advanced gasification system and the high quality of the fuel were achieved. Impurity tracing through the process chain showed that the RME scrubber serves as an efficient impurity removal unit. High tar, NH_3, and BTEX separation efficiencies were achieved, but there is a dependency on the scrubber operating temperature.

(v) For grid injection, upgrading steps are necessary independent of the applied process configuration. However, the type of upgrading steps and the optimal process conditions in the methanation reactor might differ. For the DFB + H_2 and the SER process configuration, less upgrading effort might be possible given the right process conditions.

Depending on the given circumstances and the defined goals, the most suitable process configuration might differ, as Table 4 shows. DFB + H_2 might be favored if renewable hydrogen is readily available from a technical and economic perspective, and the goal is the maximization of biomass utilization. If no hydrogen is available, the SER process configuration is an interesting alternative to the DFB-Std process configuration.

Optimized process concepts, including upgrading steps and economic and ecologic comparisons of the different routes, should be investigated to provide a more precise basis for decision-making. Furthermore, SNG production from biogenic residual material would be an ecologically and economically interesting alternative.

Supplementary information The online version contains supplementary material available at https://doi.org/10.1007/s13399-023-04341-3.

Acknowledgements This study is part of the research project ReGas4Industry (871732) and receives financial support from the research program "Energieforschung" funded by the Austrian Climate and Energy Fund. Furthermore, this study was carried out within the doctoral college CO_2Refinery at TU Wien. The authors acknowledge TU Wien Bibliothek for financial support through its Open Access Funding Programme. Furthermore, the authors would like to thank the Test Laboratory for Combustion Systems at TU Wien for the analytical

measurements and the fellow members of the research group Industrial Plant Engineering and Application of Digital Methods for their support during the test campaigns.

Author contribution Alexander Bartik: conceptualization, methodology, investigation, writing, review & editing, visualization; Florian Benedikt: conceptualization, methodology, investigation, writing, review & editing, supervision, project administration, funding acquisition; Josef Fuchs: methodology, investigation, validation, writing, review & editing; Hermann Hofbauer: conceptualization, review & editing, supervision, project administration, funding acquisition; Stefan Müller: validation, review & editing, supervision, funding acquisition.

Funding Open access funding provided by TU Wien (TUW).

Data availability Data will be made available upon request.

Declarations

Ethical approval Not applicable.

Competing interests Author Hermann Hofbauer is the editor of the Journal Biomass Conversion and Biorefinery. Apart from that, the authors declare that they have no relevant financial or non-financial interests to disclose.

References

1. IEA (2021) World energy outlook 2021, IEA, Paris. https://www.iea.org/reports/world-energy-outlook-2021. Accessed 23 May 2023
2. Rönsch S, Schneider J, Matthischke S, Schlüter M, Götz M, Lefebvre J, Prabhakaran P, Bajohr S (2016) Review on methanation – From fundamentals to current projects. Fuel 166:276–296. https://doi.org/10.1016/j.fuel.2015.10.111
3. Götz M, Lefebvre J, Mörs F, McDaniel Koch A, Graf F, Bajohr S, Reimert R, Kolb T (2016) Renewable power-to-gas: a technological and economic review. Renew Energy 85:1371–1390. https://doi.org/10.1016/j.renene.2015.07.066
4. Thunman H, Seemann M, Berdugo Vilches T, Maric J, Pallares D, Ström H, Berndes G, Knutsson P, Larsson A, Breitholtz C, Santos O (2018) Advanced biofuel production via gasification – lessons learned from 200 man-years of research activity with Chalmers' research gasifier and the GoBiGas demonstration plant. Energy Sci Eng 6(1):6–34. https://doi.org/10.1002/ese3.188
5. Schildhauer TJ, Biollaz SM (2016) Synthetic natural gas from coal, dry biomass, and power-to-gas applications. Wiley, Hoboken
6. Gassner M, Baciocchi R, Maréchal F, Mazzotti M (2009) Integrated design of a gas separation system for the upgrade of crude SNG with membranes. Chem Eng Process 48(9):1391–1404. https://doi.org/10.1016/j.cep.2009.07.002
7. Mevissen N, Schulzke T, Unger CA, an Bhaird SM (2009) Thermodynamics of autothermal wood gasification. Environ Prog Sustain Energy 28(3):347–354. https://doi.org/10.1002/ep.10393
8. Larsson A, Gunnarsson I, Tengberg F (2018) The GoBiGas project - demonstration of the production of biomethane from biomass via gasification. Technical Report, December 2018. https://doi.org/10.13140/RG.2.2.27352.55043
9. Gassner M, Maréchal F (2008) Thermo-economic optimisation of the integration of electrolysis in synthetic natural gas production from wood. Energy 33(2):189–198. https://doi.org/10.1016/j.energy.2007.09.010
10. Barbuzza E, Buceti G, Pozio A, Santarelli M, Tosti S (2019) Gasification of wood biomass with renewable hydrogen for the production of synthetic natural gas. Fuel 242:520–531. https://doi.org/10.1016/j.fuel.2019.01.079
11. Grigoriev SA, Fateev VN, Bessarabov DG, Millet P (2020) Current status, research trends, and challenges in water electrolysis science and technology. Int J Hydrog Energy 45(49):26036–26058. https://doi.org/10.1016/j.ijhydene.2020.03.109
12. Dincer I (2012) Green methods for hydrogen production. Int J Hydrog Energy 37(2):1954–1971. https://doi.org/10.1016/j.ijhydene.2011.03.173
13. Karatza D, Konstantopoulos C, Chianese S, Diplas S, Svec P, Hristoforou E, Musmarra D (2021) Hydrogen production through water splitting at low temperature over Fe_3O_4 pellet: Effects of electric power, magnetic field, and temperature. Fuel Process Technol 211:106606. https://doi.org/10.1016/j.fuproc.2020.106606
14. Safari F, Dincer I (2020) A review and comparative evaluation of thermochemical water splitting cycles for hydrogen production. Energy Conv Manag 205:112182. https://doi.org/10.1016/j.enconman.2019.112182
15. Castro J, Leaver J, Pang S (2022) Simulation and techno-economic assessment of hydrogen production from biomass gasification-based processes: a review. Energies 15(22):8455. https://doi.org/10.3390/en15228455
16. Singh T, Alhazmi A, Mohammad A, Srivastava N, Haque S, Sharma S, Singh R, Yoon T, Gupta VK (2021) Integrated biohydrogen production via lignocellulosic waste: opportunity, challenges & future prospects. Bioresour Technol 338:125551. https://doi.org/10.1016/j.biortech.2021.125511
17. Fuchs J, Schmid JC, Müller S, Hofbauer H (2019) Dual fluidized bed gasification of biomass with selective carbon dioxide removal and limestone as bed material: a review. Renew Sust Energ Rev 107:212–231. https://doi.org/10.1016/j.rser.2019.03.013
18. Bartik A, Benedikt F, Lunzer A, Walcher C, Müller S, Hofbauer H (2020) Thermodynamic investigation of SNG production based on dual fluidized bed gasification of biogenic residues. Biomass Convers Biorefinery 11:95–110. https://doi.org/10.1007/s13399-020-00910-y
19. Brellochs J (2014) "Experimentelle Untersuchung und Prozess-Simulation der AER-Biomassevergasung zur Erzeugung eines regenerativen Erdgassubstitutes", Dissertation, Universität Stuttgart, 1st edn. Cuvillier, Göttingen (ISBN: 9783954048830)
20. Bartik A, Fuchs J, Pacholik G, Föttinger K, Hofbauer H, Müller S, Benedikt F (2022) "Experimental investigation on the methanation of hydrogen-rich syngas in a bubbling fluidized bed reactor utilizing an optimized catalyst. Fuel Process Technol 237:107402. https://doi.org/10.1016/j.fuproc.2022.107402
21. Gómez L, Grasa G, Martínez I, Murillo R (2022) Performance study of a methanation process for a syngas obtained from a sorption enhanced gasification process. Chem Eng Sci 267:118291. https://doi.org/10.1016/j.ces.2022.118291
22. Alamia A, Òsk Gardarsdòttir S, Larsson A, Normann F, Thunman H (2017) Efficiency comparison of large-scale standalone,

centralized, and distributed thermochemical biorefineries. Energy Technol 5(8):1435–1448. https://doi.org/10.1002/ente.201600719
23. Salbrechter K, Schubert T (2021) Combination of b-fuels and e-fuels—a technological feasibility study. Energies 14(17):5250. https://doi.org/10.3390/en14175250
24. Menin L, Vakalis S, Benedetti V, Patuzzi F, Baratieri M (2020) Techno-economic assessment of an integrated biomass gasification, electrolysis, and syngas biomethanation process. Biomass Convers Biorefinery 11(2):445–459. https://doi.org/10.1007/s13399-020-00654-9
25. Giglio E, Vitale G, Lanzini A, Santarelli M (2021) Integration between biomass gasification and high-temperature electrolysis for synthetic methane production. Biomass Bioenerg 148:106017. https://doi.org/10.1016/j.biombioe.2021.106017
26. Leimert JM, Neubert M, Treiber P, Dillig M, Karl J (2018) Combining the heatpipe reformer technology with hydrogen-intensified methanation for production of synthetic natural gas. Appl Energy 217:37–46. https://doi.org/10.1016/j.apenergy.2018.02.127
27. Witte J, Calbry-Muzyka A, Wieseler T, Hottinger P, Biollaz SM, Schildhauer TJ (2019) Demonstrating direct methanation of real biogas in a fluidised bed reactor. Appl Energy 240(2018):359–371. https://doi.org/10.1016/j.apenergy.2019.01.230
28. Pozzo M, Lanzini A, Santarelli M (2015) Enhanced biomass-to-liquid (BTL) conversion process through high temperature co-electrolysis in a solid oxide electrolysis cell (SOEC). Fuel 145:39–49. https://doi.org/10.1016/j.fuel.2014.12.066
29. Clausen LR, Houbak N, Elmegaard B (2010) Technoeconomic analysis of a methanol plant based on gasification of biomass and electrolysis of water. Energy 35(5):2338–2347. https://doi.org/10.1016/j.energy.2010.02.034
30. Hauser A, Wolf-Zoellner P, Haag S, Dettori S, Tang X, Mighani M, Matino I, Mocci C, Colla V, Kolb S, Bampaou M, Panopoulos K, Kieberger N, Rechberger K, Karl J (2022) Valorizing steelworks gases by coupling novel methane and methanol synthesis reactors with an economic hybrid model predictive controller. Metals 12(6):1023. https://doi.org/10.3390/met12061023
31. Kleiber S, Loder A, Siebenhofer M, Böhm A, Lux S (2022) Direct reduction of siderite ore combined with catalytic CO/CO_2 hydrogenation to methane and methanol: a technology concept. Chem Ing Tech 94(5):701–711. https://doi.org/10.1002/cite.202100189
32. Schmid JC, Benedikt F, Fuchs J, Mauerhofer AM, Müller S, Hofbauer H (2019) Syngas for biorefineries from thermochemical gasification of lignocellulosic fuels and residues - 5 years' experience with an advanced dual fluidized bed gasifier design. Biomass Convers Biorefinery 11:2405–2442. https://doi.org/10.1007/s13399-019-00486-2
33. Schmid JC (2014) Development of a novel dual fluidized bed gasification system for increased fuel flexibility. Dissertation, TU Wien, Vienna. https://doi.org/10.34726/hss.2014.25397
34. Karl J, Pröll T (2018) Steam gasification of biomass in dual fluidized bed gasifiers: a review. Renew Sust Energ Rev 98:64–78. https://doi.org/10.1016/j.rser.2018.09.010
35. Faust R, Berdugo Vilches T, Malmberg P, Seemann M, Knutsson P (2020) Comparison of ash layer formation mechanisms on si-containing bed material during dual fluidized bed gasification of woody biomass. Energy Fuels 34(7):8340–8352. https://doi.org/10.1021/acs.energyfuels.0c00509
36. Benedikt F (2020) Fuel flexible advanced dual fluidized bed steam gasification. Dissertation, TU Wien, Vienna. https://doi.org/10.34726/hss.2020.39988
37. Wolfesberger-Schwabl U (2013) Profiling tar behavior in dual fluidized bed biomass steam gasification, Dissertation, TU Wien, Vienna, https://permalink.catalogplus.tuwien.at/AC11451288. Accessed 23 May 2023
38. Bardolf R (2017) Optimierung eines Produktgaswäschers bei der Biomassedampfvergasung im Zweibettwirbelschichtverfahren. Dissertation, TU Wien, Vienna. https://doi.org/10.34726/hss.2017.36646
39. Kopyscinski J, Seemann MC, Moergeli R, Biollaz S, Schildhauer TJ (2013) Synthetic natural gas from wood: reactions of ethylene in fluidised bed methanation. Appl Catal A-Gen 462–463:150–156. https://doi.org/10.1016/j.apcata.2013.04.038
40. Loipersböck J, Lenzi M, Rauch R, Hofbauer H (2017) Hydrogen production from biomass: the behavior of impurities over a CO shift unit and a biodiesel scrubber used as a gas treatment stage. Korean J Chem Eng 34(8):2198–2203. https://doi.org/10.1007/s11814-017-0130-1
41. Seemann MC, Schildhauer TJ, Biollaz SMA (2010) Fluidized bed methanation of wood-derived producer gas for the production of synthetic natural gas. Ind Eng Chem Res 49(15):7034–7038. https://doi.org/10.1021/ie100510m
42. Witte J, Settino J, Biollaz SM, Schildhauer TJ (2018) Direct catalytic methanation of biogas – part I: new insights into biomethane production using rate-based modelling and detailed process analysis. Energy Conv Manag 171:750–768. https://doi.org/10.1016/j.enconman.2018.05.056
43. Rehling B (2012) Development of the 1MW Bio-SNG plant, evaluation on technological and economical aspects and upscaling considerations. Dissertation, TU Wien, Vienna. https://permalink.catalogplus.tuwien.at/AC07815367. Accessed 23 May 2023
44. Schweitzer D, Gredinger A, Schmid M, Waizmann G, Beirow M, Spörl R, Scheffknecht G (2018) Steam gasification of wood pellets, sewage sludge and manure: Gasification performance and concentration of impurities. Biomass Bioenerg 111:308–319. https://doi.org/10.1016/j.biombioe.2017.02.002

C.5 Paper V

Economic and ecological impacts on the integration of biomass-based SNG and FT diesel in the Austrian energy system

Hammerschmid, M., Bartik, A., Benedikt, F., Veress, M., Pratschner, S., Müller, S., Hofbauer, H., *Energies*, **2023**, Vol. 16(16), 6097, https://doi.org/10.3390/en16166097.

energies

MDPI

Article

Economic and Ecological Impacts on the Integration of Biomass-Based SNG and FT Diesel in the Austrian Energy System

Martin Hammerschmid *, Alexander Bartik, Florian Benedikt, Marton Veress, Simon Pratschner, Stefan Müller and Hermann Hofbauer

Institute of Chemical, Environmental and Bioscience Engineering, TU Wien, Getreidemarkt 9/166, 1060 Vienna, Austria

* Correspondence: martin.hammerschmid@tuwien.ac.at

Abstract: The production of sustainable, biomass-based synthetic natural gas (SNG) and Fischer–Tropsch (FT) diesel can contribute significantly to climate neutrality. This work aims to determine the commercial-scale production costs and CO_2 footprint of biomass-based SNG and FT diesel to find suitable integration scenarios for both products in the Austrian energy system. Based on the simulation results, either 65 MW SNG and 14.2 MW district heat, or 36.6 MW FT diesel, 17.6 MW FT naphtha, and 22.8 MW district heat can be produced from 100 MW biomass. The production costs with taxes for wood-based SNG are 70–91 EUR /MWh and for FT diesel they are 1.31–1.89 EUR /L, depending on whether pre-crisis or crisis times are considered, which are in the range of fossil market prices. The CO_2 footprint of both products is 90% lower than that of their fossil counterparts. Finally, suitable integration scenarios for SNG and FT diesel in the Austrian energy system were determined. For SNG, use within the energy sector for covering electricity peak loads or use in the industry sector for providing high-temperature heat were identified as the most promising scenarios. In the case of FT diesel, its use in the heavy-duty traffic sector seems most suitable.

Keywords: gasification; methanation; Fischer–Tropsch; simulation; techno-economic assessment; CO_2 footprint

Citation: Hammerschmid, M.; Bartik, A.; Benedikt, F.; Veress, M.; Pratschner, S.; Müller, S.; Hofbauer, H. Economic and Ecological Impacts on the Integration of Biomass-Based SNG and FT Diesel in the Austrian Energy System. *Energies* **2023**, *16*, 6097. https://doi.org/10.3390/en16166097

Academic Editors: Elem Patricia Alves Rocha, Clara Mendoza Martinez and Esa Kari Vakkilainen

Received: 4 July 2023
Revised: 7 August 2023
Accepted: 14 August 2023
Published: 21 August 2023

1. Introduction

The increasingly visible climate change around the world requires sustainable solutions. The European Green Deal [1] aims to set the path to Europe's climate neutrality by 2050. Currently, only approximately 20% of Europe's gross final energy consumption is covered by renewable energy sources (RES). In Austria, even more ambitious targets are being set for climate neutrality by 2040. Considering the RES share of 36.5% based on Austria's gross final energy consumption, sustainable solutions in the whole energy system must be found quickly. The most considerable proportion of greenhouse gas emissions are caused by generating electricity, heat, cold, and fuels using fossil feedstocks like natural gas, coal, and mineral oil [2].

In addition to already proven renewable technologies, such as solar PV, wind power, hydropower, and heat pumps using environmental heat, bioenergy can contribute significantly to achieving climate neutrality. The most significant advantage of bioenergy is that there is great potential, especially in Austria, to produce the required energy sources, such as electricity, heat, and fuels, with domestic raw materials. The use of lignocellulosic biomass in the heat and power sector has already been proven for decades. Furthermore, oil crops have been used to produce biodiesel for many years. Sugar and starch crops are used within fermentation plants to produce bioethanol. Additionally, sugar and starch crops can be fed together with biodegradable municipal solid waste to anaerobic digestion plants to generate heat, power, and biomethane. Gasification technologies play a crucial role in

expanding the range of bioenergy products [3]. At TU Wien, dual fluidized bed (DFB) gasification technology has been investigated for decades. It has been proven that this technology is suitable for use with a wide range of raw materials. Almost all lignocellulosic biomass and significant parts of biogenic residues can be converted to high-quality product gas, mainly consisting of hydrogen, carbon monoxide, carbon dioxide, and methane. After purification of the produced gas, it can be converted into high-value products such as hydrogen, synthetic fuels, synthetic natural gas, or platform chemicals in addition to electricity and heat production in a gas engine or gas turbine [4].

In 2002, the first demo plant based on DFB gasification technology for the production of heat and power based on woody biomass went into operation in Güssing (AT), with a thermal fuel power of 8 MW_{th}. In the following 15 years, more than 100,000 h of operation were achieved. This successful demonstration resulted in the construction of further commercial plants on a scale of 3.8 to 15.5 MW_{th} in Oberwart (AT), Villach (AT), Senden (DE), Nongbua (TH), and Wajima (JP) in the last two decades. Many plants have been forced to shut down recently due to high production costs for heat and electricity using high-quality wood chips. As a result, research work in recent years has been focusing on using lower-grade feedstocks [5] and producing higher-grade synthesis products such as synthetic natural gas (SNG) [6] or Fischer–Tropsch (FT) diesel. In 2009, the world's first fluidized bed methanation pilot plant, with a SNG power of 1 MW_{SNG}, was integrated into the existing DFB plant in Güssing. The largest DFB plant to date, with a scale of 33 MW_{th}, was commissioned in Gothenburg (SE) in the frame of the GoBiGas project in 2013 [7]. In the GoBiGas project, the product gas was used to produce 20 MW SNG in a fixed-bed methanation synthesis process. In 2022, a DFB plant using lower-grade feedstocks with a scale of 1 MW_{th} was commissioned in Vienna (AT) at a waste processing location. Additionally, the product gas in Vienna can be converted in a FT slurry reactor to FT products [8–10]. Due to the large number of DFB facilities, nearly 200,000 industrial operating hours could be collected, demonstrating the DFB gasification process. Therefore, the DFB gasification process itself has already reached the commercial scale. The DFB demo plant in Vienna helps to test and investigate the use of lower-grade feedstocks in an industrial operational environment, thereby increasing the technological readiness level. From a scientific and technical point of view, fixed-bed methanation has been successfully demonstrated in Gothenburg. However, the Gothenburg plant was forced to shut down for economic reasons. Alternatively, fluidized bed methanation can be used for SNG production with the advantage that, instead of a multi-stage fixed bed methanation, only a single-stage fluidized bed methanation unit is required for the production of the desired raw-SNG. To commercialize fluidized bed SNG and FT diesel production based on product gas from DFB gasification, a further demo plant in an operational environment, covering the process from biomass supply until product use, is required to check the findings of the pilot plants in long-term test runs [11].

Based on a study from TU Wien [11], the Austrian Government decided to fund the establishment of a 5 MW_{th} demonstration plant for the biomass-based production of SNG and FT diesel. With the help of this demo plant, the remaining knowledge gaps in terms of long-term behavior should be closed. The findings should be used to promote the commercialization of DFB technology in connection with SNG and FT diesel production in Austria. Numerous researchers have investigated the technical feasibility of the primary process units of the assessed process routes. The technical feasibility of the DFB gasification process with different feedstocks, bed materials, and gasification temperatures has been investigated intensively at the pilot scale [4,5,12]. Additionally, it was demonstrated at the pilot scale that DFB gasification, coupled with oxyfuel combustion, can capture an almost pure CO_2 stream in the flue gas in addition to a high-quality product gas [13–15]. Furthermore, intensive development work has already been carried out concerning the layout and design of DFB plants [16]. Moreover, the large-scale demonstration of DFB plants [7] and studies on their implementation in existing industries [17] have been executed. Furthermore, the necessary gas cleaning steps following the gasification process have been

successfully demonstrated [18,19]. The experimental validation and demonstration of the methanation unit [6,20–22] and FT synthesis [23–27] have also been conducted.

Summing up, the technical feasibility of the production of biomass-based SNG and FT diesel has been proven. After the first operation phase with the 5 MW_{th} demo plant, the remaining knowledge gaps can be clarified, and commercialization can start. Assessments for similar process routes regarding the production costs [28,29] and the CO_2 footprint [29,30] have been conducted and presented in the literature. However, neither a techno-economic nor an environmental analysis have been performed yet based on, from the current view, optimized commercial-scale concepts with the goal of reaching the status of drop-in fuels according to the Austrian gas grid feed-in guidelines [31] and synthetic fuel standards [32]. This analysis is urgently needed to determine a suitable integration strategy for the two products in the Austrian energy system. Furthermore, the investigation of energy system integration scenarios allows us to study socio-economic impacts such as sectoral competitiveness.

For this reason, this paper investigates commercial-scale concepts for producing wood-based SNG and FT diesel at a thermal fuel power of 100 MW for integration in the Austrian energy system. In detail, the paper discusses the following sections:

- Potential analysis of biogenic feedstock suitable for DFB gasification in Austria;
- Modelling of commercial scale concepts for the production of biomass-based SNG and FT diesel;
- Techno-economic and ecological assessment of both routes;
- Development of integration scenarios for biomass-based SNG and FT diesel in the Austrian energy system.

Based on the developed commercial scale concepts, the mass and energy balances of both process routes are calculated. The simulation results are the basis for determining the production costs and CO_2 footprints. To consider the economic impact of the crises arising from the Ukrainian war and COVID-19 on the Austrian energy market, the techno-economic analyses are based on the reference years 2019 (pre-crisis level) and 2022 (crisis level). With the help of the production costs, the CO_2 footprint, and the Austrian biomass potential, the substitution possibilities, the influence on the sectoral greenhouse gas emissions, and the sectoral gross value added can be calculated. Finally, suitable integration scenarios can be proposed for using biomass-based SNG and FT diesel in the Austrian energy system. Concluding, based on existing literature, the paper provides a novel comprehensive techno-economic and ecological assessment of the commercial-scale production of biomass-based SNG and FT diesel with the aim of reaching the status of drop-in fuels according to the Austrian gas grid feed-in guidelines and synthetic fuel standards. Thus, the techno-economic and ecological impact on various Austrian energy sectors can be calculated by substituting fossil natural gas and diesel with biomass-based SNG and FT diesel.

2. Materials and Methods

In the following section, all applied methods are discussed. The biomass potential analysis builds the basis for defossilization capacities in the Austrian energy system. Furthermore, commercial scale concepts are presented to provide information approximately assumptions within the process simulation. Additionally, the methodologies for the techno-economic and ecological assessment are explained. Finally, scenarios for integrating biomass-based SNG and FT diesel into the Austrian energy system are discussed.

2.1. Potential Analysis of Biogenic Feedstock

For the discussion of the integration possibilities of DFB plants into the Austrian energy system, it is necessary to determine the biomass potential for such plants in Austria. The evaluation of the biomass potential until 2050 is based on studies from the Austrian biomass association [33], the feasibility study "Reallabor" [11], and studies from Dißauer et al. [34] and Hammerschmid et al. [35]. A fluidized bed gasifier is able to process various raw and residual materials since fluidized beds have proven to be robust and fuel-flexible

for the thermo-chemical conversion of various feedstocks [4,5,11]. The following defined biomass potentials refer to the year 2050 and can be understood as reduced technical potentials [35,36]. The reduced technical potential in 2050 can be seen as the additional amount of biomass made available by political and social changes and efforts without endangering sustainable agriculture and forestry. Table 1 lists the technical biomass potential from different literature studies. The value for woody biomass ranges between 50–126 PJ/a, including forest biomass, bark, and sawmill by-products. Thus, a reduced technical potential of 75 PJ/a is assumed in this study. A range of 100–200 PJ/a can be determined for the technical biomass potential of agricultural raw materials and residues, which comprise short-rotation wood, straw, beet leaves, corncobs, grapevine pruning, and miscanthus within this study. The available values of the mentioned studies are partly based on very ambitious expansion targets for short-rotation wood and miscanthus. Furthermore, ambitious targets for the energetic utilization of straw were adopted. To ensure sustainable agriculture, a lower reduced technical potential of 80 PJ/a is assumed for the present study. Furthermore, the technical biomass potential of other biogenic residues and waste are investigated, including waste wood, sewage sludge, manure, and biogenic rejects from several industries. The mentioned studies list an additional technical biomass potential of 10–67 PJ/a, which corresponds to a reduced technical biomass potential of 30 PJ/a.

Table 1. Analysis of reduced technical biomass potential in 2050.

Property Classes and Components	Additional Technical Biomass Potential 2050 (Study Dißauer et al. [34])	Additional Technical Biomass Potential 2050 (Study Biomass Association [33])	Additional Technical Biomass Potential 2050 Scenario "High" and "Biomasse Max" (Study Kranzl et al. [37])	Additional Reduced Technical Biomass Potential 2050 (Present Study)
Woody biomass	126 PJ/a	50 PJ/a	110 PJ/a	75 PJ/a
Agricultural raw materials and residues	126 PJ/a	200 PJ/a	100 PJ/a	80 PJ/a
Other biogenic residues and waste	67 PJ/a	50 PJ/a	10 PJ/a	30 PJ/a

In total, an additional reduced technical biomass potential of 185 PJ/a is defined within this potential analysis based on literature values. Additionally, the potential analysis in [11] showed that a plant size of 100 MW_{th} builds up a good compromise between low specific investment costs due to economy of scale and sustainable biomass procurement. At this point, it must be mentioned again that, in any case, attention must be paid to sustainable agricultural and forestry management.

2.2. Commercial Scale SNG and FT Production Concepts

The underlying commercial-scale process concepts of the FT diesel and SNG routes are presented as a basis for the techno-economic and ecological assessment and scenarios for technology roll-out. The conceptual design of the biomass-based FT diesel and SNG route described in this chapter is based on experience through the operation of laboratory, pilot, and demonstration plants. Furthermore, commercial DFB plants were scientifically monitored. The scalability of all the investigated individual process units has already been demonstrated in other applications, at least on a demonstration scale.

Figure 1 depicts the proposed process routes for producing SNG and FT products from woody biomass on a 100 MW_{th} scale. The process flowsheet is divided into four main sections: resource supply, gasification, gas cooling, cleaning, and synthesis, and gas upgrading. Both process routes only differ in the synthesis and gas upgrading steps, depending on the desired product. Otherwise, the same process layout can be utilized,

which reduces the engineering efforts for both routes. Note that the process routes are meant as standalone SNG or FT production routes and are only displayed together to save space and showcase their similarity. Furthermore, only the main process units are shown in the simplified process flow diagram (PFD). Heat displacement and regeneration steps are omitted for better legibility. Process simulation of this flow sheet was performed with the process simulation software IPSEpro 8.0. The process simulation is based on wood chips as the fuel. The assumed biomass composition can be found in the Supplementary Materials. Furthermore, no variations were considered with regard to fuel. However, experiments have shown that the main components of the resulting product gas hardly change, but the impurities vary strongly due to the fuel variation [5]. Consequently, more impurities in the product gas would require a more extensive product gas cleaning section. Moreover, research is still needed for the large-scale use of low-grade fuels such as sewage sludge in DFB gasification. Therefore, the developed plant concept only applies to woody biomass. A detailed list of the assumptions and process parameters used for the simulation is shown in the Supplementary Materials.

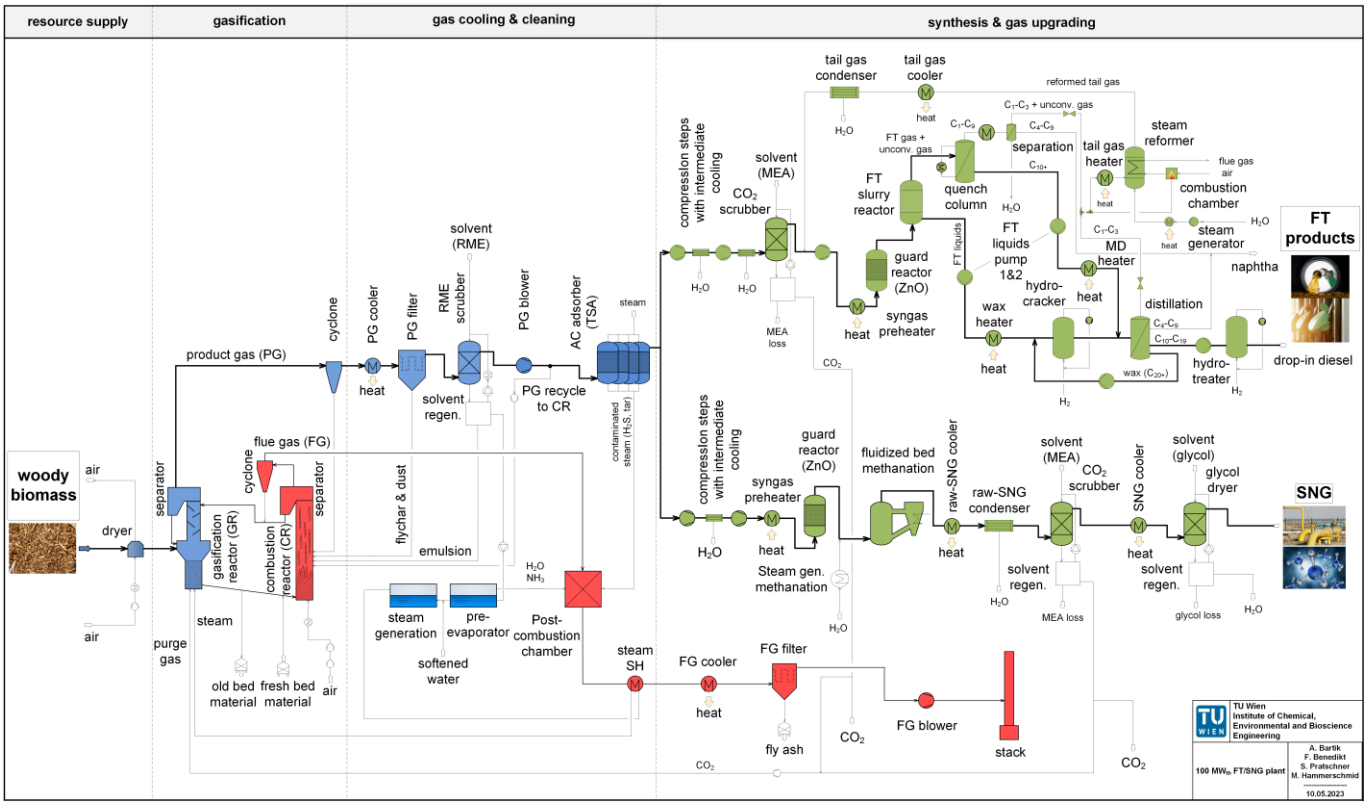

Figure 1. Simplified process flow diagram of the 100 MW_{th} FT and SNG routes (note: FT and SNG production are standalone routes but are displayed together in this picture).

The resource supply section consists of the on-site fuel handling and storage, as well as a dryer to reduce the moisture content of the fuel to an optimal and constant level for gasification, which is approximately 20%. In this study, the considered fuel is woody biomass (cf. Section 2.1).

The heat required for drying is supplied internally through heat displacement. The gasification section at approximately 820 °C is based on the advanced DFB steam gasification technology, utilizing a mixture of olivine and limestone as a bed material (80/20 wt.%) in contrast to the classical, industrially proven DFB steam gasification. The product gas, which mainly consists of H_2, CO, CO_2, CH_4, and H_2O, leaves the gasification reactor and is cooled to 180 °C in heat exchangers (PG cooler). In the coarse gas cleaning section, dust is removed in a baghouse filter (PG filter) and tars are separated in a biodiesel scrubber

at 40 °C based on the solvent rapeseed methyl ester (RME). Additionally, water vapor condenses in the biodiesel scrubber and enables the separation of water-soluble substances from the product gas, like ammonia (NH_3). The tar-rich RME and the condensed water are directed into a phase separator (solvent regen). Here, the liquid separates into a clear RME phase, an emulsion phase, and a water phase. The clear RME phase is recirculated to the scrubber, while the water phase is evaporated, superheated, and reused as a gasification agent in the gasification reactor. In this way, the freshwater consumption of the DFB system is reduced. The emulsion phase consists of a mixture of RME, absorbed tars, and water, and is utilized as additional fuel in the combustion reactor. Downstream of the biodiesel scrubber, part of the product gas is recirculated to the combustion reactor to provide the necessary heat for gasification. This way, there is no need for an external fuel supply to the combustion reactor during the process. In the fine gas cleaning section, all remaining impurities that harm the catalysts during the synthesis processes and are unwanted in the final product are removed. Activated carbon filters (AC filters) remove light aromatic compounds such as benzene, toluene, or naphthalene, as well as sulfur compounds such as hydrogen sulfide (H_2S). The activated carbon filters are operated through temperature swing adsorption (TSA), and the regeneration is carried out with steam at 250 °C [38]. The contaminated steam is disposed of in the post-combustion chamber. At this point, the requirements of the FT and SNG processes, and, therefore, the process chains, start to differ.

For the SNG route, the product gas is compressed to 10 bar in a two-stage inter-cooled compressor and preheated to 250 °C. ZnO acts as a protection layer against sulfur breakthrough. The conversion of syngas to raw-SNG takes place in a cooled fluidized bed methanation reactor at 320 °C in the presence of a nickel catalyst. A thermodynamic equilibrium model is used for this stage. After heat recovery, a condenser separates water from the raw SNG, and the gas enters an amine scrubber for CO_2 removal. The condensed water is fully reused within the process, e.g., for steam regeneration of the activated carbon or for steam addition upstream of the methanation reactor. In the last step, the gas is dried in a glycol scrubber and transferred to the natural gas grid following the specifications of the Austrian gas grid (ÖVGW G B210 [31]).

The product gas is compressed in three stages to 21 bar for the FT route. After the second compression step, CO_2 is removed in an amine scrubber at 10 bar, and recycled tail gas from the steam reformer is added to the product gas stream. Similar to the SNG route, the syngas is preheated, passes a ZnO guard bed and enters a FT slurry reactor at 230 °C. For the simulation of the FT reactor, the extended Anderson–Schulz–Flory distribution from Förtsch et al. [39], with modeling parameters according to Pratschner et al. [40], and a single-pass CO conversion of 50% are assumed. Liquid FT products are withdrawn from the slurry reactor and pumped into a hydrocracker. The hydrocracker converts long-chain FT products with hydrogen on a platinum catalyst to shorter molecules and thus increases the output of the desired diesel fraction. A consecutive distillation separates the product from the hydrocracker into different molecular weight fractions. Gaseous molecules (C_1–C_3) are directed to the steam reformer, and C_4–C_9 molecules are sold as a naphtha fraction to a refinery. Long-chain waxes (C_{20+}) are recycled to the hydrocracker and converted to low-boiling hydrocarbons (C_1–C_{19}). The properties of the desired diesel fraction (C_{10}–C_{19}) are further adjusted in a hydrotreater, allowing the production of drop-in diesel fuel with similar properties to its fossil counterpart, according to DIN EN 15940 [32]. The gaseous phase leaving the FT slurry reactor consists of molecules with different chain-lengths and unconverted syngas. Thus, a quench column condenses C_{10+} hydrocarbons pumped to the fractional distillation. A further condensation step separates a naphtha fraction from the remaining gas. C_1–C_3 molecules and unconverted syngas are brought to a steam reformer to reclaim CO and H_2. The necessary heat for the steam reformer is provided through the combustion of a partial flow (15%) of the gas itself. The reformed tail gas is then reintroduced to the process upstream of the FT slurry reactor for further conversion.

Furthermore, CO_2 and district heat are generated as side products from these processes. Additionally, for the FT route, a naphtha fraction can be sold to the refinery. CO_2 is a main

component in the product gas and is separated in amine scrubbers with an assumed purity of 95%. After upgrading, the CO_2 is sold and creates additional revenues. District heat is a result of the thermal nature of the involved processes. Heat sources and sinks are matched in this study so that no external heat supply is required. Nevertheless, heat at temperature levels above 100 °C remains, which can be utilized as district heat and create additional revenues. The processes also generate water at various steps along the process chains (e.g., RME scrubber, condensation steps, etc.), which is assumed to be internally reused for steam production (e.g., gasification agent, regeneration of activated carbon, etc.). Because of the water and hydrogen content of the biomass, typically more water is produced than consumed. Therefore, wastewater disposal costs are included for the effluent streams. However, a potentially necessary water upgrading for the internally recycled water is neglected. For the DFB gasification process itself, the internal use of steam as a gasification agent from the condensed water phase from the RME scrubber, with pre-evaporation to remove unwanted impurities via the post-combustion chamber, is industrially proven.

2.3. Techno-Economic and Ecological Assessment

The techno-economic and ecological assessment is performed based on the process simulation of the biomass-based SNG and FT diesel route. The techno-economic investigation follows the net present value method, which analyzes a pending investment by discounting future payments and revenues to the present. The levelized costs of products (*LCOP*) in terms of synthetic natural gas and FT diesel are calculated according to Equation (1). Thus, the *LCOP* are influenced by the total capital investment costs of the plant (I_0), the annual expenditures (E), the annual revenues of secondary products ($R_{sec.\ prod.}$), and the annual quantity of the produced main product ($M_{t,main\ prod.}$). The discounting of the revenues, expenditures, and the annual quantity of the produced main product is considered using the cumulative discount factor (*CDF*) according to Equation (2), which is a function of the interest rate (i) and the plant lifetime (n) [41–44]. The total capital investment costs of the biomass-based SNG and FT diesel route with a 100 MW_{th} thermal fuel power scale are based on the visualized methodology in Figure 2. For the techno-economic assessment, the process route is divided into two sections. The first plant section, from the biomass feeding system until the primary product gas cleaning, has been built already several times worldwide at a commercial scale with a plant size from 8–32 MW_{th} [11]. According to the order of magnitude method [11,45], the inflation-adjusted total capital investment costs of the plants in Güssing, Oberwart, and Senden are used to determine the total capital investment costs of an average DFB plant with a thermal fuel power of 15 MW_{th}. The final total capital investment costs for a 100 MW_{th} scale for the first plant section are calculated using the cost-scaling method [11] according to Equation (3). The total capital investment costs of the second plant section are calculated via the cost-scaling of inflation-adjusted literature values according to Equation (3). The purchased equipment costs are multiplied by a Lang factor of 4.87 for solid-fluid-processing plants, according to Peters et al. [46], to consider all additional costs like instrumentation and control, piping, or electrical equipment. The expenditures and revenues are calculated based on simulation results and cost rates for all operating utilities. Two base years for calculating the *LCOP* for SNG and synthetic FT diesel are selected, namely 2019 and 2022. The year 2019 provides an investigation concerning the pre-crisis level. The increased energy prices after COVID-19 and the Ukraine war are reflected by the base year 2022. For the SNG process route, the expenditures are compensated by the revenues from the sale of district heat and captured CO_2. In the FT process route, naphtha is produced as a by-product in addition to CO_2 and district heat. Additionally, the resulting *LCOP* values are based on a plant lifetime of 20 years. Further details on calculating the total capital investment costs and the considered cost rates and assumptions for the techno-economic assessment are summarized in the Supplementary Materials.

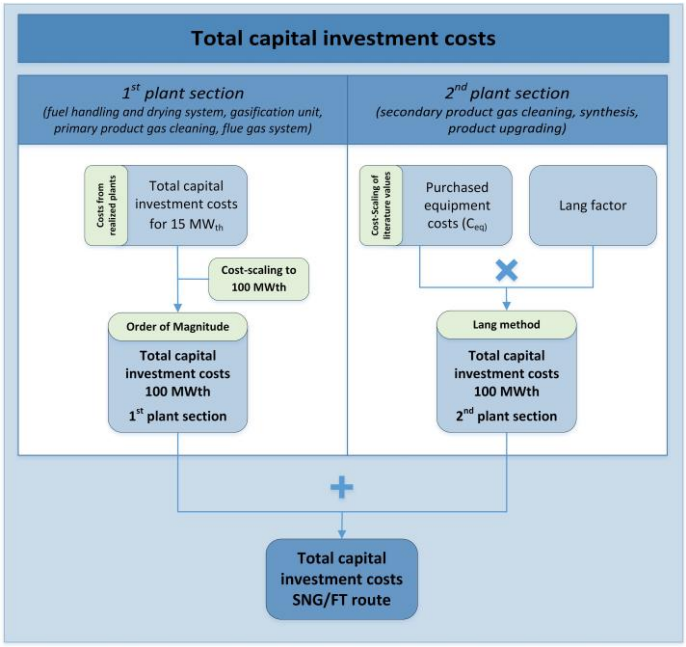

Figure 2. Methodology for the calculation of total capital investment costs [11,45].

The resulting *LCOP*s for both routes are compared with the market prices of their fossil equivalents and *LCOP*s of alternative renewable routes. Finally, a sensitivity analysis is conducted to analyze the influences of assumed cost rates on the resulting *LCOP* values. For further details on the determination of the *LCOP*, a reference is made to [46]

$$LCOP = \frac{I_0 + \left(E - R_{sec.prod.}\right) \cdot CDF}{M_{t,main\ prod.} \cdot CDF} \quad (1)$$

$$CDF = \frac{(1+i)^n - 1}{i \cdot (1+i)^n} \quad (2)$$

$$C_{eq,design} = C_{eq,base} * \left(\frac{S_{design}}{S_{base}}\right)^r * Z * \left(\frac{CEPCI_{base\ year}}{CEPCI_{\frac{2019}{2022}}}\right) \quad (3)$$

Additionally, an ecological assessment of both process routes is conducted to analyze the CO_2 footprint of the produced synthetic products. The process balance boundaries are defined by a Well-to-Tank approach [47,48]. The calculation of greenhouse gas emissions is based on the unit CO_2 equivalents (CO_2e) in order to achieve a standardization of the climate impact of different greenhouse gases. Therefore, the CO_2 footprint of both process routes is determined by calculating the direct and indirect greenhouse gas emissions of the main utilities, including the built-in steel and concrete, via ecological factors. The ecological factors are mainly based on databases from the Federal Environmental Agency of Austria [49], Germany [50], and the database of the software tool GEMIS 5.0 [51]. For the ecological factor of the consumed electricity, it is assumed that green electricity is used [49]. In accordance with the IEA [49], the energy allocation method was applied to allocate the resulting absolute CO_2e emissions to the primary and secondary products. The functional unit for the techno-economic and ecological assessment is MWh_{SNG} for the SNG route and l_{Diesel} for the FT route. At this point, it must be mentioned that for a holistic life cycle assessment of the two biomass-based products, many other ecological factors such as acidification potential, eutrophication, and land use have to be considered in addition to the CO_2 footprint. Further details on calculating the ecological footprint are summarized in the Supplementary Materials.

2.4. Scenarios for Integrating Biomass-Based SNG and FT Diesel in the Austrian Energy System

The techno-economic and ecological assessment of the 100 MW biomass-based SNG and FT route form the basis for discussing the scenarios for integrating biomass-based SNG and FT diesel into the Austrian energy system. The techno-economic assessment explained in Section 2.3 is based on woody biomass. Other feedstocks like energy crops, straw, or sewage sludge are mostly cheaper than woody biomass. However, the more complex gas cleaning process in the case of non-woody biomass also induces higher investment and operating costs. Furthermore, the ecological assessment is also based on woody biomass. The use of different feedstocks influences the resulting CO_2 footprint. Nevertheless, for the following scenarios, the whole biomass potential from the potential analysis is considered, assuming that the production costs and CO_2 footprint of SNG and FT diesel remain constant independent of the feedstock. In total, six scenarios for integrating drop-in FT diesel or SNG into the Austrian energy system are discussed. The underlying demand for natural gas and diesel is based on 2021 [2,52]. Below, the scenarios considered are explained, showing the broad integration possibilities of the two products.

(a) SNG use in the energy sector

The first scenario is based on the use of SNG in the energy sector for defossilization of existing heat, combined heat and power, and power plants. Due to the increasing share of fluctuating renewable energy sources in the Austrian power grid, further flexibility options have to be installed to ensure the security of supply. On the one hand, this can be achieved through the increased interconnection to the European power grid with corresponding national grid reinforcement and grid expansion projects, as well as the installation of additional storage facilities [53]. On the other hand, existing gas-fired power plants could be retained for peak load coverage and still be defossilized with SNG. Additionally, gas-fired heat plants based on biomass-based SNG can decrease the CO_2 footprint of existing district heating systems directly. Within this scenario, the natural gas consumption from the energy sector is completely substituted with biomass-based SNG based on industry prices. The defossilization potential assumes that the natural gas consumption in the energy sector remains constant until 2050.

(b) SNG use in the private and public sector (without mobility)

In the second scenario, the use of SNG in the private and public sector is considered, which means that existing gas boilers in private households, public and private services, and aggregates in the agriculture and forestry sector are retained and driven by biomass-based SNG. Of course, renewable heat supply in the private sector can also be achieved via other technologies, such as heat pumps or solar thermal, but the necessary high inlet temperatures in old apartments, as they are found in Vienna, can only be achieved satisfactorily by district heat or wood-fired boilers [54]. Therefore, the defossilization of existing gas infrastructure in the public and private sector using biomass-based SNG can also contribute to a sustainable energy system. The following techno-economic assessment in this scenario is based on household prices. The defossilization potential assumes that the natural gas consumption in this sector remains constant until 2050.

(c) SNG use in the industry

The third scenario for integrating biomass-based SNG in the Austrian energy system is integration in the manufacturing sector. Natural gas in burners is used in different sectors like the chemical, pulp and paper, cement, or steel industries to provide high-temperature heat for several production processes. Integrating biomass-based SNG in the industry would be an easy way to provide the necessary high-temperature heat without any changes in the current utilized process chains [55]. Furthermore, the material use of natural gas in the industry sector could be easily substituted with biomass-based SNG. The techno-economic assessment in this scenario is based on industry prices. The defossilization potential assumes that the natural gas consumption in the industry sector remains constant until 2050.

(d) FT diesel in private and public transport

Therein, the use of biomass-based FT diesel as drop-in fuel in conventional diesel cars and buses is considered. For evaluating the defossilization potential, it is assumed, according to [35], that the number of diesel cars and the associated diesel demand will be reduced by half until 2050. The number of diesel buses will remain constant until 2050. The techno-economic assessment in this scenario is based on petrol station market prices for private consumers.

(e) FT diesel in heavy-duty traffic

The fifth scenario is based on integrating biomass-based FT diesel in the heavy-duty traffic sector. In this sector, freight transport with light and heavy commercial vehicles (LCV and HCV) and the diesel demand in agriculture and forestry is considered. Furthermore, the diesel demand for inland navigation and railway is discussed. For calculating the defossilization potential in this scenario, it is assumed that the number of LCVs will be reduced, simultaneously with the number of cars, by half until 2050 [35]. The number of diesel-driven HCVs, tractors, ships, and trains will remain constant until 2050 [35]. For the techno-economic assessment, the mean value of the petrol station market price for private consumers and the stock market diesel price is considered.

(f) FT diesel in heat and power

Finally, the sixth scenario includes the integration of FT diesel in the heat and power sector. Therein, the diesel demand in the manufacturing and the public and private sectors is considered. Similar to the use of SNG in industry, FT diesel can provide high-temperature heat. The diesel demand in the public and private service sectors can be mainly attributed to, e.g., emergency diesel aggregates in hospitals and other critical infrastructure. The diesel demand in the manufacturing sector is assumed to remain constant until 2050, whereas a reduction by half is assumed for the public and private sector due to a substitution with other renewable technologies [35]. The techno-economic assessment is based on the stock market diesel price.

These six scenarios are further investigated and compared to discuss the techno-economic and ecological impact of each integration possibility. Therefore, the natural gas and diesel demand in 2050 is estimated in all sectors and compared with the SNG and FT diesel potential. Furthermore, the CO_2 reduction potential ($CO_2e_{red,sector\ i}$) through the substitution of natural gas with SNG or fossil diesel with FT diesel is investigated in each scenario (see Equation (4)). For this, the annual amount of sectoral used gas or diesel ($E_{gas/diesel,sector\ i}$) is multiplied by the difference in CO_2 footprints between the renewable biomass-based product and its fossil counterpart (FP) and divided by the absolute annual CO_2 emissions in the respective sector ($CO_2e_{tot,sector\ i}$). Finally, the techno-economic comparison between the SNG and FT diesel production costs with the market prices (MP) of the fossil counterpart shows the economic competitiveness (EC) of both products (see Equation (5)). The comparison of the total additional costs or savings per year with the gross value added (GVA) shows the economic impact in the respective sector. The GVA is calculated from the gross production values achieved, reduced by all advance outlays. Simplified, GVA could be described as a company's revenue minus expenses for all kinds of utilities. The resulting GVA is ultimately shared among all the stakeholders involved, namely the employees, the company owners, and the state. Consequently, the EC determines the percentage by which the sectoral GVA or, in approximation, the profit changes as a result of switching to biomass-based SNG or FT diesel.

$$CO_2e_{red,sector\ i} = \frac{E_{gas/diesel,sectori} * \left(FP_{fos.gas/diesel} - FP_{SNG/FTdiesel}\right)}{CO_2e_{tot,sectori}} \quad (4)$$

$$EC_{sector\ i} = \frac{E_{gas/diesel,sectori} * \left(MP_{fos.gas/diesel} - LCOP_{SNG/FTdiesel}\right)}{GVA_{total,sector\ i}} \quad (5)$$

Finally, alternative options for using SNG and FT diesel are discussed, which can contribute to a sustainable energy system in the individual sectors. Consequently, in addition to a quantitative comparison of the individual scenarios based on techno-economic and ecological footprints, a qualitative comparison of possible alternatives can be used to find the most suitable application for SNG and FT diesel.

3. Results and Discussion

In this chapter, all results are visualized and discussed. First of all, the input and output streams of both commercial scale routes for producing wood-based SNG and FT diesel with a thermal fuel power input of 100 MW_{th} are determined. Then, the techno-economic and ecological competitiveness of each route, regarding levelized production costs and CO_2 footprints, is assessed. Finally, the integration of biomass-based SNG and FT diesel in several sectors of the Austrian energy system is discussed.

3.1. Input- and Output Streams of Commercial SNG and FT Production Plants

In Section 2.2, the commercial scale concepts for both investigated routes were presented. Based on these concepts, the process simulation results in terms of input and output streams for both routes are presented in this chapter. In Table 2, the input and output streams for the production of wood-based SNG based on 100 MW_{th} scale are summarized. Thus, it can be concluded that approximately 65 MW of SNG can be generated from 100 MW_{th} woody biomass. In addition, approximately 14.2 MW of district heat and 6150 Nm^3/h of CO_2 for storage or utilization can be recovered.

Table 2. Input and output streams for producing wood-based SNG related to a thermal fuel power of 100 MW.

Plant Input			Plant Output		
Input Stream	**Unit**	**Value**	**Output Stream**	**Unit**	**Value**
Biomass (wood)	kg/h	33,250	Synthetic natural gas	Nm^3/h	6840
	$kW_{before\ drying}$	94,360		kW	64,960
	$kW_{after\ drying}$	100,000	District heat	kW	14,170
Fresh bed material (80% olivine and 20% limestone)	kg/h	150	Captured CO_2 for storage or utilization	Nm^3/h	6150
Fresh scrubber solvent (rapeseed methyl ester)	kg/h	110	Ash and dust	kg/h	350
Fresh amine (monoethanolamine)	kg/h	18.4	Waste water	kg/h	320
Fresh glycol	kg/h	0.1			
Electricity	kW	4340			

Table 3 shows the input and output streams for the production of wood-based FT diesel based on a 100 MW_{th} scale. Therein, it can be seen that through the gasification of woody biomass with subsequent gas cleaning, FT synthesis, and FT upgrading, approximately 36.6 MW of drop-in FT diesel can be produced. Additionally, 22.8 MW district heat, 17.6 MW FT naphtha, and 3790 Nm^3/h of CO_2 can be recovered.

In comparison, the SNG process yields a higher energetic efficiency than the FT process. About 79% of the chemical energy from the woody biomass can be transferred to SNG and district heat, whereas 77% is found in FT diesel, naphtha, and district heat. Furthermore, more CO_2 needs to be captured in the SNG process due to a higher CO_2 capture rate and less carbon in the product per molecule of CH_4 compared to FT products. Thus, more amine is also needed for the scrubber. In the FT process route, more electricity is required to reach higher synthesis pressure levels. Additionally, hydrogen is needed to upgrade FT products in the hydrocracker and hydrotreater. The presented simulation results are the basis for the calculation of the techno-economic and ecological results.

Table 3. Input and output streams for producing wood-based FT diesel related to thermal fuel power of 100 MW.

Plant Input			Plant Output		
Input Stream	**Unit**	**Value**	**Output Stream**	**Unit**	**Value**
Biomass (wood)	kg/h	33,250	FT diesel	L/h	3850
	$kW_{before\ drying}$	94,360		kW	36,563
	$kW_{after\ drying}$	100,000	FT naphtha	L/h	2000
Fresh bed material (80% olivine and 20% limestone)	kg/h	150		kW	17,561
Fresh scrubber solvent (rapeseed methyl ester)	kg/h	110	District heat	kW	22,823
Fresh amine (monoethanolamine)	kg/h	11.5	Captured CO_2 for storage or utilization	Nm^3/h	3790
Hydrogen (for hydrocracking and hydrotreating)	kg/h	26.3	Ash and dust	kg/h	350
Electricity	kW	6120	Waste water	kg/h	2635

3.2. Techno-Economic Results of Commercial SNG and FT Production Plants

Based on the simulation results, a techno-economic assessment determines the levelized production costs for both commercial-scale routes. The underlying methodology for determining the production costs for wood-based SNG and FT diesel is explained in Section 2.3.

Figure 3 visualizes the production costs of wood-based SNG for the 100 MW_{th} scale. They are compared with the household and industry market prices of fossil natural gas based on the pre-crisis year 2019 and crisis year 2022. The production costs for SNG consist of approximately one-third each, namely, of fuel, operation and maintenance, and investment costs. For the base year 2019, the production costs of SNG, including taxes, are around 70 EUR /MWh. For 2022, the production costs rose to approximately 91 EUR /MWh. The increase in production costs is attributable to all three previously mentioned cost drivers. While the investment costs increased by 37% and the fuel costs by 27%, the most significant price increase, with 57%, was seen for operation and maintenance (O&M) costs. This is due to the doubling of the industrial electricity price from 2019 to 2022. However, the price increases were partially compensated by the rising purchase prices for district heat and CO_2. Meanwhile, market prices for fossil natural gas doubled in the household sector and tripled in the industrial sector during the period under consideration. Consequently, production costs of wood-based SNG are at household market price levels in 2019 and at industrial market price levels in 2022 compared to fossil natural gas.

In Figure 4 (left), the determined production costs excluding taxes for wood-based SNG for 2019 are compared with those for alternatives based on renewable energy sources (RES), according to Terlouw et al. [56] and Götz et al. [57]. These alternatives comprise e-fuels based on renewable electricity and CO_2 from biogenic sources and biomethane based on manure and corn silage. The comparison shows that the production costs for biomethane are 20–55% higher than the SNG production costs based on woody biomass in the 100 MW scale. The e-fuels' production costs are 175%higher than the production costs for wood-based SNG. In this comparison, the plant scale for biomethane is considerably lower, which is unfavorable regarding the economy of scale, and biomethane plants are not being built much larger. In the case of e-fuels, the high production costs can be attributed primarily to the high dependency on the underlying electricity price, which is the main price driver.

In Figure 4 (right), the sensitivity analysis of the SNG production costs based on the year 2022 is visualized. The most significant influence on SNG production costs is caused by the annual operating hours, the plant lifetime, the fuel costs, and the investment costs. Consequently, high plant availability and lifetime, and minimization of investment and fuel costs must be realized to keep production costs low. Furthermore, a moderate influence on SNG production costs is induced by interest rate, electricity price, maintenance, insurance

and administration costs, and earnings through captured CO_2 and district heat. Other operating utility costs have little to no impact on SNG production costs.

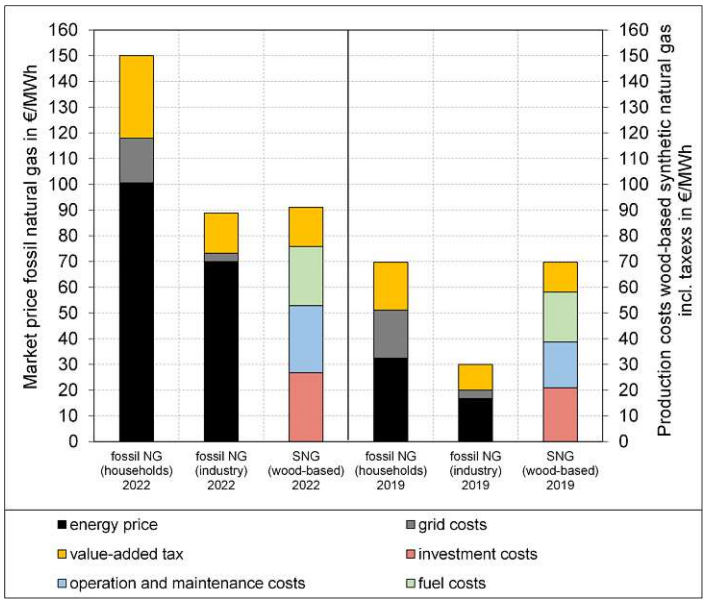

Figure 3. Comparison of production costs of wood-based SNG with the market price of fossil counterparts based on the years 2019 and 2022.

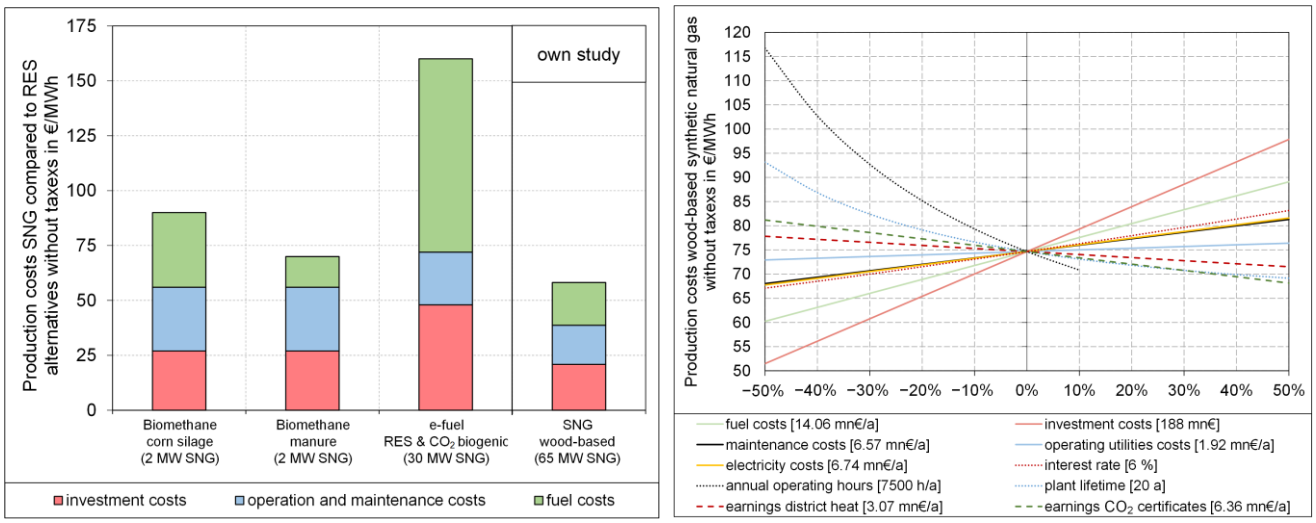

Figure 4. Comparison of production costs of wood-based SNG with RES alternatives (**left**, base year 2019) [56,57] and sensitivity analysis of production costs of wood-based SNG (**right**, base year 2022).

In Figure 5, the FT diesel production costs are compared to the stock market and petrol station prices for fossil diesel based on the pre-crisis year 2019 and the crisis year 2022. The FT diesel production costs are in the range of the petrol station prices but above stock market prices for fossil diesel in both reference years. Furthermore, the FT diesel production costs comprise 20–23% fuel costs, 36–39% operation and maintenance costs, and 40–41% investment costs, dependent on the base year. The FT diesel production costs with taxes are approximately 1.31 EUR /L for 2019 and 1.89 EUR /L for 2022. The production costs increase from 2019 compared to 2022 is in the same range as mentioned for the SNG process route.

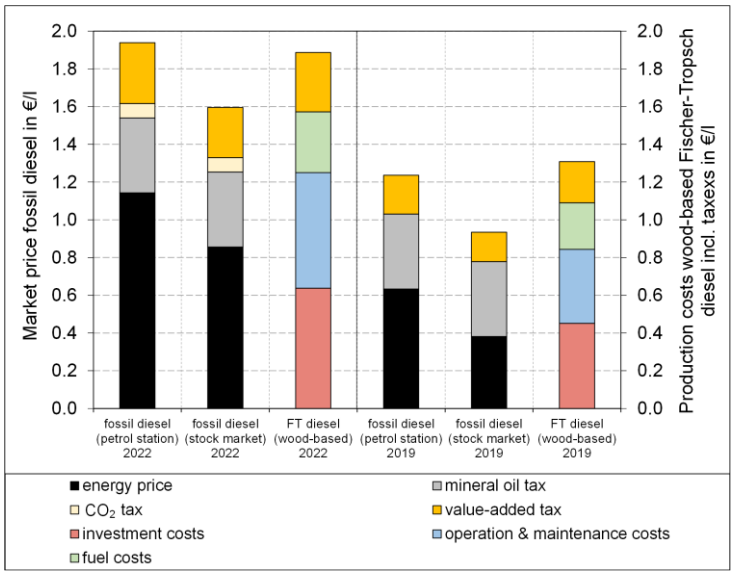

Figure 5. Comparison of wood-based FT diesel production costs with market price of fossil counterpart based on the years 2019 and 2022.

Additionally, the yearly operation and maintenance costs of the FT diesel route are 67–74% higher compared to the SNG route. This is because of the higher consumption of catalysts and electricity and higher maintenance needs. The investment costs of the FT diesel production route are approximately 70% higher than the investment costs of the SNG process route, while the fuel costs remain constant.

In Figure 6 (left), the FT diesel production costs excluding taxes, based on 2019, are compared with renewable alternative routes published by Maniatis et al. [58] and Pratschner et al. [59]. The biodiesel production routes fatty acid methyl ester (FAME) and hydroprocessed ester and fatty acid (HEFA) based on used cooking oil show production costs of 0.86–0.87 EUR /L and are approximately 26% cheaper than the wood-based FT diesel at 100 MW scale. The jatropha oil-based biodiesel from the HEFA route is more expensive than the FT diesel due to the higher fuel costs. E-fuels based on RES electricity and industrial CO_2 are approximately two to three times more expensive than wood-based FT diesel due to the high dependency on the electricity price.

The sensitivity analysis regarding the wood-based FT diesel production costs for 2022 is visualized in Figure 6 (right). Similar to the SNG route, the main influences are the annual operating hours, the plant lifetime, and the investment costs. However, the sensitivity to varying fuel costs is lower in comparison to the SNG route due to their lower share within the overall production costs.

If the techno-economics of the biomass-based SNG and FT diesel routes are compared in an energy-related manner, it is noticeable that the production costs of SNG at 70–91 EUR /MWh are much lower than FT diesel with 137–198 EUR /MWh. This results from the much higher investment costs for the production of FT diesel due to the significantly more complex product upgrading steps. Furthermore, the O&M are higher because more electricity is required for compression to a higher pressure level in synthesis and hydrogen is needed in upgrading.

3.3. Ecological Results of Commercial SNG and FT Production Plants

In analogy to the techno-economic, the egologic assessment expressed by the CO_2 footprint of both process routes is conducted. The underlying methodology for determining the CO_2 footprint for wood-based SNG and FT diesel is explained in Section 2.3.

Figure 7 (left) shows a breakdown of the CO_2 footprint of the wood-based SNG production route. The CO_2 footprint per produced unit of SNG is 0.027 $kgCO_2e/kWh_{SNG}$. The direct and indirect emissions of wood are responsible for approximately 77% of the

total CO_2 footprint. About 10% are related to using rapeseed methyl ester as a scrubber solvent. All the other utilities, like steel, concrete, bed material, activated carbon, zinc oxide, nickel catalyst, amine, glycol, and green electricity, cause the remaining 13% of the overall CO_2 footprint. Regarding the CO_2 footprint for electricity, it must be mentioned that the calculation is based on the utilization of green electricity. If the CO_2 footprint of the Austrian electricity mix were chosen, the total CO_2 footprint of the produced SNG would increase by 37% to 0.037 $kgCO_2e/kWh_{SNG}$.

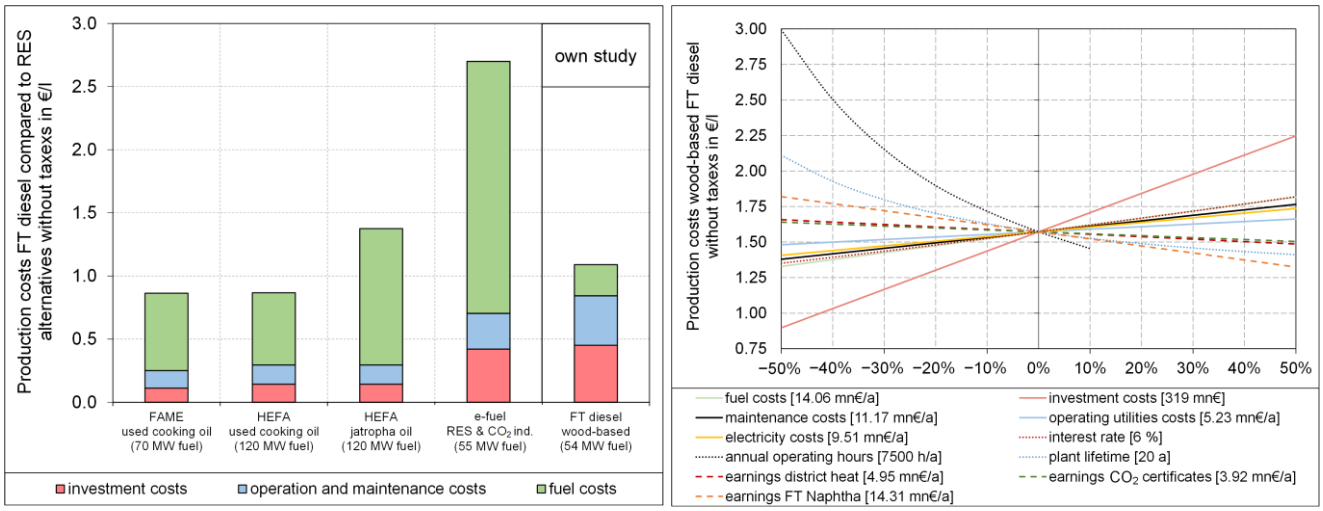

Figure 6. Comparison of wood-based FT diesel production costs with RES alternatives (**left**, base year 2019) [58,59] and sensitivity analysis of production costs FT diesel (**right**, base year 2022).

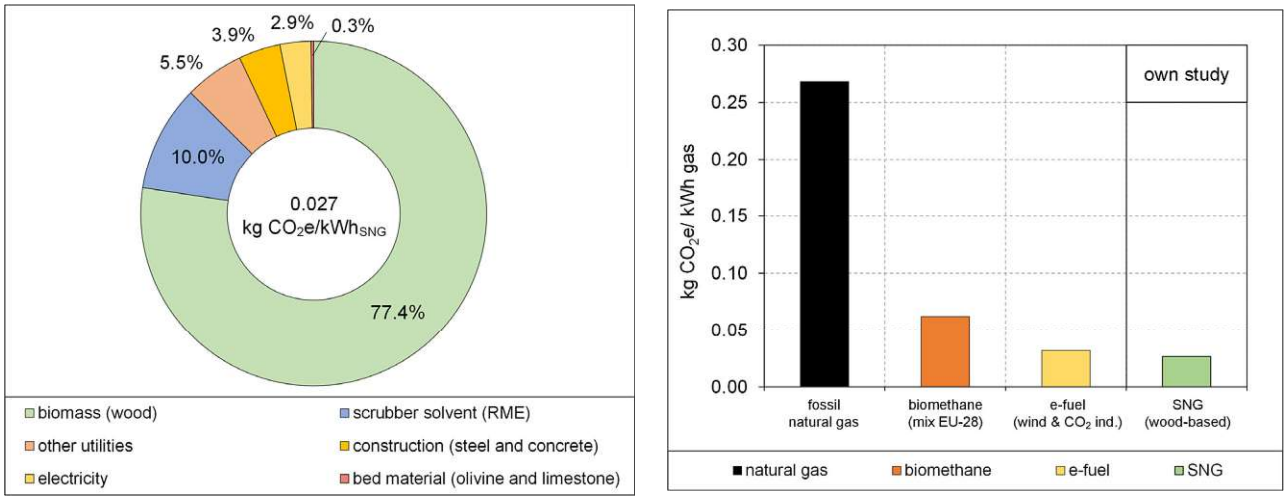

Figure 7. Breakdown of the CO_2 footprint of wood-based SNG (**left**) and comparison with fossil and RES alternatives (**right**) [30,49,60].

In Figure 7 (right), a comparison of the CO_2 footprint from wood-based SNG with that from fossil natural gas, according to Federal Environmental Agency Austria [49], and from RES alternatives, according to a study from Jungmeier et al. [30,60], is shown. Therein, it can be seen that using wood-based SNG at 100 MW scale instead of fossil natural gas can save 90% of CO_2 emissions. Furthermore, the CO_2 footprint of wood-based SNG is also lower compared to the renewable alternatives biomethane and e-fuel. The CO_2 footprint per kWh of biomethane, based on the average substrate mix within the European Union, is more than double as high as the value of synthetic natural gas, mostly caused by the emissions due to the use of corn silage or energy plants. The CO_2 footprint of e-fuels using

renewable electricity and biogenic CO_2 is also in the range of wood-based SNG and quite low. However, the CO_2 footprint of e-fuels using fossil electricity is much higher than that of fossil natural gas. Finally, it has to be mentioned that for the CO_2 footprint of the biomass-based SNG, the 6150 Nm^3/h of captured CO_2 during gas upgrading are not considered. If this is considered a CO_2 sink, a negative CO_2 footprint of 0.127 $kgCO_2e/kWh_{SNG}$ could be achieved, and thereby, a below zero emission technology is possible.

In Figure 8 (left), the breakdown of the CO_2 footprint for the wood-based FT diesel is shown. The CO_2 footprint of the wood-based FT diesel is 0.269 $kgCO_2e/l_{FT\ diesel}$. The distribution of CO_2 emissions is very similar to the SNG process route. Due to the larger consumption of different catalysts in the synthesis and upgrading step, the category "other utilities" has a slightly larger impact on the CO_2 footprint compared to the SNG route. The electricity consumption is also slightly higher due to the higher pressure level in the synthesis step. Additionally, hydrogen is required in the upgrading steps of the FT diesel, which also accounts for a small share of the CO_2 footprint. The CO_2 footprint of the electricity is based on green electricity. If the CO_2 footprint of the Austrian electricity mix were chosen for calculating the CO_2 footprint of electricity and hydrogen, the total CO_2 footprint of the produced FT diesel would increase by 64% to 0.440 $kgCO_2e/l_{FT\ diesel}$.

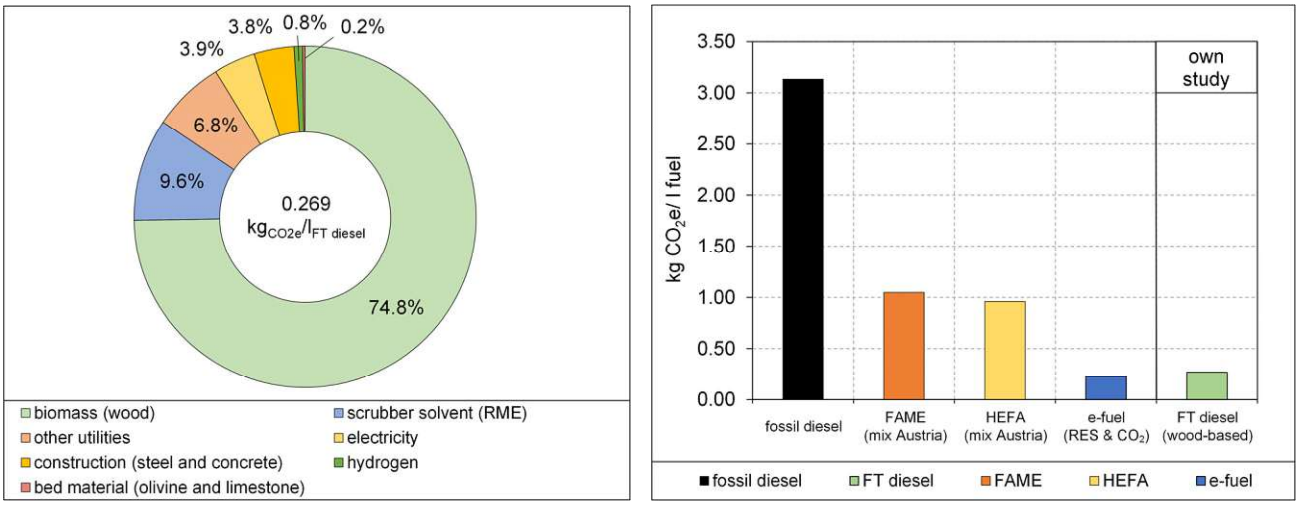

Figure 8. Breakdown of the CO_2 footprint of wood-based FT diesel (**left**) and comparison with fossil and RES alternatives (**right**) [49,61,62].

In Figure 8 (right), the CO_2 footprint of the wood-based FT diesel is compared with that of fossil diesel, according to Federal Environmental Agency Austria [49], and of RES alternatives, according to studies from Aichmayer et al. [61] and Pratschner et al. [62]. The CO_2 footprints of the wood-based FT diesel and the e-fuels, both based on green electricity, are the lowest and more than 90% lower compared to the CO_2 footprint of fossil diesel. If using fossil-based electricity as an energy source for e-fuels, the CO_2 footprint is much higher than the CO_2 footprint of fossil diesel. The CO_2 footprint of the FAME and HEFA process routes based on an Austrian fuel mix is 65–70% lower compared to the fossil diesel. If cooking oil is used as a feedstock for the FAME and HEFA processes, CO_2 footprints in the same range as those of e-fuels and wood-based FT diesel can be achieved. Similar to the SNG process route, the capturing of CO_2 is not considered. By taking the capture of approximately 3790 Nm^3/h of CO_2 in the upgrading step into account as a CO_2 sink, a footprint of 0.657 $kgCO_2e/l_{FT\ diesel}$ could be achieved.

If the CO_2 footprints of the two biomass-based products are compared, hardly any difference can be detected. The energy-related CO_2 footprint of FT diesel is 0.028 $kgCO_2e/kWh_{FT\ diesel}$, nearly the same as the SNG footprint of 0.027 $kgCO_2e/kWh_{SNG}$. The reason is that the same amount of biomass is used for the production of an energy-related product unit, with approximately the same energetic process efficiencies. In contrast to the techno-economy,

the higher electricity demand and the use of hydrogen have not as strong of a impact, since green electricity with a very low CO_2 footprint was assumed.

3.4. Integration of Biomass-Based SNG and FT Diesel in the Austrian Energy System

The biomass potential analysis (from Section 2.1) and the techno-economic (from Section 3.2) and ecological (from Section 3.3) results form the basis for discussing integration possibilities of biomass-based SNG and FT diesel in the Austrian energy system. Based on the biomass potential analysis, an additional biomass potential of 185 PJ/a can be determined in Austria in the year 2050. It should be mentioned that this potential does not consider competitive use by other biomass-based technologies. Considering the energetic efficiencies for the SNG and FT diesel process route, 120 PJ/a of SNG or 67.5 PJ/a of FT diesel can be produced out of the raised biomass potential. Additionally, the by-products of FT diesel, naphtha, district heat, and captured CO_2, are produced. In Figure 9, the annual Austrian energy demand for fossil natural gas and fossil diesel, distributed to six sectors related to the scenarios explained in Section 2.4, is compared to the biomass-based SNG and FT diesel potential in 2050. It can be seen that there is enough potential to substitute the whole natural gas demand in the energy sector or private and public sector, or nearly the whole industry sector. Instead of producing SNG, biomass-based FT diesel can substitute approximately half of the fossil diesel demand in private and public transport sectors or the heavy-duty traffic sector, or the whole demand in the heat and power sector.

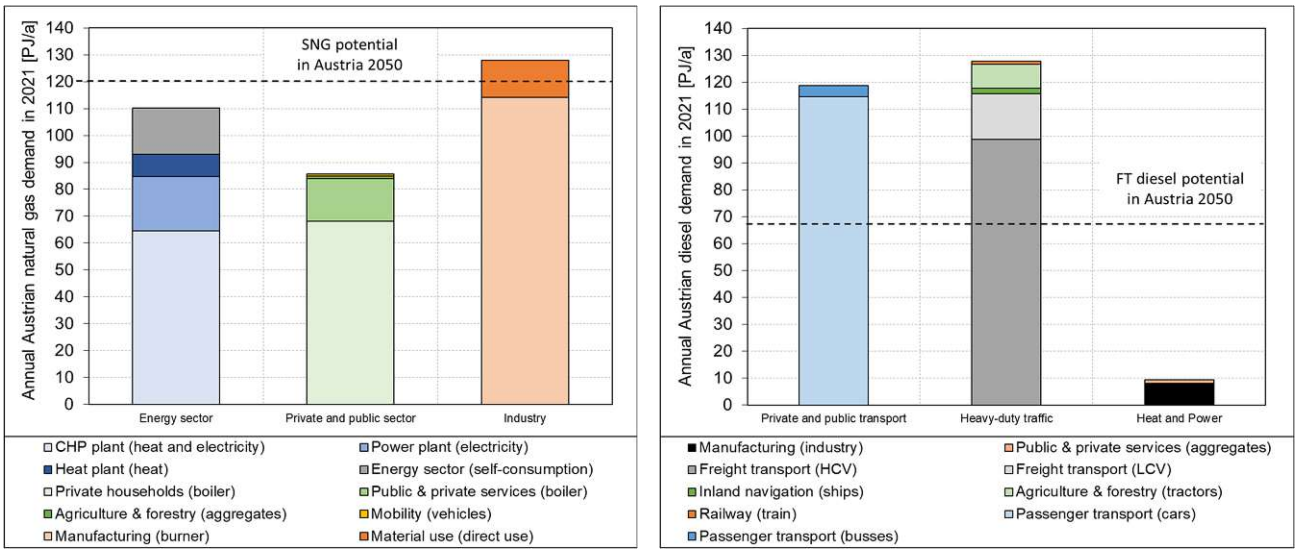

Figure 9. Annual Austrian energy demand for natural gas (**left**) and diesel (**right**) in 2021 compared to the SNG and FT diesel potential in 2050.

In Table 4, the six scenarios for the use of SNG and FT diesel as drop-in fuels in several sectors are summarized and compared. Therein, the substituted fossil natural gas and fossil diesel demands are compared with the change in the sectoral gross value added (*GVA*) for the pre-crisis year 2019 and crisis year 2022 and the CO_2 reduction potential of the sector.

It can be seen that the highest sectoral CO_2 reduction, 89%, can be reached in the energy sector through a nearly complete defossilization of the electricity and district heat mix with SNG. Regarding the economic impact, it can be seen in Figure 3 that the SNG production costs in the pre-crisis year 2019 were more than double and in the crisis year 2022, nearly on the same level compared to the related industrial natural gas market prices. This comparison shows that by integrating SNG into the energy sector, the electricity and heat price can be decoupled from the natural gas price. However, because cheaper alternative electricity and heat production technologies like wind power or solar PV exist, the SNG use in the energy sector should be focused on gas-fired power plants for the coverage of peak-loads.

Table 4. Comparison of possible implementation scenarios of biomass-based SNG and FT diesel in the Austrian energy system.

Implementation Scenarios	Natural Gas or Diesel Demand in 2050	Substituted Natural Gas or Diesel Demand in 2050	Additionally Produced by-Products	Sectoral CO_2 Reduction Potential	Economic Competitiveness (Change of Sectoral *GVA*)		Possible Renewable Alternatives
					2019	2022	
SNG use in energy sector	110 PJ/a [1]	110 PJ/a	24 PJ/a district heat	89.1%	−12.4%	−0.5%	Peak-load power coverage • increased interconnection to the European power grid • additional storage facilities • sector coupling Provision of district heat • heat pumps • biomass heating plants • solar thermal systems • waste heat utilization • hydrogen
SNG use in private and public sector (without mobility)	85 PJ/a [1]	85 PJ/a	18.5 PJ/a district heat	70.6%	0%	8.6%	Provision of decentral heat • heat pumps • solar thermal systems • wood-fired boilers • district heat
SNG use in industry	128 PJ/a [1]	120 PJ/a	26.2 PJ/a district heat	30.3%	−2.0%	−0.1%	Provision of high-temperature heat • waste heat recovery • hydrogen • high-temperature heat pumps

Table 4. *Cont.*

Implementation Scenarios	Natural Gas or Diesel Demand in 2050	Substituted Natural Gas or Diesel Demand in 2050	Additionally Produced by-Products	Sectoral CO_2 Reduction Potential	Economic Competitiveness (Change of Sectoral *GVA*) 2019	2022	Possible Renewable Alternatives
FT diesel in private and public transport	61.5 PJ/a [2]	61.5 PJ/a	38.4 PJ/a district heatand 29.6 PJ/a FT naphtha	40.2%	−0.2%	0.2%	Alternative mobility options • battery electric vehicles • fuel cell electric vehicles • hydrogenated vegetable oil • e-fuels
FT diesel in heavy-duty traffic	119 PJ/a [2]	67.5 PJ/a	42.2 PJ/a district heatand 32.5 PJ/a FT naphtha	58.5%	−1.8%	−0.8%	Alternative mobility options • battery electric vehicles (limited) • fuel cell electric vehicles • hydrogenated vegetable oil • e-fuels • compressed natural gas vehicles
FT diesel in heat and power	9 PJ/a [3]	9 PJ/a	5.5 PJ/a district heat and4.2 PJ/a FT naphtha	2.6%	−0.1%	−0.1%	Provision of high-temperature heat • wood-fired boilers • waste heat recovery • hydrogen • high-temperature heat pumps (limited usability)

[1] gas demand remains constant until 2050. [2] diesel demand for cars and LCV was reduced by half compared to 2021, because of vehicle fleet predictions [35]/diesel demand for busses and other heavy-duty traffic vehicles remain constant until 2050. [3] diesel demand for aggregates in public and private sector was reduced by half compared to 2021/diesel demand in manufacturing remains constant until 2050.

SNG use in the private and public sector also helps to reduce the sectoral CO_2 footprint by more than 70%, while raising the sectoral *GVA*. This would mean that using SNG in private households in times of crisis would help relieve household budgets. In comparison with alternative decentralized heat production technologies, it has to be mentioned that heat pumps and district heat should be used preferentially, because biomass-based SNG is not infinitely available. However, using SNG in private households, where no district heat or other renewable options are available, could be favorable.

Furthermore, the industry can use SNG to defossilize the gas demand for burners and direct material use without major changes in the process chains. In this way, nearly a third of the industrial CO_2 emissions can be reduced. The economic impact in this scenario is limited, with a sectoral *GVA* change of up to 2%. Consequently, the use of SNG could be a viable option in the defossilization process of the industry where the use of heat-pumps or waste heat cannot be realized.

In addition to the three integration scenarios for biomass-based SNG, three scenarios for integrating FT diesel in the Austrian energy system are discussed. According to the biomass potential, approximately half of the private and public transport diesel demand can be substituted with FT diesel. Consequently, according to future vehicle fleet predictions [35], it was assumed that only half of the diesel demand for cars could be replaced by synthetic fuels, thus leading to a sectoral CO_2 reduction of approximately 40%, while the sectoral *GVA* remains nearly constant. However, besides FT diesel, there are several alternative options for the public and private transport sector, first and foremost e-mobility.

The use of FT diesel in the heavy-duty traffic sector would be another option for using biomass-based products in the Austrian energy system. If the entire biomass potential is used to produce FT diesel for the heavy-duty traffic sector, the sectoral CO_2 footprint can be reduced by over 58%, while the sectoral *GVA* would be reduced by up to 2%. Furthermore, alternative options in this sector are, to date, limited; thus, the integration of FT diesel into the heavy-duty traffic sector is a promising solution. Moreover, it must be mentioned that the use of FT diesel in mobility can only take place if this fuel is approved for use in the most common diesel engines, regardless of the standard to be met.

The last scenario is based on the use of FT diesel in the heat and power sector, which comprises public and private heat production and the diesel demand in the manufacturing sector. The substitution of the diesel demand in this sector can only lead to a sectoral CO_2 reduction of 2–3%, much less than in the other scenarios. Consequently, it can be concluded that using high-quality FT diesel in the heat and power sector is not a viable option.

The scenarios examined aim to ensure that the released biomass can be used in either one sector or another. This means that several scenarios can only be implemented if the total amount of biomass used does not exceed the calculated biomass potential of 185 PJ/a.

4. Conclusions and Outlook

Based on a study from TU Wien [11], the Austrian Government could be convinced to fund the establishment of a 5 MW demonstration plant for the biomass-based production of SNG and FT diesel. The remaining knowledge gaps regarding the long-term behavior of different process units and utilities can be clarified within this demonstration phase. This includes exemplifying the technical investigation of the influence of fluctuating fuel qualities on product quality, the lifetime of catalysts and other utilities, and the required maintenance intervals with regard to plant availability. Furthermore, non-technical aspects, such as the examination of the all-season regional provision of biomass and the creation of social acceptance of the novel technology, should be investigated. In addition to the knowledge gaps described above, the competitive use of biomass must also be mentioned here as a possible limitation for the roll-out process.

After this demonstration phase, the lessons learned should be used to roll out the investigated technology commercially in Austria. This publication investigated the commercial scale concepts for producing wood-based SNG and FT diesel based on a 100 MW_{th} scale.

The simulation of both process routes showed that the energetic efficiency of the SNG process route is 79%, slightly higher compared to the 77% of the FT diesel process route. At the same time, it must be mentioned that within the SNG process, 65% of the chemical energy of the biomass can be converted to the main product, SNG. In comparison, within the FT process, only 36.6% of the biomass input is converted to the main product, FT diesel.

The techno-economic assessment showed that biomass-based SNG and FT diesel production costs can compete with the market prices of their fossil counterparts. The production costs of wood-based SNG related to the pre-crisis year 2019 are approximately 70 EUR /MWh. The market price range for fossil natural gas in the same year was 30–70 EUR /MWh, depending on the quantity purchased in industrial and household sectors. Based on the crisis year 2022, the SNG production costs were 91 EUR /MWh, slightly higher due to inflation. However, the market price for fossil natural gas increased to 89–150 EUR /MWh. Thus, it can be seen that the SNG production costs based on 2019 are in the range of the household prices, and when based on 2022, in the range of industrial market prices. Consequently, wood-based SNG production can help to decouple the domestic natural gas price level from the global market price level. The production costs for wood-based FT diesel are 1.31–1.89 EUR /L in the reference years 2019 and 2022. In comparison, the petrol station price level for fossil diesel was between 1.24–1.94 EUR /L. This comparison shows that the FT diesel production costs approximately match the petrol station price level, independent of the reference year. The economical comparison also showed that biomass-based SNG and FT diesel can compete with other renewable alternatives. The energy-related comparison of production costs for both biomass-based products shows that FT diesel, with 137–198 EUR /MWh, costs approximately twice as much as SNG, with 70–91 EUR /MWh. The reason for this is the much higher investment costs for the FT diesel route due to the more complex product upgrading and the additional costs for the higher electricity and hydrogen demand.

Furthermore, the CO_2 footprints of the wood-based SNG and FT diesel were determined. The CO_2 footprint for wood-based SNG is 0.027 $kgCO_2e/kWh_{SNG}$, and it is 0.269 $kgCO_2e/l_{FT\ diesel}$ for wood-based FT diesel, which are more than 90% lower than their fossil counterparts. Compared to renewable alternatives, wood-based SNG and FT diesel are among the products with the lowest CO_2 footprint. The energy-related comparison of the two biomass-based products shows hardly any differences, since the higher consumption of electricity and hydrogen due to the use of green electricity is not significant. Moreover, it has to be mentioned that if the additional CO_2 capturing in both process routes were considered, the production of wood-based SNG and FT diesel would create a CO_2 sink.

Moreover, six integration scenarios for producing biomass-based SNG and FT diesel were investigated to find possible applications in the Austrian energy system. The biomass potential analysis, based on several literature studies, showed that, in 2050, an additional biomass potential of 185 PJ/a would be available. Hence, a potential for biomass-based SNG of 120 PJ/a or biomass-based FT diesel of 67.5 PJ/a can be assumed. The scenarios demonstrated the various application possibilities for biomass-based SNG and FT diesel. Therein, the sectoral change of gross value added and the CO_2 reduction potential were calculated to investigate the economic and ecological impacts. The most promising applications for biomass-based FT diesel and SNG are summarized below:

- SNG use for covering electricity peak loads in the energy sector ➔ helps to prevent blackouts and to decouple the domestic electricity market from the gas market;
- SNG use in the industry sector for the provision of high-temperature heat ➔ economically feasible and a good option, when no waste heat or heat pumps can be used;
- FT diesel in heavy-duty traffic ➔ economically feasible and an excellent option to facilitate the defossilization of inland navigation, railway, freight transport, agriculture, and forestry.

Further, the use of biomass-based FT diesel in private and public transport, as well as the use of biomass-based SNG in the private and public heat provision sector, could

be an additional economically favorable option to accelerate the transition phase towards defossilization of these sectors. However, the sectoral view neglects the fact that individual enterprises and households certainly experience different economic and ecological impacts from transitioning to sustainable FT diesel and SNG, since the used energy sources and energy quantities can vary significantly.

To accelerate the rollout of the two biomass-based technologies, regulatory measures must be applied. The associated EU directive on the expansion of renewable energy sources in the EU (RED II) [63] already set mandatory quotas for the share of advanced biofuels, such as FT diesel, until 2030. Furthermore, the Austrian Renewable Energy Expansion Act [64] specifies that a fixed annual amount of biomethane, such as SNG, must be fed into the grid by 2030. A further increase in quotas with associated financial support measures would help to accelerate the roll-out process.

Besides determining the energetic efficiency, production costs, and CO_2 footprint, further sustainability indicators like the acidification potential, ground air quality, eutrophication, land use, payback time, or changes in gross domestic products should be investigated. Future research should focus on validating the calculated sustainability indicators after the scale-up to the demonstration plant. The process simulation focused mostly on each unit's mass and energy balances to define the main streams of the whole process unit. More detailed simulation models based on experimental test rigs can help to refine the whole process chain. In addition, future research should focus on biomass price changes caused by greater demand. The biomass price depends very much on the market situation and is dominated by supply and demand. Therefore, an increase in biomass use must be expected to lead to an increase in biomass price, unless regulatory measures follow. The continuous improvement of the sustainability criteria for the use of biomass must contribute to sustainable agriculture and forestry in Austria.

Summing up, the extensive investigation of biomass-based SNG and FT diesel production showed significant potential and enables the implementation of different defossilization strategies in the Austrian energy system. Nevertheless, the technical feasibility must first be tested within the framework of long-term trials in the planned demonstration plant.

Supplementary Materials: Supplementary data to this article can be found online at https://www.mdpi.com/article/10.3390/en16166097/s1.References [65–130] are cited in the Supplementary Materials.

Author Contributions: Conceptualization, M.H., A.B., F.B., M.V., S.P. and H.H.; methodology, M.H., A.B., F.B. and S.P.; validation, M.H., A.B. and S.P.; investigation, M.H., A.B., F.B. and S.P.; resources, M.H., A.B., S.P. and F.B.; writing—original draft, M.H. and A.B.; writing—review and editing, F.B., M.V., S.P., S.M. and H.H.; visualization, M.H. and A.B.; supervision, S.M. and H.H.; project administration, F.B. and H.H.; funding acquisition, F.B. and H.H. All authors have read and agreed to the published version of the manuscript.

Funding: Open Access Funding by TU Wien. The present work contains results of the project "Reallabor zur Herstellung von FT-Treibstoffen und SNG aus Biomasse und biogenen Reststoffen für die Land- und Forstwirtschaft" (101471), which is being conducted within the "DaFNE" research program funded and processed by the Federal Ministry for Sustainability and Tourism.

Data Availability Statement: Selected data that support the findings of this study are available from the corresponding author, M. Hammerschmid, upon reasonable request.

Acknowledgments: The authors acknowledge TU Wien Bibliothek for financial support through its Open Access Funding Programme.

Conflicts of Interest: The authors declare no conflict of interest.

Abbreviations

AC	activated carbon
AT	Austria
C_1–C_3	gaseous short-chain hydrocarbons recycled in Fischer–Tropsch tailgas
C_4–C_9	naphtha fraction (raw product for producing gasoline)
C_{10}–C_{19}	middle distillate fraction (after upgrading equivalent to diesel)
C_{10+}	middle distillate fraction and long-chain waxes
C_{20+}	long-chain waxes
CH_4	methane
CO	carbon monoxide
CO_2	carbon dioxide
CO_2e	carbon dioxide equivalent
DE	Germany
DFB	dual fluidized bed
EC	economic competitiveness
FAME	fatty acid methyl ester
FT	Fischer–Tropsch
GEMIS	software tool with database for life cycle analysis
GVA	gross value added
H_2	hydrogen
H_2O	water
H_2S	hydrogen sulfide
HCV	heavy commercial vehicles
HEFA	hydroprocessed ester and fatty acid
IEA	International Energy Agency
IPSEpro 8.0	software tool for process simulation from company SimTech GmbH
JP	Japan
LCOP	levelized costs of products
LCV	light commercial vehicles
MP	market prices
NH_3	ammonia
O&M	operation and maintenance
PFD	process flow diagram
PG	product gas
PV	photovoltaic
raw-SNG	synthetic natural gas after methanation unit and before upgrading
RES	renewable energy sources
RME	rapeseed methyl ester
SE	Sweden
SNG	synthetic natural gas
TH	Thailand
TSA	temperature swing adsorption
ZnO	zinc oxide
Symbols:	
%	percent
CDF	cumulative discount factor
$CEPCI_{\frac{2019}{2022}}$	Chemical Engineering Plant Cost Index based on 2019 or 2022
$CEPCI_{base\ year}$	Chemical Engineering Plant Cost Index based on base year of literature
$C_{eq,base}$	equipment costs based on base year and base scale of literature
$C_{eq,design}$	overall costs for installed equipment based on 2019 or 2022
$CO_2e_{red,sector\ i}$	carbon dioxide reduction potential in sector i
$CO_2e_{tot,sector\ i}$	total carbon dioxide equivalent in sector i
E	annual expenditures
$EC_{sector\ i}$	economic competitiveness in sector i based on 2019 or 2022

$E_{gas/diesel,sector\ i}$	substituted annual fossil gas or diesel demand in sector i
$FP_{fos.gas/diesel}$	carbon dioxide equivalent footprint of fossil natural gas or diesel
$FP_{SNG/FTdiesel}$	carbon dioxide equivalent footprint of biomass-based SNG or FT diesel
$GVA_{total,sector\ i}$	total gross value added in sector i based on 2019 or 2022
i	interest rate
I_0	total capital investment costs of plant
l	liter
$LCOP$	levelized costs of products
$LCOP_{SNG/FTdiesel}$	levelized costs of products for SNG or FT diesel based on 2019 or 2022
l_{Diesel}	liters of diesel
$MP_{fos.gas/diesel}$	market prices of fossil natural gas or diesel in 2019 or 2022
$M_{t,main\ prod.}$	annual quantity of the produced main product
MW	megawatt
MWh	megawatt hours
MWh_{th}	megawatt hours of thermal fuel power
MWh_{SNG}	megawatt hours of synthetic natural gas
n	plant lifetime
PJ/a	petajoule per year
r	scaling factor
$R_{sec.prod.}$	annual revenues of secondary products
S_{base}	base scale
S_{design}	desired scale
Z	overall installation factor

References

1. European Union. The European Green Deal. 2019. Available online: https://commission.europa.eu/system/files/2019-12/european-green-deal-communication_de.pdf (accessed on 2 July 2023).
2. Anderl, M.; Bartel, A.; Frei, E.; Gugele, B.; Gössl, M.; Mayer, S.; Heinfellner, H.; Heller, C.; Heuber, A.; Köther, T.; et al. *Klimaschutzbericht 2022*; Federal Environmental Agency: Vienna, Austria, 2022. Available online: https://www.umweltbundesamt.at/fileadmin/site/publikationen/rep0816.pdf (accessed on 2 July 2023).
3. Kaltschmitt, M.; Hartmann, H.; Hofbauer, H. *Energie aus Biomasse: Grundlagen, Techniken und Verfahren*, 3rd ed.; Springer Vieweg: Berlin/Heidelberg, Germany, 2016. [CrossRef]
4. Schmid, J.C.; Benedikt, F.; Fuchs, J.; Mauerhofer, A.M.; Müller, S.; Hofbauer, H. Syngas for biorefineries from thermochemical gasification of lignocellulosic fuels and residues—5 years' experience with an advanced dual fluidized bed gasifier design. *Biomass Convers. Biorefinery* **2021**, *11*, 2405–2442. [CrossRef]
5. Benedikt, F.; Schmid, J.C.; Fuchs, J.; Mauerhofer, A.M.; Müller, S.; Hofbauer, H. Fuel flexible gasification with an advanced 100 kW dual fluidized bed steam gasification pilot plant. *Energy* **2018**, *164*, 329–343. [CrossRef]
6. Bartik, A.; Benedikt, F.; Fuchs, J.; Hofbauer, H.; Müller, S. Experimental investigation of hydrogen-intensified synthetic natural gas production via biomass gasification: A technical comparison of different production pathways. *Biomass Convers. Biorefinery* **2023**. [CrossRef]
7. Thunman, H.; Seemann, M.; Berdugo Vilches, T.; Maric, J.; Pallares, D.; Ström, H.; Berndes, G.; Knutsson, P.; Larsson, A.; Breitholtz, C.; et al. Advanced biofuel production via gasification—Lessons learned from 200 man-years of research activity with Chalmers' research gasifier and the GoBiGas demonstration plant. *Energy Sci. Eng.* **2018**, *6*, 6–34. [CrossRef]
8. Cleantech Cluster. Erstes Produkt der Fischer-Tropsch-Pilotanlage in Wien-Simmering kommt in Flottentest zum Einsatz. 2023. Available online: https://www.cleantech-cluster.at/partnerunternehmen-im-ctc/ctc-partnernews-umwelt/detail/news/erstes-produkt-der-fischer-tropsch-pilotanlage-in-wien-simmering-kommt-in-flottentest-zum-einsatz (accessed on 28 May 2023).
9. Kadlez, D.; Benedikt, F.; Bartik, A.; Müller, S.; Hofbauer, H.; Karel, T.; Binder, M.; Huber, M.; Egger, A.; Hochstöger, D.; et al. First results of mass and energy balances of a 1 MW advanced dual fluidized bed steam gasification demonstration plant. In Proceedings of the Central European Biomass Conference, Graz, Austria, 18–20 January 2023.
10. Kuba, M.; Karel, T.; Fürsatz, K.; Binder, M.; Hannl, T.; Huber, M.; Hochstöger, D.; Egger, A.; Weber, G.; Haslinger, W.; et al. Second generation biomass gasification: The Syngas Platform Vienna—Current status and outlook. In Proceedings of the Central European Biomass Conference, Graz, Austria, 18–20 January 2023.
11. Hofbauer, H.; Mauerhofer, A.M.; Benedikt, F.; Hammerschmid, M.; Bartik, A.; Veress, M.; Haas, R.; Siebenhofer, M.; Resch, G. *Reallabor zur Herstellung von Holzdiesel und Holzgas aus Biomasse und Biogenen Reststoffen für die Land- und Forstwirtschaft*; TU Wien: Vienna, Austria, 2020; Available online: https://dafne.at/projekte/ftsng-reallabor (accessed on 2 July 2023).
12. Fuchs, J.; Schmid, J.C.; Müller, S.; Hofbauer, H. Dual fluidized bed gasification of biomass with selective carbon dioxide removal and limestone as bed material: A review. *Renew. Sustain. Energy Rev.* **2019**, *107*, 212–231. [CrossRef]

13. Schmid, M.; Beirow, M.; Schweitzer, D.; Waizmann, G.; Spörl, R.; Scheffknecht, G. Product gas composition for steam-oxygen fluidized bed gasification of dried sewage sludge, straw pellets and wood pellets and the influence of limestone as bed material. *Biomass Bioenergy* **2018**, *117*, 71–77. [CrossRef]
14. Schmid, M.; Hafner, S.; Scheffknecht, G. Experimental Parameter Study on Synthesis Gas Production by Steam-Oxygen Fluidized Bed Gasification of Sewage Sludge. *Appl. Sci.* **2021**, *11*, 579. [CrossRef]
15. Schweitzer, D.; Beirow, M.; Gredinger, A.; Armbrust, N.; Waizmann, G.; Dieter, H.; Scheffknecht, G. Pilot-Scale Demonstration of Oxy-SER steam Gasification: Production of Syngas with Pre-Combustion CO_2 Capture. *Energy Procedia* **2016**, *86*, 56–68. [CrossRef]
16. Karl, J.; Pröll, T. Steam gasification of biomass in dual fluidized bed gasifiers: A review. *Renew. Sustain. Energy Rev.* **2018**, *98*, 64–78. [CrossRef]
17. Kuba, M.; Benedikt, F.; Fürsatz, K.; Fuchs, J.; Demuth, M.; Aichernig, C.; Arpa, L.; Hofbauer, H. Integration of dual fluidized bed steam gasification into the pulp and paper industry. *Biomass Convers. Biorefinery* **2021**. [CrossRef]
18. Loipersböck, J.; Weber, G.; Rauch, R.; Hofbauer, H. Developing an adsorption-based gas cleaning system for a dual fluidized bed gasification process. In Proceedings of the International Conference on Polygeneration Strategies, Vienna, Austria, 18–20 November 2019; Hofbauer, H., Müller, S., Eds.; TU Wien: Vienna, Austria, 2019. [CrossRef]
19. Bardolf, R. Optimierung eines Produktgaswäschers bei der Biomassedampfvergasung im Zweibettwirbelschichtverfahren. Ph.D. Thesis, TU Wien, Vienna, Austria, 2017.
20. Rehling, B. Development of the 1MW Bio-SNG Plant, Evaluation on Technological and Economical Aspects and Upscaling Considerations. Ph.D. Thesis, TU Wien, Vienna, Austria, 2012.
21. Schildhauer, T.J.; Biollaz, S.M.A. Reactors for Catalytic Methanation in the Conversion of Biomass to Synthetic Natural Gas (SNG). *Chimia* **2015**, *69*, 603–607. [CrossRef] [PubMed]
22. Seemann, M.C.; Schildhauer, T.J.; Biollaz, S.M.A. Fluidized Bed Methanation of Wood-Derived Producer Gas for the Production of Synthetic Natural Gas. *Ind. Eng. Chem. Res.* **2010**, *49*, 7034–7038. [CrossRef]
23. Gruber, H. Synthesis and Refining of Biomass- Derived Fischer-Tropsch Paraffin Waxes. Ph.D. Thesis, TU Wien, Vienna, Austria, 2020.
24. Sauciuc, A.; Abosteif, Z.; Weber, G.; Potetz, A.; Rauch, R.; Hofbauer, H.; Schaub, G.; Dumitrescu, L. Influence of operating conditions on the performance of biomass-based Fischer–Tropsch synthesis. *Biomass Convers. Biorefinery* **2012**, *2*, 253–263. [CrossRef]
25. Guilera, J.; Díaz-López, J.A.; Berenguer, A.; Biset-Peiró, M.; Andreu, T. Fischer-Tropsch synthesis: Towards a highly-selective catalyst by lanthanide promotion under relevant CO_2 syngas mixtures. *Appl. Catal. A Gen.* **2022**, *629*, 118423. [CrossRef]
26. Müller, S.; Groß, P.; Rauch, R.; Zweiler, R.; Aichernig, C.; Fuchs, M.; Hofbauer, H. Production of diesel from biomass and wind power—Energy storage by the use of the Fischer-Tropsch process. *Biomass Convers. Biorefinery* **2018**, *8*, 275–282. [CrossRef]
27. Rauch, R.; Hrbek, J.; Hofbauer, H. Biomass gasification for synthesis gas production and applications of the syngas. *WIREs Energy Environ.* **2014**, *3*, 343–362. [CrossRef]
28. Thunman, H.; Gustavsson, C.; Larsson, A.; Gunnarsson, I.; Tengberg, F. Economic assessment of advanced biofuel production via gasification using cost data from the GoBiGas plant. *Energy Sci. Eng.* **2019**, *7*, 217–229. [CrossRef]
29. Neuling, U.; Kaltschmitt, M. Techno-economic and environmental analysis of aviation biofuels. *Fuel Process. Technol.* **2018**, *171*, 54–69. [CrossRef]
30. Jungmeier, G.; Canella, L.; Pucker-Singer, J.; Beermann, M. *Geschätzte Treibhausgasemissionen und Primärenergieverbrauch in der Lebenszyklusanalyse von Pkw-basierten Verkehrssystemen*; Joanneum Research Forschungsgesellschaft: Graz, Austria, 2019.
31. Österreichische Vereinigung für das Gas- und Wasserfach. *Richtlinie G B210—Gasbeschaffenheit: Gas Quality*; Österreichische Vereinigung für das Gas- und Wasserfach: Vienna, Austria, 2021; Available online: https://shop.austrian-standards.at/action/de/public/details/697809/OEVGW_G_B210_2021_06 (accessed on 2 July 2023).
32. *DIN EN 15940*; Kraftstoffe—Paraffinischer Dieselkraftstoff aus Synthese oder Hydrierungsverfahren—Anforderungen und Prüfverfahren. Beuth Verlag: Berlin, Germany, 2019. Available online: https://www.beuth.de/de/norm/din-en-15940/309170058 (accessed on 2 July 2023).
33. Österreichischer Biomasseverband. *Basidaten 2019 Bioenergie*; Österreichischer Biomasseverband: Vienna, Austria, 2019; Available online: https://www.biomasseverband.at/wp-content/uploads/Basisdaten_Bioenergie_2019.pdf (accessed on 2 July 2023).
34. Dißauer, C.; Rehling, B.; Strasser, C. *Machbarkeitsuntersuchung Methan aus Biomasse*; Bioenergy 2020+: Wieselburg, Austria, 2019; Available online: https://www.gruenes-gas.at/assets/Uploads/BioEenergy2020+_Machbarkeitsuntersuchung_Methan_aus_Biomasse.pdf (accessed on 2 July 2023).
35. Hammerschmid, M.; Konrad, J.; Werner, A.; Popov, T.; Müller, S. ENECO$_2$Calc—A Modeling Tool for the Investigation of Energy Transition Paths toward Climate Neutrality within Municipalities. *Energies* **2022**, *15*, 7162. [CrossRef]
36. Kranzl, L. *Bioenergy—A Key Option within all Energy Sectors. VO Economic Perspectives of Renewable Energy Systems*; Energy Economics Group (EEG), TU Wien: Vienna, Austria, 2020.
37. Kranzl, L.; Haas, R.; Kalt, G.; Diesenreiter, F.; Eltrop, L.; König, A.; Makkonen, P. *Strategien zur Optimalen Erschließung der Biomassepotenziale in Österreich bis zum Jahr 2050 mit dem Ziel einer Maximalen Reduktion an Treibhausgasemissionen*; Energy Economics Group (EEG), TU Wien: Vienna, Austria, 2008.
38. Alamia, A.; Gardarsdòttir, Ò.S.; Larsson, A.; Normann, F.; Thunman, H. Efficiency Comparison of Large-Scale Standalone, Centralized, and Distributed Thermochemical Biorefineries. *Energy Technol.* **2017**, *5*, 1435–1448. [CrossRef]

39. Förtsch, D.; Pabst, K.; Groß-Hardt, E. The product distribution in Fischer–Tropsch synthesis: An extension of the ASF model to describe common deviations. *Chem. Eng. Sci.* **2015**, *138*, 333–346. [CrossRef]
40. Pratschner, S.; Hammerschmid, M.; Müller, F.J.; Müller, S.; Winter, F. Simulation of a Pilot Scale Power-to-Liquid Plant Producing Synthetic Fuel and Wax by Combining Fischer–Tropsch Synthesis and SOEC. *Energies* **2022**, *15*, 4134. [CrossRef]
41. Hammerschmid, M.; Rosenfeld, D.C.; Bartik, A.; Benedikt, F.; Fuchs, J.; Müller, S. Methodology for the Development of Virtual Representations within the Process Development Framework of Energy Plants: From Digital Model to Digital Predictive Twin—A Review. *Energies* **2023**, *16*, 2641. [CrossRef]
42. Konstantin, P. *Praxisbuch Energiewirtschaft: Energieumwandlung, -Transport und -Beschaffung, Übertragungsnetzausbau und Kernenergieausstieg*, 4th ed.; VDI-Buch; Springer Vieweg: Berlin/Heidelberg, Germany, 2017; ISBN 978-3-662-49823-1.
43. Resch, G.; Kranzl, L.; Faninger, G.; Geipel, J. Block 1: Introduction: Energy & climate challenge and basics of economic assessment. In *VO Economic Perspectives of Renewable Energy Systems*; Energy Economics Group (EEG), TU Wien: Vienna, Austria, 2020.
44. Kost, C.; Shammugam, S.; Jülch, V.; Nguyen, H.-T.; Schlegl, T. *Stromgestehungskosten Erneuerbare Energien*; Fraunhofer-Institut für solare Energiesysteme (ISE): Freiburg, Germany, 2018.
45. Veress, M. Optimization of a Process Concept for the Industrial Production of Bio-SNG from Low-Grade Fuels. Master's Thesis, TU Wien, Vienna, Austria, 2020.
46. Peters, M.S.; Timmerhaus, K.D. *Plant Design and Economics for Chemical Engineers*, 4th ed.; McGraw-Hill Chemical Engineering Series; McGraw-Hill: New York, NY, USA, 1991; ISBN 0-07-049613-7.
47. Wulf, C.; Kaltschmitt, M. Hydrogen Supply Chains for Mobility—Environmental and Economic Assessment. *Sustainability* **2018**, *10*, 1699. [CrossRef]
48. Lichtblau, G.; Pölz, W.; Stix, S.; Winter, R. *Ökobilanzen Ausgewählter Biotreibstoffe: Projekt proVISION*; Umweltbundesamt Österreich: Vienna, Austria, 2012; Available online: https://www.umweltbundesamt.at/fileadmin/site/publikationen/rep0360.pdf (accessed on 2 July 2023).
49. Federal Environmental Agency Austria. *Berechnung von Treibhausgas (THG)-Emissionen verschiedener Energieträger*; FEA: Vienna, Austria, 2022. Available online: https://secure.umweltbundesamt.at/co2mon/co2mon.html (accessed on 20 March 2023).
50. Federal Environmental Agency Germany. *ProBas—Prozessorientierte Basisdaten für Umweltmanagementsysteme*; FEA Germany: Dessau-Roßlau, Germany, 2015. Available online: https://www.probas.umweltbundesamt.de/php/index.php (accessed on 2 July 2023).
51. *INAS GmbH*, Version 4.94. Globales Emissions-Modell Integrierter Systeme (GEMIS). Internationales Institut für Nachhaltigkeitsanalysen und -Strategien: Freiburg, Germany, 2018.
52. Gollner, M. *Gesamtenergiebilanz Österreich 1970 bis 2021*; Statistik Austria: Vienna, Austria, 2022; Available online: https://www.statistik.at/web_de/statistiken/energie_umwelt_innovation_mobilitaet/energie_und_umwelt/energie/energiebilanzen/index.html (accessed on 2 July 2023).
53. Resch, G.; Burgholzer, B.; Totschnig, G.; Lettner, G.; Auer, H.; Geipel, J.; Haas, R. *Stromzukunft Österreich 2030: Analyse der Erfordernisse und Konsequenzen eines Ambitionierten Ausbaus von Erneuerbaren Energien*; Energy Economics Group (EEG), TU Wien: Vienna, Austria, 2017; Available online: https://www.igwindkraft.at/mmedia/download/2017.07.10/1499698755049626.pdf (accessed on 2 July 2023).
54. Kranzl, L.; Müller, A.; Büchele, R. *Wärmezukunft 2050: Anforderungen an die Gebäudesanierung: Endbericht*; Energy Economics Group (EEG), TU Wien: Vienna, Austria, 2018; Available online: https://www.igwindkraft.at/mmedia/download/2018.02.05/1517825327514183.pdf (accessed on 2 July 2023).
55. Baumann, M.; Fazeni-Fraisl, K.; Kienberger, T.; Nagovnak, P.; Pauritsch, G.; Rosenfeld, D.; Sejkora, C.; Tichler, R. *Erneuerbares Gas in Österreich 2040: Quantitative Abschätzung von Nachfrage und Angebot*; Bundesministerium für Klimaschutz, Umwelt, Energie, Mobilität, Innovation und Technologie: Vienna, Austria, 2021. Available online: https://www.bmk.gv.at/themen/energie/publikationen/erneuerbares-gas-2040.html (accessed on 2 July 2023).
56. Terlouw, W.; Peters, D.; van Tilburg, J.; Schimmel, M.; Berg, T.; Cihlar, J.; Ur Rehman Mir, G.; Spöttle, M.; Staats, M.; Lejaretta, A.V.; et al. *Gas for Climate: The Optimal Role for Gas in a Net-Zero Emissions Energy System*; Navigant: Utrecht, The Netherlands, 2019; Available online: https://gasforclimate2050.eu/wp-content/uploads/2020/03/Navigant-Gas-for-Climate-The-optimal-role-for-gas-in-a-net-zero-emissions-energy-system-March-2019.pdf (accessed on 2 July 2023).
57. Götz, M.; Lefebvre, J.; Mörs, F.; Koch, A.M.; Graf, F.; Bajohr, S.; Reimert, R.; Kolb, T. Renewable Power-to-Gas: A technological and economic review. *Renew. Energy* **2016**, *85*, 1371–1390. [CrossRef]
58. Maniatis, K.; Landälv, I.; Waldheim, L.; van den Heuvel, E.; Kalligeros, S. *Final Report—Building up the Future: Sub Group on Advanced Biofeuls—Sustainable Transport Forum*; European Comission: Luxembourg, 2017; ISBN 978-92-79-69010-5.
59. Pratschner, S.; Hammerschmid, M.; Müller, S.; Winter, F. Converting CO_2 and H_2O into Fischer-Tropsch Products—A Techno-economic assessment. In Proceedings of the 27th International Symposium for Chemical Reaction Engineering—ISCRE 27, Quebec City, QC, Canada, 11–14 June 2023.
60. Jungmeier, G. Umweltbilanz von E-Fuels—Vergleich mit anderen Treibstoffen im Lebenszyklus. In Proceedings of the ÖGEW/DGMK Onlinekonferenz „Innovative Energieversorgung", Graz, Austria, 13 November 2020; Available online: https://www.wko.at/site/oegew/veranstaltungen/umweltbilanz-von-e-fuels.pdf (accessed on 2 July 2023).

61. Aichmayer, S.; Mitterhuemer, R.; Winter, R. *Biokraftstoffe im Verkehrssektor 2021*; Bundesministerium für Klimaschutz, Umwelt, Energie, Mobilität, Innovation und Technologie: Vienna, Austria, 2021; Available online: https://www.biokraft-austria.at/media/18119/biokraftstoffbericht_2021.pdf (accessed on 2 July 2023).
62. Pratschner, S.; Hammerschmid, M.; Müller, S.; Winter, F. CO_2 Footprint of Fischer-Tropsch Products produced by a Power-to-Liquid Plant. In Proceedings of the 15th Mediterranean Congress of Chemical Engineering—MECCE 2023, Barcelona, Spain, 30 May–2 June 2023.
63. European Union. Directive (EU) 2018/2001 of the European Parliament and of the Council of 11 December 2018 on the Promotion of the Use of Energy from Renewable Sources, RED II. *Off. J. Eur. Union* **2018**, *L 328/82*. Available online: https://eur-lex.europa.eu/legal-content/DE/TXT/?qid=1575559881403&uri=CELEX:32018L2001 (accessed on 12 May 2021).
64. Bundesrepublik Österreich. Erneuerbaren-Ausbau-Gesetz, EAG. 2021. Available online: https://www.parlament.gv.at/PAKT/VHG/XXVII/I/I_00733/index.shtml (accessed on 12 August 2021).
65. Ringhofer, T. Evaluierung des Biomassetrockners der Kraft-Wärme-Kopplungsanlage Oberwart. Bachelor's Thesis, TU Wien, Vienna, Austria, 2011.
66. Müller, S. Hydrogen from Biomass for Industry—Industrial Application of Hydrogen Production Based on Dual Fluid Gasification. Ph.D. Thesis, TU Wien, Vienna, Austria, 2013.
67. Benedikt, F.; Fuchs, J.; Schmid, J.C.; Müller, S.; Hofbauer, H. Advanced dual fluidized bed steam gasification of wood and lignite with calcite as bed material. *Korean J. Chem. Eng.* **2017**, *34*, 2548–2558. [CrossRef]
68. Benedikt, F.; Müller, S.; Hofbauer, H. 1 MW scale-up of the advanced fuel flexible dual fluidized bed steam gasification process by process simulation. In Proceedings of the ICPS19—International Conference on Polygeneration Strategies, Vienna, Austria, 18–20 November 2019; ISBN 978-3-9503671-1-9.
69. Wolfesberger, U. Profiling Tar Behavior in Dual Fluidized Bed Biomass Steam Gasification. Ph.D. Thesis, TU Wien, Vienna, Austria, 2013.
70. Hofbauer, H.; Rauch, R.; Bosch, K.; Koch, R.; Aichernig, C. Biomass CHP plant Güssing—A success story. In Proceedings of the Pyrolysis and Gasification of Biomass and Waste—Expert Meeting, Strasbourg, France, 30 September–1 October 2002.
71. Pröll, T.; Siefert, I.G.; Friedl, A.; Hofbauer, H. Removal of NH_3 from Biomass Gasification Producer Gas by Water Condensing in an Organic Solvent Scrubber. *Ind. Eng. Chem. Res.* **2005**, *44*, 1576–1584. [CrossRef]
72. Stidl, M. Prozesssimulation von spezifischen Anwendungsfällen der Zweibett-Wirbelschicht-Dampfvergasungs-Technologie für die Papier- und Zellstoffindustrie. Ph.D. Thesis, TU Wien, Vienna, Austria, 2012.
73. Sadegh, A.M.; Worek, W.M. *Marks' Standard Handbook for Mechanical Engineers*, 12th ed.; McGraw-Hill Education: New York, NY, USA, 2018; ISBN 9781259588518.
74. Broer, K.M.; Woolcock, P.J.; Johnston, P.A.; Brown, R.C. Steam/oxygen gasification system for the production of clean syngas from switchgrass. *Fuel* **2015**, *140*, 282–292. [CrossRef]
75. Bartik, A.; Fuchs, J.; Pacholik, G.; Föttinger, K.; Hofbauer, H.; Müller, S.; Benedikt, F. Experimental investiga-tion on the methanation of hydrogen-rich syngas in a bubbling fluidized bed reactor utilizing an optimized catalyst. *Fuel Process. Technol.* **2022**, *237*, 107402. [CrossRef]
76. Li, K.; Leigh, W.; Feron, P.; Yu, H.; Tade, M. Systematic study of aqueous monoethanolamine (MEA)-based CO_2 capture process: Techno-economic assessment of the MEA process and its improvements. *Appl. Energy* **2016**, *165*, 648–659. [CrossRef]
77. Günther, L. *Biomethanreinigung mit der Drucklosen Wäsche zur Herstellung von Biomethan und Kohlendioxid. Fachtagung "Innogas"*; DGE GmbH Presentation: Wittenberg, Germany, 2007; Available online: https://www.dge-wittenberg.de/vortraege/DGE%20Fachtagung%20WB%202006.pdf (accessed on 2 July 2023).
78. Neagu, M.; Cursaru, D.L. Technical and economic evaluations of the triethylene glycol regeneration processes in natural gas dehydration plants. *J. Nat. Gas Sci. Eng.* **2017**, *37*, 327–340. [CrossRef]
79. Kidnay, A.J.; Parrish, W.R.; McCartney, D.G. *Fundamentals of Natural Gas Processing*; CRC Press: Boca Raton, FL, USA, 2019; ISBN 9780429464942.
80. Gruber, H.; Groß, P.; Rauch, R.; Reichhold, A.; Zweiler, R.; Aichernig, C.; Müller, S.; Ataimisch, N.; Hofbauer, H. Fischer-Tropsch products from biomass-derived syngas and renewable hydrogen. *Biomass Convers. Biorefinery* **2019**, *48*, 22. [CrossRef]
81. De Klerk, A. *Fischer-Tropsch Refining*; Wiley-VCH Verlag GmbH & Co. KGaA: Weinheim, Germany, 2011; ISBN 9783527635603.
82. Schädel, B.T.; Duisberg, M.; Deutschmann, O. Steam reforming of methane, ethane, propane, butane, and natural gas over a rhodium-based catalyst. *Catal. Today* **2009**, *142*, 42–51. [CrossRef]
83. Ali, S.; Sørensen, K.; Nielsen, M.P. Modeling a novel combined solid oxide electrolysis cell (SOEC)—Biomass gasification renewable methanol production system. *Renew. Energy* **2020**, *154*, 1025–1034. [CrossRef]
84. Clariant International Ltd. *Catalysts and Adsorbents for Syngas*; Clariant International Ltd.: Muttenz, Switzerland, 2017; Available online: https://de.scribd.com/document/477562978/Clariant-Brochure-Catalysts-And-Adsorbents-For-Syngas-2017-EN-1 (accessed on 2 July 2023).
85. Petersen, A.M.; Chireshe, F.; Okoro, O.; Gorgens, J.; van Dyk, J. Evaluating refinery configurations for deriving sustainable aviation fuel from ethanol or syncrude. *Fuel Process. Technol.* **2021**, *219*, 106879. [CrossRef]
86. Fahim, M.A. *Fundamentals of Petroleum Refining*; Elsevier Science & Technology: Oxford, UK, 2010; ISBN 978-0-444-52785-1.
87. De Klerk, A. Can Fischer–Tropsch Syncrude Be Refined to On-Specification Diesel Fuel? *Energy Fuels* **2009**, *23*, 4593–4604. [CrossRef]

88. Kang, J.; Ma, W.; Keogh, R.A.; Shafer, W.D.; Jacobs, G.; Davis, B.H. Hydrocracking and Hydroisomerization of n-Hexadecane, n-Octacosane and Fischer–Tropsch Wax Over a Pt/SiO_2–Al_2O_3 Catalyst. *Catal. Lett.* **2012**, *142*, 1295–1305. [CrossRef]
89. Murali, C.; Voolapalli, R.K.; Ravichander, N.; Gokak, D.T.; Choudary, N.V. Trickle bed reactor model to simulate the performance of commercial diesel hydrotreating unit. *Fuel* **2007**, *86*, 1176–1184. [CrossRef]
90. Busca, G. *Heterogeneous Catalytic Materials*; Elsevier: Amsterdam, The Netherlands, 2014; ISBN 978-0-444-59524-9.
91. Mauerhofer, A.M.; Schmid, J.C.; Benedikt, F.; Fuchs, J.; Müller, S.; Hofbauer, H. Dual fluidized bed steam gasification: Change of product gas quality along the reactor height. *Energy* **2019**, *173*, 1256–1272. [CrossRef]
92. Schmid, J.C. Technoökonomische Fallstudien als Entscheidungsunterstützung für das Strategische Management. Master's Thesis, Fachhochschule Burgenland, Eisenstadt, Austria, 2016.
93. E-Control. *Gaspreisentwicklung*; E-Control: Vienna, Austria, 2022. Available online: https://www.e-control.at/statistik/gas/marktstatistik/preisentwicklung (accessed on 10 August 2022).
94. E-Control. *Strom- und Gaspreise in Österreich*; E-Control: Vienna, Austria, 2022; Available online: https://www.e-control.at/preismonitor (accessed on 10 August 2022).
95. Bundesministerium für Klimaschutz, Umwelt, Energie, Mobilität, Innovation und Technologie. Treibstoffpreise aktuell. Bundesministerium für Klimaschutz, Umwelt, Energie, Mobilität, Innovation und Technologie: Vienna, Austria, 2022. Available online: https://www.bmk.gv.at/themen/energie/preise/aktuelle_preise.html (accessed on 15 October 2022).
96. *Deutsche Börse*; Diesel: Frankfurt, Germany, 2022; Available online: https://www.boerse.de/charts/Dieselpreis/XC0009677813 (accessed on 15 October 2022).
97. Statistik Austria. Erzeugerpreisindex Produzierender Bereich—Österreich. Vienna, Austria; 2022. Available online: https://www.statistik.at/statistiken/volkswirtschaft-und-oeffentliche-finanzen/preise-und-preisindizes/erzeugerpreisindex-produzierender-bereich (accessed on 10 August 2022).
98. Meehan, J. Europe Monoethanolamine Prices Move Down on Import Pressure. 2013. Available online: https://www.icis.com/explore/resources/news/2013/06/19/9680122/europe-monoethanolamine-prices-move-down-on-import-pressure/ (accessed on 13 December 2019).
99. Billig, E. DBFZ Report Nr. 26. Ph.D. Thesis, Universität Leipzig, Helmholtz-Zentrum für Umweltforschung, Leipzig, Germany, 2016.
100. Thrän, D.; Pfeiffer, D. Methodenhandbuch: Stoffstromorientierte Bilanzierung der Klimagaseffekte. *Energetische Biomassenutzung* **2013**, *2013*, 4.
101. European Energy Exchange AG (EEX). *EEX EUA Spot Market—CO2 Emission Allowances*; EEX: Leipzig, Germany, 2022; Available online: https://www.eex.com/de/marktdaten/umweltprodukte/spot (accessed on 15 October 2022).
102. E-Control. *Strompreisentwicklung*; E-Control: Vienna, Austria, 2022; Available online: https://www.e-control.at/statistik/strom/marktstatistik/preisentwicklung (accessed on 10 August 2022).
103. Godula-Jopek, A.; Stolten, D. *Hydrogen Production: By Electrolysis*, 1st ed.; Wiley-VCH: Weinheim, Germany, 2015; ISBN 9783527676507.
104. Goritschnig, M.; Kreuter, K.; Novakovits, P.; Pomper, M.; Zweiler, R. Winddiesel_klienIF: Untersuchung des Lastwechselverhaltens eines Slurryreaktors zur Einkopplung von H2 und Produktion von FT-Diesel. Güssing Energy Technologies. 2017. Available online: https://www.winddiesel.at/images/Downloads/13003-BB008a_Winddiesel_kurzfassung.pdf (accessed on 15 October 2022).
105. Perry, R.H.; Green, D.W.; Maloney, J.O. *Perry's Chemical Engineers' Handbook*, 7th ed.; McGraw-Hill: New York, NY, USA, 1997; ISBN 0070498415.
106. Batidzirai, B.; Shotman, G.S.; van der Spek, M.W.; Junginger, M.; Faaij, A.P.C. Techno-economic performance of sustainable international bio-SNG production and supply chains on short and longer term. *Biofuels Bioprod. Biorefining* **2019**, *13*, 325–357. [CrossRef]
107. Brasington, R.D.; Haslbeck, J.L.; Kuehn, N.J.; Lewis, E.G.; Pinkerton, L.L.; Turner, M.; Varghese, E.; Woods, M. *Cost and Performance Baseline for Fossil Energy Plants: Volume 2, Coal to Synthetic Natural Gas and Ammonia*; DOE/NETL-2010/1402; Report for the U.S. Department of Energy; National Energy Technology Laboratory by the Research and Development Solutions, LLC (RDS): Morgantown, WV, USA, 2011.
108. Heyne, S.; Harvey, S. Impact of choice of CO_2 separation technology on thermo-economic performance of Bio-SNG production processes. *Int. J. Energy Res.* **2014**, *38*, 299–318. [CrossRef]
109. Arvidsson, M.; Morandin, M.; Harvey, S. Biomass gasification-based syngas production for a conventional oxo synthesis plant—Greenhouse gas emission balances and economic evaluation. *J. Clean. Prod.* **2015**, *99*, 192–205. [CrossRef]
110. Holmgren, K.M. *Investment Cost Estimates for Gasification- Based Biofuel Production Systems*; IVL Swedish Environmental Research Institute: Stockholm, Sweden, 2015; Available online: https://www.ivl.se/download/18.694ca0617a1de98f472a45/1628413810159/FULLTEXT01.pdf (accessed on 2 July 2023).
111. Federal Environmental Agency Germany. *ProBas—Xtra-AbbauQuarzsand-DE-2030*; Federal Environmental Agency Germany: Dessau-Roßlau, Germany, 2008. Available online: https://www.probas.umweltbundesamt.de/php/prozessdetails.php?id=%7b843DA94D-BDA7-442E-A9A3-B80D8B40E66F%7d (accessed on 20 March 2023).

112. Federal Environmental Agency Germany. *ProBas—LKW oder Lastzug*; Federal Environmental Agency Germany: Dessau-Roßlau, Germany, 2010. Available online: https://www.probas.umweltbundesamt.de/php/prozessdetails.php?id=%7b539F70D8-E544-FE35-BBCA-700578003269%7d (accessed on 20 March 2023).
113. Federal Environmental Agency Germany. *ProBas—BioRaff-IIRME-DE-2020/brutto*; Federal Environmental Agency Germany: Dessau-Roßlau, Germany, 2011. Available online: https://www.probas.umweltbundesamt.de/php/prozessdetails.php?id=\{35FD7B45-BBDF-4D1B-BEE6-7EEAA29BFDAE\} (accessed on 20 March 2023).
114. Jekel, M.; Baur, N.; Böckelmann, U.; Dünnbier, U.; Eckhardt, A.; Gnirß, R.; Grummt, T.; Hummelt, D.; Lucke, T.; Meinel, F.; et al. *Anthropogene Spurenstoffe und Krankheitserreger im Urbanen Wasserkreislauf*; Universitätsverlag der TU Berlin: Berlin, Germany, 2016; ISBN 978-3-7983-2815-0.
115. Federal Environmental Agency Germany. *ProBas—Zink*; Federal Environmental Agency Germany: Dessau-Roßlau, Germany, 2008. Available online: https://www.probas.umweltbundesamt.de/php/prozessdetails.php?id=%7b50476E3A-C90A-4AE4-A1FB-3BC08579E219%7d (accessed on 20 March 2023).
116. Federal Environmental Agency Germany. *ProBas—MetallNickel-DE-2020*; Federal Environmental Agency Germany: Dessau-Roßlau, Germany, 2008. Available online: https://www.probas.umweltbundesamt.de/php/prozessdetails.php?id=%7b65C51F09-9F88-4D3C-8858-CFBCACF98D53%7d (accessed on 20 March 2023).
117. Federal Environmental Agency Germany. *ProBas—AufbereitungTonerde-DE-2020*; Federal Environmental Agency Germany: Dessau-Roßlau, Germany, 2010. Available online: https://www.probas.umweltbundesamt.de/php/prozessdetails.php?id=\{9DFA17E4-264F-459F-90D0-8EDF677F1BC0\} (accessed on 20 March 2023).
118. Federal Environmental Agency Germany. *ProBas—Kobalt*; Federal Environmental Agency Germany: Dessau-Roßlau, Germany, 2008. Available online: https://www.probas.umweltbundesamt.de/php/prozessdetails.php?id=\{81A717DC-DA5B-4EDC-A754-03331A829E4F\} (accessed on 20 March 2023).
119. Federal Environmental Agency Germany. *ProBas—EdelmetallPt-primär-mix-Welt*; Federal Environmental Agency Germany: Dessau-Roßlau, Germany, 2008. Available online: https://www.probas.umweltbundesamt.de/php/prozessdetails.php?id=\{0E0B2A95-9043-11D3-B2C8-0080C8941B49\} (accessed on 20 March 2023).
120. Federal Environmental Agency Germany. *ProBas—Quarz, Quarzite*; Federal Environmental Agency Germany: Dessau-Roßlau, Germany, 2008. Available online: https://www.probas.umweltbundesamt.de/php/prozessdetails.php?id=\{9E9C7D4E-6240-4BF8-823A-D80C0F0C257B\} (accessed on 20 March 2023).
121. Federal Environmental Agency Germany. *ProBas—Trimethylamin*; Federal Environmental Agency Germany: Dessau-Roßlau, Germany, 2008. Available online: https://www.probas.umweltbundesamt.de/php/prozessdetails.php?id=%7bCC66D615-2F74-4C6C-8EDA-74119209C218%7d (accessed on 20 March 2023).
122. Federal Environmental Agency Germany. *ProBas—Chem-OrgPEG+DPM (Hochrein)*; Federal Environmental Agency Germany: Dessau-Roßlau, Germany, 2011. Available online: https://www.probas.umweltbundesamt.de/php/prozessdetails.php?id=%7b150EFBAB-DBA6-4752-BF86-FB34F95A1B3C%7d (accessed on 20 March 2023).
123. NREL. *H2A: Hydrogen Analysis Production Models: Case Studies 2018*; National Renewable Energy Laboratory: Denver, CO, USA, 2018. Available online: https://www.nrel.gov/hydrogen/h2a-production-models.html (accessed on 28 June 2021).
124. Federal Environmental Agency Germany. *ProBas—MetallStahl-Profile-85%Recycling-Welt-2005*; Federal Environmental Agency Germany: Dessau-Roßlau, Germany, 2012. Available online: https://www.probas.umweltbundesamt.de/php/prozessdetails.php?id=\{E0B82461-4166-4CFB-9F80-3EDFBF6B858C\} (accessed on 20 March 2023).
125. Federal Environmental Agency Germany. *ProBas—Stahl*; Federal Environmental Agency Germany: Dessau-Roßlau, Germany, 2008. Available online: https://www.probas.umweltbundesamt.de/php/prozessdetails.php?id=\{19E7D6CB-2337-4ED1-A096-3DF3961DDA87\} (accessed on 20 March 2023).
126. Federal Environmental Agency Germany. *ProBas—Beton*; Federal Environmental Agency Germany: Dessau-Roßlau, Germany, 2012. Available online: https://www.probas.umweltbundesamt.de/php/prozessdetails.php?id=\{707E23CA-304F-485C-83A6-90C0A0F1BAA6\} (accessed on 20 March 2023).
127. Wirtschaftskammer Österreich. *Statistisches Jahrbuch 2023*; Wirtschaftskammer Österreich: Vienna, Austria, 2023; Available online: https://www.wko.at/service/zahlen-daten-fakten/statistisches-jahrbuch.html (accessed on 2 July 2023).
128. Gollner, M. *Nutzenergieanalyse 1993–2021*; Statistik Austria: Vienna, Austria, 2022; Available online: https://www.statistik.at/statistiken/energie-und-umwelt/energie/nutzenergieanalyse (accessed on 2 July 2023).
129. Turner, J.; Winkler, G.; Swoboda, G. *Statistiken Sonderheft: Einkommen, Konsum und Vermögen der Haushalte—Sektorale Volkswirtschaftliche Gesamtrechnungen in den Letzten 20 Jahren*; Oesterreichische Nationalbank: Vienna, Austria, 2022. Available online: https://www.oenb.at/Publikationen/Statistik/Statistiken-Sonderhefte/2022/sektorale-vgr.html (accessed on 2 July 2023).
130. Fichtinger, M.; Grohall, G.; Helmenstein, C.; Schitnig, H.; Sengschmid, E.; Zalesak, M. *Die volkswirtschaftliche Bedeutung des österreichischen Logistiksektors: Studie im Auftrag der Wirtschaftskammer Österreich—Sparte Transport und Verkehr, der Vereinigung der Österreichischen Industrie und des Zentralverbandes Spedition & Logistik*; Economica GmbH: Vienna, Austria, 2022. Available online: https://news.wko.at/news/oesterreich/221115-Logistik-Studienbericht-EconomicaG.pdf (accessed on 2 July 2023).

Supplementary material

Economic and ecological impacts on the integration of biomass-based SNG and FT diesel in the Austrian energy system

Martin Hammerschmid[1], Alexander Bartik, Florian Benedikt, Marton Veress, Simon Pratschner, Stefan Müller and Hermann Hofbauer

TU WIEN, Institute of Chemical, Environmental and Bioscience Engineering, Getreidemarkt 9/166, 1060 Vienna, Austria

Assumptions and references for process simulation to calculate mass and energy balances for biomass-based SNG and FT route

Table S1. Assumptions for the units of the gasification, gas cooling & cleaning section

Parameter	Unit	Value/Assumption	Reference
Biomass dryer			**[65, 66]**
Water content incoming biomass	wt.-%	40	
Water content exiting biomass	wt.-%	20	
Temperature drying air inlet	°C	90	
Relative humidity drying air inlet	%	80	
Relative humidity drying air outlet	%	80	
DFB gasification reactor			**[66-68]**
Operating temperature	°C	820	
Steam to fuel ratio	$kg_{H2O}/kg_{fuel,daf}$	0.6	
Heat loss (related to thermal fuel power)	%	1	
Temperature steam	°C	400	
DFB combustion reactor			**[66-68]**
Lambda	kg/kg	1.25	
CO slip	mol CO/mol CO_2	0.05	
Heat loss (related to thermal fuel power)	%	1	
PG filter			**[69]**
Separation efficiency dust	%	99.9	
Separation efficiency char	%	99.9	
Separation efficiency tar	%	30	
RME scrubber			**[19, 70, 71]**
Circulating solvent to gas ratio	kg_{RME}/kg_{gas}	20	
Tar concentration outlet	g/Nm^3	1.5	
Temperature exiting gas	°C	40	
Temperature incoming RME	°C	37	
Separation efficiency ammonia (inclusive downstream units)	%	99.9	
Massflow fresh RME make-up	kg/h	110	[19]
AC adsorber			**[38, 45]**
Separation efficiency tar	%	100	
Separation efficiency sulfur	%	100	
Adsorption capacity AC	wt.-%	20	
Steam regeneration temperature	°C	250	[38]
Steam amount for regeneration	kg/kg_{BTX}	9.2	[38]

[1] Corresponding author. Tel.: +43 1 58801 166856; E-mail address: martin.hammerschmid@tuwien.ac.at

Auxiliary and pressure drop			
Steam pre-evaporation (related to amount of water phase from RME scrubber)	wt.-%	5	assumed
Total pressure drop product gas route	mbar	345	assumed
Total pressure drop flue gas route	mbar	345	assumed
Blowers			**[66, 72]**
Efficiency of drive system (all units)	%	95	
Mechanical efficiency of blowers (all units)	%	98	
Isentropic efficiencies			
Drying air blower	%	80	
PG blower	%	50	
PG recycle blower	%	50	
FG blower	%	75	
FG recycle blower	%	75	
Combustion air blower 1	%	65	
Combustion air blower 2	%	45	

Table S2. Assumptions for the units of the SNG synthesis and upgrading section

Parameter	Unit	Value/Assumption	Reference
Compressor			**[73]**
Efficiency of drive system	%	95	
Mechanical efficiency of compressor	%	98	
Isentropic efficiency	%	85	
Guard reactor (ZnO)			
GHSV	h^{-1}	3800	[74]
Fluidized bed methanation reactor			
Reaction temperature	°C	320	[75]
Reaction pressure	bar	10	assumed
WHSV	Nm^3/kg_{cat} h	1.5	[75]
Steam content inlet	vol.-%	15	assumed
Pressure drop	mbar	150	assumed
Catalyst type	-	Ni/Al_2O_3	[75]
CO_2 scrubber			
Gas inlet temperature	°C	40	[76]
Gas outlet temperature	°C	60	assumed
Separation efficiency CO_2	%	97.5	assumed
Reboiler duty	$MJ/kgCO_2$	0.8	[38]
Absorption capacity	kg CO_2/kg amine	0.36	[77]
Amine make-up stream	kg/t_{CO2}	1.5	[76]
Glycol dryer			
Gas inlet temperature	°C	30	[78]
Gas outlet temperature	°C	31	[78]
Glycol regeneration temperature	°C	190	[78]
Glycol make-up stream	kg/h	0.1	[79]

Table S3. Assumptions for the units of the FT synthesis and upgrading section

Parameter	Unit	Value/Assumption	Reference
Compressor			**[73]**
Efficiency of drive system	%	95	
Mechanical efficiency of compressor	%	98	
Isentropic efficiency	%	85	
CO_2 scrubber			
Gas inlet temperature	°C	40	[76]
Gas outlet temperature	°C	60	assumed
Separation efficiency CO_2	%	80	assumed[2]
Reboiler duty	$MJ/kgCO_2$	0.8	[38]
Absorption capacity	kg CO_2/kg amine	0.36	[77]
Amine make-up stream	kg/t_{CO2}	1.5	[76]
Guard reactor (ZnO)			
GHSV	h^{-1}	3800	[74]
FT slurry reactor			
Reaction temperature	°C	230	[40]
Reaction pressure	bar	21	[40]
CO-Conversion	mol.-%	50	[40]
CO_2-Conversion (WGS activity)	mol.-%	0	[40]
α_1 (eASF distribution parameter)	-	0.78	[40]
α_2 (eASF distribution parameter)	-	0.9	[40]
β (eASF distribution parameter)	-	0.75	[40]
γ (eASF distribution parameter)	-	0.48	[40]
μ (eASF distribution parameter)	-	0.95	[40]
Naphtha compounds in liquid phase	mass.-%	0	assumed[3]
Middle distillate compounds in liquid phase	mass.-%	0.05	assumed[3]
Naphtha compounds in liquid phase	mass.-%	0.75	assumed[3]
Recirculation ratio tailgas	vol.-%	85	assumed[4]
WHSV	Nm^3/kg_{cat} h	2.0	[80]
Pressure drop	mbar	300	assumed
Catalyst type	-	Co/Al_2O_3	[81]
Quench column			
Temperature (top)	°C	70	[81]
Steam Reformer			
Reaction temperature	°C	850	[82]
Reaction pressure	bar	10	[82]
CH_4-Conversion	vol.-%	90	[82]
C_2H_4-Conversion	vol.-%	90	[82]
C_2H_6-Conversion	vol.-%	95	[82]
C_3H_8-Conversion	vol.-%	99	[82]
Steam/Carbon ratio	-	2.5	[83]
WHSV	Nm^3/kg_{cat} h	2.5	assumed
Pressure drop	mbar	300	assumed
Catalyst type	-	$NiO/CaAl_{12}O_{19}$	[84]

[2] Separation efficiency was set to adjust balance in Steam Reformer in favor of H_2/CO ratio of tailgas
[3] Liquid and gas phase distribution of FT products assumed according to phase equilibrium at process conditions
[4] Recirculation ratio assumed according to heat demand of steam reformer (15% of tailgas combusted = purge gas)

Hydrocracker			
Reaction temperature	°C	360	[81, 85, 86]
Reaction pressure	bar	40	[81, 85, 86]
Wax conversion	%	70	[86, 87]
Outlet concentration C_1-C_3	wt.-% (without wax)	5	[81]
Outlet concentration C_4-C_9	wt.-% (without wax)	20	[81]
Outlet concentration C_{10}-C_{20}	wt.-% (without wax)	75	[81]
LHSV	Nm^3_{wax}/Nm^3_{cat} h	1	[81, 85, 86]
Hydrogen make-up stream	$wt.\text{-}\%_{H2}$ /$wt.\text{-}\%_{wax}$	1	[81]
Catalyst type	-	Pt/SiO_2-Al_2O_3	[87, 88]
Hydrotreater			
Reaction temperature	°C	350	[86, 89]
Reaction pressure	bar	40	[86, 89]
LHSV	Nm^3_{MD}/Nm^3_{cat} h	2	[86, 89]
Hydrogen make-up stream	$wt.\text{-}\%_{H2}$ /$wt.\text{-}\%_{MD}$	0.3	[86]
Catalyst type	-	Ni-MoS_2/Al_2O_3	[85 ,90]

Table S4. Assumptions as well as results for biomass and gas compositions

Parameter	Unit	Value/Assumption	Reference
Biomass composition			**[5]**
Water content	wt.-%	40	
Ash content	$wt.\text{-}\%_{db}$	1	
Carbon	$wt.\text{-}\%_{db}$	50.7	
Hydrogen	$wt.\text{-}\%_{db}$	5.9	
Nitrogen	$wt.\text{-}\%_{db}$	0.21	
Sulfur	$wt.\text{-}\%_{db}$	0.01	
Product gas composition			**[91]**
Hydrogen	$vol.\text{-}\%_{db}$	45	
Carbon dioxide	$vol.\text{-}\%_{db}$	21.15	
Carbon monoxide	$vol.\text{-}\%_{db}$	23	
Methane	$vol.\text{-}\%_{db}$	9.7	
Ethylene	$vol.\text{-}\%_{db}$	1	
Ethane	$vol.\text{-}\%_{db}$	0.1	
Water content	vol.-%	30	
Ammonia	$ppm_{v,db}$	950	
Nitrogen	$ppm_{v,db}$	350	
Dust	g/Nm^3	10	
Char	g/Nm^3	10	
Tar	g/Nm^3	5	
SNG composition			**result**
Methane	vol.-%	94.62	
Hydrogen	vol.-%	2.82	
Carbon dioxide	vol.-%	2.34	
Nitrogen	vol.-%	0.12	
Carbon monoxide	vol.-%	0.093	

Relative density	-	0.564	
Wobbe index	MJ/Nm^3	50.55	
Higher heating value	MJ/Nm^3	37.95	
FT product composition (excluding C_1-C_3)			**result**
FT naphtha (C_4-C_9)	$wt.-\%_{db}$	23.67	
FT middle distillate (C_{10}-C_{19})	$wt.-\%_{db}$	37.25	
FT wax (C_{20+})	$wt.-\%_{db}$	39.08	

Assumptions and references for techno-economic assessment to calculate production costs for biomass-based SNG and FT route

Table S5. Assumptions for cost rates

Parameter	Unit	Value/Assumption	Reference
General plant parameters			**[11, 92]**
Plant lifetime	a	20	
Number of employees	-	7	
Personnel costs per employee 2022	€/a	65000	
Personnel costs per employee 2019	€/a	62500	
Operating hours plant	h/a	7500	
Operating hours district heat	h/a	5800	
Maintenance costs	$\%_{CAPEX}$/a	2.0	
Insurance, administration and other costs	$\%_{CAPEX}$/a	1.5	
Interest rate	%	6	
Consumption-related parameters			
Natural gas household price 2022	€/MWh	150	[93, 94]
Natural gas household price 2019	€/MWh	69.7	[93]
Natural gas industry price 2022	€/MWh	88.9	[93]
Natural gas industry price 2019	€/MWh	29.9	[93]
Fossil diesel price petrol station 2022	€/l	1.939 (incl. taxes)	[95]
Fossil diesel price petrol station 2019	€/l	1.236 (incl. taxes)	[95]
Fossil diesel price stock market 2022	€/l	1.595 (incl. taxes)	[96]
Fossil diesel price stock market 2019	€/l	0.934 (incl. taxes)	[96]
Wood chips price 2022	$€/t_{atro}$	95	[11]
Wood chips price 2019	$€/t_{atro}$	75	[11]
Fresh scrubber solvent (RME)[5]	$€/kg_{2013}$	0.96	[66]
Fresh amine (MEA)[5]	$€/kg_{2013}$	1.40	[98]
Fresh glycol (TEG)[5]	$€/kg_{2016}$	2.0	[99]
Activated carbon[5] (lifetime 1 year)	$€/kg_{2019}$	2.21	[11]
Zinc oxide[5] (lifetime 3 years)	$€/kg_{2013}$	20	[100]
Olivine[5]	$€/t_{2013}$	190	[66]
Limestone[5]	$€/t_{2013}$	35	[92]
Nickel catalyst[5] (lifetime 3 years)	$€/kg_{2011}$	50	[29]
Cobalt catalyst[5] (lifetime 5 years)	$€/kg_{2013}$	24	[29]
Platin catalyst[5] (lifetime 3 years)	$€/kg_{2014}$	1504	[29]
Disposal costs ash[5]	$€/t_{2013}$	90	[66]
Disposal costs waste water[5]	$€/m^3{}_{2019}$	2.5	[11]

[5] Cost rates from literature inflation-adjusted with EPI [97] from literature base to reference years 2019 and 2022

CO_2 emission allowances 2022	€/t_{CO2}	69.6	[101]
CO_2 emission allowances 2019	€/t_{CO2}	24.9	[101]
Electricity costs (industry) 2022	€/kWh_{el}	0.21	[102]
Electricity costs (industry) 2019	€/kWh_{el}	0.095	[102]
Hydrogen costs 2022	€/kg	4.5	[103]
Hydrogen costs 2019	€/kg	4.0	[103]
Revenues FT naphtha[5]	€/l_{2017}	0.78	[104]
Revenues district heat[5]	€/$MWh_{th,2016}$	30.0	[92]

Table S6. Assumptions for determination of total capital investment costs for the biomass-based SNG route

Equipment	Base scale	Base cost	Scale factor	Desired scale	Equipment costs 2022[6]	Equipment costs 2019[6]	Ref.
Resource supply + Gasification + Raw gas cleaning + Flue gas cleaning					**114 431 228 €**	**83 522 433 €**	
(biomass dryer, gasification reactor, combustion reactor, PG cyclone, PG cooler, PG filter, RME scrubber incl regeneration, PG blower, steam generation, pre-evaporator, FG cyclone, post combustion chamber, steam superheater, FG cooler, FG filter, FG blower, stack)							
DFB gasification system + gas cooling and cleaning (total capital investment costs)	15 MW_{th}	21 697 500 $€_{2020}$	0.7	100 MW_{th}	114 431 228 €	83 522 433 €	[11]
Fine gas cleaning + Syngas compression and cooling					**6 206 640 €**	**4 505 289 €**	
Activated carbon adsorber (TSA)	32 MW_{th}	945 180 $€_{2018}$	0.7	100 MW_{th}	3 043 368 €	2 221 330 €	[28]
Product gas compressor 1	224 kW_{el}	120 498 $€_{1994}$	0.84	1303 kW_{el}	1 256 400 €	917 036 €	[105]
Intermediate cooler	448 MW_{th}	4 258 200 $€_{2007}$	0.7	1.66 MW_{th}	140 785 €	102 758 €	[106]
Product gas compressor 2	224 kW_{el}	120 498 $€_{1994}$	0.84	1442 kW_{el}	1 368 204 €	998 641 €	[105]
Syngas preheater	93 m^2	19 660 $€_{1994}$	0.59	65 m^2	36 015 €	26 287 €	[105]
ZnO guard reactor	175 $MW_{SNG,HHV}$	450 000 $€_{2012}$	0.7	72 $MW_{SNG,HHV}$	361 778 €	239 237 €	[107]
Methanation					**3 713 954 €**	**2 710 785 €**	
Fluidized bed methanation	25 560 Nm^3/h	2 235 200 $€_{2010}$	0.6	27 044 Nm^3/h	3 670 316 €	2 678 934 €	[108]
Steam generator methanation	93 m^2	19 660 $€_{1994}$	0.59	90 m^2	43 638 €	31 851 €	[105]
SNG Upgrading					**5 099 018 €**	**3 721 731 €**	
Raw-SNG cooler	93 m^2	19 660 $€_{1994}$	0.59	600 m^2	133 651 €	97 551 €	[105]
Raw-SNG condenser	448 MW_{th}	4 258 200 $€_{2007}$	0.7	4.29 MW_{th}	274 085 €	200 052 €	[106]
CO_2 scrubber (MEA) incl. regeneration	54 000 Nm^3/h	6 700 000 $€_{2012}$	0.6	13 185 Nm^3/h	4 298 880 €	3 137 718 €	[109]
CO_2 recycle blower	16 992 Nm^3/h	60 702 $€_{1994}$	0.6	6 246 Nm^3/h	75 353 €	54 999 €	[105]
CO_2 recycle motor	7.5 kW_{el}	11 144 $€_{1994}$	0.56	8.9 kW_{el}	29 189 €	21 304 €	[105]
SNG cooler	93 m^2	19 660 $€_{1994}$	0.59	65 m^2	36 015 €	26 287 €	[105]
Glycol dryer incl. regeneration	41664 Nm^3/h	457 507 $€_{2016}$	0.6	6938 Nm^3/h	251 845 €	183 820 €	[78]
Total equipment costs SNG route (without DFB)					**15 019 612 €**	**10 937 805 €**	
Total capital investment costs SNG route (Lang factor = 4.87 [54])					**187 576 738 €**	**136 789 544 €**	

[6] Calculated according to equation 3 from main text in chapter 2.3

Table S7. Assumptions for determination of total capital investment costs for the biomass-based FT route

Equipment	Base scale	Base cost	Scale factor	Desired scale	Equipment costs 2022[7]	Equipment costs 2019[7]	Ref.
Resource supply + Gasification + Raw gas cleaning + Flue gas cleaning					**114 431 228 €**	**83 522 433 €**	
(biomass dryer, gasification reactor, combustion reactor, PG cyclone, PG cooler, PG filter, RME scrubber incl regeneration, PG blower, steam generation, pre-evaporator, FG cyclone, post combustion chamber, steam superheater, FG cooler, FG filter, FG blower, stack)							
DFB gasification system + gas cooling and cleaning (total capital investment costs)	15 MW_{th}	21 697 500 $€_{2020}$	0.7	100 MW_{th}	114 431 228 €	83 522 433 €	[11]
Fine gas cleaning + Syngas compression and cooling					**14 213 796 €**	**10 331 845 €**	
Activated carbon adsorber (TSA)	32 MW_{th}	945 180 $€_{2018}$	0.7	100 MW_{th}	3 043 368 €	2 221 330 €	[28]
Product gas compressor 1	224 kW_{el}	120 498 $€_{1994}$	0.84	1303 kW_{el}	1 256 400 €	917 036 €	[105]
Product gas compressor 2	224 kW_{el}	120 498 $€_{1994}$	0.84	1450 kW_{el}	1 374 800 €	1 003 455 €	[105]
CO_2 scrubber (MEA) incl. regeneration	54 000 Nm^3/h	6 700 000 $€_{2012}$	0.6	23 171 Nm^3/h	6 029 535 €	4 400 909 €	[109]
CO_2 recycle blower	16 992 Nm^3/h	60 702 $€_{1994}$	0.6	3 890 Nm^3/h	56 716 €	41 397 €	[105]
CO_2 recycle motor	7.5 kW_{el}	11 144 $€_{1994}$	0.56	5 kW_{el}	21 100 €	15 401 €	[105]
Product gas compressor 3	224 kW_{el}	120 498 $€_{1994}$	0.84	1926 kW_{el}	1 744 670 €	1 273 421 €	[105]
Syngas preheater	93 m^2	19 660 $€_{1994}$	0.59	177 m^2	64 991 €	47 436 €	[105]
ZnO guard reactor	24 925 Nm^3/h	361 778 $€_{2022}$	0.7	50 442 Nm^3/h	622 216 €	411 460 €	SNG route
Fischer-Tropsch synthesis + Tailgas recycling					**14 296 262 €**	**10 434 726 €**	
Fischer-Tropsch slurry reactor	2 420 000 kW	223 156 860 $€_{2011}$	0.75	54 124 kW	4 664 232 €	3 404 386 €	[110]
Quench column incl. separation	12.1 t/h	497 000 $€_{2011}$	0.7	29.1 t/h	1 369 811 €	999 814 €	[29]
Tail gas heater	93 m^2	19 660 $€_{1994}$	0.59	1011 m^2	181 781 €	132 680 €	[105]
Steam reformer	1 390 kmol/h	9 400 000 $€_{2007}$	0.65	1 617 kmol/h	4 182 820 €	3 053 007 €	[29]
Combustion chamber	Calculation tool (Reformer furnace)			14 815 kW	2 848 772 €	2 079 296 €	[46]
Steam generator (reformer)	36 000 kg/h	1 317 000 $€_{2011}$	0.6	6 080 kg/h	644 012 €	470 059 €	[29]
Tail gas cooler	93 m^2	19 660 $€_{1994}$	0.59	1175 m^2	198 652 €	144 994 €	[105]
Tail gas condenser	448 MW_{th}	4 258 200 $€_{2007}$	0.7	2.86 MW_{th}	206 182 €	150 490 €	[106]

Table S7. Assumptions for determination of total capital investment costs for the biomass-based FT route (continuous)

[7] Calculated according to equation 3 from main text in chapter 2.3

Equipment	Base scale	Base cost	Scale factor	Desired scale	Equipment costs 2022[8]	Equipment costs 2019[8]	Ref.
Fischer-Tropsch products upgrading					**13 500 621 €**	**9 853 995 €**	
Wax heater	93 m^2	19 660 $€_{1994}$	0.59	14 m^2	14 348 €	10 473 €	[105]
Hydrocracker	4 100 kg/h	6 018 429 $€_{2007}$	0.55	1 728 kg/h	6 233 141 €	4 549 519 €	[110]
Middle distillate (MD) heater	93 m^2	19 660 $€_{1994}$	0.59	22 m^2	19 092 €	13 935 €	[105]
Distillation	3190 MW	67 179 900 $€_{1993}$	0.65	54.1 MW	2 799 167 €	2 043 090 €	[110]
Hydrotreater	1 300 kg/h	1 611 386 $€_{2007}$	0.6	3 001 kg/h	4 434 873 €	3 236 978 €	[110]
Total equipment costs FT route (without DFB)					**42 010 679 €**	**30 620 566 €**	
Total capital investment costs FT route (Lang factor = 4.87 [54])					**319 023 235 €**	**232 644 589 €**	

[8] Calculated according to equation 3 from main text in chapter 2.3

Assumptions and references for ecological assessment to calculate CO_2 footprint for biomass-based SNG and FT route

Table S8. Assumptions for CO_2e emission factors

Parameter	Unit	Value	Reference
Consumption-related emission factors			
Biomass (wood chips)	$kg_{CO2e}/kg_{wood\ chips}$	0.049	[49]
Bed material (olivine / limestone)	$kg_{CO2e}/kg_{quartz\ sand}$	0.024	[111]
Bed material transport	$kg_{CO2e}/km/t_{sand}$	0.057	[112]
RME scrubber solvent (rapeseed methyl ester)	kg_{CO2e}/kg_{RME}	1.912	[49, 113]
Activated carbon (AC)	kg_{CO2e}/kg_{AC}	14.133	[114]
Zinc oxide (only raw material)	kg_{CO2e}/kg_{Zinc}	3.260	[115]
Nickel catalyst (only raw materials) (20% Ni and 80% Al_2O_3) ➔ for methanation and hydrotreater assumed	$kg_{CO2e}/kg_{catalyst}$	1.902	[116, 117]
Nickel catalyst (only raw materials) (14% Ni and 86% Al_2O_3) ➔ for steam reformer assumed	$kg_{CO2e}/kg_{catalyst}$	1.679	[116, 117]
Cobalt catalyst (only raw materials) (20% Co and 80% Al_2O_3) ➔ for FT slurry reactor assumed	$kg_{CO2e}/kg_{catalyst}$	2.472	[117, 118]
Platin catalyst (only raw materials) (1% Pt and 99% SiO_2) ➔ for hydrocracker assumed	$kg_{CO2e}/kg_{catalyst}$	266	[119, 120]
Amine (monoethanolamine)	kg_{CO2e}/kg_{Amine}	2.361	[121]
Glycol (Polyethylene glycol assumed)	kg_{CO2e}/kg_{PEG}	2.240	[122]
Electricity (green electricity)	kg_{CO2e}/kWh_{el}	0.014	[49]
Hydrogen (calculated via electricity consumption)	kWh_{el}/kg_{H2}	48	[123]
Construction-related emission factors			
Steel for construction and equipment	kg_{CO2e}/t_{steel}	1446	[124, 125]
Concrete for brickwork and fundament	$kg_{CO2e}/t_{concrete}$	107	[126]
Emission factors of fossil counterparts			
Fossil natural gas	kg_{CO2e}/kWh_{NG}	0.268	[49]
Fossil diesel	kg_{CO2e}/l_{Diesel}	3.134	[49]

Assumptions and references for the investigation of the sectoral integration of biomass-based SNG and FT diesel in the Austrian energy system

Table S9. Assumptions for sectoral integration of DFB products

Parameter	Unit	Value	Reference
Sectoral integration of biomass-based SNG			
Gross value added for energy sector 2019	M€/a	9 840	[127]
Gross value added for energy sector 2022	M€/a	14 520	[127]
CO_2 footprint for energy sector	Mt_{CO2e}/a	8 269	[2]
Gross value added for public and private sector 2019 (only households with gas heaters - 25% [75])	M€/a	16 825	[129]
Gross value added for public and private sector 2022 (only households with gas heaters - 25% [75])	M€/a	16 135	[129]
CO_2 footprint for public and private sector	Mt_{CO2e}/a	8 046	[2]
Gross value added for industry sector 2019	M€/a	66 790	[127]
Gross value added for industry sector 2022	M€/a	71 290	[127]
CO_2 footprint for industry sector	Mt_{CO2e}/a	26 540	[2]
Sectoral integration of biomass-based FT diesel			
Gross value added for public and private transport sector 2019 (only diesel vehicles – 73.6% of inland transport [75])	M€/a	49 533	[129]
Gross value added for public and private transport sector 2022 (only diesel vehicles – 73.8% of inland transport [75])	M€/a	47 822	[129]
CO_2 footprint for public and private transport sector	Mt_{CO2e}/a	12 246	[2]
Gross value added for heavy-duty traffic sector 2019	M€/a	22 847	[130}
Gross value added for heavy-duty traffic sector 2022	M€/a	26 769	[130]
CO_2 footprint for heavy-duty traffic sector	Mt_{CO2e}/a	9 243	[2]
Gross value added for heat and power sector 2019	M€/a	66 790	[127]
Gross value added for heat and power sector 2022	M€/a	71 290	[127]
CO_2 footprint for heat and power sector	Mt_{CO2e}/a	26 540	[2]

LEBENSLAUF

Alexander Bartik

Geburtstag [redacted]

Adresse [redacted]

Telefon [redacted]

E-Mail [redacted]

BERUFSERFAHRUNG

Seit 11/2018	**Technische Universität Wien** Projekt- und Universitätsassistent am Institut für Verfahrenstechnik, Umwelttechnik und Technische Biowissenschaften Forschungsbereich Brennstoff- und Energiesystemtechnik Experimentelle und simulative Entwicklung verfahrenstechnischer Anlagen und Prozesse Durchführung von Lehrtätigkeiten
02/2017 – 08/2017	**Technische Universität Wien** Projektmitarbeiter am Institut für Thermodynamik und Energietechnik Forschung im Bereich thermochemischer Energiespeicher
06/2013 – 09/2013	**Fill Metallbau GmbH** Monteur
09/2012	**Josko Fenster & Türen GmbH** Monteur
06/2011 – 08/2011	**FACC AG** Mitarbeiter in der Abteilung „Tool & Manufacturing Engineering" Maturaprojekt: „Optimierung von Schlauchblasverfahren"
06/2010 – 08/2010	**FACC AG** Ferialpraktikant in der Abteilung „Tool & Manufacturing Engineering" Konstruktive Tätigkeiten mit CATIA

AUSBILDUNG

11/2018 – 03/2024	**Technische Universität Wien – Doktoratsstudium Verfahrenstechnik** Dissertation: Synthetic Natural Gas from Woody Biomass

09/2016 – 11/2018	**Technische Universität Wien – Master Verfahrenstechnik** Fachrichtung Anlagen- und Apparatebau Schwerpunkt Brennstoff- und Energietechnologie Diplomarbeit „$MgO/Mg(OH)_2$ as thermochemical energy storage materials in a fluidized bed reactor" Abschluss mit Auszeichnung in Mindeststudienzeit
09/2016 – 02/2016	**University of Waterloo, Kanada – Auslandssemester** Studienfach Chemical Engineering
09/2016 – 12/2016	**Technische Universität Wien – Bachelor Verfahrenstechnik** Abschluss mit Auszeichnung in Mindeststudienzeit
09/2007 – 06/2012	**HTL Andorf** Fachrichtung Werkstoffingenieurwesen Schwerpunkt Kunststoff- und Umwelttechnik Abschluss mit Auszeichnung

WEITERE QUALIFIKATIONEN

Auszeichnungen	Verleihung des Diplomarbeitspreises der Stadt Wien (2019) Nominierung für den Würdigungspreis 2019 (Staatspreis für die österreichweit besten Diplom- und Masterabschlüsse) Viermalige Verleihung des Leistungsstipendiums der Fakultät für Maschinenbau und Betriebswissenschaften der TU Wien (2015/2016/2017/2018) Verleihung des "Best Presentation Awards" beim Minisymposium Verfahrenstechnik (2020)
Sprachen	Deutsch, Englisch (fließend)
IT Kenntnisse	MS-Office und LaTEX Prozesssimulation IPSEpro MATLAB SPS-Programmierung (Automation Studio, APROL) 3D-CAD
Sonstiges	Schulsprecher an der HTL Andorf Vorstandsmitglied und Kassier in ehrenamtlichen Vereinen

PERSÖNLICHE INTERESSEN

Bergsteigen, Klettern, Reisen, Musizieren, Skifahren